eman ta zabal zazu
Universidad del País Vasco
Euskal Herriko Unibertsitatea
ZIENTZIA ETA TEKNOLOGIA FAKULTATEA
FACULTAD DE CIENCIA Y TECNOLOGÍA

FACULTAD DE CIENCIA Y TECNOLOGÍA

DEPARTAMENTO DE INGENIERÍA QUÍMICA

PYROLYSIS AND IN-LINE CATALYTIC STEAM REFORMING OF BIOMASS AND BIOMASS/PLASTIC MIXTURES FOR H_2 PRODUCTION

TESIS DOCTORAL

Aitor Arregi Joaristi

Marzo, 2017

eman ta zabal zazu
Universidad del País Vasco
Euskal Herriko Unibertsitatea
ZIENTZIA ETA TEKNOLOGIA FAKULTATEA
FACULTAD DE CIENCIA Y TECNOLOGÍA

FACULTAD DE CIENCIA Y TECNOLOGÍA

DEPARTAMENTO DE INGENIERÍA QUÍMICA

PYROLYSIS AND IN-LINE CATALYTIC STEAM REFORMING OF BIOMASS AND BIOMASS/PLASTIC MIXTURES FOR H_2 PRODUCTION

MEMORIA

Que para optar al grado de Doctor en Ingeniería Química

presenta

Don Aitor Arregi Joaristi

Leioa, Marzo, 2017

Tesia amaitzear nagoen honetan, eskerrak ematea gustatuko litzaidake azken urte hauetan nire alboan izan diren eta lagundu didaten pertsona guztiei. Lehenik eta behin, eskerrik asko Martin Olazar eta Maider Amutio nire zuzendariei, lan hau egiteko nigan jarritako konfiantzagatik, behar izan dudan momentu guztietan laguntzeko prest egotearren eta tesi hau zuzentzen egindako lan guztiagatik. Bereziki, eskerrik asko Maider, laborategian irakatsitako guztiagatik eta emandako laguntza eta aholkuengatik. Eskerrak Javier Bilbaori ere, tesi honen zuzenketan egindako lanagatik eta baita Andres Aguayori ere, programazioarekin eskainitako laguntzagatik.

Nola ez, eskerrik asko batez ere urte hauetan nirekin laborategian egon zareten guztioi: Gartzen, Maider, Maite, Aitziber, Jon, Itsaso, Laura eta Maria. Eskerrik asko Gartzeni, lehenengo egunetik eskainitako laguntzagatik, irakatsitako guztiagatik eta emandako aholkuengatik. Maiteri, beti laguntzeko prest egotearren eta urte hauetan zehar bai laborategian eta bai laborategitik kanpo pasa ditugun momentu guztiengatik. Joni, behar izan dudan bakoitzean laguntzearren eta tesiaren amaieran emandako animo guztiengatik. Itsasori, laborategian beti nire alboan egotearren, jaso dudan laguntza ikaragarriagatik, baina batez ere, pasa ditugun momentu on guztiengatik. Eta azkenik, Laurari eta Mariari, azken aldi honetan emandako laguntza eta animo guztiengatik. Eskerrik asko benetan guztioi, plazer handi bat da zuekin lan egiteko aukera izatea. Era berean, eskerrik asko beste laborategietan zaudeten guztioi, behar izan dudan bakoitzean zuen laguntza ematearren. Momentu honetan eskerrak eman nahi nizkieke unibertsitatean egindako lagunei ere, eta bereziki, eskerrik asko Miryam eta Maitaneri, azken urte hauetan pasa ditugun momentu on guztiengatik.

Eskerrik asko Angeliki Lemonidouri, hiru hilabeteetan zehar bere laborategietan lan egiteko aukera emateagatik. Eta eskerrak baita ere, Sofia, Vicky eta Villyri, eta bereziki, Dimitris eta Andyri, hilabete horietan zehar laborategian eta batez ere, laborategitik kanpo nire alboan egoteagatik.

Lanetik aparte, eskerrak eman nahi nizkieke Eluska, Izaskun eta Gorka nire lagunei, karreran zehar Bilbon bizitako esperientzia guztiengatik eta urte horietan bizitakoa ahaztezin bihurtzeagatik. Eskerrik asko nire kuadrilla osoari, zuen alboan pasa ditudan momentu on guztiengatik eta behar izan dudanean nire alboan egoteagatik. Eta batez ere, eskerrik asko hiri Kaiet, hire azken urteetan erakutsitako guztiagatik eta nola ez, lagun paregabea izateagatik.

Bukatzeko, nire eskerrik handienak eman nahi dizkiet nire familiari eta etxeko guztiei. Eta batez ere, eskerrik asko ama eta atte, beti nire alboan egoteagatik eta nigan konfiatzeagatik, eta nola ez, Maiteri, arrebarik onena izatearren.

Eskerrik asko benetan guztioi!

Azkoitian, 2017ko martxoan

INDEX

OBJECTIVES **3**

1. INTRODUCTION **7**

1.1. SUSTAINABLE HYDROGEN PRODUCTION FROM BIOMASS **7**

1.1.1. Biomass as an alternative raw material **8**

1.1.2. Thermochemical strategies **9**

1.2. BIOMASS GASIFICATION **11**

1.2.1. Reactor configurations **17**

1.2.2. Effect of biomass characteristics **19**

1.2.3. Operating variables **20**

1.2.3.1. Temperature **20**

1.2.3.2. Steam/biomass ratio **22**

1.2.4. Catalysts **23**

1.2.5. Supercritical water gasification **26**

1.3. HYDROGEN FROM BIO-OIL **28**

1.3.1. Bio-oil production from biomass fast pyrolysis **28**

1.3.1.1. Bio-oil **28**

Composition and properties **28**

Stability **30**

1.3.1.2. Reactor configurations **31**

Bubbling fluidized bed reactor **31**

Circulating fluidized bed reactor **32**

Ablative reactor **32**

Vacuum pyrolysis **33**

Mechanical reactor **34**

Conical spouted bed reactor **34**

1.3.1.3. Bio-oil valorisation routes **38**

Previous stabilization of the bio-oil **38**

Direct use as a fuel **38**

Extraction of compounds **39**

Catalytic transformation **39**

1.3.2. Bio-oil reforming **41**

1.3.2.1. Reactor configurations **49**

1.3.2.2. Operating variables **51**

Temperature **52**

Space time **53**

Steam/C ratio **54**

1.3.2.3. Catalysts **55**

1.3.2.4. Bio-oil steam gasification **56**

1.4. PYROLYSIS AND IN-LINE REFORMING OF BIOMASS **58**

1.4.1. Reactor configurations **62**

1.4.2. Catalysts **64**

1.4.3. Plastic co-feeding **65**

2. EXPERIMENTAL 71

2.1. MATERIALS 71

2.1.1. Feeds 71

2.1.1.1. Biomass **71**

2.1.1.2. High density polyethylene (HDPE) **72**

2.1.2. Catalyst 72

2.2. PILOT PLANT 74

2.2.1. Solid feeding system 75

2.2.2. Gas feeding system 76

2.2.3. Water feeding system 77

2.2.4. Reaction system 77

2.2.4.1. Pyrolysis reactor **77**

2.2.4.2. Catalytic reforming reactor **79**

2.2.5. Product separation system 80

2.2.6. Control system 81

2.3. OPERATING CONDITIONS 82

2.3.1. Pyrolysis step 82

2.3.2. Catalytic reforming step 82

2.4. CATALYST AND PRODUCT ANALYSIS 85

2.4.1. Volatiles and permanent gases 85

2.4.1.1. Gas chromatography **85**

2.4.1.2. Gas micro-chromatography **91**

2.4.2. Fresh catalyst 93

2.4.2.1. Physical properties **93**

2.4.2.2. Reducibility and nature of metallic species **95**

2.4.3. Deactivated catalyst **96**

2.4.3.1. Metallic properties **96**

X-ray diffraction (XRD) **96**

2.4.3.2. Coke nature and content **97**

Temperature programmed oxidation (TPO) **97**

Scanning electron microscopy (SEM) **98**

Transmission electron microscopy (TEM) **98**

3. PYROLYSIS-CATALYTIC STEAM REFORMING OF BIOMASS AND BIOMASS/PLASTIC MIXTURES 103

3.1. BACKROUND OF BIOMASS PYROLYSIS AND IN-LINE REFORMING STRATEGY **103**

3.1.1. Pyrolysis temperature **104**

3.1.2. Reforming temperature **105**

3.1.3. Space time **107**

3.1.4. Steam/C ratio **107**

3.2. FIRST STEP: PYROLYSIS USING STEAM AS FLUIDIZING AGENT **108**

3.2.1. Pyrolysis of biomass **109**

3.2.1.1. Product yields **109**

3.2.1.2. Characterization of the bio-oil **112**

3.2.2. Pyrolysis of HDPE **113**

3.2.2.1. Product yields **113**

3.2.2.2. Characterization of waxes **115**

3.3. SECOND STEP: CATALYTIC STEAM REFORMING OF THE VOLATILES FROM PYROLYSIS 116

3.3.1. Reaction indices 118

3.3.2. Parametric study of biomass valorisation 120

3.3.2.1. Effect of temperature **121**

3.3.2.2. Effect of space time **125**

3.3.2.3. Effect of steam/biomass ratio **128**

3.3.2.4. Comparison with literature results **131**

3.3.3. Valorisation of biomass and HDPE mixtures 135

3.3.3.1. Initial conversion **136**

3.3.3.2. Initial product yields and concentrations **139**

3.3.3.3. Comparison of pyrolysis-reforming and gasification processes **141**

4. CAUSE AND EFFECT OF CATALYST DEACTIVATION 147

4.1. EVOLUTION OF REACTION INDICES WITH TIME ON STREAM 149

4.1.1. Valorisation of biomass 149

4.1.1.1. Effect of temperature **149**

4.1.1.2. Effect of space time **154**

4.1.1.3. Effect of steam/biomass ratio **157**

4.1.1.4. Comparison with literature results **161**

4.1.2. Valorisation of biomass and HDPE mixtures 161

4.1.2.1. Conversion **162**

4.1.2.2. Product yields and concentrations **163**

4.2. DEACTIVATED CATALYST CHARACTERIZATION 168

4.2.1. Effect of operating variables on coke deposition 170

4.2.1.1. Temperature **170**

4.2.1.2. Space time **173**

4.2.1.3. Steam/biomass ratio **175**

4.2.2. Effect of time on stream on catalyst deactivation 177

4.2.2.1. Deterioration of catalyst properties **177**

Physical properties **177**

Metallic properties **179**

4.2.2.2. Evolution of coke **179**

Temperature programmed oxidation (TPO) **179**

Scanning electron microscopy (SEM) **182**

Transmission electron microscopy (TEM) **183**

4.2.2.3. Coke formation mechanism **184**

4.2.3. Coke formation for biomass and HDPE valorisation 186

4.2.3.1. Temperature programmed oxidation (TPO) **186**

4.2.3.2. Transmission electron microscopy (TEM) **188**

4.3. REGENERATION OF THE CATALYST 191

4.3.1. Evolution of reaction indices with time on stream 192

4.3.2. Deactivated catalyst characterization 194

4.3.3. Regenerated catalyst characterization 196

5. KINETIC MODELLING OF STEAM REFORMING IN THE PYROLYSIS-REFORMING OF BIOMASS 201

5.1. KINETIC MODELLING AT ZERO TIME ON STREAM 202

5.1.1. Reaction rate equations and mass balance 202

5.1.2. Calculation of the kinetic parameters 204

5.1.3. Calculation program 205

5.1.4. Experimental results and reaction scheme 206

5.1.5. Proposed kinetic model 210

5.2. KINETIC MODELLING OF THE DEACTIVATION 214

5.2.1. Methodology 214

5.2.1.1. Consideration of deactivation in kinetic equations **214**

5.2.1.2. Calculation of the kinetic parameters **215**

5.2.2. Experimental results 215

5.2.3. Proposed kinetic model 216

6. SUMMARY 221

7. CONCLUSIONS 227

8. NOMENCLATURE 235

9. BIBLIOGRAPHY 243

10. DISSEMINATION OF RESULTS 283

10.1. PUBLICATIONS DERIVED FROM THE THESIS 283

10.2. OTHER PUBLICATIONS 284

OBJECTIVES

OBJECTIVES

This doctoral thesis is part of a broader line of research into the development of thermal and catalytic processes for the recovery of biomass and plastic wastes to obtain liquid fuels, raw materials (olefins, aromatics) and H_2. This thesis is designed to advance previous studies on the gasification of biomass and plastics (with and without catalyst), the gasification-reforming of HDPE (Erkiaga, 2014), and the pyrolysis-reforming of different plastics (Barbarias, 2015), with its overriding objective being the proposal of a new technology with two in-line reactors, i.e., a conical spouted bed reactor for biomass fast pyrolysis and a catalytic fluidized bed for the reforming step.

In order to fulfil the main objective, the following specific goals have been approached:

- The setting-up of an experimental laboratory unit with two in-line reactors (conical spouted bed reactor and fluidized bed reactor) for valorising biomass in a continuous regime, with the reforming products (H_2, CO_2, CO, H_2O) and by-products (CH_4, C_2-C_4 hydrocarbons and non-reacted bio-oil) being analyzed in-line by using chromatographic equipment. The technology previously developed in the research group using a conical spouted bed reactor and a fluidized bed reactor for plastic valorisation (Barbarias, 2015) has proven to be suitable, given that it avoids the operational problems due to the blocking of the fixed bed by coke deposition, as reported by Erkiaga (2014) using conical spouted bed-fixed bed technology.

- The assessment of the capability of the conical spouted bed reactor for the pyrolysis of biomass using steam as an inert fluidizing agent. The knowledge previously acquired in the steam pyrolysis of HDPE will be extended to biomass wastes. Moreover, the inert nature of steam at relatively low pyrolysis temperatures (500 ºC) will be verified, as this aspect is of particular interest because of the simplicity and economy of the process.

- The assessment of a commercial catalyst's capacity for reforming the volatiles derived from the pyrolysis of biomass and biomass/plastic mixtures. The use of a fluidized bed reactor presumably allows operating for a longer period of time, which improves the quality of the reaction indices and concentrations of the products in the reaction medium. The results obtained for biomass and

biomass/HDPE mixtures will allow evaluating the effect different feeds have on the reforming products.

- The effect operating conditions (temperature, space time and steam/feeding ratio) have on reaction indices and product composition, comparing the results obtained with those reported in the literature for biomass gasification, bio-oil reforming, and biomass pyrolysis-reforming. Moreover, the effect the HDPE/biomass mass ratio in the pyrolysis-reforming process has on reaction indices and product composition will be studied.

- The identification of the role of coke in catalyst deactivation, determining the nature and evolution of its composition over time, as well as the effect the nature of the coke has on its deactivating capacity. Likewise, coke precursor compounds will be identified in order to establish the deactivation kinetic equation, which is dependent on coke precursor concentration. Moreover, the effect different feeds have on catalyst deactivation will be studied.

- The regeneration of the catalyst by coke combustion with air in order to ascertain its stability for operating in successive reforming/regeneration cycles, analyzing the main reaction indices and product concentrations. Moreover, the catalyst will be characterized to explain the results previously obtained.

- The establishment of a kinetic model corresponding to zero time on stream, based on a scheme considering the reactions involved in the reforming step and calculating the kinetic parameters by fitting the experimental concentrations of the main products (H_2, CO_2, CO, H_2O) and by-products (CH_4, C_2-C_4 hydrocarbons and non-reacted bio-oil) in a wide range of operating conditions (temperature and space time).

- The integration of the deactivation kinetic equation in the kinetic model in order to obtain a full model for simulating the process, also in a wide range of operating conditions (temperature, space time and time on stream).

1

INTRODUCTION

1. INTRODUCTION

In this section, the sustainable H_2 production from biomass will be analyzed (Section 1.1), with especial emphasis on the thermochemical routes studied in the literature: gasification of biomass (Section 1.2) and bio-oil reforming (Section 1.3). Moreover, the pyrolysis-reforming of biomass will be presented as an alternative route to produce H_2 in a two-step process (Section 1.4) and the main advantages compared to the other routes will be discussed.

1.1. SUSTAINABLE HYDROGEN PRODUCTION FROM BIOMASS

H_2 world consumption has been steadily increasing during last years, reaching a value in the 400-500 billion Nm^3 range, representing a market of about \$60 billion. The main applications are related to ammonia production (49 %), oil refining (37 %), methanol production (8 %), and other uses such as food, electronic or metal industries (6 %) (Kirtay, 2011) (Figure 1.1). Furthermore, H_2 market is expected to increase in the near future in a 5-10 % per year, basically due to its consumption in refineries for treating heavy oil fractions and because of the projected demand in the transportation sector or as energetic vector (Levin and Chahine, 2010).

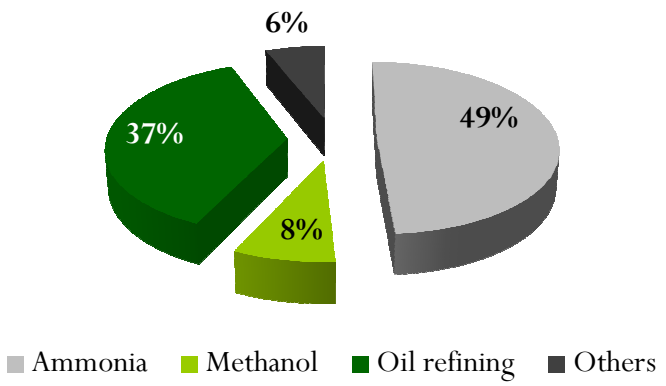

Figure 1.1. Global consumption of hydrogen.

The 96 % of the current H_2 production technologies are predominantly based on non-renewable sources (Serrano-Ruiz and Dumesic, 2011; Fermoso et al., 2012), with the most used processes being natural gas (48 %) and oil derivate (30 %) reforming, followed by coal gasification (18 %). Only the 4 % of the H_2 is obtained

by means of water electrolysis (Kothari et al., 2008) (Figure 1.2). This distribution reveals that the current generation of H_2 is associated with the consumption of fossil fuels and the emission of CO_2 in its production processes (mainly by steam reforming). In addition, H_2 is mainly consumed in the petrochemical industry for the production of automotive fuels, which in turn are CO_2 generators.

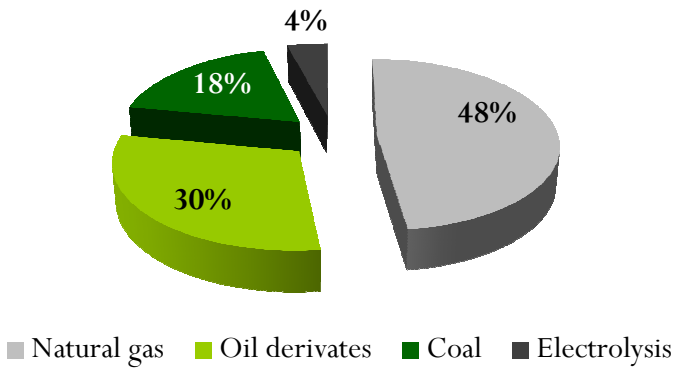

Figure 1.2. Current source of hydrogen.

1.1.1. Biomass as an alternative raw material

The urgent need to reduce the current energetic dependence on fossil fuels has promoted a large number of studies that focus on the development of existing and new processes that use biomass based materials as feedstock. The term biomass includes different organic materials and those of recent origin (non-geological), as are agro-forestry materials (agricultural, forestry and timber industry wastes), and crops and their derivatives. Wastes from food and paper industry (such as, lignin and black liquors) and organic components of municipal wastes are also considered biomass.

Nature produces 170 billion tons of biomass per year, although between 3 and 4 % is only used. Moreover, taking into account that 75 % of the biomass corresponds to carbohydrates, biomass is of especial relevance for its valorisation as raw material for obtaining fuels (bio-fuels) or for the production of chemical products, such as H_2 ("green chemistry", alternative to the one developed from petroleum) (Huber et al., 2006; Nigam and Singh, 2011).

Moreover, biomass derived fuels and chemicals can play a major role in reducing CO_2 emissions as well as become a strategic source in order to guarantee energetic

competitiveness and sustainability (Sanna, 2014). However, the establishment of a sustainable energy system should be based on biomass exploitation policies that take into account land usage in order to avoid competition with human and animal food and soil exhaustion (Popp et al., 2014). Accordingly, lignocellulosic biomass wastes and crops are regarded as the most suitable alternative feedstocks (Somerville et al., 2010; Baliban et al., 2013).

1.1.2. Thermochemical strategies

Lignocellulosic biomass can be treated using several thermochemical or biochemical processes in order to produce energy, bio-fuels and bio-chemicals (Melero et al., 2012). Thermochemical processes, such as gasification and pyrolysis, are characterized by their scalability to industrial units, where the syngas and bio-oil produced as intermediate products can be subsequently converted into valuable fuels and chemicals (Parajuli et al., 2015). These processes have the advantage of being similar to the ones already implemented in oil refineries, although need further development in order to be cost effective compared to fossil fuels (Balat and Kirtay, 2010). Figure 1.3 displays the main processes involved in a lignocellulosic thermochemical bio-refinery for the production of valuable products such as automotive fuels, light olefins and H_2.

Although each biomass conversion method has its own advantages and disadvantages, it has been reported that the H_2 production cost for gasification and pyrolysis is similar, around \$1.2-2.4/kg (slightly higher for the former), which is actually between two and three times higher than the cost of CH_4 steam reforming (Parthasarathy and Narayanan, 2014). Therefore, the choice of the most adequate one needs a thorough assessment of the economic aspects in the area where it has to be implemented, as well as the availability of biomass resources, and the existence of large catalytic conversion units that can treat the intermediate products. These aspects allow making the choice between centralized processes, in which the final product is produced at the same unit where the biomass is primarily converted, or decentralized processes, where the intermediate product (such as the bio-oil derived from flash pyrolysis) can be easily transported to catalytic conversion units.

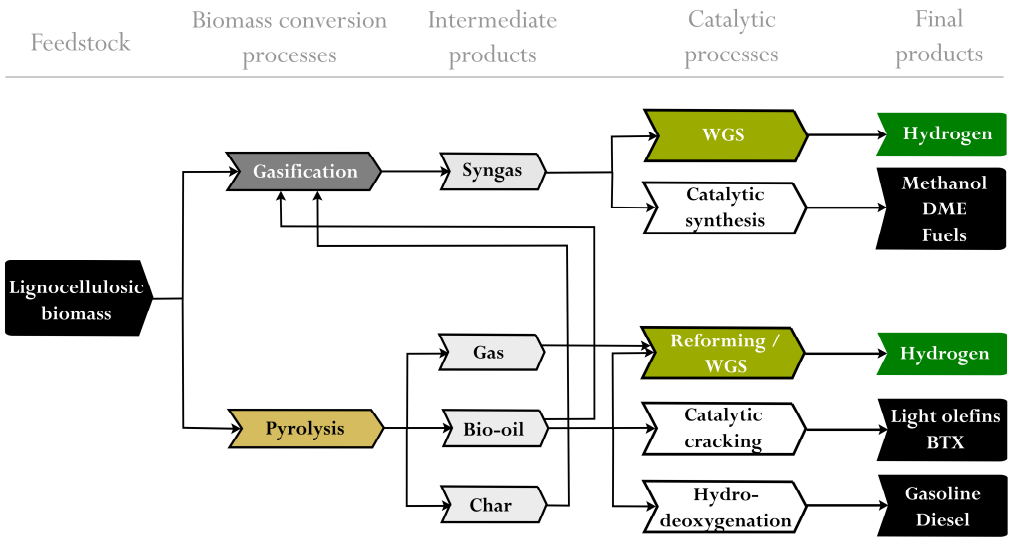

Figure 1.3. Schematic representation of the main processes involved in a lignocellulosic thermochemical bio-refinery.

The mostly studied and developed technologies for H_2 production are steam gasification (Erkiaga et al., 2013a; Ogi et al., 2013; Di Carlo et al., 2015) and the reforming of the bio-oil produced in biomass flash pyrolysis (Remiro et al., 2013a; Seyedeyn-Azad et al., 2014; Remón et al., 2015; Xie et al., 2016); however, the biomass flash pyrolysis and in-line reforming of the volatiles has recently gained attention, with several studies published over the last years (Xiao et al., 2013; Ma et al., 2014; Chen et al., 2016). In this scenario, this paper aims at reviewing the pyrolysis and in-line reforming strategy and comparing this technology with the main thermochemical biomass conversion processes for H_2 production.

1.2. BIOMASS GASIFICATION

Biomass gasification has been widely studied during last decades, which is due to the fact the gaseous product can be directly used as fuel or as intermediate product for the large scale production of fuels and chemicals (Zhang, 2010; Bulushev and Ross, 2011; Heidenreich and Foscolo, 2015; Mahinpey and Gomez, 2016; Sikarwar et al., 2016). The process characteristics entail establishing gasification plants in the regions where biomass is available because the costs for the transportation of the raw material or the formed gaseous products would be excessive (Miao et al., 2012). Figure 1.4 shows a schematic representation of the steam gasification process.

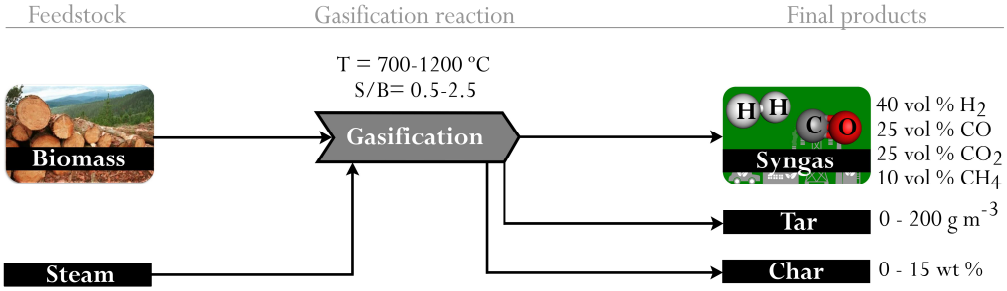

Figure 1.4. Schematic representation of the biomass steam gasification process for hydrogen production.

Biomass gasification typically takes places at temperatures around 700 and 1200 °C, using air, oxygen, steam or their mixtures as gasifying agent, which leads to a gaseous product mainly formed by H_2, CO, CO_2, CH_4 and other hydrocarbons. The use of steam enhances H_2 formation and produces a high heating value gas. Although the highly endothermic nature of steam gasification increases energy costs compared to air gasification, it avoids the need for a costly oxygen separation process (Parthasarathy and Narayanan, 2014).

The main steps involved in biomass steam gasification are drying, pyrolysis, heterogeneous char gasification and homogeneous reactions undergone by pyrolysis volatiles, i.e., reforming, cracking and Water Gas Shift (WGS) reactions. These gasification steps have been summarized in Figure 1.5 and the reactions involved are shown in eqs. (1.1)-(1.8) in Table 1.1. The use of an in-situ catalyst (primary) or in-line catalyst (secondary) favours the development of the reactions described in eqs. (1.4)-(1.8).

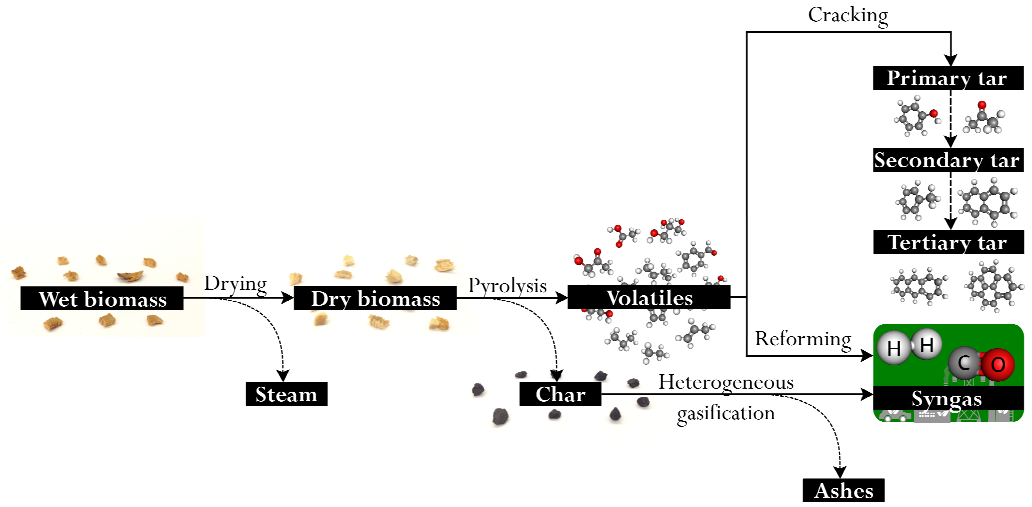

Figure 1.5. Biomass steam gasification reactions and stages.

Table 1.1. Reaction stages in biomass steam gasification.

Biomass pyrolysis:	$\text{Biomass} \rightarrow \text{gas}(CO, CO_2, CH_4, H_2 \ldots) + C_xH_yO_z + \text{char}$	(1.1)
Char steam gasification:	$C + H_2O \rightarrow CO + H_2 \quad \Delta H = 131.3 \text{ kJ mol}^{-1}$	(1.2)
Boudouard reaction:	$C + CO_2 \leftrightarrow 2CO \quad \Delta H = 162.4 \text{ kJ mol}^{-1}$	(1.3)
Tar cracking:	$C_nH_mO_k \rightarrow C_xH_yO_z + C_aH_b + CH_4 + CO + CO_2 + C$	(1.4)
Tar reforming:	$C_nH_mO_k + (n-k)H_2O \rightarrow nCO + \left(n + \frac{m}{2} - k\right)H_2$	(1.5)
Water gas shift (WGS):	$CO + H_2O \leftrightarrow H_2 + CO_2 \quad \Delta H = -41.2 \text{ kJ mol}^{-1}$	(1.6)

Table 1.1. Continued.

Methane steam reforming:	$CH_4 + H_2O \leftrightarrow CO + 3H_2 \quad \Delta H = 206.3 \text{ kJ mol}^{-1}$	(1.7)
Hydrocarbons steam reforming:	$C_nH_m + nH_2O \rightarrow nCO + \left(n + \frac{m}{2}\right)H_2$	(1.8)

In the drying step, the evaporation of the moisture contained in the biomass takes place, which is usually a fast step and takes place at low temperatures, with its influence on the overall gasification process being limited. In the pyrolysis step, biomass is thermally degraded to yield gases, condensable products and char (eq. (1.1)). The liquid product or primary tar formed in biomass pyrolysis is a complex mixture of oxygenates made up of alcohols, furans, ketones, saccharides, acids, phenols and so on (Mohan et al., 2006; Di Blasi, 2008; Kan et al., 2016). However, these compounds are in general of marked unstable nature, and under gasification conditions are rapidly cracked or reformed (eqs. (1.4) and (1.5)), or evolve towards more stable aromatic structures, such as secondary and tertiary tars (Devi et al., 2005; Font Palma, 2013). The tar contained in the syngas is a serious problem for its valorisation, given that it is polymerized or condensed below 300 ºC, and so may cause fouling, corrosion and blocking of pipes, heat exchangers and particle filters (Erkiaga et al., 2013a). Therefore, the improvement of tar cracking performance is one of the greatest challenges in the gasifier design, with the increase in residence time being an objective usually pursued. However, the total elimination of most stable tertiary tars requires temperatures of around 1250 ºC and residence times above 0.5 (Font Palma, 2013).

The presence of steam in the reaction environment promotes CH_4 (eq.(1.7)) and light hydrocarbons (eq. (1.8)) steam reforming. In addition, it also favours the displacement of WGS reaction (eq. (1.6)), which enhances H_2 production.

The char formed in the pyrolysis step is converted by steam gasification (eq. (1.2)) and Boudouard (eq. (1.3)) reactions. However, the rate of both reactions is low, even at typical gasification temperatures. This is especially true for CO_2 gasification, which is between 2 and 5 times slower that steam gasification (Di Blasi, 2009). Thus, char gasification represents the limiting step in biomass gasification and an adequate

reactor design requires a suitable residence time in order to attain high char conversion efficiency (Ollero et al., 2002; Ahmed and Gupta, 2011; Lopez et al., 2016).

Therefore, biomass steam gasification products are as follows: a gaseous fraction typically composed of 40 vol % of H_2, 25 vol % of CO, 25 vol % of CO_2 and 10 vol % of CH_4; a heavier fraction (tar), which consists of a complex mixture of aromatic hydrocarbons; and a solid fraction derived from the biomass that has not been totally gasified. The yields and properties of these products are influenced by a number of factors, with the most important ones being reactor configuration (which determines the contact mode, and therefore mass and heat transfer rates), biomass initial characteristics, operating conditions (such as temperature and steam to biomass ratio), and the use of catalysts (Pereira et al., 2012; Parthasarathy and Narayanan, 2014; Sikarwar et al., 2016). Table 1.2 shows a summary of several biomass steam gasification research papers, in which the effect of the aforementioned variables is studied. For the sake of clarity, studies using only steam as gasifying agent have been analyzed. The discussion of the results reported is detailed below.

Table 1.2. Studies involving different strategies, feeds, catalysts and operating conditions, and main results obtained (maximum H_2 production) reported in the literature for biomass steam gasification.

Reactor configuration	Biomass	Operating conditions	Catalyst	H_2 production (wt %)[a]	Gas yield ($Nm^3/kg_{biomass}$)	Tar content (g/Nm^3)	Reference
Updraft fixed bed	Pallets wood chips	T= 750 °C S/B= 1.4-2.7	None	6.4	1.3	60	Umeki et al., 2010
Fixed bed	Pine sawdust	T= 600-900 °C S/B = 0-2.8	*Primary:* dolomite	11.2	2.53	n.d.	Luo et al., 2009
Fixed bed + fixed bed reformer	Sawdust	*Gasifier:* T= 800°C; S/B= 0.6 *Secondary reactor:* T= 750-850 °C	*Secondary:* nano-Ni–La–Fe/γ - Al_2O_3	12.1	2.4	0.08	Li et al., 2009a
Entrained flow	Empty fruit bunch	T= 900 °C S/B= 0.23-2.3	None	8.5	1.8	0.5	Ogi et al., 2013
Rotary kiln	Palm shells	T= 850 °C S/B= 0.6-1	None	3.7	0.8	1.2	Iovane et al., 2013
External circulating concurrent moving bed	Pine sawdust	T= 650-800 °C S/B= 0-1.2	*Primary*: calcined olivine	9.5	2	0.7	Wei et al., 2006
Conical spouted bed	Pinewood sawdust	T= 900 °C S/B= 1	*Primary:* olivine; γ-alumina	4.4	1.15	22.4	Erkiaga et al., 2013a
Circulating spout-fluid Bed	Rice straw	T= 860-900 °C S/B= 2	*Primary*: limestone; dolomite; synthetic 0 - 20 % CaO/Al_2O_3	5.5	1.25	2.55	Xie et al., 2010
Bubbling fluidized bed	Pinewood chips	T= 750-780 °C S/B= 0.53-1.1	None	6.9	1.4	38	Gil et al., 1999
Bubbling fluidized bed	Miscanthus X Giganteus	T= 815-880 °C S/B= 1.1	*Primary:* Olivine	4.9	1.2	-	Michel et al., 2011b

Table 1.2. Continued.

Reactor configuration	Biomass	Operating conditions	Catalyst	H_2 production (wt %)[a]	Gas yield (Nm^3/ $kg_{biomass}$)	Tar content (g/Nm^3)	Reference
Bubbling fluidized bed + catalytic filter	Almonds shells	*Gasifier:* T= 808-813 °C; S/B= 1.03-1.28 *Filter:* T= 740 °C	*Primary:* olivine *Secondary:* Al_2O_3 filter; NiO (47 wt %)/MgO-Al_2O_3 filter	14.5	2.9	0.15	Rapagnà et al., 2012
Bubbling fluidized bed + fixed bed reformer	Almond shells	*Gasifier:* T= 770 °C; S/B= 1 *Secondary reactor:* T= 665-830 °C	*Primary:* calcined dolomite *Secondary:* calcined dolomite; Ni catalyst	11.0	1.98	0.2	Rapagnà et al., 1998
Bubbling fluidized bed + fixed bed reformer	Hazelnut shells	*Gasifier:* T= 850 °C; S/B= 0.7 *Secondary reactor:* T= 700-800 °C	*Primary:* olivine *Secondary:* Ni/$Ca_{12}Al_{14}O_{33}$	55 vol %[b]	-	4.2	Di Carlo et al., 2015
Bubbling fluidized bed + tubular cracker + bubbling fluidized bed reformer	White oak	*Gasifier:* T= 700 °C; S/B= 1 *Thermal tubular cracker:* T= 850 °C *Secondary reactor:* T= 900 °C	*Primary:* olivine *Secondary:* 6.6 % NiO/ 3.4 % MgO/ 4.0 % K_2O/ Al_2O_3	53.7 vol %[b]		n.d.	Yung et al., 2010
Dual fluidized bed	Wood pellets	T= 750-850 °C S/B= 0.3-0.9	None	51 vol %[b]	-	10	Göransson et al., 2011a
Dual fluidized bed	Wood pellets	T= 770-850 °C S/B= 0.74-1.1	*Primary:* olivine	4.2	1.13	11	Koppatz et al., 2011
Dual fluidized bed + fixed bed reformer	Wood chips	*Gasifier:* T= 850-900 °C *Secondary reactor:* T= 850-900 °C	*Secondary:* NiO (% 16-40) / MgO/Al_2O_3 honeycomb	45 vol %[b]	-	0.02	Pfeifer and Hofbauer, 2008

[a] H_2 production defined as g_{H2}/ 100 $g_{biomass}$. [b] H_2 concentration in the gas (vol %). n.d. Not detected

1.2.1. Reactor configurations

Biomass gasification is an extensively studied process, with a relatively high technological development. Therefore, a wide range of reactor configurations have been used, such as fixed bed (updraft and downdraft), fluidized bed, entrained flow, rotary kiln or plasma reactors (Heidenreich and Foscolo, 2015; Mahinpey and Gomez, 2016; Molino et al., 2016; Sikarwar et al., 2016). The gasification process was firstly developed in downdraft reactors, which although involves a simple technology that leads to low tar contents in the gas, has serious drawbacks, such as low heat coefficient, non-uniform bed temperature and limited capacity for scale-up. The entrained flow reactor leads to a high biomass conversion and low tar content gas, but requires a very low particle size and high capital and maintenance costs. Regarding rotary kiln reactors, the main advantages are high biomass conversion and flexibility in terms of feed type and simple construction, but they also have limited process flexibility, high maintenance costs and lead to high dust and tar content gas. Plasma reactors can produce a syngas with limited polluting compounds as the biomass ash is vitrified in the process, but requires high capital investment and maintenance costs (Molino et al., 2016). Fluidized beds are preferable for large scale applications, due to their suitable characteristics for a high biomass conversion and low tar content in the gas, such as good contact between phases and temperature control and a high operational flexibility, although a pre-treatment of the biomass is required and bed fluidization gives way to dust and ash dragging (Alauddin et al., 2010; Kaushal and Tyagi, 2012; Molino et al., 2016). Figure 1.6 displays a schematic representation of the reactors used in biomass steam gasification, based on the studies reviewed in Table 1.2.

These observations are in agreement with the information compiled in Table 1.2, where it is shown that the vast majority of studies have been carried out in fluidized bed reactors, due to the aforementioned advantages. The assessment of the effect of reactor configuration on the results shown is not straightforward, due to different scale, biomass type, operating conditions and gas and tar analysis procedures used. However, analyzing the non-catalytic gasification experiments carried out in updraft fixed bed (Umeki et al., 2010), entrained flow (Hernández et al., 2012; Ogi et al., 2013), rotary kiln (Iovane et al., 2013), plasma (Shie et al., 2010), free fall (Wei et al., 2007), fluidized bed (Gil et al., 1999; Göransson et al., 2011a) and spouted bed (Erkiaga et al., 2014) reactors, and although all the reaction configurations lead to H_2 productions between 1.3 and 8.5 wt % (with the average value being 4.6 wt %), with tar concentrations in the 4-140 g/Nm^3 range, it can be concluded that fluidized bed reactors are suitable for the biomass steam gasification process because high H_2

productions (6.9 wt %), gas yields (around 1-1.4 $Nm^3/kg_{biomass}$), H_2 concentrations (> 50 vol %) and low tar ones (20-80 g/Nm^3) are obtained (Gil et al., 1999; Göransson et al., 2011a).

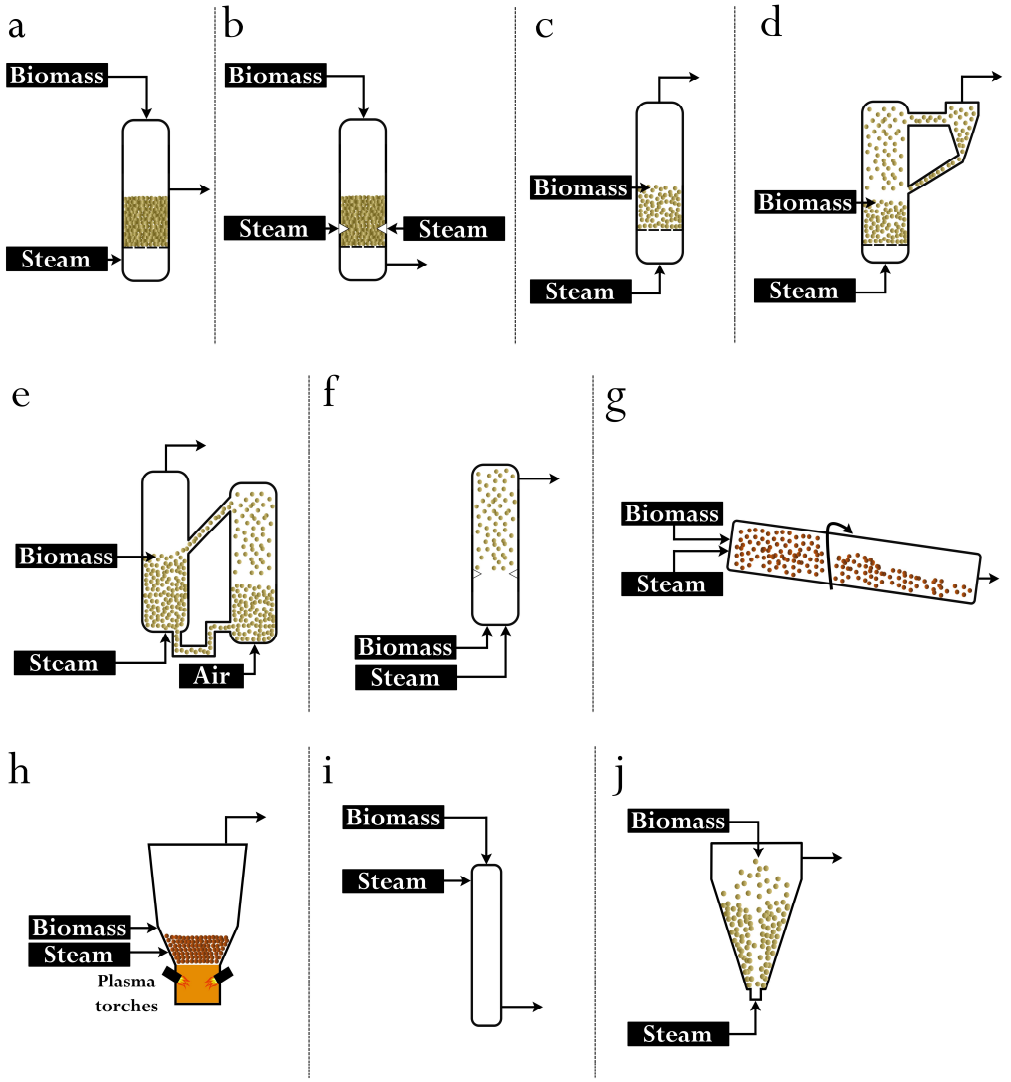

Figure 1.6. Reactor configurations for biomass steam gasification: a) updraft fixed bed; b) downdraft fixed bed; c) fluidized bed; d) circulating fluidized bed; e) dual fluidized bed; f) entrained flow; g) rotary kiln; h) plasma; i) free fall, and; j) spouted bed.

Furthermore, the scale up of this technology has been satisfactorily accomplished, solving energy requirements by means of the dual fluidized bed (DFB) configuration, which is a combination of two bubbling and/or circulating fluidized beds, with one of them acting as gasifier and the other as char combustor. The gasifier is blown with steam, obtaining a syngas with high H_2 content, whereas the char is burnt in the combustor in order to provide heat to the system (Pfeifer and Hofbauer, 2008; Göransson et al., 2011b; Koppatz et al., 2011; Wilk and Hofbauer, 2013a). However, it has been reported that the heat provided by char combustion may not be enough, and therefore additional fuel must be used in order to meet heat specifications (Corella et al., 2007). The vast majority of the current biomass steam gasification demonstration or commercial scale plants are based on this technology (Kaushal and Tyagi, 2012). Thus, among the DFB gasification technologies reviewed by Göransson et al. (2011b), the ones that must be remarked due to their capacity are the *SilvaGas*^{TM} plant in USA (40 MW_{th}) that consists of two circulating fluidized beds, the 15 MW_{th} *Blue Tower* plant in Germany, the *Güssing FICFB* plant in Austria (8 MW_{th}) and the *Charlmers GoBiGas* plant in Sweden (2 MW_{th}), the three based on a bubbling fluidized bed as gasifier and a circulating fluidized bed as combustor.

1.2.2. Effect of biomass characteristics

The main biomass characteristics affecting gasification performance are biomass type, moisture content and particle size (Parthasarathy and Narayanan, 2014). Regarding biomass type, special attention has to be paid to the ash content as, on the one hand, high ash content biomasses lead to high char yields and, on the other, ash leaves the gasifier in the form of micron size particulate matter, which has to be removed downstream by means of gas cleaning processes (Asadullah, 2014).

Concerning biomass moisture content, gasifiers can handle biomasses having moisture contents below 35 wt %, although most of them are designed for a 10-15 wt %. The main drawback of raw materials with high moisture contents lies in the loss of gasification efficiency due to the reduction of the operation temperature (Kaushal and Tyagi, 2012). Therefore, a drying pre-treatment process must be carried out for high moisture content biomasses, which increases the cost of the total process.

Furthermore, biomass particle size has a great influence on the gasification performance. Thus, smaller particles provide larger surface areas per unit mass, which increases heat and mass transfer, and therefore gasification rates, leading to

high gas yields with high H_2 concentrations and low tar contents (Kaushal and Tyagi, 2012; Parthasarathy and Narayanan, 2014). However, biomass particle size reduction below 1 mm increases exponentially grinding energy consumption (Kaushal and Tyagi, 2012). Therefore, it is essential to develop a versatile gasification technology that may handle large biomass particles without compromising heat and mass transfer phenomena.

1.2.3. Operating variables

Gasifier temperature and steam/biomass ratio (S/B) are the parameters that need to be carefully selected and controlled for improving gasification performance (Kaushal and Tyagi, 2012; Parthasarathy and Narayanan, 2014). Temperature has a great impact on gas and H_2 yields, due to the endothermicity of the reactions involved (pyrolysis (eq. (1.1)), steam reforming (eqs. (1.5), (1.7)-(1.8)), Boudouard (eq. (1.3)) and char gasification (eq. (1.2)) reactions). Furthermore, an increase in temperature hinders WGS reaction (eq. (1.6)) equilibrium. Overall, at higher temperatures a gaseous product with higher H_2 and lower CO and CH_4 concentrations is obtained, as well as a reduced tar content and char yield.

1.2.3.1. Temperature

Most of the authors that studied the influence of temperature on product yields and compositions agreed that a more severe operation led to an improved gasification performance, minimizing the tar content, as shown in Figure 1.7. Thus, Erkiaga et al. (2014) operating in a conical spouted bed reactor, concluded that gas yield and H_2 concentration increased from 0.73 $Nm^3/kg_{biomass}$ and 28 vol % at 800 ºC to 0.96 and 38 at 900 ºC, respectively (which corresponds to an increase in the H_2 production from 1.8 to 3.3 wt %). Furthermore, char yield decreased from 9 to 4.5 wt % and tar concentration from 364 to 142 g/Nm^3. Göransson et al. (2011a) studied the influence of operating conditions in a 150 KW_{th} capacity dual fluidized bed reactor, observing that an increase in gasification temperature led to a reduction in tar content, from 30 g/Nm^3 at 750 ºC to 10 g/Nm^3 at 850 ºC. However, they also observed a reduction in the H_2 composition in the gas with temperature, from 62 to 51 vol %.

Similarly, the utilization of a catalyst in the gasification bed resulted in an analogous effect of temperature on gasification operation. Xie et al. (2010) operating in a circulating spout-fluid bed with dolomite observed a tar reduction from 4.5 g/Nm^3

at 860 °C to 2.7 at 900 °C. Olivine also leads to a similar trend with temperature, with the best results being observed at the highest temperatures studied. Thus, Wei et al. (2006), operating in external circulating concurrent moving bed with olivine as primary catalyst, obtained the optimum gasification results at 800 °C, with a H_2 production of 9.5 wt %, which is equivalent to a gas yield of 2 $Nm^3/kg_{biomass}$ with a H_2 concentration of 53.3 vol %, and tar yield of 0.7 g/Nm^3. Rapagná et al. (2000) and Michel et al. (2011a), gasifying almond shells and miscanthus in a fluidized bed, attained the maximum gas yields of 1.9 and 1.2 $Nm^3/kg_{biomass}$ and H_2 productions of 9.4 and 4.9 wt %, at 820 and 880 °C, respectively. Tar contents were also found to be minimum at the highest temperature, with a value of 0.6 g/Nm^3 for the study with almond shells (Rapagnà et al., 2000). Therefore, gasification temperature will be limited by the economics of the process because higher temperatures lead to higher H_2 productions and a gas with lower tar content.

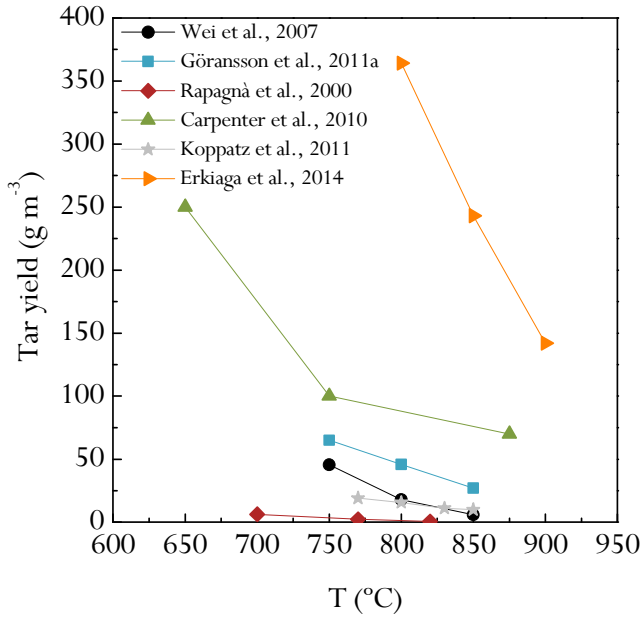

Figure 1.7. Effect of gasification temperature on tar yield (Rapagnà et al., 2000; Wei et al., 2007; Carpenter et al., 2010; Göransson et al., 2011a; Koppatz et al., 2011; Erkiaga et al., 2014).

1.2.3.2. Steam/biomass ratio

Steam/biomass ratio (S/B) also plays a crucial role in gas and H_2 yields. As the S/B is increased, the WGS reaction (eq. (1.6)) and those in the steam reforming (eqs. (1.5), (1.7)-(1.8)) are favoured, thus leading to a higher gaseous yield, i.e., H_2 and CO_2 formation is promoted and the one of CO and hydrocarbons is reduced. In addition, tar formation and char yield are hindered due to the enhancement of reforming and gasification reactions. However, the S/B ratio has to be optimized for each process because an excess of steam, on the one hand, does not entail an improvement in the quality of the product gas and, on the other hand, it considerably increases the energy consumption of the process (Kaushal and Tyagi, 2012). In fact, Kaushal and Tyagi (2012) suggested operating with S/B ratios between 0.6 and 0.85 to combine a suitable promotion of steam reforming reactions and high thermal efficiency of the process. Figure 1.8 shows some of the studies in which the effect of steam to biomass ratio on H_2 production has been studied.

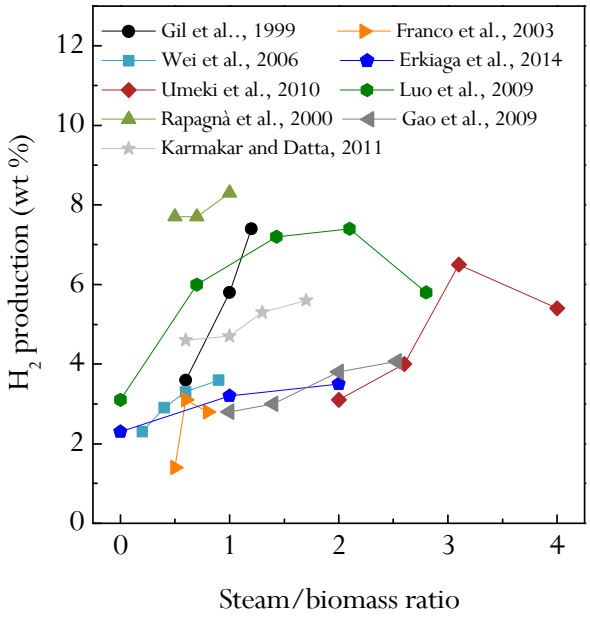

Figure 1.8. Effect of steam to biomass ratio on hydrogen production in gasification process (Gil et al., 1999; Rapagnà et al., 2000; Franco et al., 2003; Wei et al., 2006; Gao et al., 2009; Luo et al., 2009; Umeki et al., 2010; Karmakar and Datta, 2011; Erkiaga et al., 2014).

Ogi et al. (2013) observed that gasification performance was maximized for a S/B ratio of 0.96 in an entrained flow reactor, obtaining a H_2 production of 8.5 wt %, and gas yield of 1.8 $Nm^3/kg_{biomass}$ with a very low tar content of 0.5 g/Nm^3. However, Hernández et al. (2012), also in an entrained flow reactor, found that H_2 production attained the maximum value of 1.3 wt % at the maximum S/B studied (S/B ratio of 3.19). An asymptotic trend was observed by Erkiaga et al. (2014) in a conical spouted bed reactor, i.e., a further increase of the S/B ratio from 1 to 2 did not improve gasification performance, thus obtaining a maximum H_2 production and minimum tar content of 3.3 wt % and 140 g/Nm^3, respectively. In the studies where dolomite and olivine were used as in-bed catalyst, S/B ratio also had a positive effect on gasification performance. Thus, Luo et al. (2009), operating in a free fall reactor at 900 ºC, observed that even with the lowest S/B ratio of 0.73, tar was totally cracked and that the highest H_2 production was obtained with a S/B ratio of 2.1 (11.2 wt %).

1.2.4. Catalysts

The syngas that leaves the gasification reactor requires several complex and costly purification steps in order to meet specifications for the downstream catalytic conversion processes, which are designed for removing the particulate matter (micron size char and ash), the N, S and Cl containing gaseous compounds (such as NH_3, HCN, H_2S and HCl) and specially the tar components present in the gas (Devi et al., 2002; Anis and Zainal, 2011; Abdoulmoumine et al., 2015). Tar, which is a complex mixture of polycyclic aromatic compounds (larger molecules than benzene), leads to fouling of downstream equipment, and is therefore one of the major drawbacks in biomass gasification processes that has not been yet solved. Tar concentration must be reduced to less than 5 mg/Nm^3 for gas turbines, 1 mg/Nm^3 for methanol synthesis and 0.1 mg/Nm^3 for Fischer-Tropsch synthesis (Asadullah, 2014; Abdoulmoumine et al., 2015). Moreover, the nature of the tar formed in biomass gasification processes, specially its dew point, also determines the extent of its associated problems. Thus, lighter tars as monoaromatics are not condensable even at concentrations of 10 g m^{-3}, whereas polyaromatics of more than 4 rings condense at concentrations of only 1 mg m^{-3} (Anis and Zainal, 2011). Furthermore, it has been observed that steam gasification, in compassion to air gasification, leads to higher tar content in the product gas (Gil et al., 1999; Devi et al., 2002), although this tar is more suitable for being eliminated (Orío et al., 1997). Consequently, many strategies have been developed in order to obtain a tar free (or low tar content) syngas, and they can be classified into primary processes, which hinder tar formation

in the gasifier, or secondary processes, which imply a cleaning of the produced syngas. Figure 1.9 shows a scheme of both methods, which include physical cleaning, and thermal or catalytic treatments (Anis and Zainal, 2011).

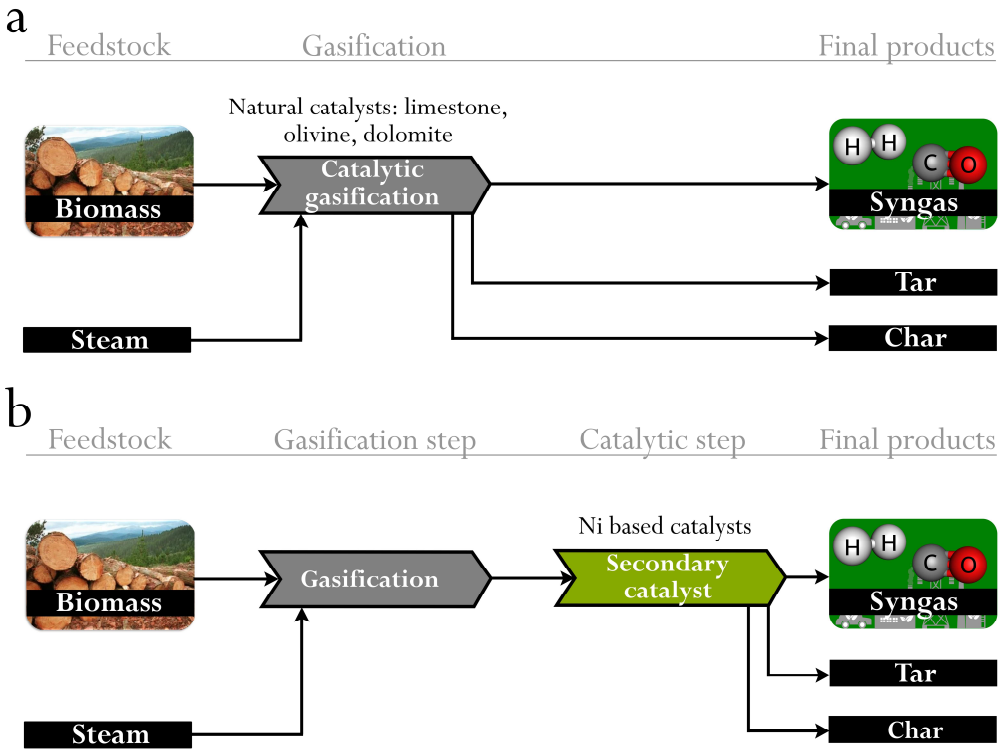

Figure 1.9. Primary (a) and secondary (b) tar reduction methods in biomass gasification.

Amongst the primary methods for tar elimination, the design of the gasifier is usually the first measure adopted. This is the case of fluidized bed gasifiers whose flexible design allows for several modifications aimed at improving tar cracking efficiency, which are as follows: increase in residence time in the freeboard region (Gil et al., 1999), location of the feeding (Wilk et al., 2013; Brachi et al., 2014) or secondary air injections in the case of air gasification (Narváez et al., 1996).

Catalytic gas cleaning methods for tar removal have the advantage of an additional increase in gas and H_2 yields, due to the enhancement of tar cracking (eq. (1.4)) and steam reforming (eqs. (1.5), (1.7)-(1.8)) reactions. The most widely used catalysts in steam gasification studies are natural minerals, such as dolomite or olivine, and Ni based catalyst (De Lasa et al., 2011; Shen and Yoshikawa, 2013; Guan et al., 2016).

The former have the advantage of their availability and low cost, whereas Ni based catalysts have a high activity for tar cracking and reforming (Chan and Tanksale, 2014). They can be used as primary catalyst, directly in the gasifier, or as secondary catalysts in downstream catalytic processes. Primary tar elimination methods have the advantage of significantly reducing process costs, but the effectiveness of the catalytic process is low due to the high deactivation by coke formation (De Lasa et al., 2011; Chan and Tanksale, 2014). Therefore, mineral based catalysts are usually employed as primary catalysts, whereas Ni based ones, which undergo significant deactivation, are mainly used in secondary reactors with a higher performance (Chan and Tanksale, 2014), although the inclusion of a second step leads to considerably higher capital cost, i.e., they are too costly for small or medium scale plants (Guan et al., 2016). Figure 1.10 shows the tar yields obtained with different catalysts by several authors.

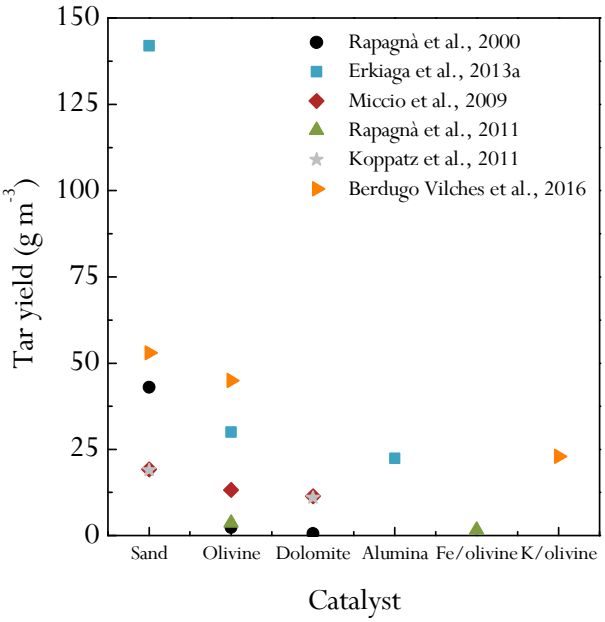

Figure 1.10. Effect of different catalyst on tar yield (Rapagnà et al., 2000; Miccio et al., 2009; Koppatz et al., 2011; Rapagnà et al., 2011; Erkiaga et al., 2013a; Berdugo Vilches et al., 2016).

1.2.5. Supercritical water gasification

Supercritical water gasification has been proposed as alternative to steam gasification for high moisture content biomass (typically > 30 wt %), such as food derivatives, algae or sewage sludge, as no drying pretreatment is required (Yakaboylu et al., 2015). The process takes place at temperatures higher than 374 ºC and pressures above 22.1 MPa, with H_2 production being enhanced at temperatures above 600 ºC (lower ones have been reported to increase CH_4 concentration). Under these conditions, supercritical water acts both as solvent and catalyst, thus leading to a very fast reaction, which produces high gas yields, with a low formation of tar and coke. Furthermore, the product gas is obtained at high pressure, which is beneficial for further applications (Guo et al., 2010a).

However, the process presents serious drawbacks for large scale feasibility. Pumping of feedstock is a technological challenge, as biomass needs to be converted into a pumpable slurry or solution, which limits the dry biomass content in the slurry to 20 wt %, depending on the biomass type. In addition, plugging by char, tar or alkaline catalysts may occur in long time runs and the severe operating conditions may lead to material corrosion problems (Calzavara et al., 2005). The high energy consumption of the process is one of the most important factors, as water has to be maintained at supercritical conditions. Therefore, it is essential to recover the heat of the products leaving the reactor in order to preheat the inlet water-biomass slurry. However, this process cannot be carried out directly in conventional heat exchangers as biomass is decomposed at the required temperature of 450 ºC, leading to blockage and fouling problems (Matsumura et al., 2005).

These drawbacks have hindered the scalability of the process, and therefore laboratory scale reactors have been used for biomass supercritical gasification studies, with most of the runs being carried out in batch reactors (Lu et al., 2006, 2012; Yanik et al., 2007, 2008; Osada et al., 2012; Ding et al., 2014; Jin et al., 2014; Elif and Nezihe, 2016; Safari et al., 2016) and, to a lesser extent, in continuous flow tubular (Antal Jr. et al., 2000; Güngören Madenoglu et al., 2011) or fluidized bed reactors (Lu et al., 2008). The largest supercritical water gasification facility implemented is the VERENA pilot plant from Karlsruhe Institute of Technology (100 kg/h), which has been designed for 700 °C, 35 MPa and a maximum solids content of 20 wt %, and includes a down-flow reactor and a biomass and water preheating step with the reactor outlet stream (Kruse, 2008; Yakaboylu et al., 2015).

In order to reduce the operating temperature and increase H_2 selectivity, several catalysts have been developed, which can be classified into alkali based (such as Na_2CO_3, K_2CO_3 or NaOH), transition metal based (Ni and Ru) and activated carbon catalysts. Although all of them have proven to be suitable for enhancing gasification and improving H_2 yield, alkali catalysts lead to corrosion and plugging problems, whereas transition metal and activated carbon based catalysts undergo a severe deactivation (Guo et al., 2010a; Azadi and Farnood, 2011).

1.3. HYDROGEN FROM BIO-OIL

1.3.1. Bio-oil production from biomass fast pyrolysis

Pyrolysis is the thermal decomposition in the absence of oxygen, and one of the most energy efficient and low cost processes for the production of liquid fuels from biomass (Balat et al., 2009; Anex et al., 2010; Wright et al., 2010). Its potential is based on the possibility of valorising all the products formed: gas, liquid (bio-oil) and solid. The char can be used as fuel, whereas the gas can be partially recirculated into the pyrolysis reactor (Bridgwater, 2012).

The main product of biomass fast pyrolysis is the bio-oil and its yield can be maximized at low pyrolysis temperatures (450-550 ºC), high heating rates (10^3-10^4 K s^{-1}) and low residence times of the volatiles (< 1 s), which are rapidly cooled when they leave the reactor, and char particles, which should be separated rapidly from the volatiles (Bridgwater et al., 1999; Huber et al., 2006). The typical yields obtained in biomass fast pyrolysis are as follows: 60-75 wt % of bio-oil, 15-25 wt % of char and 10-20 wt % of gas.

Although bio-oil composition depends on the type of biomass, it is not a limitation for considering pyrolysis as a process of broad interest, which is a relevant point for its implementation for self-sufficient energy generation in rural areas, especially in developing countries. Section 1.3.1 deals with the composition, properties and stability of the bio-oil (Section 1.3.1.1), the different pyrolysis reactors for its production and, especially, with the advantages of the conical spouted bed reactor (Section 1.3.1.2). Moreover, the most important bio-oil valorisation routes will be discussed (Section 1.3.1.3).

1.3.1.1. Bio-oil

Composition and properties

Bio-oil is a brown, polar and hydrophilic liquid obtained from biomass pyrolysis, which is constituted by depolymerization products and fragmentation of cellulose, hemicellulose and lignin contained in lignocellulosic biomass. It is a complex mixture of water and oxygenated compounds with different functional groups, in which more

than 300 compounds have been identified by GC/MS (acids, alcohols, aldehydes, esters, ketones, phenols, guaiacols, syringols, sugars, furans, alkenes, aromatics, nitrogenated and oxygenated compounds), with their molecular weight being in the 37-1000 g mol^{-1} range. The reactivity of these compounds gives to bio-oil its acid, corrosive and unstable nature.

The low pH of the bio-oil (pH ≈ 2-3) is due to the content of carboxylic acids, mainly formic acid and acetic acid. The presence of phenolic oligomers, coming from the lignin contained in the biomass and *aldol* type reactions promoted by acids, causes the polymerization of bio-oil compounds with time (ageing).

The water content in the bio-oil (in the 21-27 wt % range for wood and in the 39-51 wt % for agricultural herbaceous wastes) contributes to the high O content (around 35-40 wt %). Water comes from the free water contained in biomass, which plays an essential role when is explosively vaporized favouring heat transmission during the pyrolysis (Cai and Liu, 2007), and the water released from the decomposition of cellulose and hemicellulose.

Moreover, some char particles produced in the pyrolysis and the material used as inert for fluidization may be found in the bio-oil, which should be separated by means of cyclones or other devices. The ash content (waste remaining after combustion) in the bio-oil varies in the 0.004-0.30 wt % range (Gollakota et al., 2016). The *ASTM D 7544* norm recommends that the ash content in the bio-oil should not exceed 0.25 %, since higher contents can cause problems in pumps and injectors, and corrosion and deposition problems in combustion equipment due to the alkali metals contained in the ashes. The filtration of pyrolysis vapours is effective for reducing the ash content in the bio-oil below 0.01 % and that corresponding to metals below 10 ppm (Lu et al., 2009).

The viscosity of the bio-oil varies in the 10-100 cP range at 40 ºC, depending on the biomass used, pyrolysis conditions and water content (Mohan et al., 2006). Viscosity can be reduced by a moderate preheating (< 80 ºC) to ease bio-oil pumping and atomization. The thermal conductivity and specific heat of the bio-oil are 0.35-0.4 W m^{-1} K^{-1} and 2.5-3.5 kJ kg^{-1} K^{-1}, respectively, in the 20-60 ºC range, which is higher than that corresponding to gasoil. Moreover, it also has lower toxicity and its biodegradability rate is twice that corresponding to petroleum based fuels (Zhang et al., 2013).

Recently, a review has been published by Gollakota et al. (2016), in which a summary of bio-oil properties obtained with different biomass types has been shown (water content, viscosity, density, ultimate analysis and ashes). Moreover, these authors calculate the high heating value (HHV) and low heating value (LHV) of each bio-oil, based on ultimate analysis and using the correlations developed by Milne et al. (1989) (eq. (1.9)) and Oasmaa et al. (1997) (eq. (1.10)).

$$HHV = 0.3382\ (C) + 1.4428\ [(H) - 0.145\ (O)] \quad (1.9)$$

$$LHV = HHV - 0.2183\ (H) \quad (1.10)$$

Stability

The bio-oil can be considered a microemulsion, stabilized by H bonds and by the formation of nanomicelles and micromicelles, in which the continuous phase (aqueous solution of the products derived mainly from the decomposition of cellulose and hemicellulose) stabilizes the discontinuous one (composed mainly by macromolecules derived from lignin) (Fratini et al., 2006). The presence of acids favours the condensation-polymerization reactions of these phenolic oligomers and several reactive functional groups of the bio-oil, causing an increase in the viscosity and aging of the bio-oil during storage. Moreover, the water content in the bio-oil increases during its degradation process, reaching even the separation of two phases: aqueous phase and organic phase. Its volatility is also decreased due to the rupture of the microemulsion and the reactions via *aldol* condensation to form larger molecules (Hilten and Das, 2010), with temperature being the main variable in these reactions. Therefore, refrigeration is required during storage to avoid these degradation processes.

The addition of alcohols (mainly methanol and ethanol) has been proven to be effective for stabilizing the bio-oil during storage: a low alcohol addition (< 5 %) prevents aging reactions for few months, while higher amounts (≥ 10 %) delay it for at least one year, with viscosity increase being 20 times lower. This effect is as a consequence of: 1) physical dilution; 2) molecular dilution and changes in the microstructure of the emulsion, and; 3) reactions of the bio-oil compounds with the alcohol (esterification and acetylation), which limit further chain growth. These

reactions of the bio-oil with alcohols have a potential interest for producing commercial products (Radlein et al., 1996).

Prior to use as fuel or for catalytic valorisation, the bio-oil should be subjected to physical, thermal or catalytic treatments in order to increase its stability. The main pre-treatments studied in the literature will be discussed briefly in Section 1.3.1.3.

1.3.1.2. Reactor configurations

Fast pyrolysis technologies are versatile, simple and of relatively low cost, which explains its considerable state of development and the implementation of decentralized units in areas where the raw material is available (Balat et al., 2009; Anex et al., 2010; Bridgwater, 2012). They are in an incipient state of commercialization, but distributed all over the world by different companies, such as *Ensyn Technologies*, *Dynamotive*, *Agritherm*, *KIT*, *BTG* or *Wellman Engineering* (Bridgwater, 2010; Butler et al., 2011). These are versatile technologies, which allow valorising different types of lignocellulosic and other biomasses, such as, lignin, sewage sludge (Kim and Parker, 2008; Ben and Ragauskas, 2011), macro- and micro-algae and organic wastes (Bae et al., 2011).

The general features of fast pyrolysis technology have been summarized in several reviews, which allow analysing the progress in this field (Meier and Faix, 1999; Bridgwater and Peacocke, 2000; Mohan et al., 2006; Butler et al., 2011; Bridgwater, 2012). Different reactors have been proposed, which can be classified as follows: 1) bubbling fluidized bed (Boateng et al., 2007; Westerhof et al., 2010); 2) circulating fluidized bed and entrained flow reactor (Dai et al., 2000; Van de Velden et al., 2008); 3) ablative reactor (Peacocke and Bridgwater, 1995; Lédé et al., 2007); 4) vacuum reactor (Yang et al., 2001; Amutio et al., 2011); 5) screw reactor (Ingram et al., 2008), and; 6) conical spouted bed reactor (Aguado et al., 2000; Olazar et al., 2001; Amutio et al., 2012a). The schemes of reactor configurations for fast pyrolysis are shown in Figure 1.11.

Bubbling fluidized bed reactor

The bubbling fluidized bed reactors are the most developed technology, using sand as fluidizing solid and for maintaining the required thermal conditions in this endothermic process. These reactors have a reduced segregation (Zhang et al., 2009a) and good heat transfer between phases (DeSisto et al., 2010; Papadikis et al.,

2010), due to the high gas velocity and the low height/diameter ratio of the bed. They require a quick and efficient separation of char, whose presence favours the production of tar, and therefore should be separated by ejection. The implementation of large scale units has been carried out by companies such as *Dynamotive*, based on the *Biotherm* patent, which is a modification of the original process developed at the University of Waterloo (Scott et al., 1985). This company has installed 100 ton/day plants in West Loren (in 2006) and 200 ton/day plants in Guleph (Canada) (in 2008), increasing the scale compared to previous demonstration plants of 2-4 ton/day. *Biomass Engineering Ltd.* is building a 6 ton/day unit in Great Britain, and different units have been reported to be building in China in the 14-25 ton/day range (Wu et al., 2010). *Agri-Therm* (Canada) proposed an original design integrating a fluidized bed reactor with a char combustor, with different levels of scaling up to 19 ton/day (Berruti and Briens, 2007).

Circulating fluidized bed reactor

In circulating fluidized bed reactors (CFB), the residence time of volatiles and char (which undergoes greater attrition than in bubbling fluidized bed) are the same, which makes difficult the separation of bio-oil. In addition, as it is heated by convection, the heat transfer is less efficient and with null relative velocity between phases. A second bubbling fluidized bed is provided, in which the sand is heated by char combustion and which is recirculated to the pyrolysis reactor. *Easyn* has a 100 ton/day plant operating since 2007 and another 400 ton/day under construction in Renfrew (Canada) (Müller, 2010).

Ablative reactor

In ablative reactors, the heat required to heat the biomass particles is supplied by contact with the hot wall. The pyrolysis rate is increased by reducing the particle size and favouring the contact of these particles with the reactor wall, which is done by a mechanical or centrifugal force (Peacocke et al., 1994), favoured by the disposition of the rotary cone. A variant of this reactor is the cyclonic reactor (Lédé et al., 2007). The development of this technology has reached its maximum scale in a plant with a rotary cone reactor, with a capacity for 2-4 ton/day developed by *Biomass Technology Group (BTG) B.V.*, in collaboration with the University of Twente. *Pytec* (Germany) has manufactured a 6 ton/day mobile unit, for subsequent bio-oil combustion in diesel engines (Faix et al., 2010).

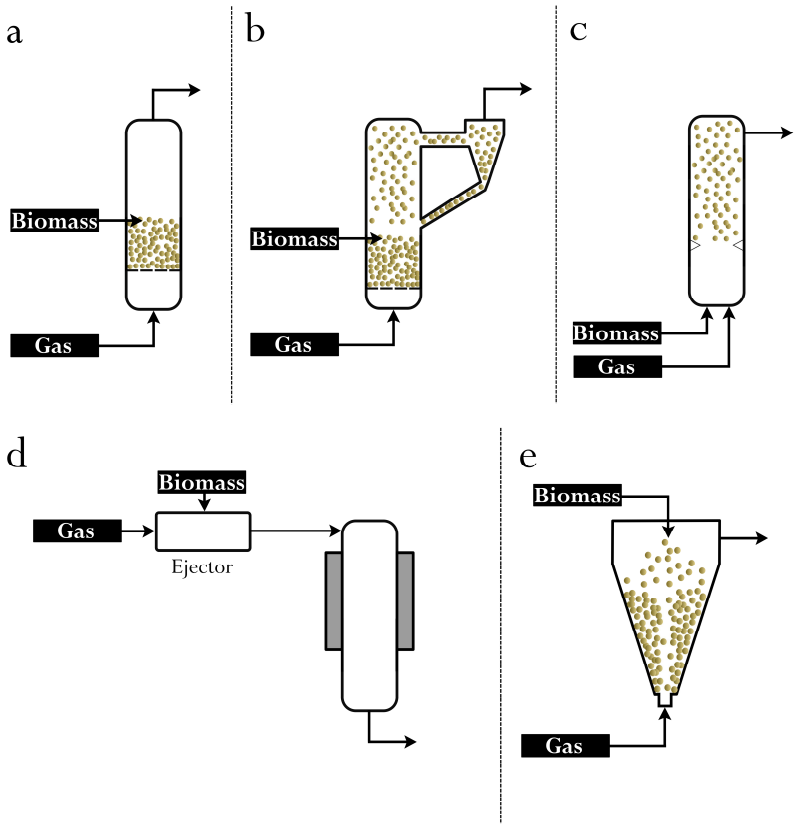

Figure 1.11. Reactor configurations for fast pyrolysis: a) bubbling fluidized bed reactor; b) circulating fluidized bed reactor; c) entrained flow reactor; d) ablative reactor, and; e) conical spouted bed reactor.

Vacuum pyrolysis

The best example of vacuum pyrolysis is the unit built by *Pyrovac* process (15 kPa and around 450 °C) (Yang et al., 2001). It is considered a fast pyrolysis method due to the reduced residence time of the volatiles, although the devolatilization is slow and requires a high residence time of the biomass particles in the reactor, which is a conveyor belt. It produces a bio-oil with high molecular weight compounds, which can be afterwards transformed in a second atmospheric pressure pyrolysis reactor.

Vacuum pyrolysis of pine sawdust has been studied by Amutio (2011) in a continuous conical spouted bed reactor, determining that bio-oil composition is slightly affected by vacuum down to 0.25 atm.

Mechanical reactor

The screw reactor (Ingram et al., 2008) does not require a carrier gas, which simplifies the design and separation of products, but has several drawbacks related to the cost of the energy required for mechanical operation. *ARBI-Tech* (Canada) is developing large-scale units and expects to market a unit of 50 ton/day (Preto, 2010). *Renewable Oil Int. LCC* (USA) has built 4 plants, with the largest one being of 4.8 ton/day (Bridgwater, 2010).

Conical spouted bed reactor

The advantages of this reactor are the features of the conventional spouted beds (cylinder with a conical base) and are promoted by the exclusively conical geometry of the reactor: simplicity of construction and design, low pressure drop, vigorous contact between particles, high heat and mass transfer rates between phases, versatility in the gas flow, low residence time of the gas and the ability to work in continuous regime for the solid.

Figure 1.12 shows the evolution of solid particles movement and the corresponding evolution of pressure drop for different gas flows rates. Using suitable gas velocities, the spouted bed regime (Figure 1.12b) and the dilute spouted bed regime (Figure 1.12d) are reached, which have their characteristic bed pressure drops and gas and solid flows patterns. In the range between spouting and dilute spouting, there is a transition regime (Figure 1.12c).

Three different areas in the bed can be differentiated in the spouted bed regime, in which the gas-solid contact has different features:

i) *Spout zone*, or central zone, with an upward solid flow. It has a low particle concentration (high porosity) and spans from the entrance of the gas to the bed surface (fountain zone), in which the particles rain back onto the annular zone.

ii) *Annular zone*, which surrounds the spout zone and the solid flow is descendent, similar to a moving bed. There is solid cross-flow from the annular to the spout zone along the interface between the two zones.

iii) *Fountain zone*, above the previous two zones, in which the particles arrive with an upward vertical trajectory, but change it to a downward one to

incorporate to the annular zone. The similarity of this zone with a fountain gives the name to this contact regime. In this area, two different regions can be differentiated: 1) a central region or fountain core, where the solids flow upwards and, 2) a peripheral region, in which the particles circulate downwards and towards the reactor wall and fall onto the annular zone.

For a gas velocity corresponding to the dilute spouted bed regime (jet spouted bed), the cyclic movement of the particles in the three regions is similar to that described for the spouted bed regime, with the peculiarity that porosity is approximately the same all over the bed (higher than 0.90).

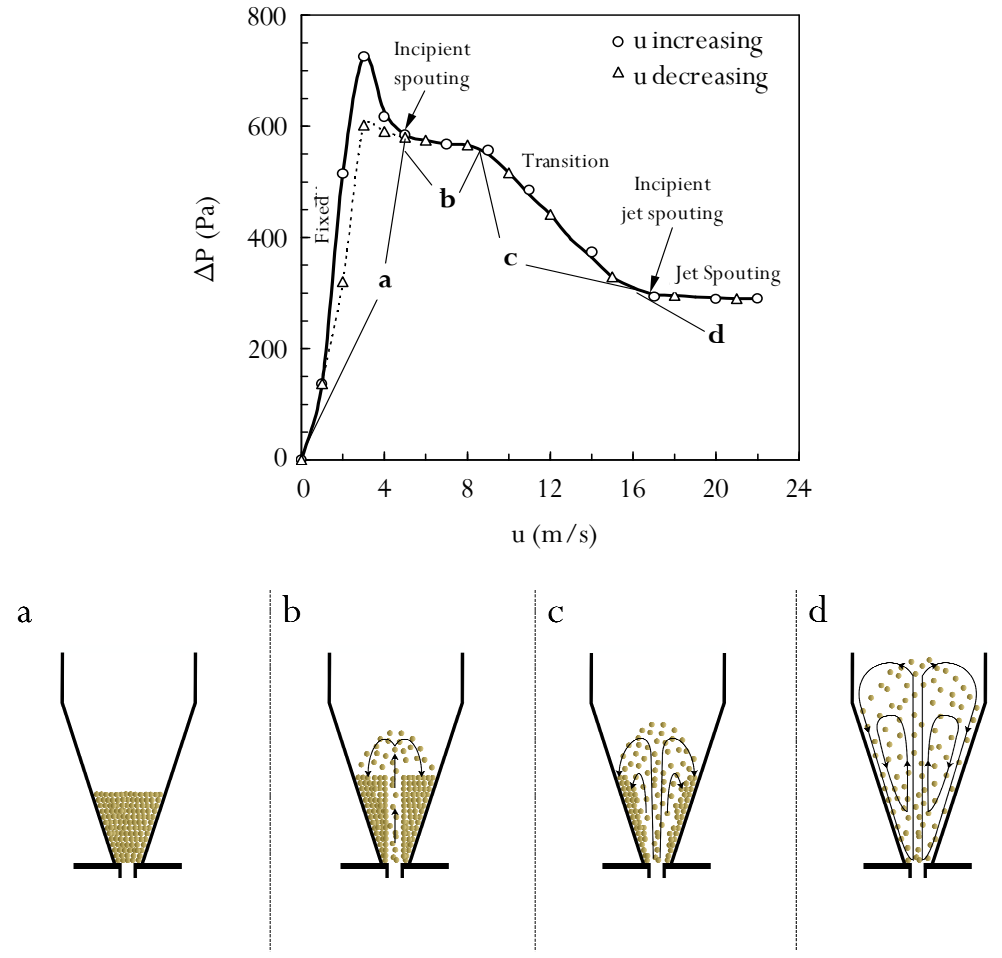

Figure 1.12. Evolution of pressure drop and particle circulation when gas velocity is increased in the conical spouted bed (Olazar et al., 1992).

The polymerization of benzyl alcohol on SiO_2-Al_2O_3 catalysts was the first application of the conical spouted bed reactor in our research group. These studies, carried out without any hydrodynamic basis for the design of the reactor, evidenced a good performance of the reactor to avoid the agglomeration of catalyst particles coated with polymer (Bilbao et al., 1987; Olazar et al., 1994a, 1997).

The development of the conical spouted bed reactor for the pyrolysis of biomass and plastics is based on hydrodynamic and contactor design studies, carried out initially with spheres and regular texture solids with density and size corresponding to Geldart group D (Olazar et al., 1992, 1993a,b, 1994b, 1995a,b, 1996, 1999; San José et al., 1993, 1998a,b). These cold hydrodynamic studies were extended to materials with low density, such as plastics (Olazar et al., 2004; San José et al., 2005a,b, 2006, 2007) and other materials with irregular texture, such as biomass (Olazar et al., 2004). A remarkable feature of the reactor is the low segregation observed when treating mixtures of solids with different size, texture and density (Olazar et al., 1993c, 2006; San José et al., 1994).

Based on the hydrodynamic knowledge and tests carried out in discontinuous prototypes, different units for the pyrolysis of lignocellulosic biomass (Amutio et al., 2012a), sewage sludge (Alvarez et al., 2015), plastics (Elordi et al., 2011a) and tires (Lopez et al., 2010) have been designed. The vigorous cyclic movement of the particles in the conical spouted bed reactor is suitable to minimize the operational limitations related to the physical steps of the pyrolysis.

The hydrodynamics of the conical spouted bed reactor for biomass (irregular material) differs from that corresponding to regular texture granular materials in the following aspects: 1) the fountain has higher height; 2) the minimum velocity of the spouted bed (to open the spout) differs from that corresponding to the full bed movement; 3) the pressure drop in the bed reaches a very pronounced peak and has a notable hysteresis, and; 4) the angle of the conical section contributes to a great extent to the stability of the bed. Consequently, there are some differences in the correlations for the calculation of hydrodynamic properties and design conditions (Olazar et al., 2004) in relation to those determined for glass spheres and solids with regular texture (Olazar et al., 1992, 1993a). The versatility of the operation is remarkable, as it may be operated with a wide range of gas velocity in a transition regime between those corresponding to incipient spouted bed (bed porosity = 0.60) and diluted spouted bed (with bed porosity $\approx$ 0.99) (Olazar et al., 1999).

Amutio (2011) has improved the development of the conical spouted bed technology in continuous regime, obtaining a maximum bio-oil yield at 500 °C (Figure 1.13). In addition, a progress has been done in strategies that are essential for the scaling-up, such as vacuum pyrolysis to reduce the inert gas flow rate (Lopez et al., 2010; Amutio et al., 2011) and autothermic pyrolysis, which in turn reduce the external energy needed for gas heating (Amutio et al., 2012b). Moreover, the technology has been scaled up to 25 kg h^{-1} for biomass pyrolysis (Makibar et al., 2011; Fernandez-Akarregi et al., 2013).

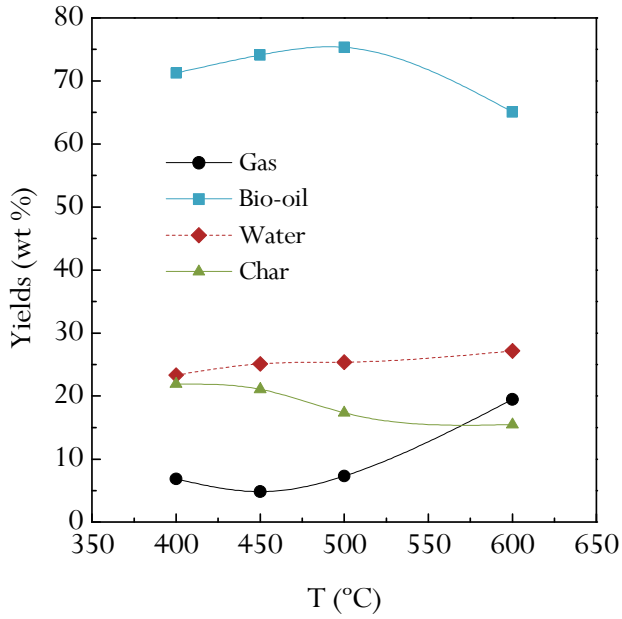

Figure 1.13. Effect of temperature on gas, liquid (bio-oil) and char yields (Amutio et al., 2012a).

The drying of materials (Altzibar et al., 2011) and the gasification of biomass (Erkiaga et al., 2014) and plastics (Erkiaga et al., 2013b) have also been carried out in units provided with a conical spouted bed reactor. The negligible segregation is an excellent feature for the use of an in situ catalyst in the pyrolysis (Elordi et al., 2011b,c, 2012a,b) and gasification (Erkiaga et al., 2013a). Furthermore, different hydrodynamic limitations of the gas and solid flow can be solved incorporating internal devices (Altzibar et al., 2013). Thus, Amutio et al. (2013) used these devices, which are necessary when pyrolysis of herbaceous materials is carried out.

1.3.1.3. Bio-oil valorisation routes

Bio-oil valorisation routes focus on adapting its composition for use as a fuel and for obtaining compounds of high interest (by extraction and/or catalytic transformation). The success or viability of each valorisation route lies in carrying out a suitable route for each geographic area.

Previous stabilization of the bio-oil

The direct use of bio-oil as a fuel is limited by its high viscosity, high water content and high corrosiveness and thermal instability, which also make problematic its long-term storage, and therefore a previous stabilization is required. Amongst the different treatments used in the literature to stabilize the bio-oil, the following techniques are worth mentioning: 1) separation of the lightest fraction of the bio-oil in order to increase its combustibility and decrease corrosiveness (Guo et al., 2010b); 2) treatment at high pressure and moderate temperatures to reduce O and water content (de Miguel Mercader et al., 2010); 3) thermal treatment to decrease the concentration of phenolic and high molecular weight compounds (Bertero et al., 2012; Bertero and Sedran, 2013); 4) esterification with low cost alcohols to reduce acidity, viscosity and corrosiveness of the bio-oil (Moens et al., 2009; Hilten et al., 2014); 5) dehydration-cracking using an in situ acid catalyst in the pyrolysis reactor to selectively reduce the concentration of some compounds, such as methoxy-phenols (Atutxa et al., 2005; Zhang et al., 2009b), and; 6) in-line transformation of pyrolysis volatiles by esterification of acids (Hilten et al., 2010) and by dehydration-cracking reactions (French and Czernik, 2010).

Direct use as a fuel

As aforementioned, the bio-oil presents several drawbacks for direct use as a fuel, due to its high water content, low heating value and high viscosity, acidity and instability. Nevertheless, the bio-oil has some environmental advantages compared to fossil fuels due to the neutral emission of CO_2 and low emissions of pollutants (mainly SO_x and NO_x) (Pütün, 2002). The bio-oil can be mixed with diesel derived from fossil fuels to contents of up to 75 wt % bio-oil. The emulsion allows achieving acceptable viscosity, density and corrosiveness (Chiaramonti et al., 2003; Ikura et al., 2003). Moreover, the combustion of bio-oil/diesel emulsion reduces the emission of particles and NO_x compared to diesel combustion. Garcia-Perez et al. (2007) investigated the stabilization of mixtures containing up to 50 wt % of bio-oil

in bio-diesel at 20 ºC, with the diesel being obtained from transesterification of triglycerides. Jiang and Ellis (2010) used octanol for the mixture of bio-oil with bio-diesel, with volume ratio being 4/6 and stirring conditions 30 ºC for 15 min.

Extraction of compounds

The extraction of bio-oil compounds can be an economically viable process, as great advances have been made in the separation techniques in recent years. Thus, these compounds can be used for different applications: 1) phenolic compounds for the synthesis of adhesives for wood (Effendi et al., 2008) and for the formulation of phenol-formaldehyde resins (Chum et al., 1989; Himmelblau, 1991); 2) levoglucosan, which can be hydrolyzed to glucose, giving rise to a rapid route for bio-ethanol production (Bennett et al., 2009); 3) binders for the manufacture of briquettes of combustible organic wastes (Goyal et al., 2008), and; 4) hydroacetaldehyde and other additives for pharmaceutical industry, timber industry, fertilizer synthesis… (Effendi et al., 2008; Uzun et al., 2010).

Catalytic transformation

In the scheme of a bio-refinery, the bio-oil plays an important role as raw material with other fuels or intermediate raw materials (such as bio-ethanol, biogas or synthesis gas), which are also derived from biomass. Figure 1.14 shows the evolution of the different techniques for the valorisation of bio-oil over the years. The valorisation has been approached in the literature through three main routes: catalytic cracking, hydrodeoxygenation and steam reforming, which will be explained briefly in this section, paying particular attention to the catalytic steam reforming process (Section 1.3.2).

In the catalytic cracking process, the deoxygenation of bio-oil is carried out with acid catalysts through simultaneous dehydration, decarbonylation and decarboxylation reactions, obtaining H_2O, CO, CO_2, hydrocarbons and coke as products. Five different stages take place during the catalytic cracking (Domine et al., 2008): 1) dehydration reactions; 2) hydrocarbons cracking; 3) H_2 production; 4) H_2 consumption, and; 5) formation of large molecules by C-C bonds. This process is a versatile strategy to improve the quality of bio-oil (Graça et al., 2009; Gayubo et al., 2010a; Hew et al., 2010; Bertero et al., 2012; Bertero and Sedran, 2013) and produce higher value added compounds, such as olefins (Gayubo et al., 2010b; Gong et al., 2011; Hong et al., 2013) and BTX aromatics (Valle et al., 2010; Rezaei et al.,

2014). The process can be carried out in units designed specifically for its production or in existing refinery units (such as FCC units), co-feeding bio-oil together with the usual feed, with this strategy being more interesting for large-scale viability. The catalytic cracking of bio-oil can also be done by in situ cracking of the volatiles in the pyrolysis reactor (catalytic pyrolysis), obtaining partially deoxygenated liquids, with a higher content of aromatic compounds and phenols (Carlson et al., 2009; Mullen et al., 2011; Park et al., 2012).

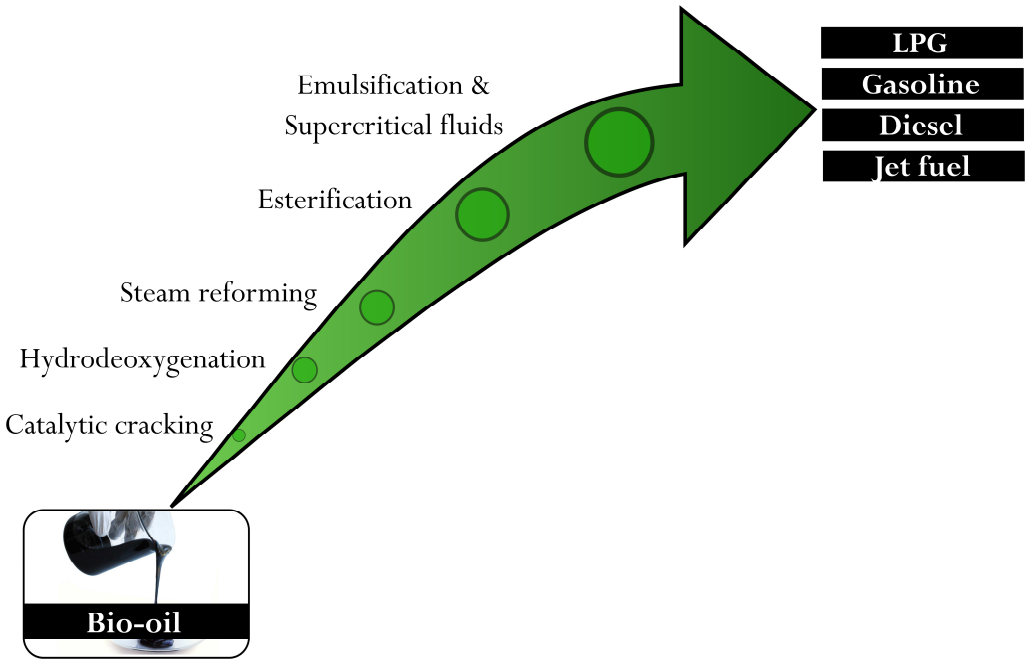

Figure 1.14. Evolution of bio-oil upgrading techniques over the years (Gollakota et al., 2016).

In the hydrodeoxygenation (HDO) process, the improvement of bio-oil properties for use as fuel is carried out over metallic catalysts at high pressures (≥ 70 bar) and moderate temperatures (300 – 600 °C), with the consumption of H_2 being around 490 – 710 $L/L_{bio\text{-}oil}$ (Zacher et al., 2014).The O contained in the bio-oil is removed as H_2O, CO_2 and CO, through the following reactions: 1) dehydration; 2) decarboxylation; 3) decarbonylation; 4) hydrogenation of unsaturated compounds; 5) hydrogenolysis with rupture of C-O bonds and release of H_2O, and; 6) hydrocracking, with C-C bond breakage in the high molecular weight compounds (Mortensen et al., 2011). The result is a highly deoxygenated liquid product, reaching values even around 0.2 wt % of total O (Elliott et al., 2012). Some of the

most relevant results and conclusions obtained about HDO process in the literature are as follows: 1) the ketones group is easily and selectively hydrogenated to methylene group above 200 ºC (Laurent and Delmon, 1994); 2) the carboxyl group undergoes parallel reactions of hydrogenation and decarboxylation, which lead to the formation of alkanes (Laurent and Delmon, 1994); 3) the guaiacols cause deactivation of catalyst by coke formation (González-Borja and Resasco, 2011), and; 4) high water contents can reduce the catalyst activity up to one third of the initial one (González-Borja and Resasco, 2011).

The esterification process and supercritical fluids have gained increasing attention in recent years. On the one hand, the esterification process of corrosive and acid components in the bio-oil is a simple pre-treatment to improve the stability of the bio-oil during storage and transport. The addition of small concentrations of ethanol or methanol (< 10 %) improves the stability of the bio-oil, through the formation of esters by reactions with carboxylic acids and aldehydes. The bio-oil resulted after esterification leads to lower aging rate and viscosity (Boucher et al., 2000; Chen et al., 2014; Gollakota et al., 2016). On the other hand, the new method for bio-oil upgrading using supercritical fluids takes advantage of the properties of supercritical reaction medium, improving the quality and properties of the bio-oil (Gollakota et al., 2016).

1.3.2. Bio-oil reforming

The catalytic steam reforming of bio-oil (Figure 1.15) is one of these routes that has been considerably researched, using different reactor configurations, catalysts and operating conditions. The higher energy density of the bio-oil compared to biomass is an important factor to be considered, given that transportation costs can be decreased, with the biomass pyrolysis being carried out in different geographical zones and the bio-oil afterwards valorised in a centralized large scale catalytic conversion unit. In this process, the bio-oil obtained in the prior pyrolysis of biomass is subjected to the catalytic steam reforming and the individual reactions involved are shown in Table 1.3.

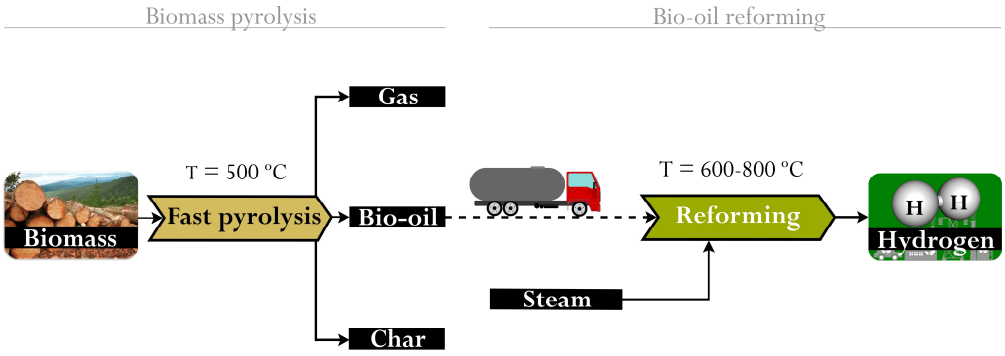

Figure 1.15. Schematic representation of fast pyrolysis of biomass and bio-oil reforming process for hydrogen production.

Table 1.3. Reaction stages involved in bio-oil reforming.

Boudouard reaction:	$C + CO_2 \leftrightarrow 2CO \quad \Delta H = 162.4 \text{ kJ mol}^{-1}$	(1.3)
Bio-oil cracking:	$C_nH_mO_k \rightarrow C_xH_yO_z + C_aH_b + CH_4 + CO + CO_2 + C$	(1.4)
Bio-oil reforming:	$C_nH_mO_k + (n-k)H_2O \rightarrow nCO + \left(n + \frac{m}{2} - k\right)H_2$	(1.5)
Water gas shift (WGS):	$CO + H_2O \leftrightarrow H_2 + CO_2 \quad \Delta H = -41.2 \text{ kJ mol}^{-1}$	(1.6)
Methane steam reforming:	$CH_4 + H_2O \leftrightarrow CO + 3H_2 \quad \Delta H = 206.3 \text{ kJ mol}^{-1}$	(1.7)
Hydrocarbons steam reforming:	$C_nH_m + nH_2O \rightarrow nCO + \left(n + \frac{m}{2}\right)H_2$	(1.8)
Inter-conversion:	$C_nH_mO_k \rightarrow C_xH_yO_z$	(1.11)

Table 1.3. Continued.

Methanation:	$CO + 3H_2 \leftrightarrow CH_4 + H_2O$	(1.12)
	$CO_2 + 4H_2 \leftrightarrow CH_4 + 2H_2O$	(1.13)

The main reactions are the reforming of the oxygenated compounds in the bio-oil (eq. (1.5)), CH_4 (eq. (1.7)) and light hydrocarbons (C_nH_m) (eq. (1.8)), and the WGS reaction (eq. (1.6)), which are promoted by the presence of the catalyst. Moreover, it should be considered that high temperatures are needed in reforming of bio-oil due to the endothermic nature of reforming reactions. High temperature also favours secondary reactions, such as Boudouard (eq. (1.3)), bio-oil cracking (eq. (1.4)), interconversion (eq. (1.11)) or methanation (eqs. (1.12) and (1.13)) reactions.

The aforementioned difficulties related to bio-oil properties and its feeding problems boosted the use of bio-oil model compounds in the feed, which helps understanding the mechanisms of reforming reactions, with acetic acid (Basagiannis and Verykios, 2006; Takanabe et al., 2006a,b; Bimbela et al., 2007, 2012; Hu and Lu, 2010; Assaf et al., 2013; Pant et al., 2013; Wang et al., 2014a,b; Gil et al., 2015), acetone (Wang et al., 1997, 1998; Rioche et al., 2005; Hu and Lu, 2009; Navarro et al., 2014, 2015; Xie et al., 2015a,b) and ethanol (Alberton et al., 2007; Trane-Restrup et al., 2013; González-Gil et al., 2015; Quitete et al., 2016) being among others the most studied ones. Nevertheless, although some works have been published concerning reforming of phenols (Tan et al., 2014; Wang et al., 2014a,b; Xie et al., 2015a,b; Artetxe et al., 2016) and especially, m-cresol (Marquevich et al., 1999; Wu and Liu, 2010; Xu et al., 2013; Lan et al., 2014a; Garcia-Garcia et al., 2015; Mei et al., 2016), furans (Xu et al., 2013; Lan et al., 2014a; Trane-Restrup and Jensen, 2015), saccharides (Marquevich et al., 1999; Hu and Lu, 2009) and aromatic compounds such as toluene (Yoon et al., 2010; Wang et al., 2012; Artetxe et al., 2017) or m-xylene (Hu and Lu, 2009), cyclic oxygenated compounds (phenols, saccharides and furans) are less investigated, but they are supposed to be responsible for the catalyst deactivation by coke deposition (Trane-Restrup and Jensen, 2015). Most studies related to bio-oil model compounds have been carried out in fixed bed reactors, although there are some studies in fluidized bed reactors (Román Galdámez et al., 2005; Kechagiopoulos et al., 2007; Ramos et al., 2007; Medrano et al., 2009; Gil et al., 2015; Montero et al., 2015), which is a feasible solution in order to avoid problems related to bed blocking by deposition of high amounts of coke. Although

most studies investigate the reforming of these compounds separately, the joint valorisation of different compounds is of great interest, given that the different reactivity of these compounds when they are alone or in a mixture and the interactions between them can vary the results.

Consequently, this strategy focuses on the valorisation of the bio-oil aqueous fraction and, especially, raw bio-oil, which has recently gained increasing attention. Therefore, Table 1.4 and Table 1.5 summarize some of these studies, in which reforming of bio-oil aqueous fraction (Table 1.4) and raw bio-oil (Table 1.5) have been performed. Although different reactors and operating conditions have been used, a discussion of the main results has been detailed below. In this section, the values of H_2 production are generally given as g of H_2 per 100 g of organic compounds in the feed, and otherwise it will be specified in each case. Moreover, H_2 yield is based on the maximum allowable by stoichiometry.

Table 1.4. Studies involving different strategies, feeds, catalysts and operating conditions, and main results obtained (maximum H_2 yield or production) reported in the literature for the reforming of bio-oil aqueous fraction.

Reactor configuration	Biomass	Catalyst	Operating conditions	Conversion	H_2 yield (%)[a]	H_2 production (wt %)[b]	Reference
Bench scale bubbling fluidized bed	Pine sawdust	C11-NK	T= 800-850 °C $G_{C1}HSV$= 700-1000 h^{-1} S/C= 7-9	95	89	16.8[*] 3.0[c]	Czernik et al., 2002
Nozzle-fed fixed bed	Beech wood	Ru/MgO/Al_2O_3	T= 700-800 °C GHSV= 4880-16570 h^{-1} S/C= 7.2	100	100[d]	-	Basagiannis and Verykios, 2007a
Spouted bed	Pine wood	Ni/olivine	T= 850 °C S/C= 5.37 O_2/C=1, 0.3, 0	100	43	-	Kechagiopoulos et al., 2009
Fluidized bed	Sawdust	Ni/dolomite Ni/modified dolomite	T= 600-800 °C WHSV= 1.5 h^{-1} S/C= 2-10	-	73	-	Li et al., 2009b
Laboratory-scale fixed bed	Rice hull	Commercial: Z417 Ni/CeO_2-ZrO_2 *Ni loading= 5-12 wt %* *Ce loading= 5-10 wt %*	T= 450-800 °C Water/bio-oil= 3.2-5.8	-	69.7	-	Yan et al., 2010a
Fluidized bed	Pine wood	Ni-Al Ni-Ca-Al Ni-Mg-Al	T= 650 °C $G_{C1}HSV$= 12000-5400 h^{-1} S/C= 7.64	83.26	-	13.3	Medrano et al., 2011
Fixed bed	Corn stover	G90-LDP	T= 500-700 °C WHSV= 0.87 h^{-1} S/C= 4-18	80	65	12.5	Ortiz-Toral et al., 2011
Bench scale fixed bed	Pine wood	Ni/Al coprecipitated catalysts *Ni loading= 23-33 wt %*	T= 600-800 °C Space time= 0-5 g_{cat} min $g_{organic}^{-1}$ S/C= 5.58	82.62	77	13.8	Bimbela et al., 2013
Fixed bed	Pine wood sawdust	Ni-Mo supported on modified sepiolite	T= 600-800 °C WHSV= 0.9-5.4 h^{-1} S/C= 2-25	98	67.5	-	Liu et al., 2013

Table 1.4. Continued.

Reactor configuration	Biomass	Catalyst	Operating conditions	Conversion	H_2 yield (%)[a]	H_2 production (wt %)[b]	Reference
Fixed bed / fluidized bed	Pine sawdust	Ni/La_2O_3-αAl_2O_3	T_1= 500 °C T_2= 500-800 °C Space time= 0.10-0.45 g_{cat} h $g_{bio\text{-}oil}^{-1}$ S/C=12	100	96	15.6* 10.1[c]	Remiro et al., 2013b
Fixed bed or fluidized bed	Pine sawdust	Ni/Al-Mg-O modified with Co or Cu	T= 650 °C Space time= 4 g_{cat} min $g_{orcanic}^{-1}$ S/C= 7.6	80	-	13.8	Remón et al., 2013
Fixed bed	Biomass	$Ni\text{-}MgO/Al_2O_3$ *Ni loading=0-33.3 wt %* *MgO loading= 0-12.8 wt %*	T= 850 °C WHSV= 30 h^{-1} Oil/Water= 1:2, 1:1, 2:1	-	85	10.5* 3.4[c]	Seyedeyn-Azad et al., 2014
Fixed bed / fixed bed	Corn stalk	Ni-Al modified with Ca, Ce, Mg, Mn and Zn	T_1= 400 °C (volatilization) T_2= 600-900 °C Space time= 1.67 g_{cat} min $g_{bio\text{-}oil}^{-1}$ S/C= 3.54-9	90.4	57.2	10.4*	Yao et al., 2014
Fluidized bed or spouted bed	Pine / poplar wood	Ni-Co/Al-Mg	T= 650 °C Space time= 4 g_{cat} min $g_{orcanic}^{-1}$ S/C= 7.6	96.5	-	18.2	Remón et al., 2015

[a] H_2 yield referred to the maximum allowable by stoichiometry. [b] H_2 production defined as $g_{H2}/100g_{organic}$. [c] H_2 production defined as $g_{H2}/100g_{bio\text{-}oil}$.
[d] H_2 selectivity. * calculated by H_2 yield and bio-oil composition.

Table 1.5. Studies involving different strategies, feeds, catalysts and operating conditions, and main results obtained (maximum H_2 yield or production) reported in the literature for the reforming of raw bio-oil.

Reactor configuration	Biomass	Catalyst	Operating conditions	Conversion	H_2 yield (%)[a]	H_2 production (wt %)[b]	Reference
Fixed bed	Beech wood	Pt, Pd, Rh supported on Al_2O_3 and $CeZrO_2$	T= 650-950 °C GHSV=3090 h^{-1} S/C= 5-10.8	-	75	14.5[c*]	Rioche et al., 2005
Fixed bed	Biomass	C12A7-O^-/M catalysts *M= Mg, K, Ce*	T=250-750 °C GHSV= 10000 h^{-1} S/C=1.5-9	96	80	20.1[*] 12.4[c*]	Wang et al., 2007
Fixed bed / fixed bed	Sawdust	1- Dolomite 2- Ni/MgO	T_1=700-900 °C T_2=600-800 °C $(W_BHSV)_1$=0.5-5 h^{-1} $(GHSV)_2$=1800-14400 h^{-1} $(S/C)_1$=1-16 $(S/CH_4)_2$=1-4	100	81.1	13.2[c*]	Wu et al., 2008a
Fixed bed	Sawdust	Ni-CNT *Ni loading= 5, 15, 35 wt %*	T= 350-550 °C GHSV= 12000 h^{-1} S/C= 2.0-6.1	94.9	92.5	17.5[*]	Hou et al., 2009
Fixed bed or fluidized bed	Rice husk	Ni/MgO-La_2O_3-Al_2O_3	T_{fixed}= 650-950 °C $LHSV_{fixed}$=0.8-2.5 h^{-1} S/C_{fixed}=3-14 $T_{fluidized}$= 500-800 °C $LHSV_{fluidized}$=0.2-1.5 h^{-1} $S/C_{fluidized}$=8-20	-	75.88	17.6[*]	Lan et al., 2010
Fluidized bed	Rice husk	NiO/MgO	T= 500-800 °C WHSV= 0.2-0.8 h^{-1} S/C= 8-20	-	56.3	13.1[*]	Xu et al., 2010

Table 1.5. Continued.

Reactor configuration	Biomass	Catalyst	Operating conditions	Conversion	H_2 yield (%)[a]	H_2 production (wt %)[b]	Reference
Fixed bed	Biomass	Ni/Al_2O_3 $Ru-Ni/Al_2O_3$ $Ni-MgO/Al_2O_3$ *Ni loading= 0-18 wt %* *Ru loading= 0.5 wt %*	T= 750-950 °C W_BHSV= 13 h^{-1} S/C= 5	81	85	14.3[c*]	Salehi et al., 2011
Fixed bed	Sawdust	NiCo/Ce-Zr-O *Ni loading=2-10 wt %* *Co loading=2-10 wt %*	T= 850 °C WHSV= 2.62 h^{-1}	-	72.15	13.2[*]	Zhang et al., 2012
Fixed bed	Biomass	Ni/ZrO_2 Ni/Al_2O_3 *Ni loading= 0-18 wt %*	T=850 °C W_BHSV=13 h^{-1} S/C=5	-	92	20.1[*] 15.5[c*]	Seyedeyn Azad et al., 2012
Fixed bed / fluidized bed	Pine sawdust	1- Dolomite 2- Ni/La_2O_3-αAl_2O_3	T_1= 500 °C T_2= 600-800 °C $G_{C1}HSV$= 8000-156000 h^{-1} S/C= 1-15	100	95	15.4[*] 11.7[c*]	Remiro et al., 2013a
Fixed bed	Maize stalk	$Ni-Ce/Al_2O_3$ *Ni loading=5.1-20.4 wt %*	T= 700-900 °C W_BHSV= 8-24 h^{-1} S/C= 1-9	-	71.4	11.1[c*]	Fu et al., 2014
Fixed bed or fluidized bed	Pine sawdust	Ni/Co-Al-Mg	T= 650 °C $G_{C1}HSV$= 13000 h^{-1} S/C= 7.6	95	-	17.0[*]	Remón et al., 2014
Fixed bed	Corn cob	$Ce-Ni/Co-Al_2O_3$	T= 650-850 °C LHSV= 0.08-0.23 h^{-1} S/C= 9-15	-	85	11.7[*] 6.6[c*]	Xie et al., 2016

[a] H_2 yield referred to the maximum allowable by stoichiometry. [b] H_2 production defined as $g_{H2}/100g_{organic}$. [c] H_2 production defined as $g_{H2}/100g_{bio\text{-}oil}$. [*] calculated by H_2 yield and bio-oil composition.

1.3.2.1. Reactor configurations

The main reactor configurations used for the reforming of both aqueous fraction and raw bio-oil are shown in Figure 1.16, in which one-step (Figure 1.16a, b and c) and two-step processes (Figure 1.16d and e) are differentiated.

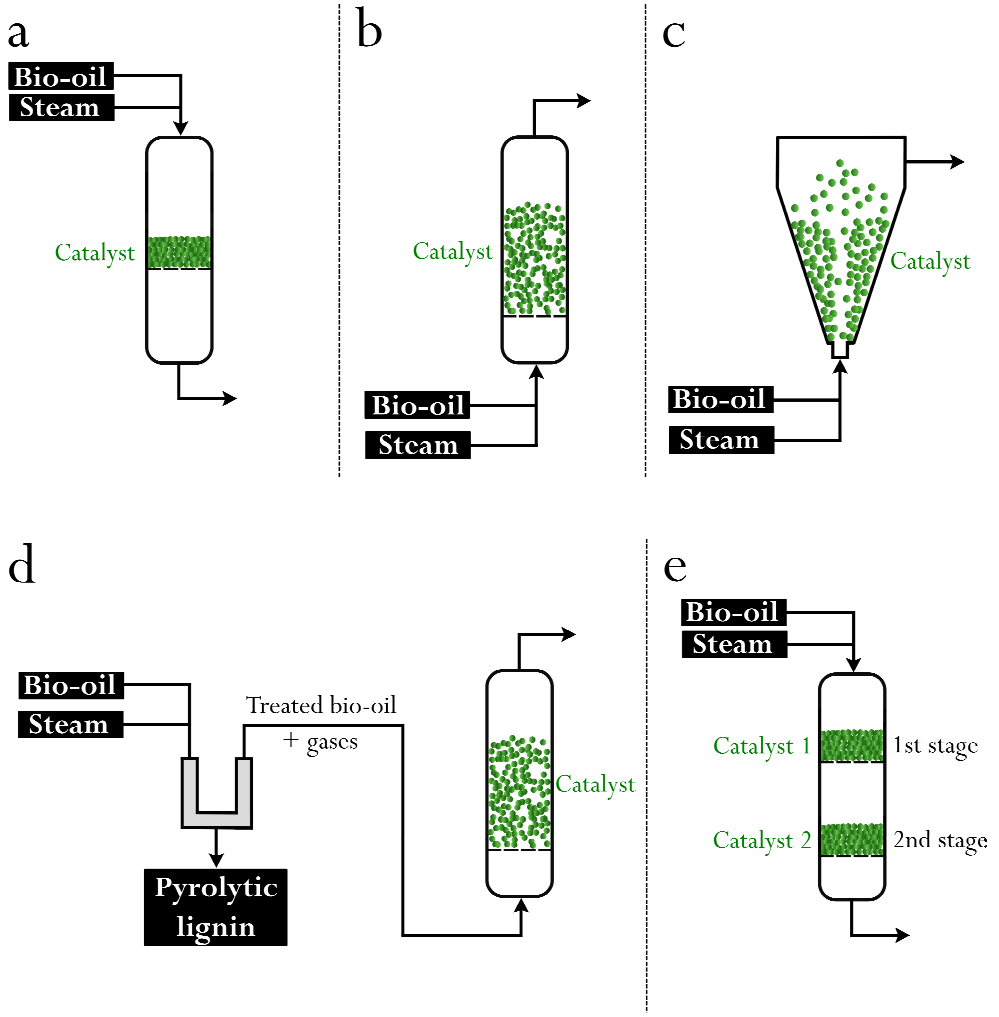

Figure 1.16. Reactor configurations for bio-oil reforming process: a) fixed bed reactor; b) fluidized bed reactor; c) spouted bed reactor; d) two-stage fixed-fluidized bed reactor, and; e) two-stage fixed bed reactor.

Many studies of reforming of bio-oil aqueous fraction are found in the literature, which have been carried out mainly in fixed (Garcia et al., 2000; Basagiannis and Verykios, 2007a; Yan et al., 2010a; Ortiz-Toral et al., 2011; Bimbela et al., 2013; Liu et al., 2013; Seyedeyn-Azad et al., 2014; Remón et al., 2015) (Figure 1.16a) and fluidized bed (Czernik et al., 2002; Li et al., 2009b; Medrano et al., 2011) (Figure 1.16b) reactors. Nevertheless, a spouted bed reactor was used for the reforming of the bio-oil aqueous fraction by Kechagiopoulos et al. (2009) (Figure 1.16c), and they did not observe coke deposits. Therefore, although reforming performs better in fixed bed reactors than in other technologies, they lead to a higher production of coke. It should be taken into account that bio-oil can be thermally decomposed forming high amounts of coke on the catalyst surface, which block the reactor, and therefore fluidized bed reactors are more suitable than fixed bed reactors for bio-oil reforming processes (Czernik et al., 2002). Remón et al. (2013) compared a fixed bed and a fluidized bed reactor for the steam reforming of bio-oil aqueous fraction and reported a higher initial activity when a fixed bed reactor was used, obtaining 80 % conversion and 13.8 wt % H_2 production over 2 h operation using a coprecipitated NiCo/AlMg catalyst, although lower deactivation was achieved in the fluidized bed reactor. The same authors also compared a fluidized bed reactor and spouted bed reactor for the reforming of different aqueous fractions of pine wood and poplar wood (Remón et al., 2015). They observed higher initial conversion and H_2 production for pine wood bio-oil reforming, obtaining a maximum conversion of 96.5 % and H_2 production of 18.2 wt % when the reforming process was carried out in fluidized bed reactor.

Similarly to the reforming of the bio-oil aqueous fraction, the reforming of raw bio-oil has also been performed mainly in fixed bed (Rioche et al., 2005; Wang et al., 2007; Hou et al., 2009; Salehi et al., 2011; Seyedeyn-Azad et al., 2011, 2012; Zhang et al., 2012; Fu et al., 2014; Xie et al., 2016) and fluidized bed (Czernik et al., 2007; Xu et al., 2010; Lan et al., 2014b) reactors. Furthermore, some authors made a comparison between fixed and fluidized bed reactors. Higher conversion and H_2 yield were obtained by Remón et al. (2014) in a fixed bed reactor compared to fluidized bed reactor. Nevertheless, Lan et al. (2010) reported lower carbon deposition in the fluidized bed reactor than in the fixed bed reactor, obtaining carbon contents of around 2.3 wt % and 0.3 wt %, respectively, at 650 ºC in 60 min on stream.

Moreover, some authors used a two-stage system for bio-oil reforming. The steam reforming of bio-oil aqueous fraction (Valle et al., 2013; Remiro et al., 2013b,c), raw bio-oil (Remiro et al., 2013a) and bio-oil/bio-ethanol mixtures (Valle et al.,

2014; Remiro et al., 2014) was investigated by Remiro et al. and Valle et al. using a two-stage thermal-catalytic process, in which the pyrolytic lignin was deposited by repolymerization of certain bio-oil components in the first stage and the treated bio-oil together with the gases formed in the first step were in-line reformed in a fluidized bed reactor (Figure 1.16d). Yao et al. (2014) used a two-stage fixed bed reactor (Figure 1.16e), where firstly the bio-oil aqueous fraction was volatilized at 400 °C and subsequently the reforming step was carried out on modified Ni-Al catalysts. Moreover, Wu et al. (2008a) used a two-stage fixed bed reactor system in order to avoid the direct contact between the bio-oil and the catalyst. Thus, the bio-oil was reformed in the first stage using dolomite as catalyst and, subsequently, the volatiles were purified using a Ni/MgO catalyst in the second stage.

Nevertheless, although different reactors have been used for bio-oil reforming, the main issue to be solved is related to raw bio-oil feeding, which causes several problems in the reforming reactions. Basagiannis et al. (2007a) reported coke deposition on the reactor wall due to the polymerization of unstable compounds in the bio-oil. Although the feeding system was cooled, Kechagiopoulos et al. (2009) reported plugging of the injection nozzle, due to the thermal instability of the aqueous fraction of the bio-oil used for the process, which required a new injection-cooling system to feed adequately the bio-oil fraction. Moreover, some authors reported aging problems of the bio-oil, which have been solved by adding different alcohols such as methanol (Czernik et al., 2007) or ethanol (Remiro et al., 2014) in order to stabilize the bio-oil and reduce its viscosity. Thus, the improvement of bio-oil feeding systems is essential for a satisfactory scaling up of bio-oil reforming process.

1.3.2.2. Operating variables

Temperature, space time and S/C ratio are the most important operating variables to be considered in reforming processes. In general, most studies reveal that the use of higher temperature, lower space velocity and higher S/C ratio lead to higher H_2 yields due to the enhancement of reforming reactions, at the same time as they maintain catalyst activity for a longer time on stream (Czernik et al., 2002). Although a detailed comparison of results is difficult, the most relevant ones on the effect operating conditions have on product yields and, especially, on H_2 production, have been summarized in this section.

Temperature

Temperature is one of the key variables that should be taken into account in reforming processes. On the one hand, higher temperatures enhance reforming kinetics of oxygenated compounds of the bio-oil and, therefore, higher H_2 yield and production are obtained in the reforming of bio-oil aqueous fraction (Yan et al., 2010a; Bimbela et al., 2013; Liu et al., 2013; Yao et al., 2014) and raw bio-oil (Salehi et al., 2011; Seyedeyn-Azad et al., 2011; Fu et al., 2014; Lan et al., 2014b). Figure 1.17 displays the effect of temperature on H_2 yield in several bio-oil reforming processes studied in the literature.

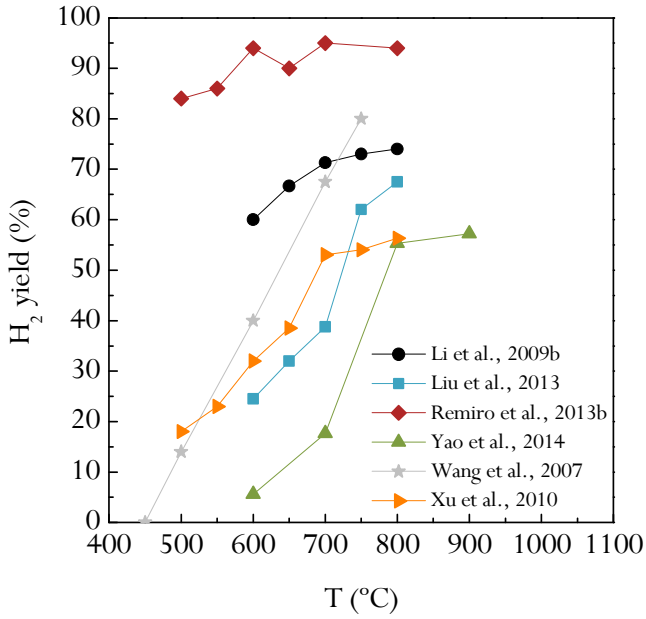

Figure 1.17. Effect of reforming temperature on hydrogen yield in bio-oil reforming processes (Wang et al., 2007; Li et al., 2009b; Xu et al., 2010; Liu et al., 2013; Remiro et al., 2013b; Yao et al., 2014).

However, most studies reveal that as temperature is increased CO_2 concentration decreases and CO concentration increases due to the thermodynamic limitations of the WGS reaction (Basagiannis and Verykios, 2007a; Remiro et al., 2013b; Yao et al., 2014).

On the other hand, using high temperatures the coke deposition can be reduced given that its in situ gasification is promoted (Wu et al., 2008a; Lan et al., 2010; Lemonidou et al., 2013; Remiro et al., 2013b). Thus, the effect of temperature on catalyst deactivation is also of great interest, given that high temperatures lead to lower coke deposits due to their gasification (Lan et al., 2010), although at the same time Ni sintering can be produced. Remiro et al. (2013b) studied the effect of reforming temperature on coke deposition in the reforming of bio-oil aqueous fraction. As temperature was increased lower coke deposition on the catalyst surface was observed, decreasing from 3.3 wt % at 500 ºC until 0 wt % at 800 ºC. Nevertheless, they observed that catalyst deactivation was also caused by Ni sintering due to the high temperature used in the reforming process, which lead to a higher Ni crystallite size as reaction temperature was increased, from 12.0 nm at 600 ºC until 23.9 nm at 800 ºC. A similar effect was also reported by the same authors in the reforming of raw bio-oil (Remiro et al., 2013a), obtaining coke contents of 3.35 and 1.14 wt % at 600 and 700 ºC, respectively. Wu et al. (2008a) studied the effect of temperature on catalyst deactivation in reforming of raw bio-oil, in which coke deposition was reduced as temperature was increased in the 700-900 ºC range from 1.97 to 0.52 wt %.

Space time

Space time is an important variable whose effect has been studied by several authors in the reforming of bio-oil. Most studies reported that higher space times enhance reforming (eq. (1.5)) and WGS (eq. (1.6)) reactions, and therefore higher H_2 yields are obtained in both reforming of aqueous bio-oil (Medrano et al., 2011; Bimbela et al., 2013; Liu et al., 2013) and raw bio-oil (Seyedeyn-Azad et al., 2011; Remiro et al., 2013a; Fu et al., 2014; Lan et al., 2014b; Xie et al., 2016). Consequently, CO concentration decreases and CO_2 concentration increases, at the same time as secondary products such as CH_4 and light hydrocarbons produced from mainly cracking reactions disappear (Basagiannis and Verykios, 2007a; Medrano et al., 2011; Bimbela et al., 2013).

Moreover, a higher space time gives way to a higher lifespan of the catalyst with time on stream. Therefore, two different $G_{C1}HSV$ values (126000 and 62300 h^{-1}) were studied by Garcia et al. (2000) in the steam reforming of bio-oil aqueous fraction and, at the highest space time value, H_2 yield remained constant for more than 22 min, while at low space time it started decreasing from the first minutes. Remiro et al. (2013b) reported that at the low space time bio-oil conversion decreased

considerably, while above 0.22 g_{cat} h $g_{bio\text{-}oil}^{-1}$ conversion was maintained almost constant for 5 h on stream.

Steam/C ratio

The most important effect of S/C ratio is the enhancement of the WGS reaction, which favours the formation of H_2 and CO_2 as main products. Figure 1.18 shows the effect of steam to C ratio on H_2 yield in several bio-oil reforming studies.

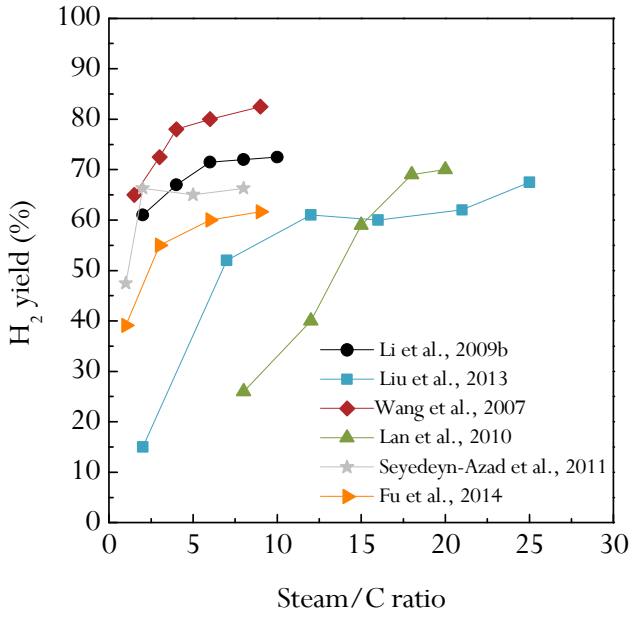

Figure 1.18. Effect of steam to C ratio on hydrogen yield in bio-oil reforming studies (Wang et al., 2007; Li et al., 2009b; Lan et al., 2010; Seyedeyn-Azad et al., 2011; Liu et al., 2013; Fu et al., 2014).

When S/C ratio was increased from 2 to 5 by Li et al. (2009) in the reforming of bio-oil aqueous fraction, H_2 yield was significantly affected, although above this value the influence of S/C ratio was less pronounced. Seyedeyn-Azad et al. (2011) reported an enhancement of the reforming and WGS reactions in the reforming of raw bio-oil, especially when S/C ratio was increased in the 1-2 range, whereas conversion and H_2 yield were not improved at higher S/C ratios. Thus, it should be pointed out that there is an optimum S/C ratio, above which H_2 yield is not improved due to excess of steam in the reaction medium (Yan et al., 2010a; Ortiz-

Toral et al., 2011; Liu et al., 2013; Fu et al., 2014). Moreover, most studies reported that CO, CH_4 and light hydrocarbons yields are decreased as S/C ratio is increased (Wang et al., 2007; Li et al., 2009b; Yan et al., 2010a; Remiro et al., 2013a; Lan et al., 2014b).

In addition, at high S/C ratios water adsorption on the catalyst surface is enhanced, favouring the gasification of coke, and therefore improving the overall reforming process (Garcia et al., 2000; Wang et al., 2007; Fu et al., 2014). Thus, when S/C ratio was increased by Li et al. (2009b), lower coke yield was obtained, with the decrease being more pronounced from 2 to 5.

1.3.2.3. Catalysts

Different catalysts have been studied in the literature in the reforming of bio-oil aqueous fraction and raw bio-oil, although Ni based are the most used ones (Garcia et al., 2000; Czernik et al., 2007; Trane et al., 2012; Lemonidou et al., 2013; Guan et al., 2016). Nevertheless, some authors also used noble metals, which are very active for reforming reactions, although its high cost is a drawback for its industrial implementation. Thus, Rioche et al. (2005) studied Rh and Pt catalysts supported on Al_2O_3 and $CeZrO_2$ in the reforming of raw bio-oil, obtaining a maximum H_2 yield of 75 % using 1 % Pt/$CeZrO_2$ catalyst, with these values being noticeably higher compared to Al_2O_3 supported catalysts.

Furthermore, different promoters have also been studied in order to improve catalyst activity and stability, with Ce, La, Mg and Ca being the most studied ones (Garcia et al., 2000; Medrano et al., 2011; Salehi et al., 2011; Valle et al., 2013). Different Ni-Al catalysts modified with Ca, Ce, Mg, Mn and Zn were used by Yao et al (2014) in the reforming of bio-oil aqueous fraction at 800 ºC and a S/C ratio of 3.54. The highest H_2 yield of 56.46 % was obtained when Ni-Mg-Al catalyst was used, followed by Ni-Ce-Al (55.30 %) and Ni-Zn-Al (52.01 %) catalysts.

Moreover, increasing attention is being paid to the use of CO_2 adsorbents in reforming processes, given that the thermodynamic equilibrium of bio-oil reforming reaction is shifted, and therefore higher H_2 yields are obtained (Yan et al., 2010b; Nahil et al., 2013; Remiro et al., 2013a,c; Xie et al., 2015a). Thus, Remiro et al. (2013c) used dolomite as CO_2 adsorbent in the catalytic steam reforming of bio-oil aqueous fraction, obtaining full conversion of the bio-oil and H_2 yields around 99 %. They also performed the reforming of raw bio-oil using dolomite (Remiro et al.,

2013a), obtaining a H_2 yield of 82 % at 600 ºC, $G_{C1}HSV$= 7000 h^{-1} and S/C ratio of 1.1. Nevertheless, further studies dealing with reaction/regeneration cycles are required in order to study the loss of activity of the adsorbents.

Concerning catalyst deactivation, some authors reported high deactivation due to coke deposition on catalyst surface. Catalyst deactivation leads to secondary reactions, such as thermal decomposition of bio-oil (eq. (1.4)) and Boudouard (eq. (1.3)) reactions. Although it has not been extensively studied in the literature, some authors reported that H_2 and CO_2 yields decrease and CO, CH_4 and hydrocarbons yields increase with time on stream due to the attenuation of oxygenated compound reforming and the enhancement of the secondary reactions in the reforming of bio-oil (Czernik et al., 2002; Medrano et al., 2011; Liu et al., 2013; Remiro et al., 2013b). Moreover, coke deposition may also be attributed to the repolymerization of the phenolic compounds in the bio-oil (Rennard et al., 2010) and to the secondary reactions of CH_4 decomposition and Boudouard reaction.

1.3.2.4. Bio-oil steam gasification

Bio-oil gasification has been proposed as an alternative to biomass gasification for syngas production, with the aim of reducing the expensive biomass transport costs (Li and Hu, 2014). Therefore, as in the case of bio-oil reforming, several decentralized pyrolysis plants coupled with a centralized bio-oil gasification facility would be required in order to take advantage of the economies of scale (Li et al., 2015) (Figure 1.19). In addition, the pyrolysis char may also be upgraded with the bio-oil, by feeding it as bio-slurry, thus taking advantage of the potential of biomass pyrolysis char to produce H_2 (Trippe et al., 2011). In this way, the biomass that has an energy density of about 2 GJ/m^3 is upgraded to a bio-slurry with a density of 25 GJ/m^3, thereby considerably reducing the transport costs (Sikarwar et al., 2016). It has been reported that bio-oil gasification becomes more attractive economically than biomass gasification for large scale plants, low energy density biomass and very long transport distances. However, improvements in biomass pyrolysis efficiency and gasification plants' capital costs would make bio-oil gasification cost-competitive also in smaller distances (Braimakis et al., 2014).

The differences between bio-oil gasification and reforming are vague and sometimes are not well distinguished in the literature. In this thesis, gasification has been considered as the process that takes place at higher temperatures than bio-oil reforming (around 800-1400 ºC), and is carried out non-catalytically or in the

presence of primary mineral catalysts, as in biomass gasification. Therefore, bio-oil gasification produces a syngas with a similar composition than the one obtained in biomass gasification, whereas bio-oil reforming yields a gas with higher H_2 content. The lower H_2 yield and energy efficiency and higher costs of bio-oil gasification are responsible for the lower technological development of this thermochemical route (Zhang et al., 2013).

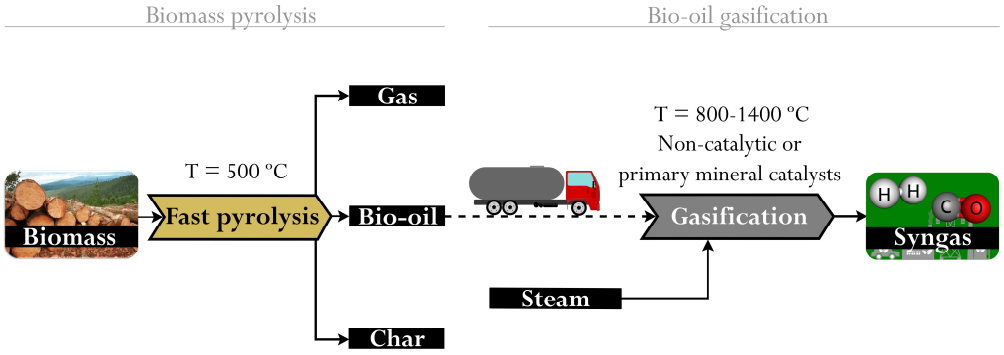

Figure 1.19. Schematic representation of the bio-oil steam gasification process for hydrogen production.

The H_2 productions (defined in this section as $g_{H2}/100\ g_{bio\text{-}oil}$) obtained by several authors in the literature vary in a wide range, as a result of differences in the bio-oils used, reactor configurations and operating conditions. In the non-catalytic studies analyzed, the average H_2 production can be established at around 4 wt %, although values between 1.4 and 12.6 wt % have been reported. Thus, Panigrahi et al. (2003), operating in a fixed bed micro-reactor at 800 ºC, obtained the maximum H_2 production of 4.4 wt % with a S/C ratio of 2. A similar value of 4 wt % was attained by Kan et al. (2010), also in a fixed bed at 800 ºC and a S/C of 10.6. Furthermore, Latifi et al. (2015), operating in a Jiggle bed reactor at 800 ºC, without adding additional steam to the bio-oil, observed a H_2 production of 3.5 wt %. Van Rossum et al. (2007) obtained a lower H_2 production of 1.4 wt % in a fluidized bed at 790 ºC and S/C of 1.9. However, the tar content reported in the gas was of 2.6 g/Nm^3, which is significantly lower than the average values obtained in biomass non-catalytic gasification processes. Finally, Chhiti et al. (2011) reached the highest H_2 production of 12.6 wt % at 1400 ºC and S/C ratio of 8.3 in a laboratory scale high temperature entrained flow reactor.

1.4. PYROLYSIS AND IN-LINE REFORMING OF BIOMASS

Among the different thermochemical routes aforementioned for H_2 production from biomass, the two-stage pyrolysis-reforming strategy has been gaining increasing attention recently (Figure 1.20), given that it has several advantages in relation to gasification process due to the separation of pyrolysis and reforming steps in different zones. Thus, this process allows for independent temperature optimization in the pyrolysis and reforming steps (Park et al., 2010). Moreover, compared to catalytic gasification process, the direct contact between the feedstock and its impurities with the reforming catalyst is avoided (Wu and Williams, 2010a). In addition, the reforming step is carried out at lower temperature in relation to catalytic gasification, and therefore catalyst deactivation by sintering can be avoided (Barbarias et al., 2016a,b,c), especially when Ni is used as active phase, which is the most widely used catalyst in reforming of oxygenated compounds and hydrocarbons. In addition, the gasification process does not focus on H_2 production, but syngas is the main product. The quality and concentration of the syngas depends on the gasifying agent used, and therefore subsequent catalytic processes are needed to enhance H_2 production. Moreover, highly active steam reforming catalysts allow for attaining complete conversion of biomass derived volatiles, with the gas product being free of tars, which is a remarkable advantage over conventional gasification.

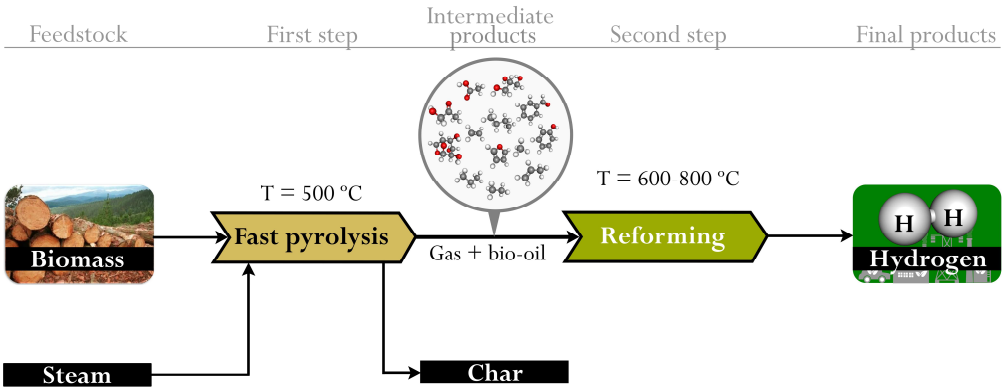

Figure 1.20. Schematic representation of the pyrolysis-reforming of biomass.

Regarding bio-oil reforming, volatiles from biomass are valorised in-line, and therefore condensation and volatilization of the intermediate compounds from biomass pyrolysis are not required, which avoids the difficult handling of these products in addition to possible mass loss and re-polymerization during the raw bio-

oil volatilization step. Moreover, the main advantage of the pyrolysis-reforming process lies in its ease scaling up with continuous feed.

Although the routes described in previous sections such as direct gasification or bio-oil reforming have been extensively studied in the literature, the operating problems reported by some authors in these processes have made the two-step process an interesting alternative for H_2 production from biomass. The reactions involved in the reforming of biomass pyrolysis volatiles are those aforementioned for bio-oil reforming in Table 1.3, i.e., the reforming of bio-oil (eq. (1.5)), CH_4 (eq. (1.7)), light hydrocarbons (eq. (1.8)) and WGS (eq. (1.6)) reactions are the main reactions. Moreover, when the catalyst is deactivated, secondary reactions such as cracking (eq. (1.4)), interconversion (eq. (1.11)), methanation (eqs. (1.12) and (1.13)) or Boudouard (eq. (1.3)) reactions may take place.

Therefore, the following section focuses on an in-depth review on this process, in which the most relevant factors affecting product distribution will be discussed. Among others, the type of the reactor for both pyrolysis and reforming steps and their configuration plays an essential role for the process. Therefore, a comparison of the most relevant results in the literature using different feeds, catalyst and operating conditions for the two-stage pyrolysis-reforming process is summarized in Table 1.6. The results have been arranged according to the reactor configuration used in each study.

Table 1.6. Studies involving different strategies, feeds, catalysts and operating conditions, and main results obtained (maximum H_2 production) reported in the literature for the pyrolysis and in-line reforming of biomass.

Reactor configuration	Biomass	Catalyst	Operating conditions	H_2 concentration (vol %)	H_2 production (wt %)[a]	Reference
Fixed bed / fixed bed	Wood sawdust	10 wt % Ni/Al_2O_3	T_P= 300, 400, 500, 600 °C (40 °C min^{-1}) T_R= 800 °C Steam flow rate= 4.74 g h^{-1} (second step)	38.1	2.2	Olaleye et al., 2014
Fixed bed / fixed bed	Wood sawdust	nano Fe-Zn/Al_2O_3 *Zn/Al ratio: 1:1, 1:2, 1:3, 1:4*	T_P= 500 °C (40 °C min^{-1}) T_R= 800 °C Steam flow rate= 0.05 g min^{-1} (second step)	40	1.9	Chen et al., 2015
Fixed bed / fixed bed	Wood sawdust	$Ni/CaAlO_x$ *Ca/Al molar ratio:* 1:3, 1:2, 1:1, 2:1, 3:1	T_P= 500 °C (40 °C min^{-1}) T_R= 800 °C Steam flow rate= 0.05 g min^{-1} (second step)	45	3.1	Chen et al., 2016
Fixed bed / fixed bed	Cellulose	15 wt % Ni/Al_2O_3	T_P= - T_R= 800 °C Steam flow rate= 0, 0.01, 0.02, 0.1, 0.2 g min^{-1} (second step)	-	5.9	Zou et al., 2016
Fixed bed / fixed bed	Rice husk / sugar cane bagasse / wheat straw	Dolomite 10 wt % Ni/dolomite	T_P= 950 °C (20 °C min^{-1}) T_R= 950 °C Steam flow rate= 0.1 g min^{-1} (second step) Steam/biomass ratio= 1.37	59.1	5.1	Waheed and Williams, 2013
Fixed bed / fixed bed	Pine wood chip / pig manure compost	Ni-brown coal char	T_P= 700 °C (10 °C min^{-1}) T_R= 450-700 °C	-	10.0	Xiao et al., 2013
Fixed bed / fixed bed	Sewage sludge	Commercial Ni/Al_2O_3	T_P= 900 °C (10 °C min^{-1}) T_R= 400-750 °C Space velocity= 4000-8000 h^{-1} Steam partial pressure= 30-53 kPa (second step)	70	11.6	Cao et al., 2014

Table 1.6. Continued.

Reactor configuration	Biomass	Catalyst	Operating conditions	H_2 concentration (vol %)	H_2 production (wt %)[a]	Reference
Fixed bed / fixed bed	Rice husk	Raw, char, Fe char, Ni-Fe/char, Ni-Fe char and Ni char	T_P= 800 °C T_R= 600-900 °C	31.5	5.5	Shen et al., 2014a
Fixed bed / fixed bed	Rice husk	Ni-rice husk char (RHC)	T_P= 750 °C T_R= 500-900 °C	24.3	-	Shen et al., 2015
Fluidized bed / fixed bed	Pine wood chip / pig manure compost	Ni/Al_2O_3 and Ni-brown coal char	T_P= 530-700 °C T_R= 550-710 °C Space velocity= 9100-11300 h^{-1} S/C ratio= 0-3 (first step)	60	9.3	Xiao et al., 2011
Screw-kiln / fixed bed	Wood pellets	NiO/Al_2O_3 NiO/CeO_2/Al_2O_3 NiO/SiO_2	T_P= 500 °C T_R= 760 °C Biomass feed rate= 0.24 kg h^{-1} Steam (second step)	44.4	-	Efika et al., 2012
Fluidized bed / entrained flow / fixed bed	Timber wood sawdust	NiO/MgO	T_P= 600 °C T_G= 700, 750, 800, 850 °C T_R= 700, 750, 800, 850 °C Steam/biomass ratio= 3 (first step) Biomass/catalyst ratio= 1	51	7.6	Ma et al., 2014

[a] H_2 production defined as g_{H2}/100 $g_{biomass}$.

1.4.1. Reactor configurations

The main reactors used in the literature for biomass pyrolysis are bubbling fluid beds, circulating fluid beds and transporter beds, rotating cone, ablative reactor, vacuum reactor, screw kiln reactor and spouted bed reactor (Bridgwater, 2012), which have been described in Section 1.3.1.2. The kind of pyrolysis reactor and its features are relevant factors, given that they condition the distribution of pyrolysis products and their yields. Thus, bubbling fluidized bed reactors are the most developed technology, using sand as fluidizing solid because it allows an excellent gas-solid contact, and therefore improves heat transfer (Bridgwater, 2012). Moreover, it should be taken into account that the product stream of the pyrolysis step is the feed of the subsequent reforming step, which is usually carried out in fixed or fluidized bed reactors. Although the use of fixed bed reactors is more extended, fluidized bed reactors avoid operational problems related to bed blockage by coke deposition in the reforming step (Lan et al., 2010; Erkiaga et al., 2015). Thus, Figure 1.21 shows the different reactor configurations studied in the literature for this two-step process.

The group headed by Prof. Williams carries out the process in discontinuous mode, using a two-stage fixed bed reactor (Figure 1.21a), in which the biomass is pyrolyzed in the first stage and the volatiles from the pyrolysis circulate through the catalytic reforming step, with wood sawdust being the feedstock used for most of the studies (Olaleye et al., 2014; Chen et al., 2016), although other materials, such as cellulose (Zou et al., 2016), rice husk, sugar cane bagasse and wheat straw (Waheed and Williams, 2013) or biomass/plastic mixtures (Alvarez et al., 2014a; Kumagai et al., 2015) have also been investigated. This two-stage fixed bed reactor strategy has also been used by Xiao et al. (2013) and Cao et al. (2014) for the pyrolysis-reforming of different materials, such as pine wood chip, pig manure compost and sewage sludge. The process developed by the research group headed by Prof. Yoshikawa consists also in a two-step pyrolysis-reforming reactor, in which pyrolysis and reforming zones are also separate (Shen et al., 2014a,b, 2015).

Although most studies in the literature are carried out in laboratory-scale batch reactors, Xiao et al. (2011) worked in a two stage fluidized-fixed bed configuration with continuous biomass in the feed, with the pyrolysis step being carried out in a fluidized bed reactor of silica sand and the reforming step in a fixed bed reactor on a commercial Ni/Al_2O_3 and Ni/BCC (brown coal char) bed (Figure 1.21b). Wang et al. (2013a) used a similar configuration, in which continuous pyrolysis of cellulose was carried out at the lower section of the reactor (fluidized bed) and the upper

section is the reactor for catalytic reforming step (fixed bed). Koike et al. (2013) and Li et al. (2013, 2014) studied the pyrolysis-reforming process in a continuous feed laboratory scale dual-bed reactor, which includes a primary bed for biomass pyrolysis and a secondary catalyst bed for the reforming of pyrolysis products. A different reactor configuration was used by Efika et al. (2012), which was provided by a screw-kiln reactor for the continuous biomass pyrolysis and a fixed bed reactor for the reforming of pyrolysis vapours (Figure 1.21c).

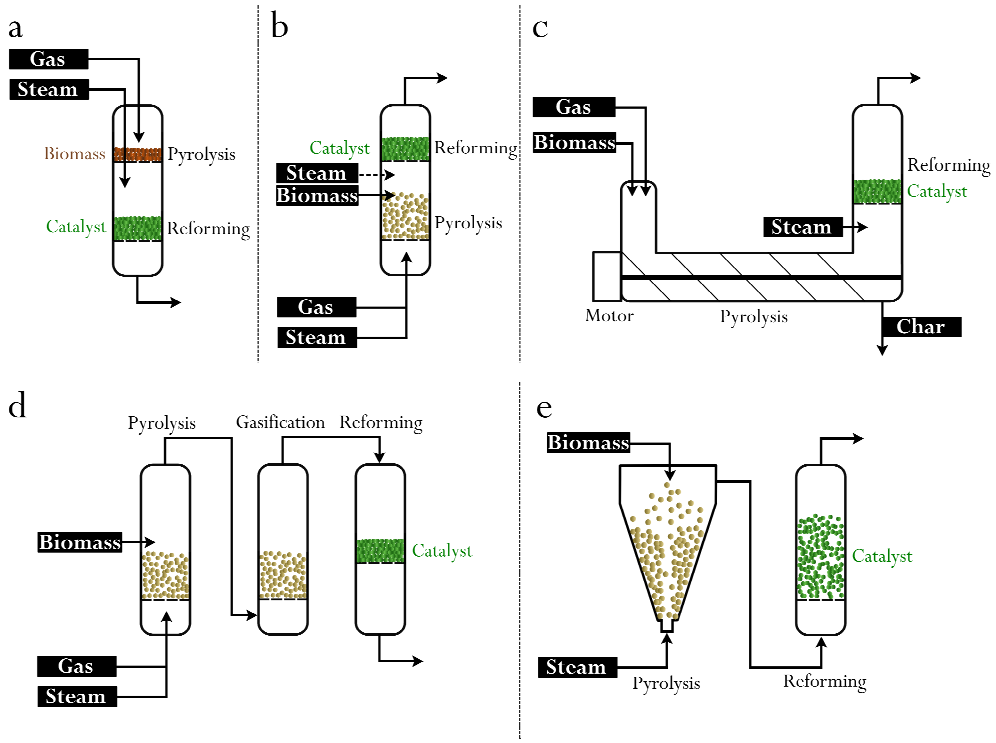

Figure 1.21. Reactor configurations for pyrolysis and in-line catalytic steam reforming of biomass: a) fixed – fixed bed reactor; b) fluidized – fixed bed reactor; c) screw kiln – fixed bed reactor; d) fluidized bed, entrained flow and fixed bed reactor, and; e) spouted bed – fluidized bed reactor.

Ma et al. (2014) improved this two step process introducing another stage between the pyrolysis and reforming reactors for gas-solid simultaneous gasification (Figure 1.21d). Therefore, a first fluidized bed stage for biomass pyrolysis has been used, followed by the second stage of entrained flow gasification and subsequently the fixed bed catalytic steam reforming reactor.

In this thesis, a different system configuration has been used for the pyrolysis-catalytic steam reforming of biomass and biomass/HDPE mixtures, in which a conical spouted bed reactor has been used for pyrolysis step and the volatiles stream has been introduced in a fluidized bed reforming reactor (Figure 1.21e). In previous works of the research group, Erkiaga et al. (2015) studied the pyrolysis and in-line catalytic steam reforming of HDPE using a conical spouted bed-fixed bed configuration, where operational problems were reported due to bed blockage by coke deposition. Therefore, Barbarias et al. (2016a) installed a fluidized bed reactor as reforming reactor, which allows working continuously without operational problems for longer period of time. Moreover, this technology has many possibilities for industrial implementation, due to the suitability of the conical spouted bed for the pyrolysis step (Lopez et al., 2009; Elordi et al., 2011a; Artetxe et al., 2012a; Alvarez et al., 2014b, 2015; Amutio et al., 2015), which has been satisfactorily scaled up for the continuous pyrolysis of 25 kg h^{-1} of biomass (Fernandez-Akarregi et al., 2013; Makibar et al., 2015).

Thus, some of the technologies currently used for the pyrolysis-reforming process have some issues to resolve due to the discontinuous mode of the process. Nevertheless, as described above, great progress has been made recently, especially for the implementation of continuous biomass feed integrated into different kinds of reactors and configurations, with all these improvements contributing to the successful scaling up of the process.

1.4.2. Catalysts

Although different catalysts can be used for reforming of oxygenated compounds, the most used ones are those based on Ni and Co due mainly to its low cost in relation to noble metals, such as, Pt, Pd, Ru or Rh. Efika et al. (2012) investigated three different catalysts: NiO/Al_2O_3, $NiO/CeO_2/Al_2O_3$ and NiO/SiO_2 (prepared by an incipient wetness method and by a sol-gel method). The sol-gel NiO/SiO_2 catalyst produced the highest gas yield, while $NiO/CeO_2/Al_2O_3$ was the catalyst with the lowest gas production. Nevertheless, NiO/Al_2O_3 was the catalyst giving the highest H_2 concentration of 44.4 vol %. Koike et al. (2013) compared three different catalysts and the lower coke formation was observed for $Ni+MnO_x/Al_2O_3$ followed by $Ni+CeO_2/Al_2O_3$ and Ni/Al_2O_3 catalysts. Li et al. (2014) investigated Ni-Cu/Mg/Al bimetallic catalysts with different Cu/Ni ratios, obtaining higher activity and lower deactivation by coke when Cu/Ni ratio was 0.25, with the results being better compared to monometallic Ni/Mg/Al and Cu/Mg/Al catalysts. Chen et al.

(2015) studied Fe-Zn/Al_2O_3 nanocatalysts with different Zn/Al ratios (1:1, 1:2, 1:3 and 1:4), and a maximum H_2 concentration and production of 40 vol % and 1.9 wt %, respectively, were obtained when 1:1 ratio was used. They have also investigated Ni/$CaAlO_x$ catalysts with different Ca/Al molar ratios (1:3, 1:2, 1:1, 2:1 and 3:1) (Chen et al., 2016) and H_2 concentration and production of 45 vol % and 3.1 wt %, respectively, were obtained when a Ca/Al molar ratio of 1:2 was used.

Concerning catalyst supports, although Al_2O_3 is commonly used, different kinds of supports can be found in the literature. Li et al. (2013) reported a higher activity for Co catalyst when they are supported on $BaAl_{12}O_{19}$ than on other supports, such as Al_2O_3, ZrO_2, SiO_2, MgO and TiO_2 due to its high dispersion. Moreover, Waheed and Williams (2013) made a comparison of dolomite and 10 wt % Ni-dolomite catalysts, and a better performance of Ni-dolomite catalyst was reported, obtaining a maximum H_2 concentration and production of 59.1 vol % and 5.1 wt %, respectively, when rice husk was valorised.

Furthermore, the use of char is gaining increasing attention recently and several studies using it as support have been published. Thus, Xiao et al. (2011) compared a commercial Ni/Al_2O_3 catalyst and Ni/BCC (brown coal char), and higher H_2, CO and CH_4 yields, lower tar content and higher resistance to coke deposition were observed when Ni/BCC catalyst was used. The group headed by prof. Yoshikawa also studied Ni-Fe catalysts (Shen et al., 2014a) and Ni catalysts (Shen et al., 2014b, 2015) supported on rice husk char (RHC). They reported higher tar removal efficiency with RHC Ni and RHC Ni-B catalysts, 96.9 and 98.6 %, respectively, compared to Ni-Fe char catalyst, for which a maximum efficiency of 92.3 % was achieved. It should be pointed out that the recovery of the char from the pyrolysis step is of great interest for the viability of the process.

1.4.3. Plastic co-feeding

The production of H_2 by pyrolysis and in-line catalytic steam reforming of plastics is an alternative which has not been extensively studied in the literature, although it is probably the most promising route for plastic valorisation due to its operational advantages. On the one hand, the impurities contained in the plastic waste remain in the pyrolysis reactor, which avoids their contact with the reforming catalyst and its deactivation; on the other hand, an independent temperature optimization can be carried out in the thermal degradation and the catalytic steam reforming steps (Park

et al., 2010), which is a great advantage compared to the direct gasification, as the material costs and the sintering problems of the reforming catalyst are minimized.

The pioneering studies of pyrolysis and in-line steam reforming of plastics have been carried out by Czernik and French in an experimental unit made up of two fluidized bed reactors for the pyrolysis and reforming steps, using a Ni based commercial catalyst in the reforming step (Czernik and French, 2006). Operating with continuous PP feed (1 g min^{-1}) and at pyrolysis and reforming temperatures of 650 and 800 ºC, respectively, a H_2 production of 34.0 wt % was obtained, obtaining a tar-free gas product. The H_2 production was reduced to 24.0 wt % when operating under autothermal conditions by co-feeding air (ER 0.25) into the reforming step. Interestingly, the process was able to operate under steady state conditions for 10 h without detectable catalyst deactivation.

The research group headed by Prof. Williams has widely studied the pyrolysis and reforming of waste plastics over different catalysts (Wu and Williams, 2009a,b,c,d, 2010a,b; Acomb et al., 2014; Saad et al., 2015). These studies were carried out in a laboratory reactor made up of two fixed bed reactors and operating in batch regime. The plastic sample was of around 1 g and was heated in the pyrolysis reactor (40 ºC min^{-1} to 500 ºC), with the volatiles formed being subsequently treated in the reforming reactor at 800 ºC. Using a Ni-Mg-Al catalyst the H_2 production was of 24.0 and 30.3 wt % for PP and HDPE, respectively (Wu and Williams, 2010a), which were below those reported by Czernik and French (2006). The two step process developed by Namioka et al. (2011) and Park et al. (2010) for the pyrolysis and reforming of PP was based on two fixed bed reactors operating in continuous regime (1 g min^{-1}). A maximum H_2 production of 34.2 wt % was obtained at a reforming temperature of 630 ºC, obtaining full conversion of liquid hydrocarbons to gaseous products (and coke).

In our research group, the pyrolysis and in-line reforming of HDPE was studied by Erkiaga et al. (2015) using a conical spouted bed-fixed bed configuration. The pyrolysis was carried out at 500 ºC and the reforming step at 700 ºC over a Ni commercial catalyst. The reforming catalyst promoted the complete conversion of pyrolysis volatiles to yield gases, with the H_2 production and yield being 34.5 wt % and 81.5 %, respectively (based on the the maximum allowed by stoichiometry).The main challenge of this process was coke formation (4.4 wt % of the plastic in the feed) which blocked reactant flow in the fixed bed reforming reactor. These operational problems were avoided in a latter study replacing the fixed bed by a fluidized bed reactor for the reforming step (Barbarias et al., 2016a). Thus, operating

at the same temperatures in the pyrolysis and reforming steps the H_2 production and yield increased to 38.1 wt % and 92.5 %, respectively (based on the maximum allowed by stoichiometry). This improvement clearly remarks the advantages of using a fluidized bed reactor for the reforming step.

As a consequence of the good results obtained in the pyrolysis-reforming of HDPE in previous studies, the joint valorisation of biomass and plastics is another alternative regarded as a feasible joint valorisation route (Figure 1.22). On the one hand, the low H content and high O content of the biomass are drawbacks for high H_2 production; on the other hand, the catalyst undergoes a considerable deactivation by coke. Furthermore, the co-feeding solves the seasonal limitations of biomass availability and contributes to attenuating the environmental problems associated with waste plastic management. Consequently, the valorisation of biomass and plastic mixtures allows increasing H_2 production and attenuating catalyst deactivation compared to only biomass in the feed.

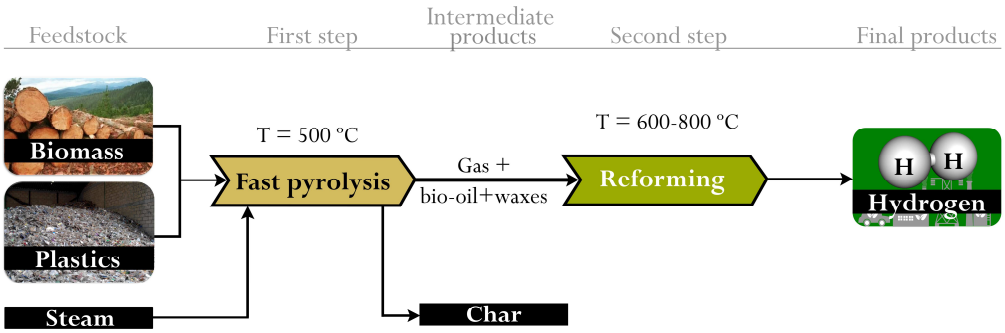

Figure 1.22. Schematic representation of the pyrolysis-reforming of biomass and plastics mixtures.

Although pyrolysis is considered a suitable route for the valorisation of waste plastics on a large-scale, and particularly for polyolefins (Wong et al., 2015; Anuar Sharuddin et al., 2016; Kunwar et al., 2016), studies involving pyrolysis and in-line catalytic steam reforming of biomass-plastic mixtures are very scarce. Alvarez et al. (2014a) studied the co-feeding of polypropylene in the pyrolysis-reforming of biomass in a batch laboratory scale reactor, and they obtained higher gas yields and higher H_2 productions than those for only biomass in the feed. In the same experimental unit, Kumagai et al. (2015) performed the pyrolysis-reforming of a biomass/polypropylene mixture on a Ni-Mg-Al-Ca catalyst synthesized by co-precipitation and they obtained a maximum H_2 production of 6.0 wt % when the catalyst was calcined at 500 °C.

2

EXPERIMENTAL

2. EXPERIMENTAL

2.1. MATERIALS

2.1.1. Feeds

Biomass and high density polyethylene (HDPE) are the materials fed into the pyrolysis and in-line catalytic steam reforming process.

2.1.1.1. Biomass

The biomass used is forest pine wood waste *(pinus insignis)* from the wood industry (sawmill), which has not being treated with any product and whose main properties are summarized in Table 2.1. The biomass has been crushed, ground and sieved to a particle size between 1-2 mm in order to ease the feeding operation. This particle size allows continuously feeding with low flows and providing the heat transfer required for the pyrolysis step.

Table 2.1. Pine wood sawdust characterization.

Ultimate analysis (wt %)	
Carbon	49.33
Hydrogen	6.06
Nitrogen	0.04
Oxygen	44.57
Proximate analysis (wt %)	
Volatile matter	73.4
Fixed carbon	16.7
Ash	0.5
Moisture	9.4
HHV (MJ kg^{-1})	**19.8**

The ultimate analysis has been determined in a *LECO CHN-932* and *VTF-900* elemental analyzer. The ultra-microbalance *SARTORIUS M2P* (precision ± 0.001 mg) is connected in-line to a computer for the processing of the data provided by the analyzer. As observed in Table 2.1, the amount of N is almost negligible, so its empirical formula is as follows: $CH_{1.47}O_{0.67}$. Furthermore, the proximate analysis (volatile matter, fixed carbon and ashes) has been determined in a thermogravimetric analyzer *TA Instruments TGA Q5000IR*. First of all, the sample is heated in inert atmosphere to 900 ºC and the corresponding mass loss is attributed to the volatile matter. Then, air is introduced, which leads to the combustion of fixed carbon, with the remaining amount of solid corresponding to the ashes. Finally, the higher heating value (HHV) has been measured in a *Parr 1356* isoperibolic bomb calorimeter.

2.1.1.2. High density polyethylene (HDPE)

The high density polyethylene (HDPE) was provided by *Dow Chemical* (Tarragona) in the form of chippings with a particle diameter of around 4 mm. The main properties of the polymer have been summarized in Table 2.2. The HDPE has been fed as supplied, due to the good performance of the conical spouted bed reactor for pyrolysing this size plastic materials. The properties of the plastics, average molecular weight, particle density and polydispersity (ratio between the weight average molecular weight and the number average molecular weight) have been provided by the suppliers. The high heating value (HHV) has been determined in a differential scanning calorimeter (*Setaram TG-DSC 11*) and in an isoperibolic bomb calorimeter *(Parr 1356)*.

Table 2.2. Properties of the plastic material (HDPE) used in the process.

	M_W (g mol^{-1})	Polydispersity	ρ (kg m^{-3})	HHV (MJ kg^{-1})
HDPE	46200	2.9	940	43

2.1.2. Catalyst

The reforming catalyst is a CH_4 reforming commercial catalyst called ReforMax® 330 (G90LDP), which has been provided by *Süd Chemie*. The original catalyst has a shape of perforated rings (19 x 16 mm), but it was ground and sieved to 0.4-0.8 mm, which is the suitable particle size to attain a stable fluidization regime.

The metallic phase is Ni supported on Al_2O_3, which is doped with Ca, with the content of NiO being 14 wt %. Due to the confidentiality agreement signed with the company, the composition of the catalyst cannot be revealed. However, its chemical formulation is based on NiO, $CaAl_2O_4$ and Al_2O_3.

2.2. PILOT PLANT

The general scheme of the pilot plant used in the pyrolysis and in-line catalytic steam reforming process is shown in Figure 2.1. The development of this plant is based on the previous experience of the research group in cold fluid dynamic studies (Olazar et al., 1992, 1993b,d, 1994a,c) and the design and use of other plants, with the conical spouted bed reactor, in the pyrolysis and gasification of biomass (Aguado, 1999; Amutio, 2011; Erkiaga, 2014), pyrolysis of tyres (Velez, 2004; Arabiourrutia, 2007; Lopez, 2008), pyrolysis and gasification of plastics (Gaisan, 2002; Elordi, 2010; Artetxe, 2012; Erkiaga, 2014) and pyrolysis and in-line reforming of plastic wastes (Barbarias, 2015).

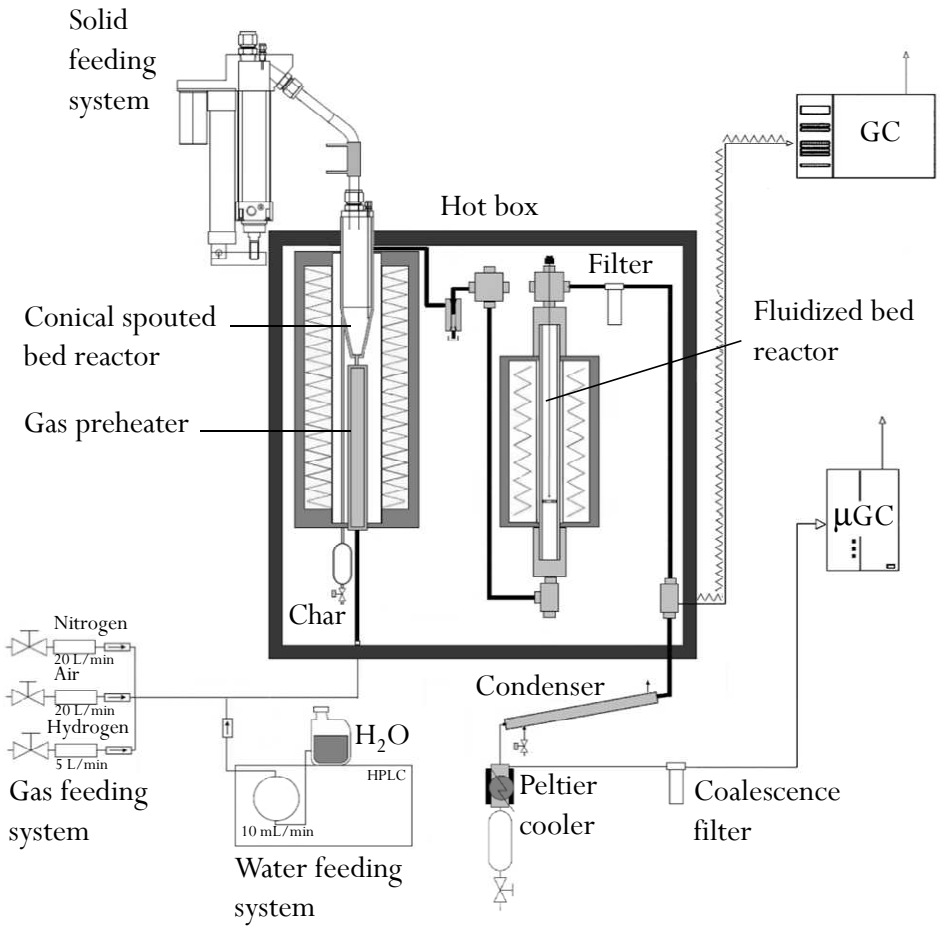

Figure 2.1. Scheme of the laboratory scale pyrolysis-reforming plant.

The pilot plant consists of the following components: 1) solid feeding system; 2) gas feeding system; 3) water feeding system; 4) reaction system; 5) product separation system; 6) control system, and; 7) gas analysis system.

Furthermore, the unit is provided with a differential pressure gauge for detecting increases in pressure drop caused by filter clogging, and therefore the need for its replacement. Below, each component of the pilot plant is described.

2.2.1. Solid feeding system

The system for feeding the solid (biomass and HDPE) into the pyrolysis reactor (Figure 2.2) consists of a dosage cylinder with 20 mm in internal diameter, provided with 40 cm stroke piston, which pushes the solid towards the top of the feeding system. In order to ease the solid dosage, the feeding system is provided with a vibrator, which is activated by a switch on the control unit.

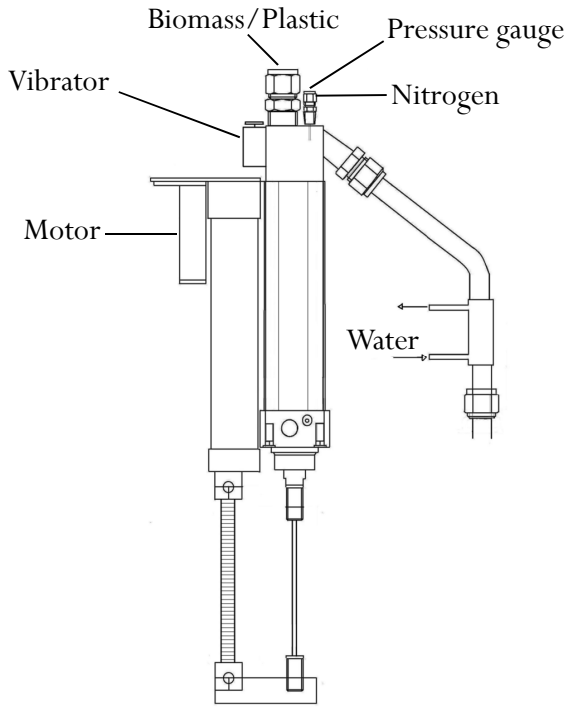

Figure 2.2. Solid feeding dispenser.

The different feeds are loaded into the dispenser through an inlet located at the top of the feeding system. By ascending the piston, the biomass and/or HDPE fall into the reactor through a 3/4" tube, which is cooled with tap water, in order to avoid the melting of the material before the reactor inlet (bigger problem with HDPE). A very small flow rate of an inert gas (N_2) is fed through a 1/8" tube to ease the solid flow into the reactor and avoid the condensation of pyrolysis volatiles and steam in the dispenser.

The rate of ascent of the piston is regulated by a *Toho 204* controller, programmed for a speed between 0 and 100 %, where the value 100 corresponds to the maximum ascent velocity of 35 mm min^{-1}, i.e., the maximum flow rate of 2 g min^{-1} of biomass and 5.5 g min^{-1} of HDPE.

2.2.2. Gas feeding system

N_2, air and H_2 are fed into the lower part of the pyrolysis reactor. Accordingly, the following components have been installed:

- *Manual valves (HOKE).* They allow the entrance of each gas to the system by manual opening. Three valves have been installed, one for each gas line, with the maximum design pressure and temperature being 345 bar and 232 °C, respectively.

- *Mass flow controllers (MFCs).* Three mass flow controllers *(Bronkhorst High-Tech)* have been used in order to control the flow rate of each of the three gas supply lines. The three MFCs have a maximum design pressure of 8 bar, and inlet and outlet pressures of 4 and 1 bar, respectively. The N_2 and air flow controllers provide a maximum flow rate of 20 L min^{-1}, while the H_2 controller provides 5 L min^{-1}.

- *Non-return valves (HOKE):* They are located after the mass flow controllers and avoid the flow in the opposite direction. The maximum design pressure and temperature of these valves are 414 bar and 177 °C, respectively. The three gas lines are joined together to give a single input gaseous stream into the reactor.

2.2.3. Water feeding system

The steam required for the reforming step and for the fluidization of both conical spouted bed and fluidized bed reactors is generated by a high pressure pump *Gilson 307*. It is a positive displacement pump, with a maximum design flow being of 10 mL min^{-1}. The water circulates through a pressure regulating valve *(back pressure)*, which avoids the flow in the opposite direction in the line and generates an overpressure of 34 bar in the pump head in relation to the reaction system, improving the operation of the pump. The water is vaporized prior to entering the gas preheater in a spiral pipe wound around the heating cartridge, which is located inside the hot box.

2.2.4. Reaction system

The reaction system consists of the following elements: 1) pyrolysis reactor (conical spouted bed reactor), and; 2) catalytic reforming reactor (fluidized bed reactor). These elements are located inside a forced convection oven, which is an 800 x 800 x 800 mm stainless steel box. This oven has two heating cartridges of 1500 W each one and two centrifugal fans to cause forced convection, in order to maintain the box temperature at 300 ºC. This external oven avoids the condensation of heavy compounds before and after the fluidized bed reactor, which in the latter case is essential to avoid the condensation of volatile products prior to chromatographic analysis.

2.2.4.1. Pyrolysis reactor

The pyrolysis reactor is a spouted bed reactor with a conical geometry, with a cylindrical section in the upper part (Figure 2.3). The main dimensions of the pyrolysis reactor are as follows: total height of the reactor, H_T, 298 mm, height of the conical section, H_C, 73 mm and the angle of the conical section, γ, 30 °. The diameter of the cylindrical section, D_C, is 60.3 mm, the diameter of the bed bottom, D_i, 12.5 mm and the diameter of the gas inlet, D_0, 7.6 mm. These dimensions ensure the stability of the bed, with a great versatility in operating conditions, and they have been established based on the prior knowledge of the research group in the studies dealing with the fluid dynamics of the spouted bed reactor for different materials (Olazar et al., 1992, 1993a,d, 1994c, 1995a; San José et al., 1993, 1995).

This versatility allows working with a wide range of gas flow rates, so that when the velocity of the particles is increased, the collisions between particles and their energy

are maximized, avoiding the segregation of the bed. Furthermore, the high velocity of the gas reduces the residence time in the reactor, from values around 1 s to close to 20 ms (Olazar et al., 1994b; San José et al., 1995), minimizing the transformation of the volatiles by secondary reactions, and therefore maximizing the bio-oil yield in biomass pyrolysis (Amutio et al., 2012a) and waxes yield in HDPE pyrolysis (Elordi et al., 2011a). The high velocity of both gas and solid contributes to improving the heat transfer between phases (Makibar et al., 2011). These characteristics explain the good performance of the conical spouted bed reactor in processes such as flash pyrolysis, and particularly, in the pyrolysis of irregular texture, non-uniform size and/or sticky materials, whose use has serious limitations with other G-S contact technologies.

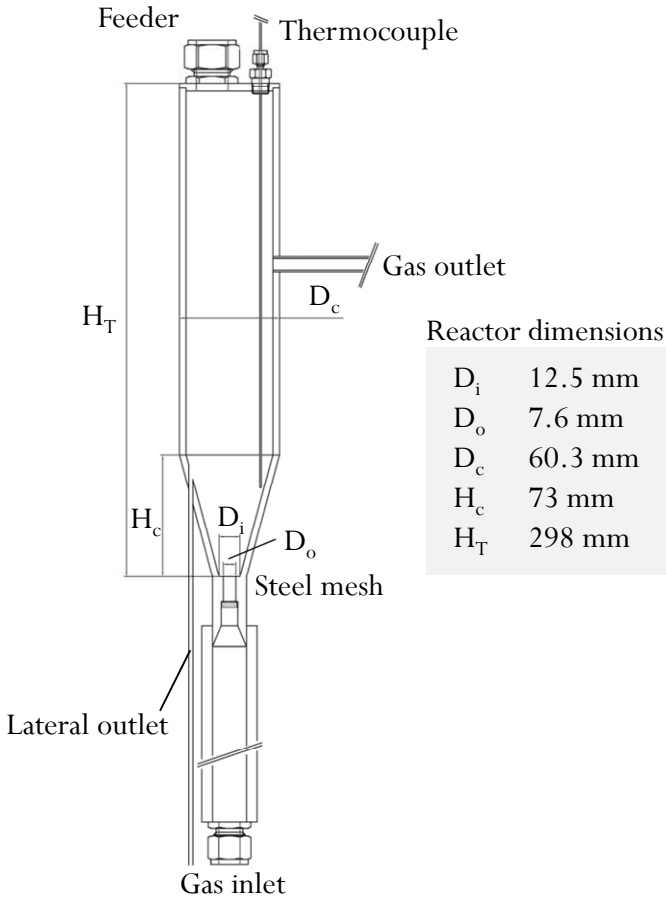

Figure 2.3. Scheme of the conical spouted bed reactor and its main dimensions.

In addition to the solid feeding tube, the reactor is equipped with a 1/8" entrance in the upper part, where a thermocouple is placed to control the temperature of the bed. Furthermore, a gas preheater is located below the conical spouted bed reactor, which consists of a stainless steel cylindrical shell, with 31 mm in height and 2.7 cm in internal diameter. The gas preheater is filled with stainless steel pipes that increase the surface area for heat transfer and heat the gases to the reaction temperature.

The gas preheater and conical spouted bed reactor are located inside an oven consisting of a stainless steel shell with the walls filled with ceramic fibre. The oven is 52 cm long, with 1250 W power, and provides the heat required to reach the reaction temperature and preheat the gaseous stream to the reaction temperature.

Moreover, the char formed is continuously removed from the pyrolysis reactor by means of a lateral outlet pipe to avoid its accumulation in the bed. This separation is achieved in the conical spouted bed reactor due to the different trajectories described by char particles in this system, which has been reported in previous studies by the research group (Lopez et al., 2009; Amutio et al., 2012b).

2.2.4.2. Catalytic reforming reactor

The reforming reactor is a cylindrical steel fluidized bed reactor (Figure 2.4), with a length of 440 mm and an internal diameter of 38.1 mm. It is located inside an oven consisting of a stainless steel shell with the walls filled with ceramic fibre. This oven is 305 mm long and 550 W power, and provides the heat required to maintain the reaction temperature, which is controlled by a thermocouple inside the catalyst bed.

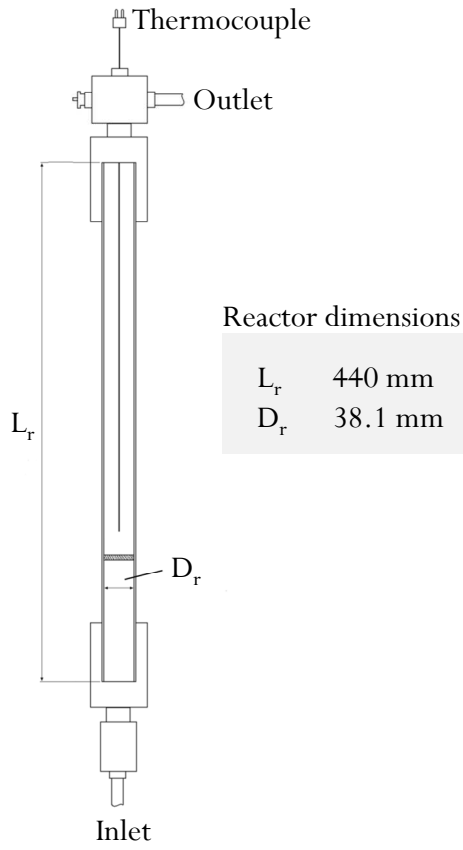

Figure 2.4. Scheme of the fluidized bed reactor and its main dimensions.

2.2.5. Product separation system

The pilot plant consists of a S-G separation system provided with a cyclone and a filter.

- *Cyclone*. The product gases from the pyrolysis step circulate through a cyclone, in order to remove the char and sand particles entrained from the bed. The gas accesses from a lateral inlet and leaves the cyclone from the upper part.

- *Filter*. The gases from the reforming reactor circulate through a filter, in order to remove the small particles of the catalyst formed by attrition and entrained from the bed.

Once the outlet stream from the reforming reactor has passed through a filter, this stream circulates to a "T" junction, where a sample is taken for its analysis by gas chromatography and the remaining is addressed to the L-G separation system consisting of the following elements:

- *Condenser*. The gaseous stream accesses to a condenser made up of a double shell tube, where the gas circulates through the internal tube and the water at room temperature through the shell.

- *Separation tank*. This tank has a capacity of 150 ml and is designed to separate the less volatile products by condensation. Accordingly, the volatiles are cooled to 2-3 ºC using a Peltier cell, which is activated automatically when the control unit is switch on. The non-condensed products (gases) leave the tank from the upper part, while the liquids leave it from the lower part.

- *Coalescence filter (SMC)*. The purpose of this filter is to retain the micro-droplets (fog) in the gaseous stream by coalescence. The maximum design pressure of this filter is 10 bar.

2.2.6. Control system

The main process variables are controlled and monitored by a computer, using a program called *Adkir*, which has been specifically designed for this purpose. A digital communication via *RS-485* allows sending set point values to the devices (controllers, programmable automata, etc.) and, at the same time, reading the actual values of the process.

The application *Adkir* can manage protocols of different manufacturers and even work with each one of the elements, based on different communication speeds, number of bits of the message, different parities, etc. The advantage of using *RS-485* communication is that it allows inserting up to 256 devices.

This program is useful for monitoring the process variables, given that it allows a variety of possibilities to plot real-time graphics. It also allows plotting both measured variables and the performance of different controllers, as well as a suitable adjustment of control parameters.

2.3. OPERATING CONDITIONS

2.3.1. Pyrolysis step

The previous experience of the research group in the pyrolysis of biomass (Aguado, 1999; Aguado et al., 2000; Amutio, 2011; Amutio et al., 2012a) and plastics (Elordi, 2010; Elordi et al., 2011a; Artetxe, 2012; Artetxe et al., 2012a) has been essential in order to set the suitable operating conditions of the pyrolysis step.

The selected temperature has been 500 °C in the pyrolysis of biomass, plastics and different biomass/plastic mixtures. In the case of biomass, below this temperature the biomass is not completely degraded and above this temperature the liquid fraction (bio-oil) decreases (Amutio et al., 2012a), while in the case of plastics, below 500 °C the pyrolysis kinetic is very low and the defluidization of the bed is inevitable, due to the adhesion of the particles to form agglomerates (Elordi et al., 2011a).

The steam flow rate and particle size of the sand in the conical spouted bed reactor, and catalyst and sand in the fluidized bed reactor, are conditioned by fluid dynamic requirements of both reactors in-line, given the former is spouted and the latter fluidized using a common gas flow. Based on a fluid dynamic runs in both reactors, a water flow rate of 3 mL min^{-1} has been established, which corresponds to a steam flow of 3.73 NL min^{-1} (1.2 times the minimum velocity in the spouted bed reactor), with 50 g of sand with a particle diameter between 0.3 and 0.355 mm. Under these conditions, a vigorous movement of the bed is achieved and, in the case of the plastics, no agglomeration of the sand particles coated with molten plastic is produced. In the case of biomass, the char produced in this first step is collected in a vessel through a lateral outlet in the conical spouted bed reactor (Figure 2.3).

2.3.2. Catalytic reforming step

Once fluid dynamic runs have been carried out in the fluidized bed reactor at the reforming temperature (between 550 and 700 °C), with the total gas flow rate being the volatile stream leaving the spouted bed and the bed amount 25 g, particle diameters have been established between 0.4-0.8 mm and 0.3-0.355 mm for the catalyst and sand, respectively, as the most suitable sizes. The fluidization velocity corresponding to these conditions is between 3 and 4 times the minimum one.

Under these conditions, complete fluidization of the bed is guaranteed, even when the catalyst has high coke content and, furthermore, the attrition of the catalyst is moderated.

In the steam reforming of biomass pyrolysis products, the variables studied are as follows: temperature, space time and steam/biomass ratio (S/B). Table 2.3 summarizes the parameters and operating conditions used in the runs.

Table 2.3. Studied parameters and operating conditions in the reforming step of biomass.

Studied parameter		Operating conditions
Temperature	550, 600, 650, 700 ºC	20 g_{cat} min $g_{volatiles}^{-1}$ S/B= 4
Space time	2.1, 4.2, 8.3, 12.5, 16.7, 25 g_{cat} min $g_{biomass}^{-1}$	600 ºC S/B= 4
	2.5, 5, 10, 15, 20, 30 g_{cat} min $g_{volatiles}^{-1}$	
Steam/biomass ratio	S/B 2, 3, 4, 5	600 ºC 20 g_{cat} min $g_{volatiles}^{-1}$
Steam/C ratio	S/C 3.9, 5.8, 7.7, 9.7	

It should be noted that a minimum reaction temperature of 550 ºC has been established, given that below this temperature the conversion of biomass pyrolysis volatiles is very low, causing operational problems and carbonaceous material (coke) on the catalyst. The ceiling of the reaction temperature is conditioned by the reduction temperature of the catalyst (710 ºC), so that at higher temperatures irreversible deactivation of the catalyst by Ni sintering occurs.

Similarly, the effect of space time has been studied between 2.1 and 25 g_{cat} min $g_{biomass}^{-1}$, which correspond to 2.5-30 g_{cat} min $g_{volatiles}^{-1}$or catalyst masses between 1.6 and 18.8 g.

The effect of steam/biomass ratio has been studied in the 2-5 range (corresponding to a steam/C molar ratio between 3.9 and 9.7), which has been attained by keeping

the water flow at 3 mL min^{-1} and varying the amount of biomass fed into the process from 0.6 to 1.5 g min^{-1}, in order to ensure suitable fluid dynamic conditions.

Once the optimum operating conditions have been established for the pyrolysis and in-line catalytic steam reforming of biomass, different mixtures of biomass and high density polyethylene (HDPE) in the feed have been studied. Table 2.4 summarizes the different HDPE/biomass mixtures used for this study and the corresponding operating conditions.

Table 2.4. Studied parameters and operating conditions in the reforming step of different biomass/plastic mixtures.

Studied parameter		Operating conditions
HDPE/biomass mass ratio	0/100, 25/75, 50/50, 75/25, 100/0 wt %	700 °C 16.7 g_{cat} min $g_{feeding}^{-1}$ Steam/feed ratio (S/F)= 4

Moreover, different samples of the catalyst have been taken throughout time on stream in the valorisation of biomass, in order to study the evolution of coke formation and the deterioration of the catalyst properties with time on stream.

Finally, the regeneration of the catalyst has been carried out by coke combustion with air, using a temperature ramp up to 700 °C, in order to burn completely the coke formed on the catalyst.

2.4. CATALYST AND PRODUCTS ANALYSIS

2.4.1. Volatiles and permanent gases

The analysis of the products has been carried out in-line, using a gas chromatograph for volatile products and gas micro-chromatograph for permanent gases. A sample of the reforming reactor outlet stream (prior to condensation) has been injected into the gas chromatograph by means of a line thermostated at 280 ºC, once it has been diluted with an inert gas, using a suction pump connected to the vent of the chromatograph. The sampling point of the permanent gases is placed after the liquid condensation system and several samples have been taken in each run operating always under steady state conditions, in order to check the reproducibility of the experiments.

2.4.1.1. Gas chromatography

The gas chromatograph *HP 6890* is equipped with a sampling valve, an injector, a column and a flame ionization detector (FID).

The scheme of the sampling valve of the chromatograph is shown in Figure 2.5. In the "off" position, the sample flows through the *loop* by a suction pump connected to the vent. The H_2, which acts as carrier gas, circulates through the column and finally, reaches the detector. The sampling valve is rotated by means of a pneumatic actuator, which passes to "on" position, with the consequent inversion of the flows. In this position, the H_2 circulates through the *loop*, so that its content is sent to the injector. The injector is of *split/splitless* type, where a small part of the sample is injected into the column and the remaining is sent to vent.

The column used is a HP Pona, 50 m long, 0.2 mm in internal diameter and a coating thickness of 0.5 μm, and the temperature program used in the chromatographic oven is shown in Figure 2.6: 2 min at 40 ºC in order to obtain a good light hydrocarbon separation; a sequence of 15 ºC min^{-1} up to 305 ºC and 8 min at this temperature to ensure that all products are outside the column.

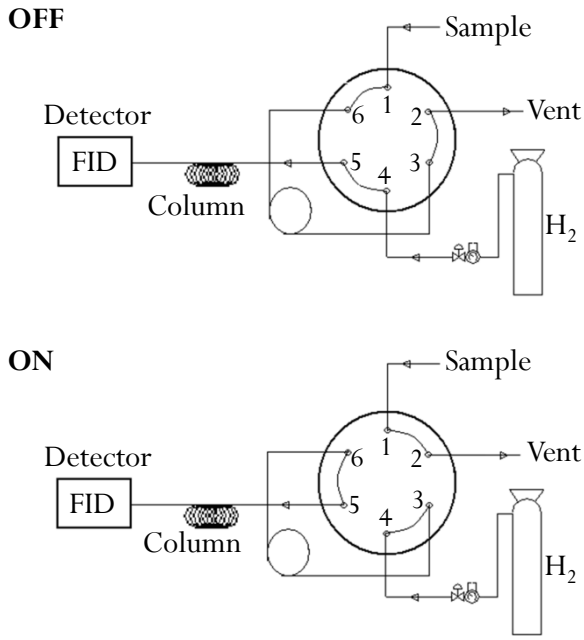

Figure 2.5. Sampling system of *HP 6890* chromatograph.

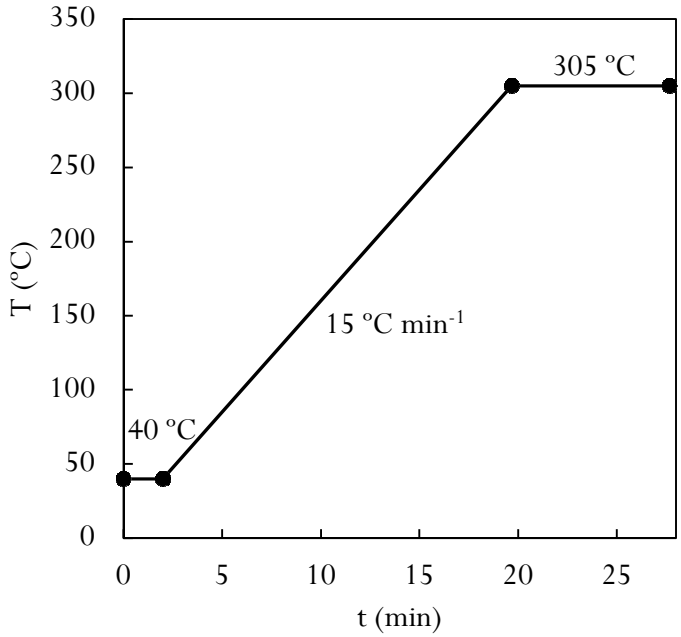

Figure 2.6. Temperature program of *HP 6890* chromatographic oven.

The *HP 6890* chromatograph is equipped with a FID detector, which gives an area/mass proportional result for pure hydrocarbons (Harmanos, 1997). Nevertheless, heteroatomic compounds are not oxidized in the same way as hydrocarbons, so the chromatographic area does not correspond proportionally to the product mass. In the case of oxygenated compounds, as oxygen is not burnt, the area is smaller than that corresponding to the mass of these compounds. Therefore, response factors must be calculated for the main oxygenated compounds in the product stream when using the FID detector.

These factors have been calculated using standard mixtures. Apart from a known concentration of the most significant oxygenated compounds in product stream, a given hydrocarbon has also been fed (with a different retention time to avoid peak overlapping), which allows establishing the response factors corresponding to each oxygenated compound compared to the hydrocarbon. Bearing in mind that the response factor for hydrocarbons is equal to unity, the factors corresponding to the oxygenated compounds in the product stream have been calculated using the following expression:

$$\frac{f_{ox}}{f_{HC}} = \frac{m_{ox}}{m_{HC}} \frac{A_{HC}}{A_{ox}} \qquad (2.1)$$

where f_{ox} and f_{HC} are the response factors, m_{ox} and m_{HC} the masses and A_{ox} and A_{HC} the chromatographic areas of oxygenated compounds and hydrocarbons, respectively.

Table 2.5 shows the factors for the main compounds of pine wood sawdust pyrolysis volatiles. It should be noted that the response factors depend on the nature of the compound (type of bond between C and O) and the relative proportion of C, H and O. Acids have a high response factor, although in the case of benzoic acid the factor is considerably reduced, given that the proportion of O is lower than in the case of lighter acids. It is also noteworthy that levoglucosan and other saccharides have high response factors, whereas those for phenols are low.

Table 2.5. Response factors of the most significant oxygenated compounds in the biomass pyrolysis volatiles.

Compound	M_W (g mol^{-1})	Formula	Response factor
Methanol	32	CH_4O	3.5
Acetaldehyde	45	C_2H_5O	2.2
Formic acid	46	CH_2O_2	4.7
Acetone	58	C_3H_6O	2.2
Acetic acid	60	$C_2H_4O_2$	4.6
2-propanol	60	C_3H_8O	2.2
Propanoic acid	74	$C_2H_6O_2$	4.0
Glycerine	92	$C_3H_8O_3$	3.6
Phenol	94	C_6H_6O	1.2
Furfural	96	$C_5H_4O_2$	2.4
2-furanmethanol	98	$C_5H_6O_2$	2.4
Cyclohexanone	98	$C_6H_{10}O$	1.5
Catechol	110	$C_6H_8O_2$	1.8
Benzoic acid	122	$C_7H_6O_2$	1.4
Guaiacol	124	$C_7H_8O_2$	1.6
Vanillin	152	$C_8H_8O_3$	2.2
Levoglucosan	162	$C_6H_{10}O_5$	5.0
Eugenol	164	$C_{10}H_{12}O_2$	1.4

In order to ease the calculation, an average response factor has been used for light oxygenated compounds and another one for heavy oxygenated compounds because all these compounds are non-converted bio-oil and they only appear when the catalyst is completely deactivated, i.e., they are not products of interest in the process, but by-products. These factors are shown in Table 2.6.

Table 2.6. Average response factors of the non-converted light and heavy products in the reforming step.

Compounds	Retention time (min)	Average response factor
Light	<6.5	2.75
Heavy	>6.5	1.75

An example of a chromatogram is shown in Figure 2.7 for the catalytic reforming of biomass (separated into two graphs, a and b), which corresponds to the experiment carried out at 600 ºC, with a space time of 20 g_{cat} min $g_{volatiles}^{-1}$, steam/biomass ratio of 4 and zero time on stream (fresh catalyst). As observed, the catalyst has a high activity, and therefore, C_1-C_3 fraction is the main one and there are not oxygenated compounds without reforming in the product stream.

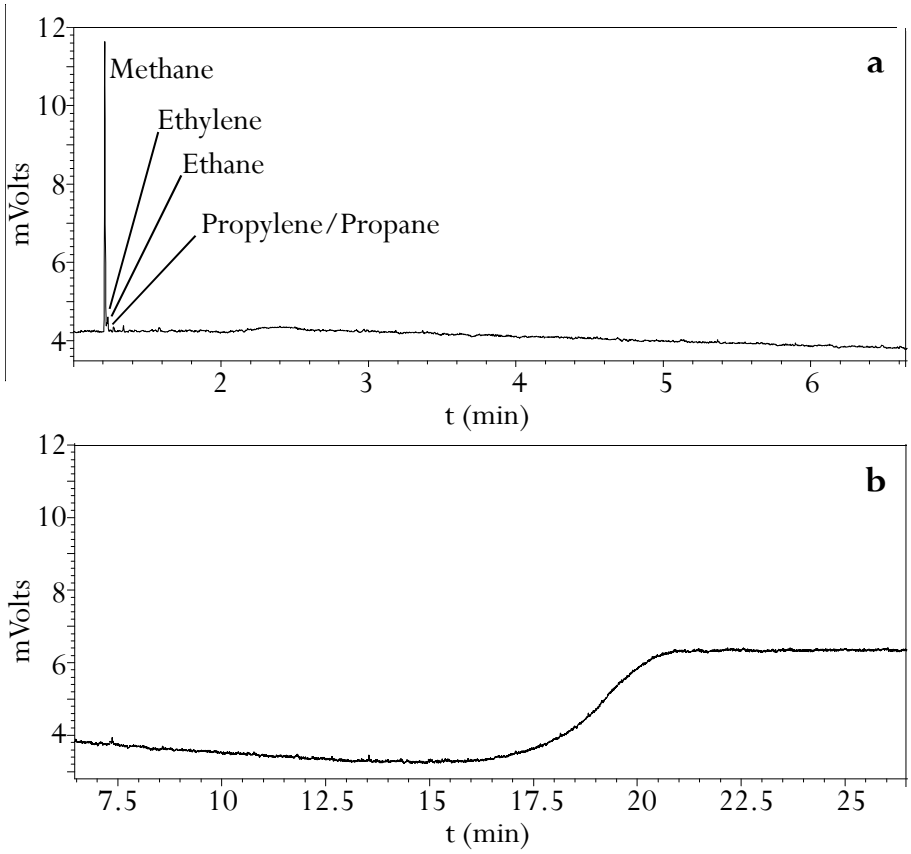

Figure 2.7. Chromatograph obtained in the catalytic reforming of biomass pyrolysis products, a) light fraction, b) heavy fraction. Operating conditions: 600 ºC; space time, 20 g_{cat} min $g_{volatiles}^{-1}$; S/B ratio, 4; zero time on stream.

Furthermore, the results shown in Figure 2.8 correspond to the same experimental conditions described above, but at 110 min on stream (deactivated catalyst).

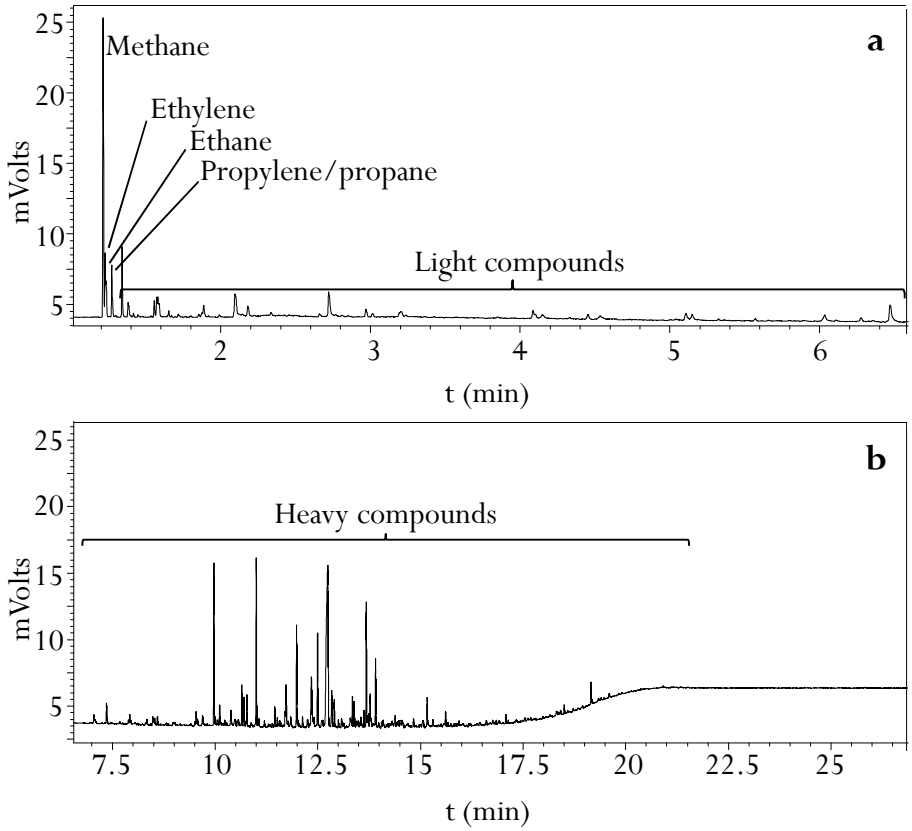

Figure 2.8. Chromatograph obtained in the catalytic reforming of biomass pyrolysis products, a) light fraction, b) heavy fraction. Operating conditions: 600 ºC; space time, 20 g_{cat} min $g_{volatiles}^{-1}$; S/B ratio, 4; 110 min on stream.

The non-condensable gas fraction (C_1-C_4) is the main one and appears in the first 3 min. As observed, methane, ethane and ethylene on the one hand, and propane and propylene on the other hand, appear in a single peak, and therefore a micro-chromatograph is required for their quantification. Subsequently, until 6.5 min, the lighter fraction of non-converted bio-oil compounds appear and then, the heavier ones.

2.4.1.2. Gas micro-chromatography

The gas micro-chromatograph *Varian 4900* has been used to quantify the concentration of H_2, CH_4, CO and CO_2 and determine the ratio between ethane/ethylene and propane/propylene, given that these compounds overlap in the gas chromatograph (GC). This micro-chromatograph has four different channels with four analytical modules, including injector, column and detector.

- *Analytic channel 1* provided with a molecular sieve capillary column, Molecular Sieve 5 (10 x 0.12 mm) and micro TCD detector. This channel is configured for the analysis of H_2, O_2, N_2, CH_4 and CO.

- *Analytic channel 2* consisting of a capillary column Porapak Q (PPQ, 10 m x 0.32 mm) and micro TCD detector. This channel is configured for the analysis of CH_4, CO_2, ethylene, ethane, propylene and propane and oxygenated compounds.

- *Analytic channel 3* consisting of a capillary column type Plot Alumina (10 m x 0.32 mm) and micro TCD detector. This channel is configured for the analysis of ethane, ethylene, propane, propylene and C_4-C_6 hydrocarbons and the isomers of butenes and pentenes.

- *Analytic channel 4* provided with a capillary column CPSil (8 m x 0.02 mm) and micro TCD detector. This channel is configured for the analysis of C_6-C_{12} hydrocarbons and oxygenated compounds.

The chromatographic channels 1, 2 and 3 have a microinjector module with reflux *(backflush)* with variable injection volume. The system (Figure 2.9) enables programming of the flows and the flow inversion in each column in order to avoid the entering of undesired compounds in the channels. It consists of a pre-column and an analytical column, both connected to a pressure point, which makes possible the inversion of the gas carrier flow through the pre-column at a given time called *backflush* time. When the desired compounds are transferred to the analytical columns, where the separation of components is to be carried out, the *backflush* valve is activated. This reverses the flow in the pre-column and the remaining compounds in it are sent to vent.

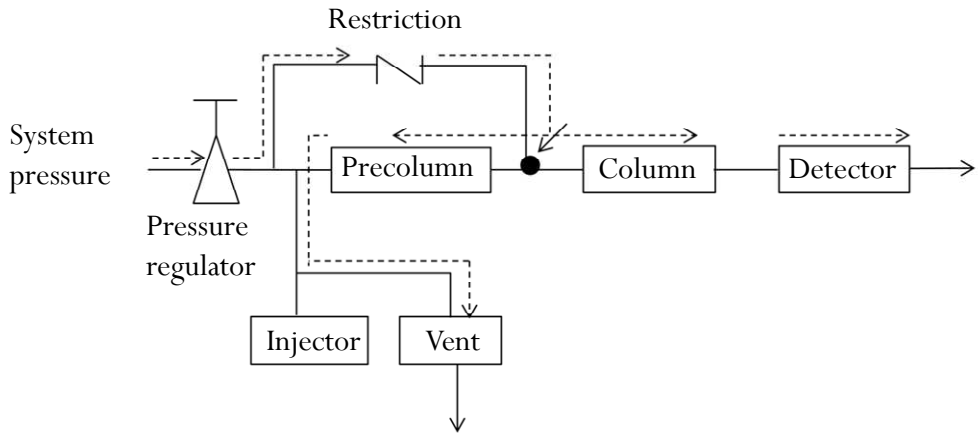

Figure 2.9. Flow chart of the reflux system in the micro-chromatograph *Varian 4900*.

The micro-chromatograph also allows the thermostatic control of the injection system, with independent temperature control up to 110 °C, of the sample inlet system and sample line of each channel. In Table 2.7, the conditions of the chromatograph analysis method are shown.

Table 2.7. Conditions of the micro-chromatograph *Varian 4900* analysis method.

Parameter	MS5	PPQ	Alumina	CPSil
Column temperature (°C)	80	95	110	120
Injector temperature (°C)	110	110	110	110
Pressure (psi)	20	20	23	20
Backflush time (s)	12	9	9	-
Injection time (ms)	20	50	20	50
Analysis time (s)	240	240	240	240

In order to determine the mass fraction of each compound based on the chromatographic peak area, some correction factors are necessary, which are shown in Table 2.8.

Table 2.8. Response factors in the micro-GC *Varian 4900* for the identified compounds.

Compound	TCD 1	TCD 2	TCD 3
Hydrogen	376	-	-
Methane	4.2	2.1	-
Carbon monoxide	3.5	-	-
Carbon dioxide	-	1.7	-
Ethylene	-	2.8	4.3
Ethane	-	2.8	4.2
Propylene	-	1.8	3.5
Propane	-	1.7	3.3

2.4.2. Fresh catalyst

As already commented in Section 2.1.2, a commercial Ni reforming catalyst called ReforMax® 330 (G90LDP), provided by *Süd Chemie* and used in industry for CH_4 reforming, has been used for the experiments, with the generic formulation being NiO, $CaAl_2O_4$, Al_2O_3. The selection of this catalyst is motivated mainly on its availability, avoiding problems of reproducibility in catalyst preparation, since a significant amount of catalyst is needed in the scheduled experimentation. Moreover, the fact that it is a commercial catalyst ensures the continuity of the research and its use by other researchers. Secondly, this catalyst showed a good performance in previous studies by the research group in ethanol reforming, with small differences with respect to Ni and Co catalysts supported on Al_2O_3 and SiO_2, which have been specifically prepared (Vicente, 2012), as well as in the reforming of HDPE pyrolysis products (Barbarias, 2015).

2.4.2.1. Physical properties

The BET surface area and the properties of the porous structure of the catalyst have been determined using a N_2 adsorption-desorption *Micromeritics ASAP 2012* apparatus, which uses the technique of the static volume, i.e., the adsorption is measured using material balance equations, state equations for the gas and pressure measurements. The experimental procedure consists in degasifying the sample at 150 ºC for 8 h to remove any impurity in the sample, followed by an adsorption-desorption of N_2

(99.9995 % purity) in multiple equilibrium stages until the saturation of the sample at cryogenic temperature (liquid N_2).

Figure 2.10 shows the isotherms of N_2 adsorption-desorption and Table 2.9 the values of surface area, pore volume and average pore size, which have been calculated based on the isotherms plotted in Figure 2.10. This commercial catalyst has not been analyzed by ICP-AES because a confidentiality agreement was signed with the supplier.

The isotherms presents a characteristic hysteresis of H3 isotherms and above a relative pressure of 0.4 shows the typical cycle of hysteresis of mesoporous materials (the average pore size is 122 Å), with a high N_2 adsorption close to relative pressures of unity.

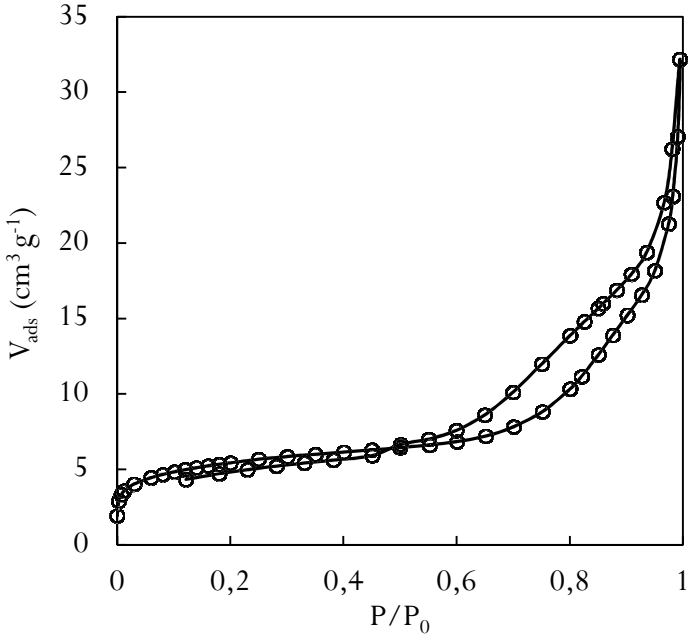

Figure 2.10. N_2 adsorption-desorption isotherm of the catalyst ReforMax® 330.

Table 2.9. Metallic content and physical properties of the catalyst.

Catalyst	NiO content (wt %)	S_{BET} ($m^2 g^{-1}$)	V_{pore} ($cm^3 g^{-1}$)	d_{pore} (Å)
ReforMax® 330	14	19	0.04	122

2.4.2.2. Reducibility and nature of metallic species

The temperature programmed reduction (TPR) enables the determination of the different reducible metallic species of the catalyst (different oxidation states or different metal-support interactions) and the temperature in which the reduction occurs.

This qualitative analysis technique of metallic oxides consists of exposing the solid to a reducing gas flow (usually H_2 diluted in an inert gas), while a lineal temperature sequence is maintained. The reduction velocity is determined by measuring continuously the H_2 consumed, which allows knowing the nature of the reduced species in the sample. This analysis has been carried out in a *Micromeritics AutoChem 2920*, where a stream of 10 vol % of H_2 in Ar (50 cm^3 min^{-1}) circulates through the sample (50-100 mg). Then, the sample is heated from room temperature to 900 ºC, with a constant heating rate of 5 ºC min^{-1}, while the temperature and TCD detector signals are recorded continuously. The water formed during the reduction is retained by a guard bed of 1-propanol/N_2 (liq.), located between the sample and the detector, in order to avoid the interference in the TCD signal.

Figure 2.11 shows the TPR profile of the catalyst, which has been essential to establish the temperature needed for its reduction, prior to use in the reforming step. As is well-known, the profile does not only depend on the nature of metallic functions, but also on the metal-support interactions. Independent of the metal, the easiest catalysts to be reduced are those supported on ZnO and SiO_2 (fully reduced below 500 ºC), whereas the catalysts supported on α-Al_2O_3, promoted or not, need higher temperatures (~900 ºC) for their full reduction (as shown in Figure 2.11).

The TPR profile shows a main peak at around 550 ºC, attributed to the reduction of NiO interacting with the α-Al_2O_3 support, and another peak at 700 ºC, which corresponds to the spinel $NiAl_2O_4$, based on the generic composition provided by the supplier. Due to confidentiality reasons, the XRD results have not been published in this thesis, but it is evident they are similar to other Ni-Al catalysts because their composition is analogous to those used in the literature for the steam gasification of biomass and pyro-gasification (without feeding water) (Arauzo et al., 1994, 1997; García et al., 1999, 2002) prepared by co-precipitation by these authors.

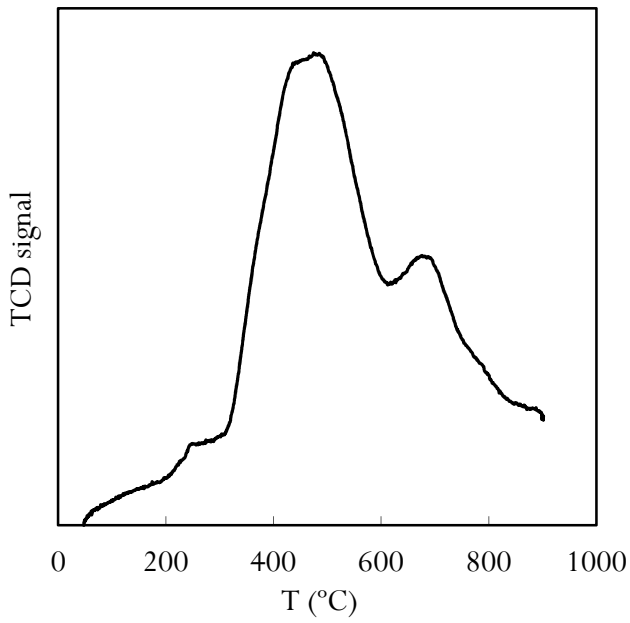

Figure 2.11. TPR profile of ReforMax® 330 catalyst.

2.4.3. Deactivated catalyst

2.4.3.1. Metallic properties

X-ray diffraction (XRD)

X-ray diffraction (XRD) is a non-destructive technique for analyzing the structure of crystalline solids, providing information about the crystallographic orientation, identification of phases, crystallite size and polymorphism, among others. In this method, a monochromatic X-ray beam impinges on the crystalline material and the intensity of the beam elastically scattered (diffracted) is measured as a function of the diffracted 2θ angle.

XRD analyses were carried out at the SGIker service in the University of the Basque Country (EHU/UPV). High angle patterns were collected by using a *Philips X'Pert PRO* automatic diffractometer operating at 40 kV and 40 mA, in theta-theta configuration, secondary monochromator with CuKα1 radiation (= 1.5418 Å) and a

PIX cell solid state detector. Data were collected from 10 to 70 º (step size= 0.02606 º and time per step= 300 s) at room temperature. A fixed divergence and antiscattering slit giving a constant volume of sample illumination were used.

This technique has been used to determine the average size of the metallic active sites of the catalyst, applying the equation of Debye-Scherrer.

$$d_{MO} = \frac{k\lambda}{\beta \cos\theta} \qquad (2.2)$$

where d_{MO} is the average crystallite size; k, Scherrer constant, whose general value is 0.9; λ, the length of the radiation wave (average kα =1.541874 Å); θ, is the position of the diffraction peak corresponding to the metal to be analyzed (in this case, Ni); β, the width of the average width of the diffraction peak of the sample, which should be corrected taking into account the contribution of the measuring equipment (0.08 º).

2.4.3.2. Coke nature and content

In order to analyze the effect of coke deposition, the physical properties of the used catalysts have been measured by N_2 adsorption-desorption, using the methodology described in Section 2.4.2.1. Moreover, the nature and location of coke on the catalyst have also been studied by the following techniques: 1) temperature programmed oxidation (TPO), which also allows calculating the content of coke; 2) SEM (scanning electron microscopy) images, and; 3) TEM (transmission electron microscopy) images.

Temperature programmed oxidation (TPO)

The amount of coke deposited on the deactivated catalysts has been determined by means of air combustion in a *TA Instruments TGA Q5000* thermogravimetric (TG) apparatus, coupled in-line with a *Balzers Instruments Thermostar* mass spectrometer (MS), which has been connected by a thermostatic line.

The total coke content deposited on the catalyst is usually calculated by the difference between the initial and final mass of the sample during the TPO experiment. Nevertheless, this method is unviable when the mass of the sample increases throughout the combustion, given that the Ni of the catalyst is oxidized in

parallel to the combustion. As an alternative method, a mass spectrometer connected in-line with the thermogravimetric apparatus has been used, which is suitable to determine low coke contents (< 10 wt %). This mass spectrometer records the signals 14, 18, 28 and 44, which correspond to N_2, H_2O, CO and CO_2, respectively. For the calculation of coke content of the catalyst, the signal of CO_2 has only been used due to several reasons: 1) the H_2O formed during the combustion cannot be distinguished from the moisture, and; 2) the combustion is complete, with the content of CO at the outlet stream being insignificant, given that the CO is immediately oxidized to CO_2, which is activated by the metallic function of the catalyst. Consequently, coke content (C_C, wt %) is defined as follows:

$$C_C = \frac{m_{CO_2} \cdot 12 g_C / 44 g_{CO_2}}{W} \cdot 100 \qquad (2.3)$$

where m_{CO2} is the mass of CO_2 generated in the combustion and W the mass of catalyst after the coke is burnt.

The following procedure has been carried out: stripping with He (10 mL min^{-1}) to remove the impurities; stabilization of temperature at 100 ºC to have the initial temperature constant in all experiments; combustion with air (50 mL min^{-1}) up to 800 ºC by following a 5 ºC min^{-1} ramp, maintaining that temperature for 30 min for obtaining complete coke combustion; finally, the sample was cooled down to room temperature.

Scanning electron microscopy (SEM)

The *Scanning Electron Microscopy* (SEM) has been carried out in a *JEOL JSM-6400* apparatus, with a W filament. The acceleration voltage applied to the electron beam was 20 kV and the intensity was between $6 \cdot 10^{-11}$ y $6 \cdot 10^{-10}$ A. The studied solids were prepared in the form of tablets and they have been adhered to a bronze support with colloidal Ag paste, for the subsequent application of the technique described above.

Transmission electron microscopy (TEM)

The nanometric images of the catalysts have been obtained using a transmission electron microscope *Philips CM200* with a supertwin lens (punctual resolution of 0.235 nm), provided with a EDX microanalysis system *(Energy-dispersive X-ray*

spectroscopy), with the resolution being 137.4 eV. The samples have been placed in a double inclination sample holder (*Philips PW6595/05*), where vacuum is generated and the images are obtained.

3

PYROLYSIS – CATALYTIC STEAM REFORMING OF BIOMASS AND BIOMASS/PLASTIC MIXTURES

3. PYROLYSIS - CATALYTIC STEAM REFORMING OF BIOMASS AND BIOMASS/PLASTIC MIXTURES

In this process, the pyrolysis has been carried out in a conical spouted bed reactor and the volatiles produced have been fed in-line to the catalytic steam reforming step in a fluidized bed reactor. Figure 3.1 shows the scheme of this original continuous two-step process used for the production of H_2 from biomass and biomass/HDPE mixtures. Section 3.1 aims at reviewing studies dealing with biomass pyrolysis and in-line reforming and studying the effect of operating conditions. Then, the main results obtained in this thesis in both pyrolysis and reforming steps are shown. In Section 3.2, the characterization of the volatiles produced in the pyrolysis of biomass and HDPE using steam as fluidizing agent are described, and subsequently, the results of the catalytic steam reforming step are shown (Section 3.3).

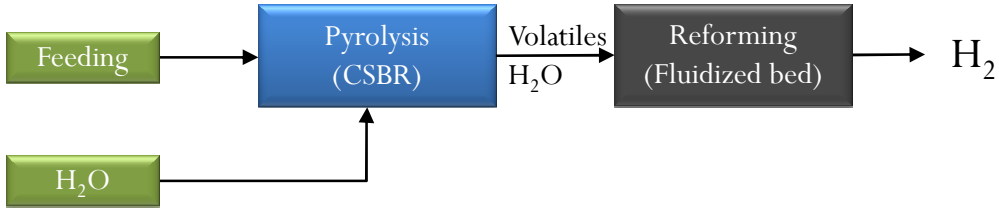

Figure 3.1. Scheme of the two-step process.

3.1. BACKROUND OF BIOMASS PYROLYSIS AND IN-LINE REFORMING STRATEGY

The different thermochemic routes for biomass valorisation have been summarized in Section 1, in which the effect of operating variables on product distribution in the biomass gasification and bio-oil reforming processes has been detailed. In this section, the effect of the most significant operating variables (pyrolysis and reforming temperatures, space time and steam to C ratio) in the two-step pyrolysis-reforming strategy will be analyzed.

3.1.1. Pyrolysis temperature

Gas, bio-oil and char are the products obtained in biomass pyrolysis, whose yields depend specially on operating conditions and reactor features. It is noteworthy that pyrolysis temperature is a relevant factor in the two-step process, given that the volatile products obtained in the pyrolysis step subsequently circulate through the catalyst bed in the reforming step, where steam reforming of bio-oil and gases takes place. Therefore, maximization of bio-oil and gases and minimization of char fraction is required to maximize volatile production in the pyrolysis step, and therefore the H_2 production in the reforming step. The bio-oil fraction obtained in lignocellulosic biomass pyrolysis processes is maximum (between 50 and 75 wt %) at temperatures of around 500 ºC (Park et al., 2008; DeSisto et al., 2010; Westerhof et al., 2010; Amutio et al., 2012a). Thus, in the pyrolysis and in-line catalytic steam reforming of biomass, the pyrolysis step is usually performed at temperatures between 500 and 600 ºC when pine wood waste is used (Efika et al., 2012; Li et al., 2013; Ma et al., 2014; Chen et al., 2015, 2016). Nevertheless, the pyrolysis temperature commonly used in the literature is much higher, between 750 and 950 ºC, when other types of biomasses are used as feedstock, such as rice husk, sugar cane bagasse, wheat straw, sewage sludge or pyrochar (Waheed and Williams, 2013; Cao et al., 2014; Shen et al., 2014a,b, 2015). Even though the effect of pyrolysis temperature on H_2 yield has not been extensively studied in the literature, Xiao et al. (2011) investigated the influence of pyrolysis temperature between 530 and 700 ºC in the pyrolysis-reforming of pig manure compost and they reported higher reforming gas yields when increasing temperature, which is explained because high temperatures produce higher gas yields and enhance tar cracking and char gasification (Xiao et al., 2013). The same trend was observed by Olaleye et al. (2014) in the pyrolysis-reforming of wood sawdust when pyrolysis temperature was increased in the 300-600 ºC range.

It should be noted that in some studies steam has been fed as fluidizing agent in the first step of pyrolysis. This strategy of using steam for pyrolysis eases the configuration of the process because there is no need for separating the inert gas from the product stream at the outlet of the reformer, given that steam may be easily condensed. Nevertheless, a suitable steam/C ratio must be established (explained in detail later on), given that evaporation and condensation costs are relevant for the overall economy of the process.

3.1.2. Reforming temperature

The product yields obtained in the reforming step depend especially on the reforming temperature, given that steam reforming reactions of the oxygenated compounds and hydrocarbons (CH_4 and C_2-C_4 hydrocarbons) produced from biomass pyrolysis are endothermic reactions, and they are therefore favoured at high temperatures. Nevertheless, the WGS reaction is an exothermic reaction which is enhanced at low temperatures, and therefore the optimum reforming temperature to enhance H_2 production should be found. Consequently, most studies reveal that high reforming temperatures enhance steam reforming reactions and lead to high conversion or gas yield and low tar yields (Xiao et al., 2011; Li et al., 2014), at the same time as H_2 production is also enhanced (Figure 3.2).

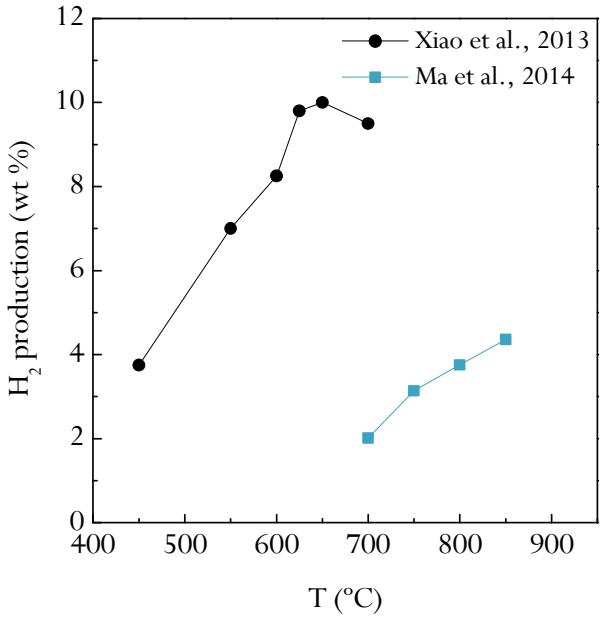

Figure 3.2. Effect of temperature on hydrogen production in pyrolysis-reforming studies (Xiao et al., 2013; Ma et al., 2014).

Wang et al. (2013a) observed high differences in tar yield when reforming temperature was increased from 500 to 850 ºC, i.e., tar yield decreases from around 20 wt % to 0 wt % at the highest temperature. Moreover, higher conversion of aromatic compounds was obtained above 700 ºC, whereas non-aromatic compounds are converted below this temperature. Xiao et al. (2013) also obtained lower tar

yields above 600 ºC, with the minimum tar content observing at 700 ºC, although the highest H_2 production of 10.0 wt % was achieved at 650 ºC. Higher activity of the catalyst was also reported by Koike et al. (2013) when temperature was increased from 550 to 650 ºC, with a considerable reduction in the amount of coke deposited, which is the main deactivation cause of the catalyst in the pyrolysis-reforming of biomass (Efika et al., 2012; Nahil et al., 2013; Waheed and Williams, 2013) and bio-oil reforming processes (Davidian et al., 2007; Wu et al., 2008b; Lan et al., 2010; Remiro et al., 2013b; Yao et al., 2014). Moreover, Ma et al. (2014) studied the influence of reforming temperature, using a pyrolysis temperature of 600 ºC and a gasification temperature of 850 ºC prior to reforming, which led to carbon conversion increase from 75.95 to 82.20 wt % when reforming temperature was increased from 700 to 850 ºC, obtaining a maximum H_2 concentration and production of 51 vol % and 7.6 wt %, respectively, at the highest temperature. These values were high compared to the two-stage pyrolysis-reforming process, in which a maximum conversion and H_2 production of 66.18 wt % and 4.4 wt %, respectively, were reported at a reforming temperature of 850 ºC. Shen et al. (2015) also reported a slight increase in tar conversion efficiency from 92.3 to 100 wt % when a Ni/C catalyst was used and temperature was increased in the 500-900 ºC range.

Concerning H_2 production, Waheed and Williams (2013) used a high reforming temperature (950 ºC) for the pyrolysis-reforming of rice husk, sugar cane bagasse and wheat straw, obtaining a maximum H_2 production of 5.1 wt % when rice husk and wheat straw were fed, whereas 4.9 wt % was obtained with sugar cane bagasse on 10 wt % Ni/dolomite catalyst, with these values being higher than those obtained with only dolomite.

In the same way, by increasing the reforming temperature, the concentrations of H_2 and CO in the gaseous stream increase, which is explained by the endothermic nature of the reforming reactions (for both oxygenated compounds and CH_4). Thus, Ma et al. (2014) obtained a maximum H_2 concentration of around 51 vol % at a reforming temperature of 850 ºC. Xiao et al. (2011) achieved H_2 concentrations of around 60 vol % when high steam/C ratios were used (~ 3 mol/mol), which corresponds to a maximum H_2 production of 9.3 wt %. Cao et al. (2014) obtained a H_2 concentration of 66.6 vol % at 500 ºC on a commercial Ni/Al_2O_3 catalyst, with the maximum value being 70.0 vol % when a temperature of 550 ºC was used, although the maximum H_2 production (11.6 wt %) was obtained at a temperature of 650 ºC.

3.1.3. Space time

The reforming space time is another important factor in order to ensure a tar-free gas product to be used for different applications. When space time is increased, steam reforming and WGS reactions are enhanced, favouring the formation of H_2, CO_2 and hindering that of CO. This conclusion was reported by Xiao et al. (2011), who observed a slight increase in H_2 production from 6.2 to 7.3 wt % and in CO_2 from 70.0 to 87.1 wt % when space velocity was reduced from 11000 to 9200 h^{-1}, whereas CO and CH_4 decrease from 23.0 to 19.9 wt % and from 9.1 to 2.9 wt %, respectively. Cao et al. (2014) also observed that higher total gas yield and H_2 production were obtained and lower coke was deposited on the catalyst when space time was increased. Higher tar reforming efficiency was reported by Shen et al. (2015), which increased from 50.1 to 99.8 % when catalyst mass was increased from 3 to 10 g, using a Ni/C catalyst and a reforming temperature of 700 ºC. Moreover, this catalyst is highly stable, as evidenced by the almost constant tar reforming efficiency (99.6 %) after 5 reforming cycles.

3.1.4. Steam/C ratio

Among the different reforming agents, steam is one of the most used in the literature and the S/C ratio is a relevant factor in reforming processes. Efika et al. (2012) studied the reforming process without and with steam, and the enhancement of gas yield with steam addition was reported, increasing from 40.5 to 45.3 wt % without catalyst and up to 54.0 wt % when NiO/SiO_2 catalyst was used. Moreover, H_2 concentration increased from 14.0 (sand without steam) to 18.2 vol % (sand with steam) and to 44.4 vol % when NiO/Al_2O_3 catalyst was used. Cao et al. (2014) also studied the effect of steam partial pressure between 30 and 53 kPa, obtaining a higher H_2 yield and lower carbon deposition at high steam partial pressure values. Zou et al. (2016) studied the influence of steam addition between 0 and 0.2 g min^{-1}, obtaining a maximum H_2 production of 5.9 wt % between 0.05 and 0.1 g min^{-1} of steam addition, without any improvement above this value.

3.2. FIRST STEP: PYROLYSIS USING STEAM AS FLUIDIZING AGENT

The continuous pyrolysis of pine wood sawdust and biomass/HDPE mixtures has been carried out in a pilot plant provided with a conical spouted bed reactor (Section 2.2). The operating conditions used for this step have been previously described in Section 2.3.1 and they are based on the experience of the research group in the pyrolysis of biomass and HDPE, which allowed establishing the most appropriate conditions in order to operate with high reproducibility involving the main products, i.e., bio-oil and waxes for biomass and plastics, respectively.

In previous works, the good performance of the conical spouted bed reactor was reported in the pyrolysis of both biomass (Amutio et al., 2012a) and polyolefins (Elordi et al., 2011a; Artetxe et al., 2012b). The vigorous cyclic movement of the particles in the conical spouted bed reactor allows handling solids of irregular texture, as is the case of biomass particles. Moreover, the sand/biomass ratio in the bed for suitable fluidization is lower than in fluidized beds, and the biomass mass flow rate per reactor volume unit is therefore higher. Versatility in the gas flow is also noteworthy, which allows operating from the minimum spouting regime to a very dilute spouting regime (San José et al., 1993; Cui and Grace, 2008). In the case of plastics, the use of this reactor ensures the uniform coating of the plastic and avoids the agglomeration of the particles coated with melted plastic and the subsequent defluidization of the bed (Artetxe et al., 2012b). It should be also noted that the conical spouted bed may operate in isothermal regime and without defluidization problems. Furthermore, the conical spouted bed reactor is of easy design (Olazar et al., 1993a), given that it does not require distributor plate and has low pressure drop (Olazar et al., 1993d). These characteristics of the conical spouted bed reactor lead to a well-defined, reproducible and constant product stream, which can be valorised in-line by different alternatives in a second reactor. In fact, reproducibility is essential to study the effect of operating conditions in the second step. In turn, the results obtained in the conical spouted bed reactor by continuous feeding of wastes allowed the scaling-up of this technology for biomass pyrolysis to a unit of 25 kg/h (Makibar et al., 2015).

The strategy of feeding steam to the pyrolysis reactor simplifies the operation of the process and favours the reforming step, given that the dilution of the volatiles in the pyrolysis unit with N_2 is avoided, and therefore the reaction rate is increased. However, the use of steam requires a high energy cost for its vaporization. Therefore, Section 3.2 deals with the pyrolysis of biomass and HDPE using steam as

fluidizing agent in the conical spouted bed reactor, the effect of steam on product distribution and a comparison of these results with those obtained using N_2 as fluidizing agent.

It should be noted that Erkiaga (2014) and Barbarias (2015) have verified that steam acts as an inert gas in the pyrolysis of HDPE, PP, PET and PS in a conical spouted bed reactor at 500 ºC. This study will confirm the inert nature of the steam in the pyrolysis of biomass and HDPE.

3.2.1. Pyrolysis of biomass

3.2.1.1. Product yields

Table 3.1 shows the product yields obtained in the pyrolysis of biomass at 500 ºC under the conditions described in Section 2.3.1. The fast pyrolysis of pine wood sawdust in a conical spouted bed reactor leads to a wide distribution of products, which can be grouped into three fractions: gases, bio-oil and char. At this temperature, the bio-oil fraction is maximized, obtaining a yield of around 75 wt %, which will be the feed of the reforming step together with the gaseous fraction.

As commented above, the pyrolysis step was carried out in steam environment, given that the steam required in the reforming step was introduced in the pyrolysis reactor, where it plays the role of a fluidizing agent. It should be noted that, even operating with N_2 as fluidizing agent, there is a significant steam concentration in the reaction environment because the water yield in the biomass pyrolysis process is above 25 wt % (Amutio et al., 2012a). Thus, the results were similar to those previously reported by Amutio et al. (2012a) in the pyrolysis of the same biomass but using N_2 as fluidizing agent. Kantarelis et al. (2013) observed certain differences in the biomass pyrolysis product yields and composition when comparing steam and N_2 pyrolysis. However, the same authors stated based on a simulation study that the differences between steam and N_2 pyrolysis are negligible in terms of heat transfer and product formation rate (Mellin et al., 2014).

Regarding the gaseous fraction, its yield was 7.3 wt % and is made up of CO, CO_2 (similar yield for both, 3.3 wt %) and a low concentration of CH_4, C_2-C_4 hydrocarbons and H_2. The main product obtained in the pyrolysis step is the liquid product or bio-oil, whose yield is 75 wt % due to the excellent features of this reactor for biomass fast pyrolysis, especially, its high heat transfer rate, short

residence time and rapid char removal from the reaction environment (Amutio et al., 2012a). The main products of the bio-oil, which is a complex mixture of oxygenated compounds, are as follows: phenols (16.5 wt %), ketones (6.4 wt %), saccharides (4.5 wt %), furans (3.3 wt %), acids (2.7 wt %), alcohols (2.0 wt %) and aldehydes (1.9 wt %). Furthermore, a water yield of 25 wt % is also obtained, which acts also as a reforming agent in the second reforming step.

These two fractions (gases and bio-oil) are the volatile products, which are driven to the fluidized bed reactor to be reformed. The molecular formula corresponding to the stream of biomass pyrolysis volatiles entering the reforming reactor, without taking into account the steam, has been determined based on the compositions of the gas and bio-oil fractions: $CH_{1.93}O_{0.92}$.

Table 3.1. Yields of biomass pyrolysis products (wt %) at 500 ºC.

Compound	Yield (wt %)
Gas	**7.33**
Carbon dioxide	3.27
Carbon monoxide	3.38
Hydrogen	0.004
Methane	0.36
Ethylene	0.09
Ethane	0.06
Propylene	0.07
Propane	0.05
Others	0.03
Unidentified	0.01
Bio-oil	**75.33**
Acids	2.73
Acetic acid	1.11

Table 3.1. Continued.

Aldehydes	1.93
Formaldehyde	0.35
Acetaldehyde	0.16
Alcohols	2.00
Methanol	0.69
Glycerine	1.11
Ketones	6.37
Acetone	0.67
Acetol	1.53
Cyclohexanone	1.23
Phenols	16.49
Alkyl-phenols	1.80
Cresols	0.67
Catechols	7.16
Pyrocatechol	4.08
Guaiacols	7.53
Guaiacol	1.86
Furans	3.32
2-Furanmethanol	0.75
Saccharides	4.46
Levoglucosan	2.78
Others	0.06
Unidentified	12.61
Water	25.36
Char	**17.34**

Under the conditions studied, char yield is of around 17 wt % and its recovery is of great interest for the economy of the process, with its main application being, amongst others, the production of adsorbent (Alvarez et al., 2014c; Wang et al., 2015), fertilizers (Uchimiya et al., 2015), catalyst support (Domínguez et al., 2013; Ren et al., 2014; Shen et al., 2014b) and soil amender (Smith et al., 2013).

3.2.1.2. Characterization of the bio-oil

In Figure 3.3, the results obtained in the simulated distillation of the bio-oil obtained at 500 °C are plotted and they are compared with those obtained for gasoline and gasoil. It can be observed that 40 wt % of the organic compounds in the bio-oil correspond to the range of light naphtha (< 160 °C), 30 wt % to heavy naphtha (between 160-200 °C) and the other 30 wt % to medium distillates (between 200-350 °C). It should be pointed out that the boiling point of the whole organic content in the bio-oil ranges from that of gasoline to that of gasoil. Moreover, 45 wt % of the bio-oil could be used as gasoline and the remaining 65 wt % as automotive fuel.

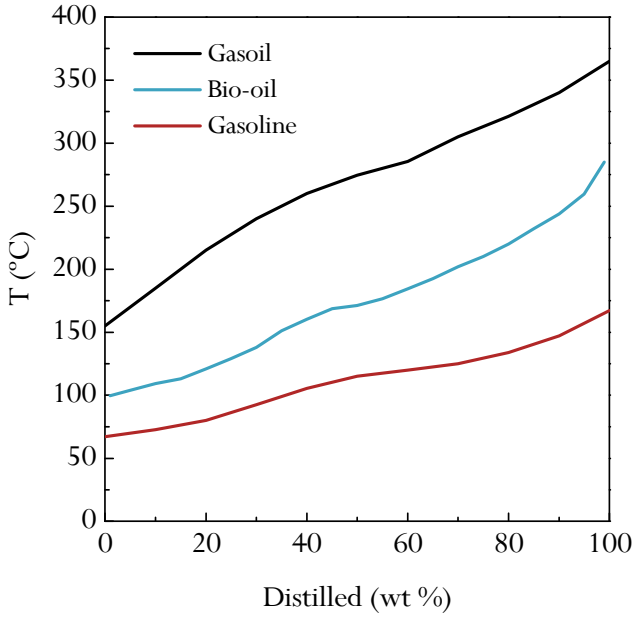

Figure 3.3. Comparison between the simulated distillation curves of the liquid obtained in the pyrolysis of pine wood sawdust at 500 °C and those of commercial fuels.

3.2.2. Pyrolysis of HDPE

3.2.2.1. Product yields

Table 3.2 shows the product yields of pyrolysis of HDPE at 500 ºC and under the conditions described in Section 2.3.1. The products have been grouped as follows: C_1-C_4, C_5-C_{11} (gasoline), C_{12}-C_{20} (diesel) and waxes (C_{21+}). As pointed out above, the steam required for the steam reforming step has been introduced in the pyrolysis step in order to use it as fluidizing agent in the conical spouted bed reactor. Thus, the pyrolysis step has been conducted under steam environment instead of using an inert gas such as N_2, which is the most commonly used gas in the pyrolysis processes. A comparison between the two mentioned strategies has been done for HDPE pyrolysis in previous studies (Erkiaga et al., 2015; Barbarias et al., 2016a) and a small effect of steam on product distribution was reported, which is due to the low temperature used for the process and the good behaviour of the conical spouted bed reactor, i.e., low residence time for the volatiles avoiding secondary reactions. Thus, the results obtained were similar to those previously reported by Elordi et al. (2011a), in which N_2 was used as fluidizing agent. The volatiles stream from HDPE pyrolysis is mainly composed of diesel fraction (C_{12}-C_{20}) and waxes (C_{21+}), with the total yield being up to 90 wt %. The high waxes yields obtained in the conical spouted bed reactor are due to the high heat and mass transfer rates in the reactor and the low residence time of the waxes, which lead to the minimization of depolymerization reactions. Furthermore, from an operational point of view, the characteristic solid flow in this reactor avoids the blocking of the bed even though there is a high wax content. Thus, Predel and Kaminsky (2000) obtained a similar diesel and waxes yields in a fluidized bed at 500 ºC, but operational problems were reported due to carbonaceous deposits. Furthermore, Williams and Williams (1999) obtained 90 wt % gasoline, diesel and waxes in the pyrolysis of LDPE in a fluidized bed at 500 ºC.

Moreover, a low yield of light olefins (1.15 wt %) and light alkanes (0.35 wt %) are obtained and they are mainly composed of propylene and butenes. Non-aromatic C_5-C_{11} yield is around 5.5 wt %, which is mainly composed of isoparaffins and olefins, and the yield of C_5-C_{11} aromatic compounds is negligible (0.28 wt %).

The compounds of the C_{12}-C_{20} fraction have been grouped according to the nature of the chemical bonds and the proportion paraffins:olefins:diolefins is 1.00:1.40:0.34 (in mass), which corresponds to a lower olefinic stream in relation to that obtained in a fluidized bed reactor at 514 ºC by Predel and Kaminski (2000) (1.00:2.20:0.25),

and more olefinic than that obtained by del Remedio Hernandez et al. (2007) (1.00:1.21:0.25) at 500 ºC.

Table 3.2. Yields of HDPE pyrolysis products (wt %) at 500 ºC.

Compound	Yield (wt %)
C_1-C_4	**1.50**
Methane	0.03
Ethane	0.06
Ethylene	0.08
Propane	0.08
Propylene	0.50
Butanes	0.18
Butenes	0.57
C_5-C_{11}	**5.86**
Paraffins	0.34
Isoparaffins	2.50
Aromatics	0.28
Naphthenes	0.19
Olefins	2.56
C_{12}-C_{20}	**25.64**
Diolefins	3.22
Olefins	13.07
Paraffins	9.35
Waxes	**67.00**
C_{21}-C_{40}	29.50
C_{40+}	37.50

3.2.2.2. Characterization of waxes

Figure 3.4 shows the simulated distillation curves corresponding to the waxes obtained in the pyrolysis of HDPE at 500 ºC. The waxes have retained a light fraction (C_{20-}) corresponding to components within the gasoline and diesel fraction. Furthermore, two fractions (light waxes and heavy waxes) have been quantified and they have been defined as follows: 1) light waxes, C_{21}-C_{40} fraction, which correspond to compounds with boiling point between 343 and 525 ºC, and; 2) heavy waxes, with higher boiling temperatures. It can be observed that 27 wt % corresponds to the retained lighter fraction (C_{20-}) and 42 wt % to light waxes, with the remaining being heavy waxes.

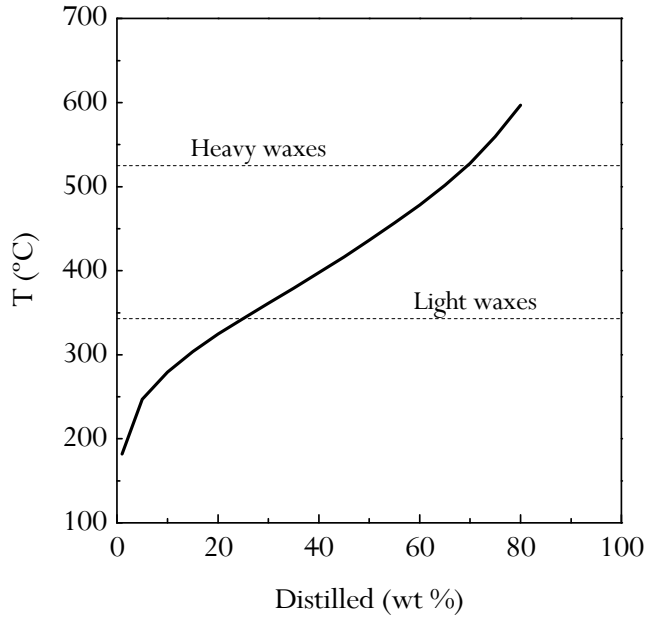

Figure 3.4. The simulated distillation curve of the waxes obtained in the pyrolysis of HDPE at 500 ºC.

3.3. SECOND STEP: CATALYTIC STEAM REFORMING OF THE VOLATILES FROM PYROLYSIS

In this section, the catalytic steam reforming of volatiles from the pyrolysis of different wastes, such as biomass and HDPE, has been investigated (Figure 3.1). This process allows producing H_2-rich gas in a two-step process, where each step is carried out in a different reactor, involving some advantages in relation to the one-step process. On the one hand, the temperature in each step can be optimized in order to obtain a homogeneous composition of the volatiles stream from pyrolysis and to maximize the production of H_2 in the reforming step; on the other hand, the catalyst is more effective for volatile transformation, i.e., the process is more versatile for establishing the desired catalyst/feed ratio. Therefore, a more uniform product stream will be obtained, because the catalyst is more efficient at attenuating secondary reactions.

Concerning biomass valorisation, this two-step alternative has also advantages in relation to the indirect route of bio-oil reforming, given that the physical properties of the bio-oil pose a serious drawback for this indirect route. Thus, bio-oil is unstable and polymerizes under storage, causing an increase in viscosity and average molecular weight (Demirbas, 2011). Furthermore, the incomplete vaporization of the bio-oil also involves a great challenge due to the formation of carbonaceous deposits, and therefore a decrease in the reforming conversion efficiency (Czernik and French, 2014). In order to alleviate the problems associated with bio-oil properties, most of the reforming studies in the literature have been carried out with model compounds and synthetic mixtures simulating bio-oil and tar (Trane et al., 2012; Lemonidou et al., 2013) or with the bio-oil aqueous fraction (Kechagiopoulos et al., 2009; Bimbela et al., 2013; Valle et al., 2013).

The H_2 production by biomass pyrolysis and in-line reforming of pyrolysis volatiles avoids the problems associated with bio-oil handling and vaporization. Furthermore, a fraction of the bio-oil is not discarded and all hydrocarbons of pyrolysis gases are reformed improving the potential process yields. Therefore, although it has been scarcely studied, this strategy is regarded as a feasible solution for H_2 production in small scale units (Namioka et al., 2011).

Another alternative to produce H_2 from biomass is gasification, which has been widely studied in the literature (Ahmad et al., 2016). However, biomass gasification faces several challenges related to the quality of the syngas obtained and, especially,

to its tar content, which causes serious operational problems due to the blockage by fouling of process equipment (Anis and Zainal, 2011) and limits the applications of the syngas produced (Woolcock and Brown, 2013).

In a previous paper of the research group, a combination of a conical spouted bed reactor and a fixed bed reactor was used for the pyrolysis and in-line reforming of HDPE (Erkiaga et al., 2015). The use of the fixed bed reactor leads to high amount of external and internal coke in the catalyst, which hinders gas flow (Erkiaga et al., 2015; Lopez et al., 2015a). In order to overcome the operational problems encountered when using a fixed bed in the reforming step, it has been replaced by a fluidized bed reactor for HDPE valorisation (Barbarias et al., 2016a). In this case, the effect of coke deposition on catalyst deactivation is attenuated due to the homogeneity of the activity in the bed and, moreover, the effect of steam flow on gasification of coke precursors is also more efficient. Furthermore, the use of a fluidized bed is interesting for the large-scale operation with catalyst circulation.

The knowledge of the research group on the pyrolysis of biomass (Amutio et al., 2012a) and HDPE (Elordi et al., 2011a; Artetxe et al., 2012a) has been essential in order to plan the experiments. As explained in Section 3.2, the conical spouted bed technology maximizes the volatiles yield at around 500 °C, obtaining a uniform volatile stream that is especially suitable for the reforming step.

Different reforming catalysts have been used in the literature for this purpose. Ni-based catalysts are the most common ones for the reforming of oxygenated compounds (Koike et al., 2013; Wu et al., 2013; Xiao et al., 2013) and hydrocarbons (Donatelli et al., 2010; Luo et al., 2012; Acomb et al., 2014), although noble metals, such as Pt, Pd and Rh, can also be used for reforming processes (Rioche et al., 2005; Basagiannis and Verykios, 2007b; Park et al., 2010; Namioka et al., 2011). In this case, a commercial Ni reforming catalyst has been used, which has been designed for CH_4 reforming and has a good mechanical strength. The use of this catalyst is promoted due to the good results obtained in the gasification-reforming (Lopez et al., 2015a) and pyrolysis-reforming of HDPE, using both a fixed bed (Erkiaga et al., 2015) and a fluidized bed reactor (Barbarias et al., 2016a). Moreover, the availability of the catalyst and the reproducibility of the results make it adequate for the set-up of this new technology.

In Section 3.3.1, the reaction indices have been defined in order to quantify and compare the results. First of all, a parametric study has been carried out for biomass valorisation, in which a study has been carried out on the effect of temperature in the

550-700 °C range, space time between 2.5 and 30 g_{cat} min $g_{volatiles}^{-1}$ and steam/biomass ratio between 2 and 5, on conversion and product distribution (Section 3.3.2). Moreover, the valorisation of different biomass/HDPE mixtures has also been studied in order to increase the production of H_2, analyzing the effect of biomass/HDPE mass ratio on conversion and product distribution (Section 3.3.3). In this section, a comparison between pyrolysis-catalytic steam reforming and gasification processes has been made and the production of H_2 in each of the processes has been analyzed.

3.3.1. Reaction indices

In order to quantify the process results, the following reaction indices have been defined:

- *Yield of C containing compounds (Y_i, %):* The yield of each C containing compound or fraction, i, has been calculated based on the pyrolysis volatile stream.

$$Y_i = \frac{F_i}{F_{volatiles}} \cdot 100 \qquad (3.1)$$

where F_i and $F_{volatiles}$ are the molar flow rates of product i and pyrolysis volatiles, respectively, both given in C units contained.

- *H_2 yield (Y_{H2}, %):* The H_2 yield was determined as a percentage of the maximum allowed by stoichiometry, which accounts for the H coming from the pyrolysis products from biomass (eq. (3.2)) and HDPE (eq. (3.3)) and the steam, considering the following stoichiometry:

$$C_nH_mO_k + (2n-k)H_2O \rightarrow nCO_2 + \left(2n + \frac{m}{2} - k\right)H_2 \qquad (3.2)$$

$$C_nH_m + 2nH_2O \rightarrow nCO_2 + \left(2n + \frac{m}{2}\right)H_2 \qquad (3.3)$$

$$Y_{H_2} = \frac{F_{H_2}}{F^0_{H_2}} \cdot 100 \quad (3.4)$$

where F_{H2} and F^0_{H2} are the H_2 molar flow rate obtained in the run and the maximum allowable by stoichiometry.

Generally, this reaction index is used in reforming processes, and therefore the results can be compared with other processes in which feeds of different composition have been used.

- *Conversion (X, %):* The reforming conversion has been defined similarly to the C conversion efficiency commonly used in the gasification processes, i.e., the ratio between the moles of C recovered in the gaseous product and those fed into the reforming step.

$$X = \frac{C_{gas}}{C_{volatiles}} \cdot 100 \quad (3.5)$$

Note that the C contained in the biomass char is not considered for estimating conversion, given that it is continuously removed from the conical spouted bed reactor and, is not therefore fed into the reforming step.

- *Specific gas yield (Y_{gas}, $m^3\ kg^{-1}$):* In order to compare the results obtained in the pyrolysis and in-line catalytic reforming strategy with those obtained in gasification processes, the specific gas yield has been defined as follows:

$$Y_{gas} = \frac{Q_{gas}}{m_0} \cdot 100 \quad (3.6)$$

where Q_{gas} is the volumetric flow rate of the gas produced and m_0 is the mass flow rate of biomass or/and HDPE fed into the process.

- *Gas production (P_{gas}, wt %):* Gas production is stated by mass unit of the HDPE or/and biomass in the feed in the pyrolysis-reforming process, and has been calculated as follows:

$$P_{gas} = \frac{m_{gas}}{m_0} \cdot 100 \quad (3.7)$$

where m_{gas} and m_0 are the mass flow rates of the gas produced and biomass or/and HDPE fed into the process, respectively.

- *H_2 production (P_{H2}, wt %):* The H_2 produced in the reforming step is also stated by mass unit of the HDPE or/and biomass in the feed into the pyrolysis-reforming process, and has been calculated as follows:

$$P_{H_2} = \frac{m_{H_2}}{m_0} \cdot 100 \quad (3.8)$$

where m_{H2} and m_0 are the mass flow rates of the H_2 produced and biomass or/and HDPE fed into the process, respectively.

- *Reacted steam (R_{steam}, wt %):* Reacted steam is defined as the amount of steam used in the reforming reaction by mass unit of the biomass and/or HDPE in the feed. It is calculated based on a H mass balance, considering the H contained in the pyrolysis volatile stream, the steam introduced into the process and the H_2 obtained in the reforming step.

3.3.2. Parametric study of biomass valorisation

In this section, the results of the parametric study of the reforming step of biomass pyrolysis volatiles have been described (Figure 3.5), in which the effect of temperature (Section 3.3.2.1), space time (Section 3.3.2.2) and steam/biomass ratio (Section 3.3.2.3) on conversion, product yields and gas product concentrations have been studied at zero time on stream. Moreover, these results have been compared with other strategies studied in the literature, such as gasification and bio-oil reforming. Section 4 deals with the evolution of these results with time on stream due to catalyst deactivation. The conditions for the pyrolysis step have been described in Section 2.3.1.

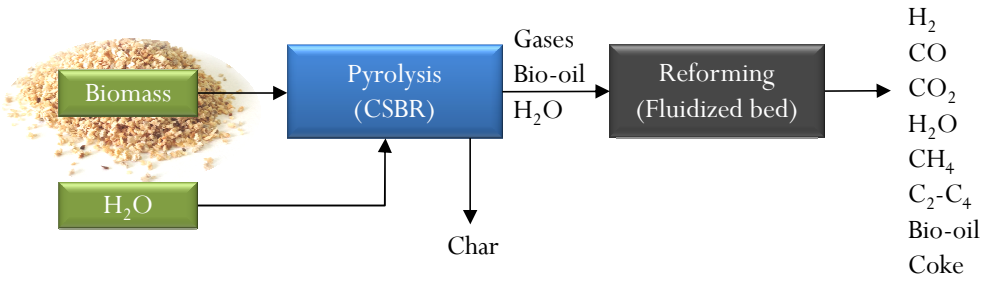

Figure 3.5. Scheme of the two-step process for biomass valorisation.

Furthermore, in order to ascertain the effect operating conditions have on the reaction indices, the following reactions have been considered:

Steam reforming: $$C_nH_mO_k + (n-k)H_2O \rightarrow nCO + \left(n + \frac{m}{2} - k\right)H_2 \quad (3.9)$$

Water gas shift (WGS): $$CO + H_2O \leftrightarrow CO_2 + H_2 \quad (3.10)$$

CH_4 steam reforming: $$CH_4 + H_2O \rightarrow CO + 3H_2 \quad (3.11)$$

C_2-C_4 hydrocarbons steam reforming: $$C_nH_m + nH_2O \rightarrow nCO + \left(n + \frac{m}{2}\right)H_2 \quad (3.12)$$

Cracking (secondary reaction): $$C_nH_mO_k \rightarrow C_xH_yO_z + C_aH_b + CH_4 + CO + CO_2 + C \quad (3.13)$$

3.3.2.1. Effect of temperature

The effect of temperature on products distribution has been studied in the 550-700 °C range. The operating conditions, namely, a relatively high space time (20 g_{cat} min $g_{volatiles}^{-1}$) and S/B ratio (4), have been established to avoid operational problems related to the low conversion of the biomass pyrolysis volatiles in the feed. The

products obtained in the reforming step can be grouped into two fractions: the gaseous products and the non-converted liquids. The main gaseous products obtained in the reforming step are H_2, CO_2, CO, and low concentrations of CH_4 and C_2-C_4 hydrocarbons, composed mainly by ethylene, ethane, propylene and propane. The non-converted product fraction is mainly made up of bio-oil oxygenated compounds leaving the pyrolysis step that have not been reformed, although changes may have undergone in their composition due to certain extent of thermal cracking in the reforming reactor.

The effect of temperature on biomass derived volatile conversion is shown in Figure 3.6. As observed, under the conditions studied, conversion is close to 60 % at 550 ºC, whereas it is full at 600 ºC. Xiao et al. (2011, 2013) studied the pyrolysis and in-line reforming of different biomasses on Ni catalysts in a fluidized-fixed bed system, and they also determined a minimum temperature of 600 ºC to attain high conversion of biomass tars.

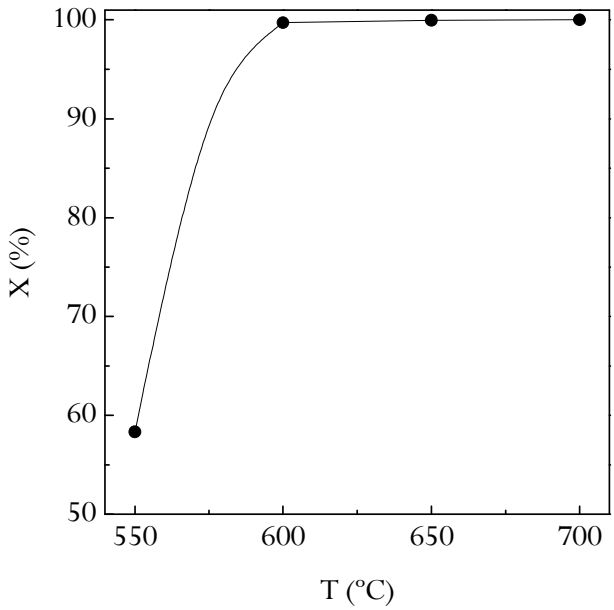

Figure 3.6. Effect of reforming temperature on conversion. Reforming conditions: space time, 20 g_{cat} min $g_{volatiles}^{-1}$; S/B ratio, 4.

Figure 3.7 shows the effect of temperature on the individual gaseous product yields (graph a) and gas composition (graph b). It should be noted that the H_2 yield is based

on the maximum allowable by stoichiometry (eq. (3.4)), but those of the other compounds (eq. (3.1)) are given by C mole unit fed into the reforming step. As observed in Figure 3.7a, the effect of temperature on H_2 yield is negligible once full conversion has been reached (above 600 ºC), with its yield being of around 93.5 % between 600 and 700 ºC. Consequently, 600 ºC is considered an optimum temperature, similarly as happens in the reforming of pure oxygenates (Lemonidou et al., 2013). In addition, operation at this relatively low temperature avoids the irreversible catalyst deactivation by Ni sintering. Although most of the studies in the literature dealing with the steam reforming of bio-oil report lower H_2 yields based on the maximum allowable by stoichiometry than those in this study (Trane et al., 2012), certain authors have reported values as high as 90 % or even slightly higher (Czernik et al., 2007; Kechagiopoulos et al., 2009; Valle et al., 2013).

Regarding H_2 production, it increased from 6.4 wt % at 550 ºC to around 11.0 wt % between 600 ºC and 700 ºC, which is higher in relation to other alternatives studied in the literature. Section 3.3.2.4 deals with a comparison between different strategies and technologies.

CO and CO_2 yields are enhanced by increasing reforming temperature from 550 to 600 ºC (Figure 3.7a). However, above 600 ºC, an increase in CO is observed at the expense of decreasing CO_2, with this trend being related to the exothermic nature of the WGS reaction (eq. (3.10)), which is hindered by temperature.

The effect of temperature on the gaseous fraction composition is not so remarkable (Figure 3.7b). In fact, H_2 concentration takes values of around 66 vol % in the range studied. A slight effect on CO_2 and, especially, on CO concentration is observed, with their evolution being explained by the effect of temperature on the WGS reaction equilibrium. The slight differences between the gas composition obtained at 550 and 600 ºC, with great differences in conversion, are explained by the fact that almost all the gases are produced by reforming. Thus, the formation of gases by secondary reactions, i.e., cracking, decarboxylation, decarbonilation and so on, are of minor significance.

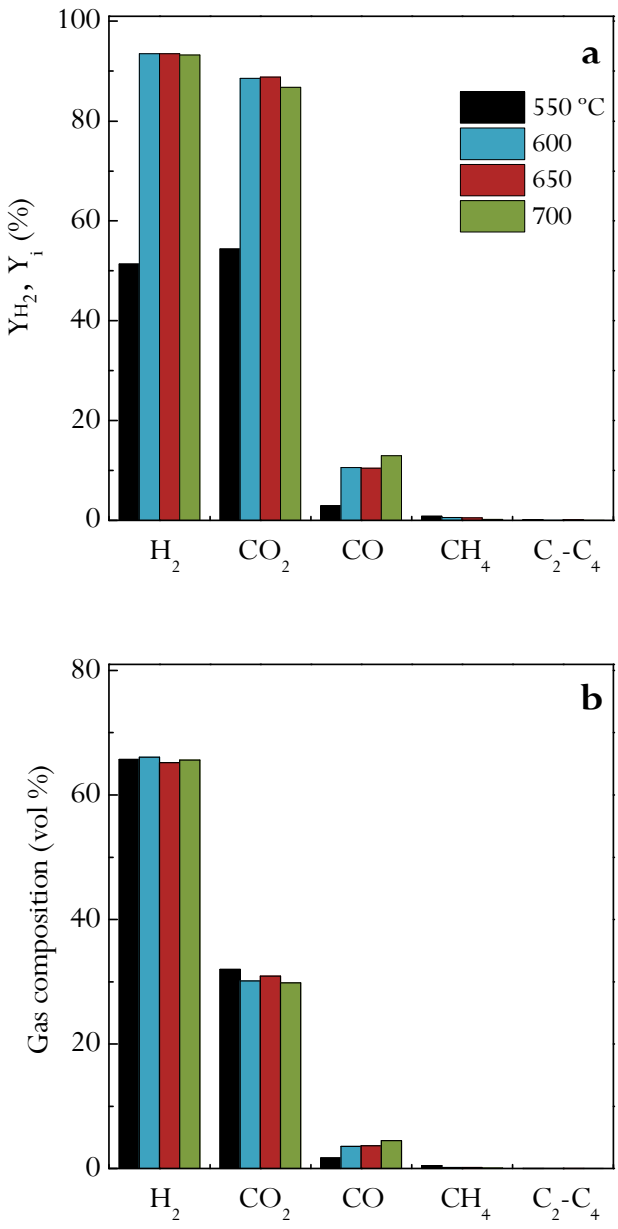

Figure 3.7. Effect of reforming temperature on the yields of the gaseous products (a) and their concentrations (on a dry basis) (b). Reforming conditions: space time, 20 g_{cat} min $g_{volatiles}^{-1}$; S/B ratio, 4.

3.3.2.2. Effect of space time

The effect of space time on biomass volatiles reforming has been studied between 2.5 and 30 g_{cat} min $g_{volatiles}^{-1}$. These experiments have been carried out at 600 ºC and a S/B ratio of 4. It should be noted that the mass of the catalyst has been varied in the experiments performed with different space time values.

As observed in Figure 3.8, a value of 20 g_{cat} min $g_{volatiles}^{-1}$ is required to attain pyrolysis volatiles full conversion. However, operating with 15 g_{cat} min $g_{volatiles}^{-1}$ the process performance is also suitable, obtaining a conversion of 98.5 %. Consequently, specific gas production increases with space time, reaching a value of 1.95 N m^3 $kg_{biomass}^{-1}$ for the highest space time studied (30 g_{cat} min $g_{volatiles}^{-1}$).

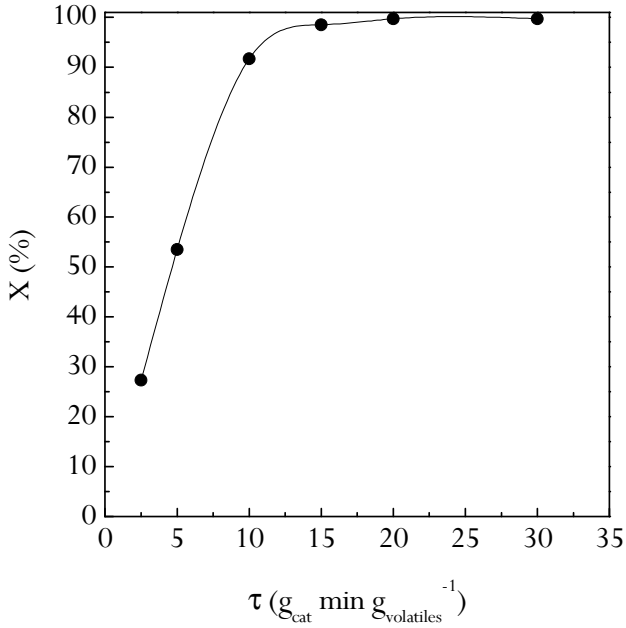

Figure 3.8. Effect of reforming space time on conversion. Reforming conditions: 600 ºC; S/B ratio, 4.

An increase in space time enhances both steam reforming (eq. (3.9)) and WGS (eq. (3.10)) reactions, and therefore the formation of H_2, CO_2 and CO is favoured, as shown in Figure 3.9a. It should be noted that, for the highest space time studied (30 g_{cat} min $g_{volatiles}^{-1}$), CO yield decreases due to the displacement of the WGS reaction. This fact, together with the intensification of CH_4 and C_2-C_4 hydrocarbon reforming,

leads to an increase in H_2 yield, reaching a value of 95.8 % of the maximum allowable by stoichiometry. A qualitatively similar effect of space time on product yields has been observed by several authors in the steam reforming of bio-oil (Seyedeyn-Azad et al., 2011; Remiro et al., 2013a; Fu et al., 2014).

Furthermore, H mass balance (considering the H content in the volatiles, the water fed into the reaction medium and the H_2 produced) allows verifying that reacted steam increases when space time is increased. This value is negative for 2.5 g_{cat} min $g_{volatiles}^{-1}$ because the inner biomass moisture is not consumed, whereas for 30 g_{cat} min $g_{volatiles}^{-1}$ the reacted steam accounts for 52.2 wt % and the H_2 produced for 11.7 wt %.

The influence of space time on gas fraction composition is shown in Figure 3.9b. As observed, the main effect of increasing space time is an increase in H_2 and CO_2 concentration and a decrease in that of CO. In addition, a remarkable improvement of CH_4 conversion is also observed.

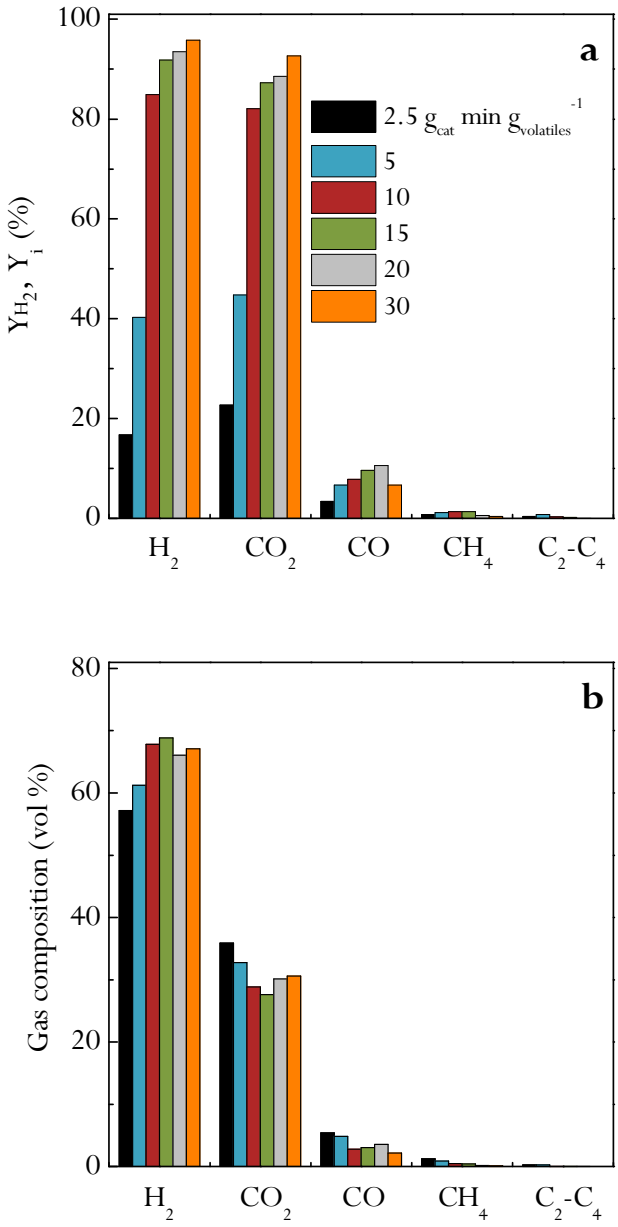

Figure 3.9. Effect of reforming space time on the yields of gaseous products (a) and their concentrations (on a dry basis) (b). Reforming conditions: 600 ºC; S/B ratio, 4.

3.3.2.3. Effect of steam/biomass ratio

The effect of S/B ratio has been studied between 2 and 5, which corresponds to steam/C molar ratios (S/C) between 3.9 and 9.7. As the same steam flow rate was used in all the range studied, which is the one required to keep an adequate spouting regime in the conical spouted bed reactor, the biomass feeding rate was varied to attain different S/B ratios. The other main operating conditions are as follows: 600 ºC and a space time of 20 g_{cat} min $g_{volatiles}^{-1}$.

Figure 3.10 shows the effect of S/B ratio on process conversion. As observed, the effect is almost negligible due to the high conversion values obtained for all the S/B ratios studied, higher than 99.5 %. This result can be attributed to the relatively high space time studied, which ensures high conversion values. Moreover, the presence of steam in the reaction medium also enhances the reaction rates for reforming reactions, eqs. (3.9), (3.11) and (3.12), and the WGS reaction, eq. (3.10).

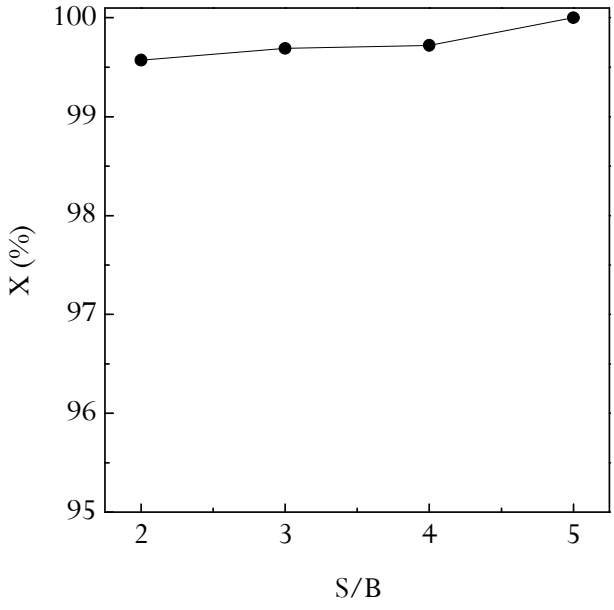

Figure 3.10. Effect of S/B ratio on conversion. Reforming conditions: 600 ºC; space time, 20 g_{cat} min $g_{volatiles}^{-1}$.

Furthermore, as observed in Figure 3.11a, the effect of S/B ratio on the yields of the individual compounds is more noticeable. Thus, an increase in S/B ratio causes a

steady increase in H_2 and CO_2 yields and a reduction in those of CO and CH_4. This result is explained because an increase in the steam partial pressure in the reaction environment enhances steam reforming reaction kinetics (eqs. (3.9), (3.11) and (3.12)), as well as the displacement of the WGS reaction equilibrium (eq. (3.10)). Thus, H_2 yield increases from 89.2 to 94.2 % when the S/B ratio is raised from 2 to 5, although a similar conversion is attained in both experiments. The yield of CO_2 increases from 84.0 to 90.1 %, whereas the opposite trend is observed for CO, i.e., a decrease from 14.4 to 8.9 %. The same effect of S/B ratio on product yields has been reported by other authors in the reforming of bio-oil and pyrolysis vapours (Xiao et al., 2011; Remiro et al., 2013a; Fu et al., 2014) and in the biomass steam gasification (Göransson et al., 2011a; Erkiaga et al., 2014).

Although process conversion efficiency improves for high S/B ratios (Trane et al., 2012), this parameter should be carefully optimized bearing in mind energy efficiency (Xiao et al., 2011), i.e., high S/B ratios require high amounts of steam to be produced and unreacted steam to be condensed at the outlet of the reformer. Considering the different factors, the optimum S/B ratios determined for biomass steam gasification are in the 0.6-0.85 range (Kaushal and Tyagi, 2012), but those for the pyrolysis-reforming strategy should be higher due to the higher steam consumption.

Another predictable effect of an increase in S/B ratio is the reduction in coke formation and the resulting attenuation in catalyst deactivation (Trane et al., 2012), which will be studied in Section 4. However, this parameter should be carefully adjusted in order to avoid a significant increase in external heat requirements (Xiao et al., 2011).

As observed in Figure 3.11b, the effect of S/B ratio on the concentration of gaseous products is qualitatively similar to the effect on product yields. H_2 concentration increases with S/B ratio to a value of 66.1 vol % for an S/B value of 5. However, CO content in the gas decreases from 5.3 to 3.0 vol % in the S/B ratio range studied. The CO_2 concentration does not follow a clear trend, with its concentration being between 30 and 32 vol %. The content of CH_4 and C_2-C_4 hydrocarbons is very low due to the relatively high space time used.

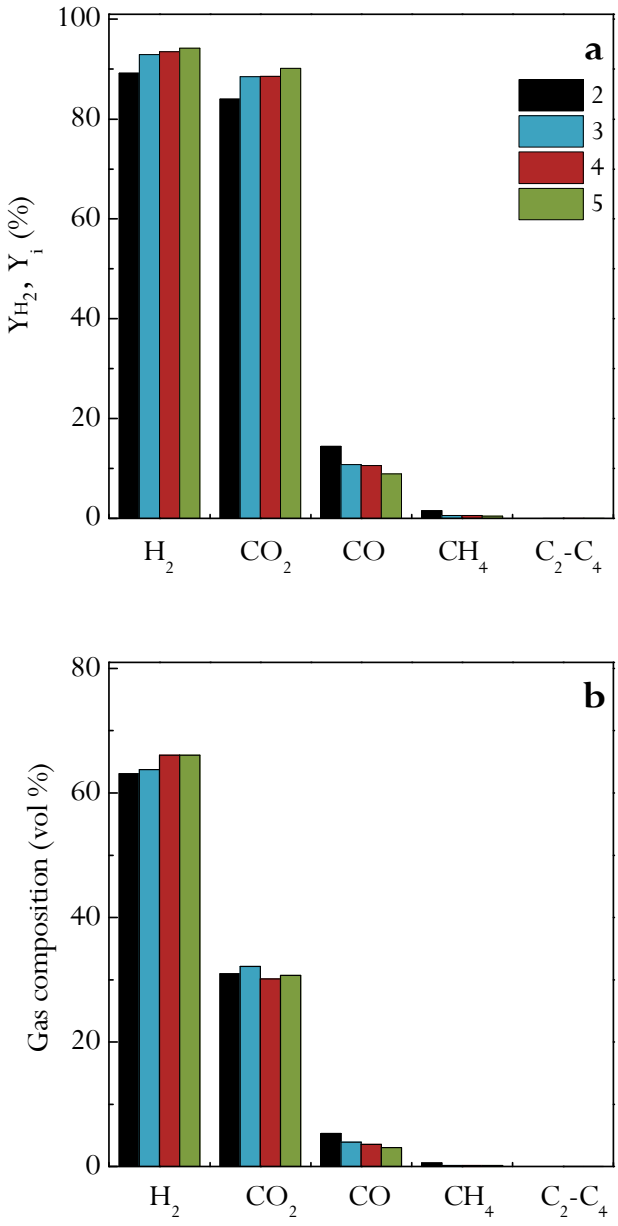

Figure 3.11. Effect of S/B ratio on the yields of the gaseous products (a) and their concentrations (on a dry basis) (b). Reforming conditions: 600 ºC; space time, 20 g_{cat} min $g_{volatiles}^{-1}$.

3.3.2.4. Comparison with literature results

This section deals with a comparison of different strategies (gasification, bio-oil reforming, oxidative bio-oil reforming and pyrolysis-reforming) for H_2 production from biomass. Table 3.3 summarizes a comparison of H_2 production and gas yields obtained in several biomass conversion processes.

As commented above, specific gas production is considerably higher in the pyrolysis-catalytic steam reforming process than those usually reported for the steam gasification of biomass, even though partial conversion of char occurs in the gasification. Thus, a maximum specific gas production of 1.95 N m^3 $kg_{biomass}^{-1}$ has been obtained in this thesis by the pyrolysis-catalytic steam reforming process, whereas it usually ranges between 0.9 and 1.2 N m^3 $kg_{biomass}^{-1}$ in the gasification operating under suitable conditions (Umeki et al., 2010; Koppatz et al., 2011; Michel et al., 2011a; Erkiaga et al., 2014), reaching values of up to 1.7 N m^3 $kg_{biomass}^{-1}$ when using in situ catalysts (Michel et al., 2011b). Nevertheless, it should be noted that the main advantage of the pyrolysis-reforming strategy compared to gasification is the capability for producing a H_2-rich gas free of tars (the main challenge in gasification) by taking advantage of highly active reforming catalysts. Therefore, the pyrolysis-reforming strategy should be conducted with relatively high space times in order to ensure a gas product completely free of tars, which would also ease its subsequent applications.

Regarding H_2 production, a value of 11.0 wt % has been achieved in this thesis. Xiao et al. (2011, 2013) reported a yield of around 10.0 wt % in the pyrolysis and in-line steam reforming of pine wood chips under optimum conditions in a fluidized-fixed bed system. Ma et al. (2014) operated in a three-step process (biomass pyrolysis in a fluidized bed reactor, gasification in an entrained flow reactor and reforming in a fixed bed) and obtained a maximum H_2 production of 7.6 wt % at the highest reforming temperature studied (850 °C). Chen et al. (2016) studied the pyrolysis and in-line steam reforming using two fixed bed reactors, in which a H_2 production of 3.1 wt % was obtained.

Table 3.3. Comparison of H_2 production and specific gas yield in different biomass conversion processes.

Reference	Strategy	Reactor	Feed	T (ºC)	Catalyst	P_{H2} (wt %)	Y_{gas} ($m^3\ kg^{-1}$)
This thesis	Pyrolysis/ reforming	Spouted bed / fluidized bed	Pine wood / pyrolysis volatiles	500/600	Ni commercial	11.0[a]	1.9[a]
Xiao et al. (2011)		Fluidized bed / fixed bed	Pine wood / pyrolysis volatiles	650/650	Ni – coal char	10.0[a]	1.9[a]
Xiao et al. (2013)		Fixed bed / fixed bed	Pine wood / pyrolysis volatiles	700/650	Ni – coal char	5.2[a]	1.12[a]
Ma et al. (2014)		Fluidized bed / fixed bed	Timber wood / pyrolysis volatiles	600/850	Ni – MgO commercial	7.6[a]	1.69[a]
Chen et al. (2016)		Fixed bed / fixed bed	Wood sawdust	500/800	Ni – Ca – AlO_x	3.1[a]	-
Bimbela et al. (2013)	Bio-oil reforming	Fixed bed	Bio-oil aqueous fraction	850	Ni – Al	13.8[b]	2.25[b]
Salehi et al. (2011)		Fixed bed	Raw bio-oil	950	Ni – Ru – Al_2O_3	14.2[c]	-
Remiro et al. (2013a)		Fluidized bed	Raw bio-oil	700	Ni – La_2O_3 – Al_2O_3	11.7[c]	1.85[c]
Kan et al. (2010)		Fixed bed	Raw bio-oil	700	Ni – Cu – Zn – Al_2O_3	10.2[c]	1.6[c]
Czernik et al. (2007)		Fluidized bed	Raw bio-oil + 10 % ethanol	850	Ni – K – Mg commercial	12.9[c]	2.1[c]
Czernik and French (2014)	Oxidative bio-oil reforming	Fluidized bed	Bio-oil aqueous fraction	850	Pt – Al_2O_3 commercial	11.0[c]	1.9[c]
Michel et al. (2011a)	Steam gasification	Fluidized bed	Miscathus giganteus	880	Olivine	4.9[a]	1.2[a]
Koppatz et al. (2011)		Dual fluidized bed	Wood pellets	850	Olivine	4.2[a]	1.13[a]
Erkiaga et al. (2014)		Spouted bed	Pine wood	900	Inert sand	3.2[a]	1[a]
Umeki et al. (2010)		Updraft	Wood chips	700-900	-	3.6[a]	1[a]
Michel et al. (2011b)		Fluidized bed	Miscathus giganteus	900	Ni – olivine	7.3[a]	1.6[a]
Rapagnà et al. (2011)		Fluidized bed	Almond shell	830	Fe – olivine	6.5[a]	1.4[a]

[a] H_2 production defined as $g_{H2}/100g_{biomass}$. [b] H_2 production defined as $g_{H2}/100g_{organic}$. [c] H_2 production defined as $g_{H2}/100g_{bio\text{-}oil}$.

The H_2 productions reported in the biomass steam gasification process vary widely depending on the operating conditions, gasification technology, original biomass properties and, especially, on the type of catalyst used. Thus, when the gasification is performed with an inert material or a primary catalyst, such as dolomite, olivine or γ-alumina, the H_2 productions are between 3.0 and 5.0 wt % (Umeki et al., 2010; Koppatz et al., 2011; Michel et al., 2011a; Erkiaga et al., 2014). The productions are higher, 7.0-8.0 wt %, when the reforming activity is increased by improving the primary catalyst with the addition of Ni or Fe (Michel et al., 2011b; Rapagnà et al., 2011).

Furthermore, a comparison of the H_2 production results with those in the indirect route of bio-oil reforming is complex due to the differences between these two strategies. Thus, in the pyrolysis and in-line reforming process the C contained in char fraction is not reformed, but the entire volatile fraction (including gases and the whole bio-oil) is treated. Nevertheless, the bio-oil reforming strategy has hardly been applied to the whole bio-oil, with the aqueous fraction being the feed in most of the cases. Furthermore, a significant fraction of the bio-oil is lost due to its incomplete vaporization (Czernik and French, 2014). Thus, problems related to phase separation of the raw bio-oil and the repolymerization of phenolic compounds, which have a great potential for H_2 production, hinder the feed of the whole bio-oil into the reforming reactor (Rioche et al., 2005).

Furthermore, the fact that H_2 yields in the bio-oil reforming studies are given on different basis, such as mass unit of organic compounds (without water), bio-oil aqueous fraction or whole bio-oil, also complicates comparison. Thus, the H_2 production obtained by Bimbela et al. (2013) in the steam reforming of the bio-oil aqueous phase on a Ni-Al catalyst was remarkably high, 13.8 wt %, but their production is given by mass unit of organic compounds in the feed. The value reported by Remiro et al. (2013a) in the reforming of raw bio-oil on a Ni/La_2O_3-Al_2O_3 catalyst is 11.7 wt %, which is based on the bio-oil fed into the reforming step. Salehi et al. (2011) obtained a maximum H_2 production of 14.2 wt % based on the raw bio-oil fed into the reformer containing a Ni/Al_2O_3 catalyst. Kan et al. (2010) studied the reforming of raw bio-oil in a fixed bed reactor at 700 ºC on a Ni-Cu-Zn-Al_2O_3 catalyst, achieving a H_2 production of 10.2 wt %. The H_2 production reported by Czernik and French (2014) in the auto-thermal reforming of bio-oil aqueous fraction on a Pt commercial catalyst was slightly lower, between 8.5 and 11.0 wt %, depending on the origin of the bio-oil used. A higher H_2 production was obtained, 12.9 wt %, by Czernik et al. (2007) in the reforming of raw bio-oil/ethanol mixture (90/10 %). Accordingly, the indirect route has a lower H_2 production capacity per

biomass mass unit compared to the direct pyrolysis-reforming strategy, even though high bio-oil yields are obtained (65-75 wt %) in the previous biomass pyrolysis process.

It should be noted that both conversion and H_2 yield are strongly influenced by bio-oil composition due to the different reactivities of the compounds in the bio-oil. Most reforming studies in the literature focus on studying the effect of operating conditions, although certain authors conducted studies dealing with the reactivity of different model compounds in the bio-oil. Thus, Remón et al. (2015) studied the catalytic reforming of acetic acid, phenol, furfural, guaiacol and levoglucosan on a Ni-Co/Al-Mg catalyst at 650 ºC, and the H_2 yield obtained with the different model compounds followed this order: phenol > furfural > acetic acid > guaiacol > levoglucosan. The lower H_2 yields of guaiacol and levoglucosan were explained by the high amount of C converted into coke. 2-methylfuran, furfural and guaiacol steam reforming were studied by Trane-Restrup and Jensen (2015) and the highest temperature (780 ºC) needed for full conversion in the reforming of guaiacol was reported, whereas full conversion was achieved at 700 ºC in the reforming of 2-methylfuran and furfural. Moreover, the highest coke deposition was observed for guaiacol followed by furfural and 2-methylfuran. Wang et al. (2014b) investigated the steam reforming of phenol, acetic acid and hydroxyacetone at 700 ºC on a Ni/nano-Al_2O_3 catalyst and conversion and H_2 yield decrease as follows: hydroxyacetone > acetic acid > phenol. Some model compounds of bio-oil were also studied by Hu and Lu (2009) at temperatures below 500 ºC for the steam reforming of acetic acid, ethylene glycol and acetone, while higher temperatures were needed for the reforming of ethyl acetate and m-xylene.

Nevertheless, the reactivity of these compounds is different when they are reformed alone or in a mixture of different oxygenated compounds. These interactions were studied by Remón et al. (2015) and a different reactivity was reported for the acetic acid depending on the medium. Thus, 100 % conversion was achieved for the reforming of an aqueous solution of acetic acid, whereas 87 % of the acetic acid was converted in the reforming of the aqueous fraction of the bio-oil. Wu et al. (2008b) studied the difference between two simulated aqueous fractions of bio-oil, a light fraction (methanol, ethanol, acetic acid and acetone mixture) and a heavy fraction (furfural, phenol, catechol and m-cresol mixture), and they report that higher temperatures are needed for reforming the heavy fraction, with coke deposition being more significant. Consequently, the difficulty is evident in studying the reactivity of the compounds of biomass pyrolysis volatiles due to the high amount of species contained and the interactions between them.

The results obtained in this work for gas yield and H_2 production, which are also shown in Table 3.3, are better than those by other technologies in the literature. These results are explained by the good performance of this original continuous two-step process, where the separation of pyrolysis and reforming steps has several advantages from an operational point of view and from the catalytic reforming performance.

3.3.3. Valorisation of biomass and HDPE mixtures

Apart from biomass wastes, HDPE has also been studied as co-feed in the pyrolysis and in-line catalytic steam reforming process due to the interest for the development of a flexible process where different wastes can be used as feedstock. The availability of biomass wastes is not constant due to seasonal changes and the addition of plastics helps maintaining a steady supply of feedstocks for the process. The main advantage of thermal treatments, especially of pyrolysis, is that residues of different nature (plastics, tyres, biomass) can be treated together, avoiding the cost of separation of solid wastes. The valorisation of biomass and HDPE mixtures as a whole is an interesting process (Figure 3.12) in order to obtain higher gas yields compared to the treatment of only biomass, given that plastics contribute to increasing the content of H in the feed, and therefore production of H_2 increases significantly. It should also be noted that catalyst deactivation is lower when HDPE is co-fed due to the lower content of oxygenated compounds in the volatile stream, which will be studied in detail in Section 4.

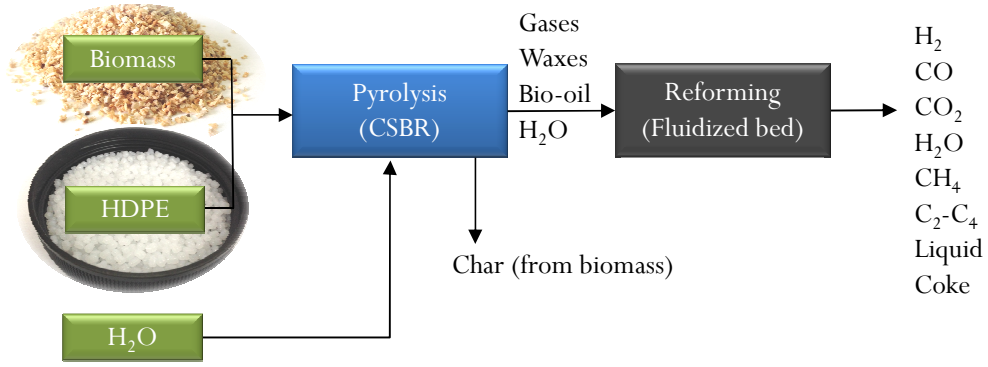

Figure 3.12. Scheme of the two-step process for the valorisation of biomass and HDPE mixtures.

The pyrolysis step of both biomass and HDPE has been studied separately at 500 ºC and the results have been summarized in Section 3.2. As observed, the spouted bed reactor performs well in the treatment of materials of different density and particle size due to the low segregation of the particles and their vigorous cyclic movement.

In this section, the reforming step has been studied by feeding HDPE/biomass mixtures of 25:75 wt %, 50:50 wt % and 75:25 wt % and the following conditions have been used: 700 ºC; space time, 16.7 g_{cat} min $g_{feeding}^{-1}$, and; steam/feed ratio, 4. These conditions have been established based on the results obtained in Section 3.3.2 for the reforming of biomass pyrolysis volatiles and on a previous study by our research group in which the reforming of HDPE pyrolysis volatiles was studied (Barbarias, 2015). These conditions guarantee the total conversion of biomass and HDPE pyrolysis volatiles and low concentrations of CH_4 and C_2-C_4 hydrocarbons in the product stream.

3.3.3.1. Initial conversion

Figure 3.13 shows the effect of HDPE/biomass mass ratio on the reforming conversion. It should be noted that, apart from the reactions described in Section 3.3.2 for the reforming of biomass pyrolysis volatiles, reactions for steam reforming and cracking of hydrocarbons should be added (eqs. (3.14)-(3.15)) in order to take into account the waxes produced in HDPE pyrolysis.

Steam reforming (hydrocarbons): $$C_nH_m + nH_2O \rightarrow nCO + \left(n + \frac{m}{2}\right)H_2 \quad (3.14)$$

Cracking (secondary reaction): $$C_nH_m \rightarrow \text{paraffins} + \text{olefins} \quad (3.15)$$

The runs performed with different HDPE/biomass mass ratios lead to high conversions because the space time used is relatively high (16.7 g_{cat} min $g_{feeding}^{-1}$). Thus, conversion is full when only biomass is fed into the process and decreases slightly when HDPE is co-fed. Nevertheless, almost complete conversion, 98 %, is also achieved with only HDPE. This difference is due to, on the one hand, the higher reactivity of oxygenated compounds from biomass pyrolysis volatiles (Czernik et al., 2007). Thus, in contrast to hydrocarbon reforming, which requires higher temperatures for obtaining full conversion (> 700 ºC), lower reforming temperatures can be used for the reforming of biomass pyrolysis volatiles (600 ºC),

as described in Section 3.3.2. On the other hand, the mass of C to be reformed when biomass is in the feed is lower than when HDPE is in the feed, which is due to two factors: 1) the biomass contains O in its molecular structure, and; 2) a significant fraction of the C is retained in the char produced in the pyrolysis step. Therefore, in the case of HDPE, around 85 g of C are reformed per 100 g in the feed, whereas in the case of biomass 35 g of C are reformed per 100 g in the feed. Consequently, the effective space time (based on the C flow rate entering the reforming reactor) is approximately 2.5 times lower for HDPE than for biomass, although the space time used is enough to guarantee a high conversion of both feeds.

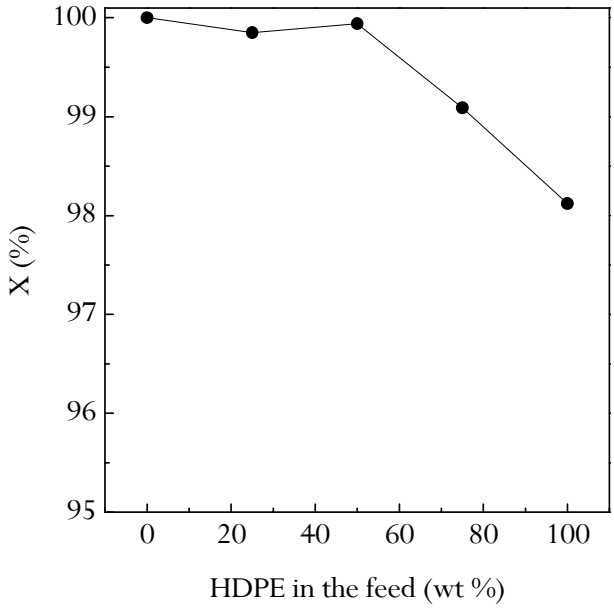

Figure 3.13. Effect of HDPE/biomass mass ratio on conversion. Reforming conditions: 700 ºC; space time, 16.7 g_{cat} min $g_{feeding}^{-1}$; S/F ratio, 4.

As observed in Figure 3.14, gas production increases lineally with the content of HDPE in the feed, obtaining a maximum value of 305.0 wt % when there is only HDPE in the feed. As mentioned above, this result is due to the higher C content of HDPE because it enhances the extent of reforming reactions (eqs. (3.9), (3.11), (3.12) and (3.14)) and leads to an increase in both the gas production and the amount of steam reacted, which also increases with HDPE content in the feed from 48.9 wt % for only biomass in the feed to 210.9 wt % for only HDPE in the feed.

The co-feeding of HDPE also has a major influence on H_2 production, which increases linearly with the HDPE content in the feed. Thus, H_2 production increases significantly from 10.9 wt % for only biomass in the feed to 37.3 wt % when there is only HDPE in the feed. This significant difference is directly related to the C and H content of the feedstocks. The linear increase of the reaction indices plotted in Figure 3.14 shows there is no significant synergetic effect when co-feeding HDPE into the pyrolysis reactor. Although other authors have verified that the co-pyrolysis of plastics and biomass have a noticeable effect on bio-oil composition (Bhattacharya et al., 2009; Xue et al., 2015), the results show that the possible effect observed on pyrolysis volatile products does not have a significant impact on the in-line reforming of these volatiles.

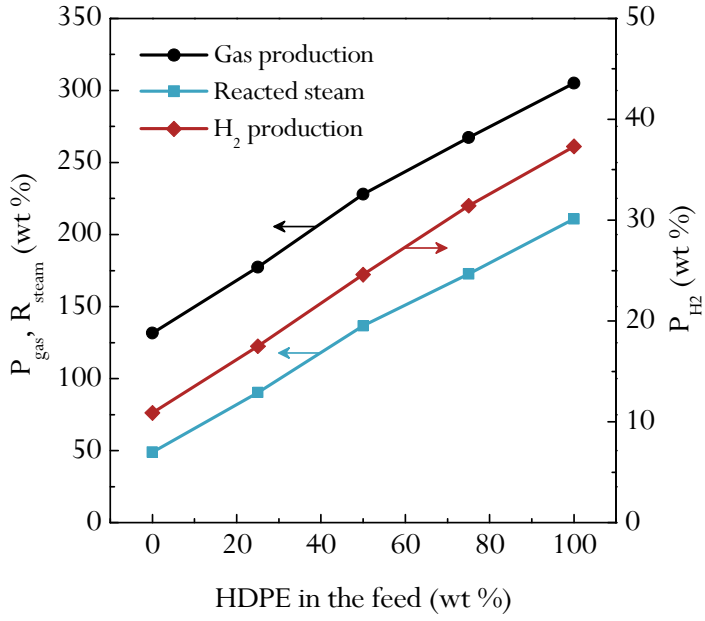

Figure 3.14. Effect of HDPE co-feeding in biomass pyrolysis and in-line reforming on gas and H_2 productions and reacted steam.

In order to compare the results in Figure 3.14 with those in the literature, it should be noted that the studies dealing with pyrolysis and in-line steam reforming of biomass and plastic mixtures are limited to those by the research group headed by prof. Williams. Thus, the influence of biomass/polypropylene ratio (between 5 and 20 wt % of PP in the feed) has been studied by Alvarez et al. (2014a) in a batch pyrolysis-reforming process on a Ni/Al_2O_3 catalyst, obtaining a maximum H_2

production of 5.5 wt %, when 20 wt % of PP was fed. Kumagai et al. (2015) have studied a Ni-Mg-Al-Ca catalyst with different Ca contents and calcination temperatures and the maximum H_2 production was 6.0 wt % when a calcination temperature of 500 ºC was used. These results are significantly lower than those obtained in this study, which is a due to the continuous mode used in this thesis.

3.3.3.2. Initial product yields and concentrations

Figure 3.15 shows the effect HDPE content in the feed has on the individual product yields (graph a) and gas composition (graph b). As observed in Figure 3.15a, there are notable differences in H_2, CO_2 and CO yields. Thus, the yields of H_2 and CO_2 decrease when HDPE content is increased from 0 to 100 wt %, from 93.2 to 85.7 % and from 87.2 to 67.4 %, respectively, while CO yield increases from 12.5 to 29.3 %. These results evidence the effect of the higher C content of HDPE. Moreover, as the same space time is used for all the experiments, a higher yield of CO and a lower yield of CO_2 are obtained when HDPE content in the feed is increased due to the lower extent of WGS reaction (eq. (3.10)). It is also observed that CH_4 and C_2-C_4 hydrocarbons yields are very low in all the cases studied, although there is a slight increase in these yields when HDPE content in the feed is increased from 0 to 100 wt %, i.e., from 0.2 to 0.8 % for CH_4 and from 0.1 to 0.7 % for C_2-C_4 hydrocarbons fraction.

H_2 concentration increases with HDPE content in the feed to 72 vol % when there is 75 wt % of HDPE in the feed (Figure 3.15b), which is due to the higher content of H and absence of O in the plastic composition. Nevertheless, the lower effective space time when HDPE is co-fed leads to lower CO_2 and higher CO concentrations in the gaseous fraction, which in the range of HDPE content studied vary from 30.2 to 20.9 vol % and from 4.3 to 9.1 vol %, respectively. The H_2 concentrations obtained in this thesis are higher than those reported by Alvarez et al. (2014a) in the pyrolysis-reforming of biomass and polypropylene mixtures, with the peak value being 52.1 vol % for 20 wt % polypropylene in the feed.

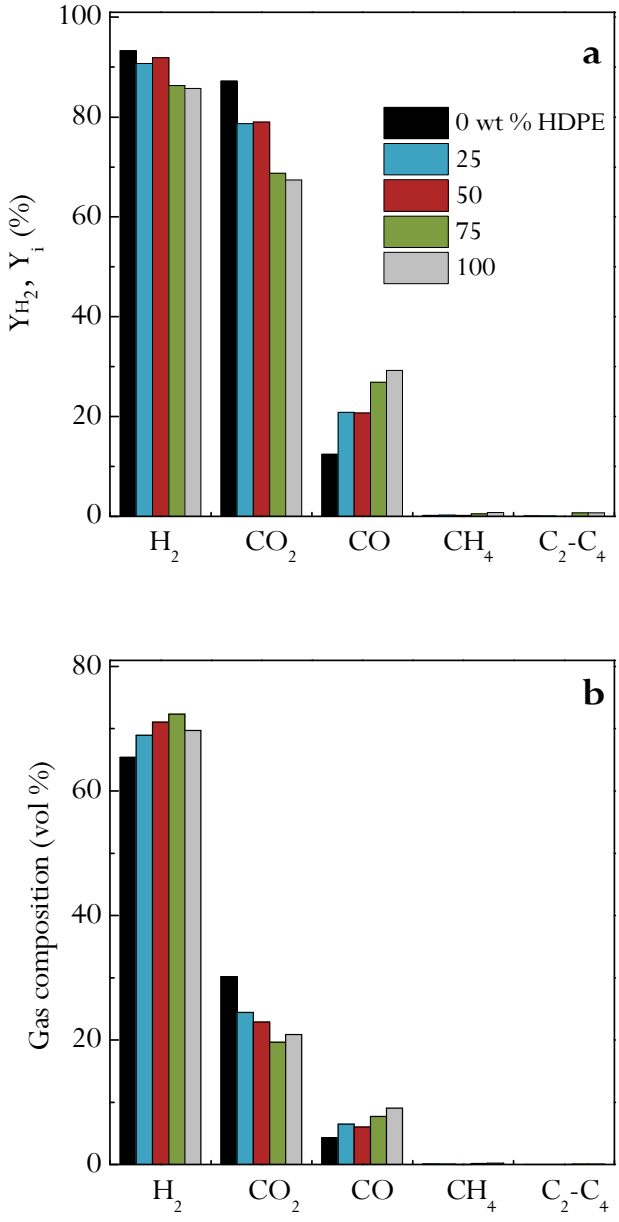

Figure 3.15. Effect of HDPE co-feeding on the product yields (a) and their concentrations (on a dry basis) (b). Reforming conditions: 700 °C; space time, 16.7 g_{cat} min $g_{feeding}^{-1}$; S/F ratio, 4.

3.3.3.3. Comparison of pyrolysis-reforming and gasification processes

In this section, two different strategies for H_2 production from biomass and HDPE mixtures have been compared, pyrolysis and in-line catalytic steam reforming and gasification processes. The co-gasification process of biomass and HDPE mixtures has been previously studied in our research group (Erkiaga, 2014; Lopez et al., 2015b). This comparison has been possible given that both pyrolysis and gasification have been carried out in a conical spouted bed reactor.

As mentioned in the previous section, there are not so many papers dealing with pyrolysis-catalytic steam reforming of biomass and plastic mixtures. Alvarez et al. (2014a) studied the co-feeding of polypropylene in pyrolysis-reforming of biomass, obtaining higher gas yield and higher H_2 production than when feeding only biomass. Kumagai et al. (2015) assayed a Ni-Mg-Al-Ca catalyst synthesized by co-precipitation method for pyrolysis-reforming of a biomass/polypropylene mixture, obtaining a maximum H_2 production of 6.0 wt % when the catalyst was calcined at low temperatures (500 ºC).

The studies dealing with steam co-gasification of biomass and polyolefins reveal the existence of positive and even synergetic effects on H_2 and gas production and tar content in the gas product (Pinto et al., 2002; Ahmed et al., 2011; Ruoppolo et al., 2012; Wilk and Hofbauer, 2013b; Narobe et al., 2014; Lopez et al., 2015b). Lopez et al. (2015b) studied the effect different mixtures of biomass and HDPE have on the steam gasification in a conical spouted bed reactor (CSBR) using dolomite as primary catalyst and they observed a reduction of 83 wt % (from 58.23 to 9.74 g N m^{-3}) in tar content when 50 wt % of plastic was co-fed. The co-gasification of biomass and plastics was also investigated by Wilk and Hofbauer (2013b) in a dual fluidized bed gasifier, with higher gas production being obtained due to the enhancement of reforming reactions. Ruoppolo et al. (2012) studied biomass and plastic chipping gasification using a pilot-scale fluidized bed gasifier and they obtained up to 32 vol % of H_2 concentration. Up to 15 vol % (dry basis) of H_2 concentration and less than 0.5 g N m^{-3} of tar content were obtained by Aznar el al. (2006) in the co-gasification of plastic and pine wood sawdust mixtures. Pinto et al. (2002) also studied the co-gasification of biomass mixed with plastic wastes, and they observed an increase in H_2 concentration to values of 50 vol %.

Tables 3.4 and 3.5 show the gas composition (vol %) in the pyrolysis-catalytic steam reforming and gasification processes, respectively, for only biomass in the feed, only

HDPE in the feed and different mixtures. The results of co-gasification in Table 3.5 have been obtained in a previous study by our research group (Erkiaga, 2014).

Table 3.4. Gas composition (vol %) in pyrolysis-catalytic steam reforming of different biomass and HDPE mixtures.

Compound	0 wt % HDPE	25 wt % HDPE	50 wt % HDPE	100 wt % HDPE
H_2	65.41	68.95	71.06	69.75
CO_2	30.18	24.47	22.88	20.88
CO	4.31	6.47	6.01	9.07
CH_4	0.08	0.09	0.05	0.24
C_2	0.02	0.01	0.00	0.04
C_3	0.00	0.00	0.00	0.02
C_4	0.00	0.00	0.00	0.00

Table 3.5. Gas composition (vol %) in co-gasification of different biomass and HDPE mixtures (Erkiaga, 2014).

Compound	0 wt % HDPE	25 wt % HDPE	50 wt % HDPE	100 wt % HDPE
H_2	39.91	40.65	56.88	57.78
CO_2	9.17	7.72	6.57	7.09
CO	28.32	28.97	27.01	27.27
CH_4	17.78	17.88	6.00	3.14
C_2	4.33	4.30	3.25	4.35
C_3	0.26	0.30	0.17	0.26
C_4	0.24	0.16	0.12	0.12

As observed, the gas composition in the pyrolysis and in-line catalytic steam reforming and gasification processes is very different. It is noteworthy that synthesis gas (CO and H_2 mixture) is the main product in the gasification process, whereas H_2 is the main product in pyrolysis-reforming process. Consequently, an additional step would be necessary in the gasification in order to achieve higher H_2 concentrations. Lopez et al. (2015a) studied an additional reforming step in a fixed bed reactor for the HDPE gasification process, enhancing H_2 concentration from 57.8 to 70.0 vol % in the 600-700 ºC temperature range.

Moreover, the H_2 productions obtained in this thesis by pyrolysis-reforming strategy of pure feeds are higher than those reported in the steam gasification processes, i.e., between 4 and 7 wt % for biomass gasification (Koppatz et al., 2011; Michel et al., 2011b; Erkiaga et al., 2013a) and in the 6-15 wt % range for polyolefin gasification (He et al., 2009; Erkiaga et al., 2013b).

Table 3.6 shows the H_2 production for the two processes studied when different HDPE/biomass mass ratios are in the feed, with the common point being the use of the conical spouted bed reactor. As observed, the highest production of H_2 achieved in the pyrolysis-catalytic steam reforming process is when 100 wt % HDPE is fed. The H_2 production has been considerably increased when the reforming step has been carried out on the Ni catalyst. This effect of the catalyst is due to the enhancement of reforming (eqs. (3.9), (3.11), (3.12) and (3.14)) and WGS (eq. (3.10)) reactions.

Table 3.6. H_2 production (wt %) with different HDPE/biomass ratios.

	0 wt % HDPE	**25 wt % HDPE**	**50 wt % HDPE**	**100 wt % HDPE**
Pyrolysis-reforming	10.89	17.49	24.59	37.30
Gasification	4.24	6.02	13.41	16.46

Thus, the catalytic steam reforming step has an important effect on the gas composition by increasing H_2 and CO_2 concentrations and decreasing CO and CH_4, which improves considerably the gas composition compared to the gasification for H_2 production. Consequently, as the pyrolysis-catalytic steam reforming process needs lower temperatures than gasification, energy efficiency of the process is increased, obtaining higher tar removal yields and H_2 productions.

4

CAUSE AND EFFECT OF CATALYST DEACTIVATION

4. CAUSE AND EFFECT OF CATALYST DEACTIVATION

The deactivation of the catalyst is an important factor for its selection, reactor design and establishment of the optimal operating strategy for industrial catalytic processes. The aim of this study is to observe the effect catalyst deactivation has on reaction indices, improve the knowledge of coke formation and attain useful information to set process operating conditions for minimizing both the evolution of coke with time on stream and its effect on catalyst activity.

It should be noted that the effect catalyst deactivation in the pyrolysis-reforming of biomass has on the reaction indices has been scarcely studied in the literature, given that most studies focus on the results obtained at zero time on stream. Nevertheless, some authors studied the deactivation of the catalyst and its influence on reaction indices in the reforming of the aqueous bio-oil fraction (Yan et al., 2010a; Medrano et al., 2011; Bimbela et al., 2013; Liu et al., 2013; Remiro et al., 2013b; Remón et al., 2013, 2015; Valle et al., 2013; Seyedeyn-Azad et al., 2014; Yao et al., 2014) and raw bio-oil reforming (Czernik et al., 2007; Seyedeyn-Azad et al., 2011, 2012; Remiro et al., 2013a; Czernik and French, 2014).

Moreover, it is well established that coke deposition is the main deactivation cause of Ni based catalysts in the pyrolysis and in-line reforming of biomass (Efika et al., 2012; Nahil et al., 2013; Waheed and Williams, 2013) and plastics (Wu and Williams, 2010c; Acomb et al., 2014), reforming of oxygenated compounds (Montero et al., 2014; Vicente et al., 2014a) and, in particular, in bio-oil reforming processes (Davidian et al., 2007; Wu et al., 2008b; Lan et al., 2010; Remiro et al., 2013b; Yao et al., 2014).

Furthermore, it should be pointed out that the use of the fluidized bed reactor is essential in order to avoid the operational problems caused by the high amount of coke deposited on the catalyst. In previous studies of our research group, Barbarias (2015) reported the good performance of the fluidized bed reactor in the pyrolysis-reforming of different types of plastics (HDPE, PP, PET and PS), which was attributed to the enhancement of coke gasification. Therefore, operation time without problems increases considerably in relation to that corresponding to the use of a fixed bed reactor (Erkiaga, 2014).

Section 4.1 deals with the effect reforming operating conditions (temperature, space time and S/B ratio) have on the evolution of reaction indices (conversion, product

yields and gaseous product concentrations). Accordingly, Section 4.1.1 summarizes the results obtained in the pyrolysis-reforming of biomass and Section 4.1.2 those obtained for the valorisation of biomass and HDPE mixtures. Moreover, Section 4.2 deals with the characterization of the deactivated catalyst, studying the effect of operating variables (Section 4.2.1) and time on stream (Section 4.2.2) on catalyst deactivation in biomass valorisation. In addition, Section 4.2.3 deals with the characterization of the coke deposited in the valorisation of biomass and HDPE mixtures. Finally, Section 4.3 approaches the regeneration with air of the deactivated catalyst in 6 consecutive reforming/regeneration cycles. Thus, the problems related to catalyst deactivation are studied in this section, which are uttermost for the kinetic modelling of the reforming process in Section 5.

4.1. EVOLUTION OF REACTION INDICES WITH TIME ON STREAM

This section addresses the parametric study of catalyst deactivation in the reforming of biomass and biomass/HDPE mixtures. The results obtained for the valorisation of biomass have been used for the kinetic modelling in Section 5.

4.1.1. Valorisation of biomass

The analysis of the products has focused on the gaseous fraction, which is made up of H_2, CO_2, CO, CH_4 and C_2-C_4 hydrocarbons. The non-converted product fraction called bio-oil is mainly made up of bio-oil compounds leaving the pyrolysis step that have not been reformed, although changes would have undergone in their composition due to certain extent of thermal cracking in the reforming reactor.

4.1.1.1. Effect of temperature

The effect of temperature on catalyst deactivation is shown in Figures 4.1-4.3, in which the results of the evolution of conversion, product yields and gaseous stream composition with time on stream are plotted, respectively. Each graph corresponds to a different reforming temperature (550, 600, 650, 700 ºC) and all the results have been obtained with a space time of 20 g_{cat} min $g_{volatiles}^{-1}$ and an S/B ratio of 4.

As observed in Figure 4.1, at 550 ºC the conversion obtained at zero time on stream is very low (< 60 %) and the decrease in the conversion with time on stream is dramatic, obtaining a value lower than 40 % in 20 min. It is noteworthy that this temperature is not high enough to reform the oxygenated compounds derived from biomass pyrolysis. However, between 600 and 700 ºC the differences of both initial conversion and evolution of conversion with time on stream are not very significant, with the decrease in activity being pronounced subsequent to 75 min in the temperature range studied. Moreover, when higher temperatures are used, the decrease in conversion is slightly slower, achieving a conversion of around 60 % in 105 min at 600 ºC, and a similar conversion in 120 min at 700 ºC. As observed, there is an acceleration of deactivation with time on stream once the catalyst starts deactivating (above 75 min), attributable to the non-reformed oxygenated compounds, which are presumably the coke precursors. This aspect should be taken into account in the deactivation model in Section 5.

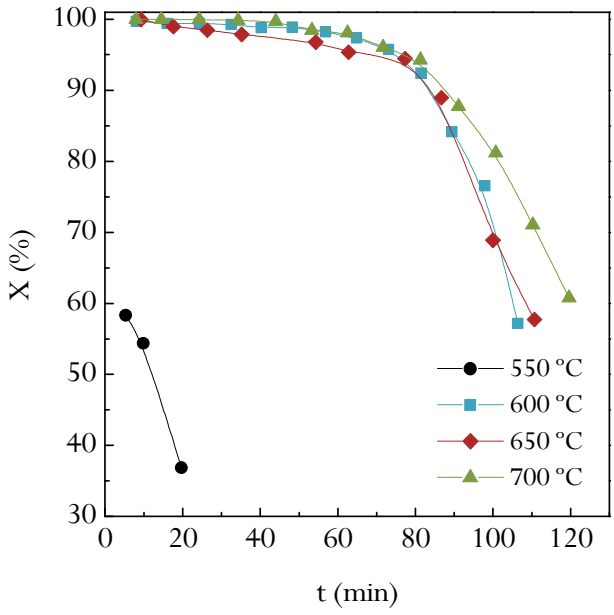

Figure 4.1. Effect of reforming temperature on the evolution of conversion with time on stream. Reforming conditions: space time, 20 g_{cat} min $g_{volatiles}^{-1}$; S/B ratio, 4.

Figure 4.2 shows the evolution of the yields of H_2, CO_2, CO, CH_4, C_2-C_4 hydrocarbons (mainly ethylene, ethane, propylene and propane) and bio-oil (non-converted fraction) with time on stream at 550 (a), 600 (b), 650 (c) and 700 °C (d). It should be pointed out that H_2 yield decreases with time on stream with the same trend shown in Figure 4.1 for the conversion. At 550 °C, H_2 yield decreases from 51.4 at zero time on stream to 27.5 % in 20 min. However, at 600 °C H_2 yield decreases slowly from 93.5 at zero time on stream to 87.8 % in 75 min, with the decrease being more pronounced until 46.4 % in a period of 30 min approximately. H_2 yield follows a similar trend at 650 and 700 °C, although the decrease is higher in relation to that observed at 600 °C for the first 75 min, decreasing from 93.5 to 78.6 % in 77 min at 650 °C and from 93.2 to 82.5 % in 72 min at 700 °C.

As observed in Figure 4.2, CO_2 yield follows a similar trend as H_2 yield with time on stream, obtaining a similar value at the different temperatures when the catalyst is deactivated. Regarding CO yield, it is maintained almost constant at 550 (~3 %) and 600 °C (~10 %), while it increases slightly with time on stream from 10.5 to 16.2 % in 110 min at 650 °C and from 12.5 to 21.4 % in 120 min at 700 °C. This increase is

attributed to the decrease in the WGS reaction rate, due to the deactivation of the catalyst and greater contribution of the cracking of bio-oil oxygenated compounds.

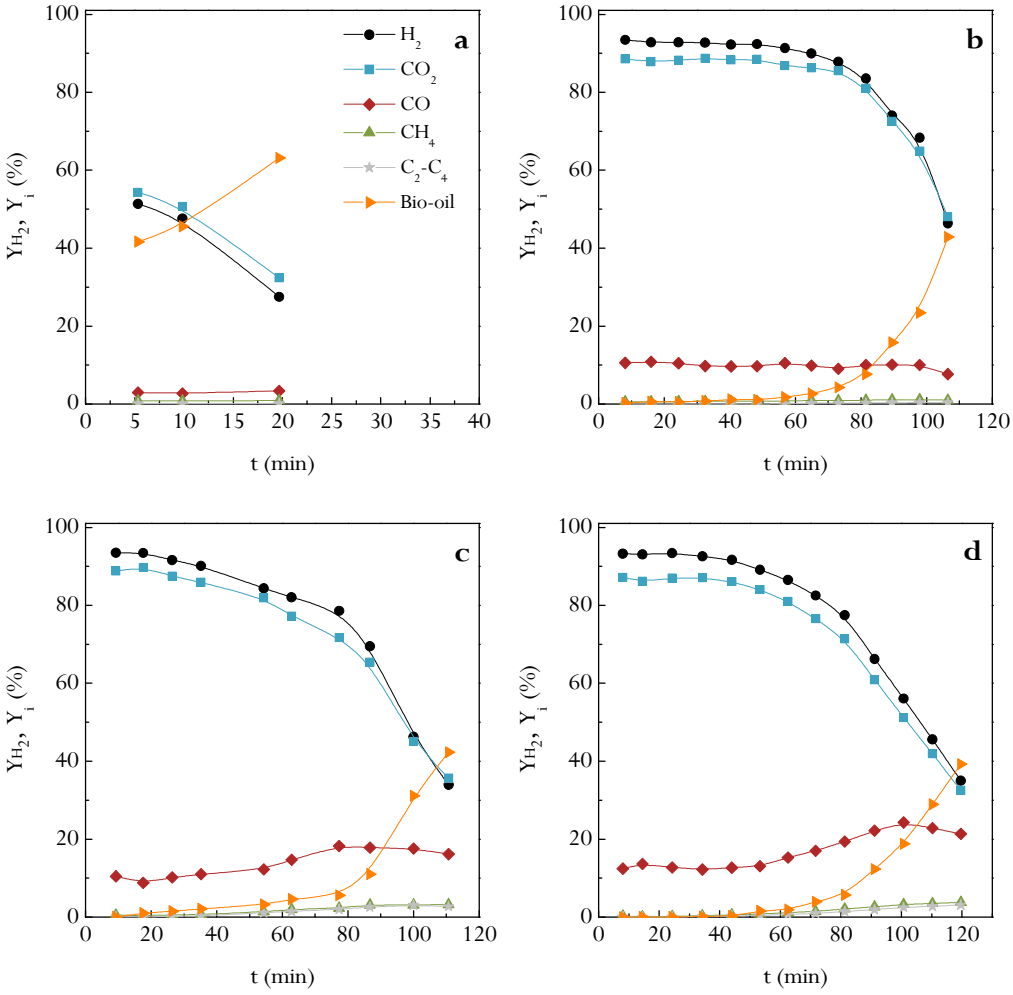

Figure 4.2. Effect of reforming temperature on the evolution of product yields with time on stream at 550 (a), 600 (b), 650 (c) and 700 °C (d). Reforming conditions: space time, 20 g_{cat} min $g_{volatiles}^{-1}$; S/B ratio, 4.

As a consequence of the decrease in the activity for the reforming reactions, the yields of CH_4, C_2-C_4 hydrocarbons and non-converted bio-oil increase with time on stream in the whole temperature range studied, with the increase being exponential as catalyst deactivation is more severe. This trend is explained by thermal cracking

reactions of oxygenated compounds to form CH_4 and C_2-C_4 hydrocarbons, which happens in parallel with the reforming reactions. Consequently, as the rate of reforming reactions is decreased due to catalyst deactivation, thermal cracking reactions are favoured.

As aforementioned, a temperature of 550 ºC is not high enough for the reforming of oxygenated compounds, and therefore non-converted bio-oil yield increases in a pronounced way in 20 min. Between 600 and 700 ºC, the yield of non-converted bio-oil increases to 42.8 % in 105 min at 600 ºC, to 42.3 % in 110 min at 650 ºC and to 39.3 % in 120 min at 700 ºC. This effect of attenuation of the deactivation when temperature is increased is a consequence of several factors. Thus, when temperature is increased, the reforming reactions undergone by the oxygenated compounds derived from biomass pyrolysis are favoured, contributing to a lower content of oxygenates in the reaction environment. Moreover, when temperature is increased the gasification of coke is also favoured, and therefore its evolution is attenuated.

Figure 4.3 shows the effect of reforming temperature on the evolution of gaseous product concentrations with time on stream. As observed, the evolution of the gaseous products concentrations is not as pronounced as in the case of product yields. As commented in Section 3.3.2 for zero time on stream, the slight differences between the gas composition but great differences in conversion are explained by the fact that almost all the gases are produced by reforming. Nevertheless, the gas composition at 600 ºC is more constant that between 650 and 700 ºC. Thus, H_2 concentration decreases slightly from 66.1 vol % at zero time on stream to 63.5 vol % in 105 min at 600 ºC, whereas it decreases at higher temperatures from 65.2 to 55.7 vol % in 110 min at 650 ºC and from 65.4 to 56.0 vol % in 120 min at 700 ºC.

Moreover, the evolution with time on stream of CO_2 concentration also shows slight differences in the trend at different temperatures. At 600 ºC, CO_2 concentration is maintained around 30 vol %, even when the catalyst is deactivated, whereas it decreases from 30.9 to 28.1 vol % in 110 min at 650 ºC and from 30.2 to 24.3 vol % in 120 min at 700 ºC. On the contrary, CO concentration increases with time on stream in the whole temperature range studied. At 600 ºC, it increases slightly from 3.6 to 4.9 vol % in 105 min, with the increase being higher at 650 ºC and 700 ºC, from 3.7 to 12.7 vol % and from 4.3 to 16.0 vol %, respectively. CH_4 and C_2-C_4 hydrocarbons concentrations are very low at zero time on stream and their increase follow the same trend as CO concentration, with the increase being more pronounced above 650 ºC. Thus, the concentrations of CH_4 and C_2-C_4 hydrocarbons

at 600 °C are 0.6 and 0.1 vol %, respectively, in 105 min, whereas at 700 °C they are 2.7 and 1.1 vol %, respectively, in 120 min. Therefore, a higher extent of cracking reactions is noteworthy at high temperatures.

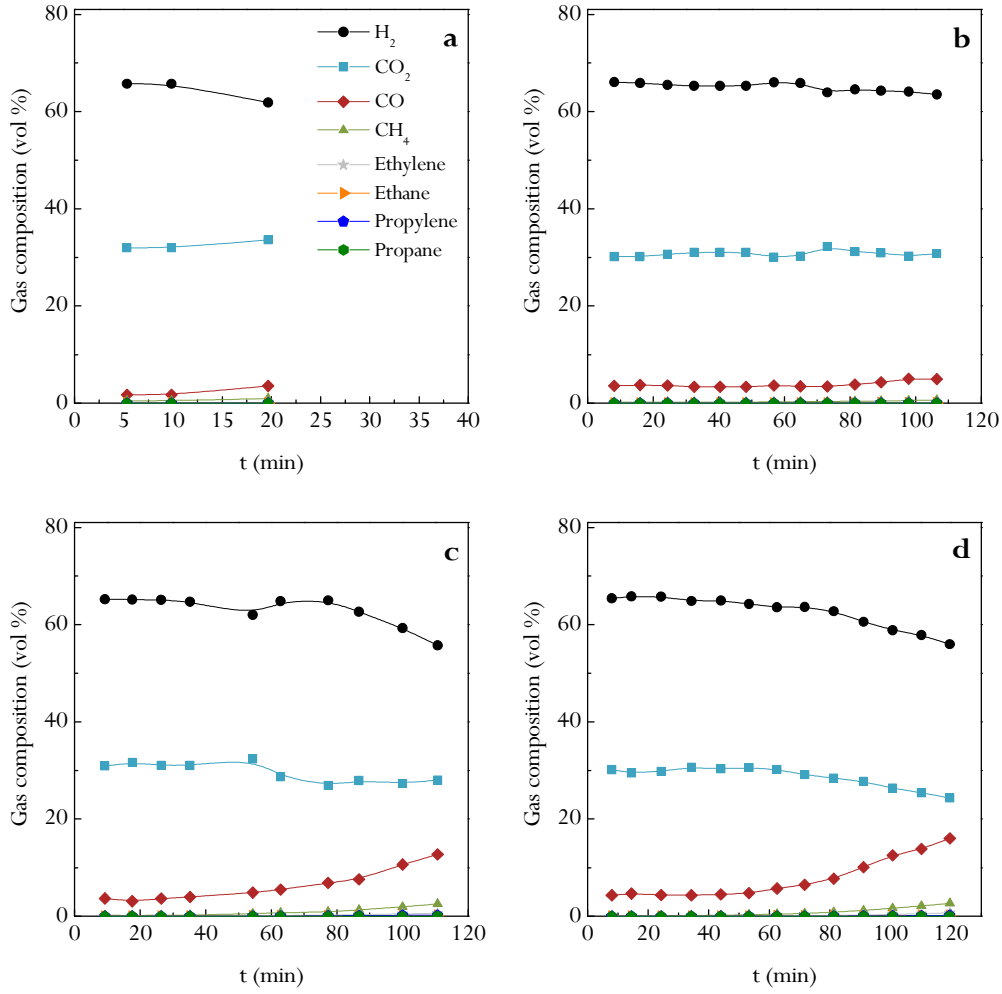

Figure 4.3. Effect of reforming temperature on the evolution of gaseous product concentrations with time on stream at 550 (a), 600 (b), 650 (c) and 700 °C (d). Reforming conditions: space time, 20 g_{cat} min $g_{volatiles}^{-1}$; S/B ratio, 4.

4.1.1.2. Effect of space time

The effect of space time on deactivation has been studied at 600 °C and an S/B ratio of 4, with experiments using 10, 15, 20 and 30 g_{cat} min $g_{volatiles}^{-1}$. The evolution with time on stream of conversion, product yields and gaseous product concentrations are plotted in Figure 4.4, 4.5 and 4.6, respectively.

As observed in Figure 4.4, the decrease in the conversion with time on stream is attenuated when space time is increased, which reveals the role of the non-converted oxygenated compounds as coke precursors. Thus, the formation of coke is attenuated when the presence of these compounds in the reaction environment is decreased. Therefore, almost full conversion is achieved in the first 140 min when a space time of 30 g_{cat} min $g_{volatiles}^{-1}$ is used, whereas it is noteworthy that catalyst deactivation is significant for times longer than 60 min with 20 g_{cat} min $g_{volatiles}^{-1}$, with the decrease in activity being pronounced subsequent to 75 min. Furthermore, with a space time below 15 g_{cat} min $g_{volatiles}^{-1}$, the decrease in conversion is significant for times longer than 20 min.

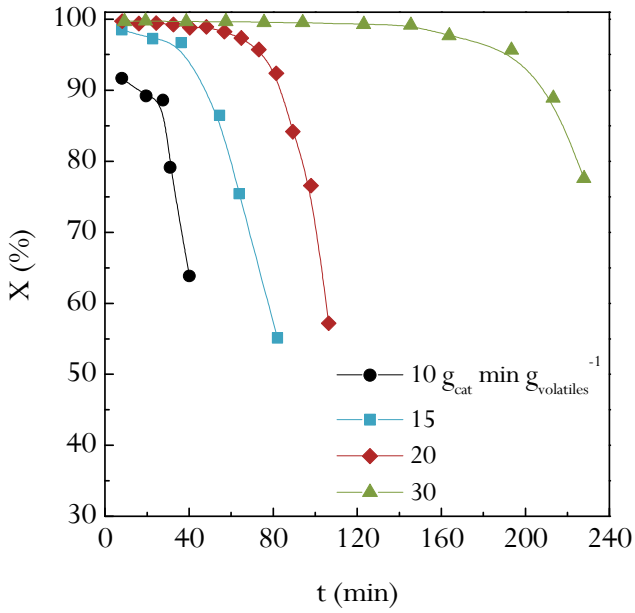

Figure 4.4. Effect of reforming space time on the evolution of conversion with time on stream. Reforming conditions: 600 °C; S/B ratio, 4.

Figure 4.5 shows the effect of space time on the evolution of product yields with time on stream. As mentioned in Section 3.3.2.2, the effect of space time on the initial CO and CO_2 yields is noteworthy. As observed in Figure 4.5, when space time is increased from 10 to 20 g_{cat} min $g_{volatiles}^{-1}$, the initial CO yield increases from 7.9 to 10.6 % and the initial CO_2 yield increases from 82.1 to 88.6 %. However, the initial CO yield decreases to 6.7 % and that of CO_2 increases to 92.6 % for the highest space time studied. Therefore, when space time is increased, at low space time values both reforming and WGS reactions are favoured, whereas at high space time values the WGS reaction is more favoured than reforming reaction.

Concerning the evolution of product yields, the decrease in H_2 yield as time on stream is increased is lower at high space time values, with the decrease being from 84.9 to 55.0 % in 40 min with 10 g_{cat} min $g_{volatiles}^{-1}$ and from 95.8 to 63.3 % in 230 min with 30 g_{cat} min $g_{volatiles}^{-1}$.The effect of space time on the decrease of CO_2 yield follows a similar trend. Furthermore, CO yield does not follow a clear trend, with its value being between 6 and 10 %. The slight effect of space time indicates that the decrease expected for the reduction in the reforming rate due to deactivation is compensated with the formation of CO by cracking of oxygenates. In addition, the presence of CO will also favour catalyst deactivation according to the WGS reaction. However, the deactivation of reforming reactions is also evident, given that the yields of CH_4 and C_2-C_4 hydrocarbons increase exponentially, which is explained by the increase in the non-converted bio-oil in the reaction environment. Therefore, cracking reactions are favoured, enhancing the formation of CH_4 and C_2-C_4 hydrocarbons.

Figure 4.6 shows the effect of reforming space time on the evolution of gaseous product concentrations with time on stream. The influence is small, given that H_2, CO_2 and CO concentrations are almost constant, with their values being of around 65, 35 and 5 vol %, respectively.

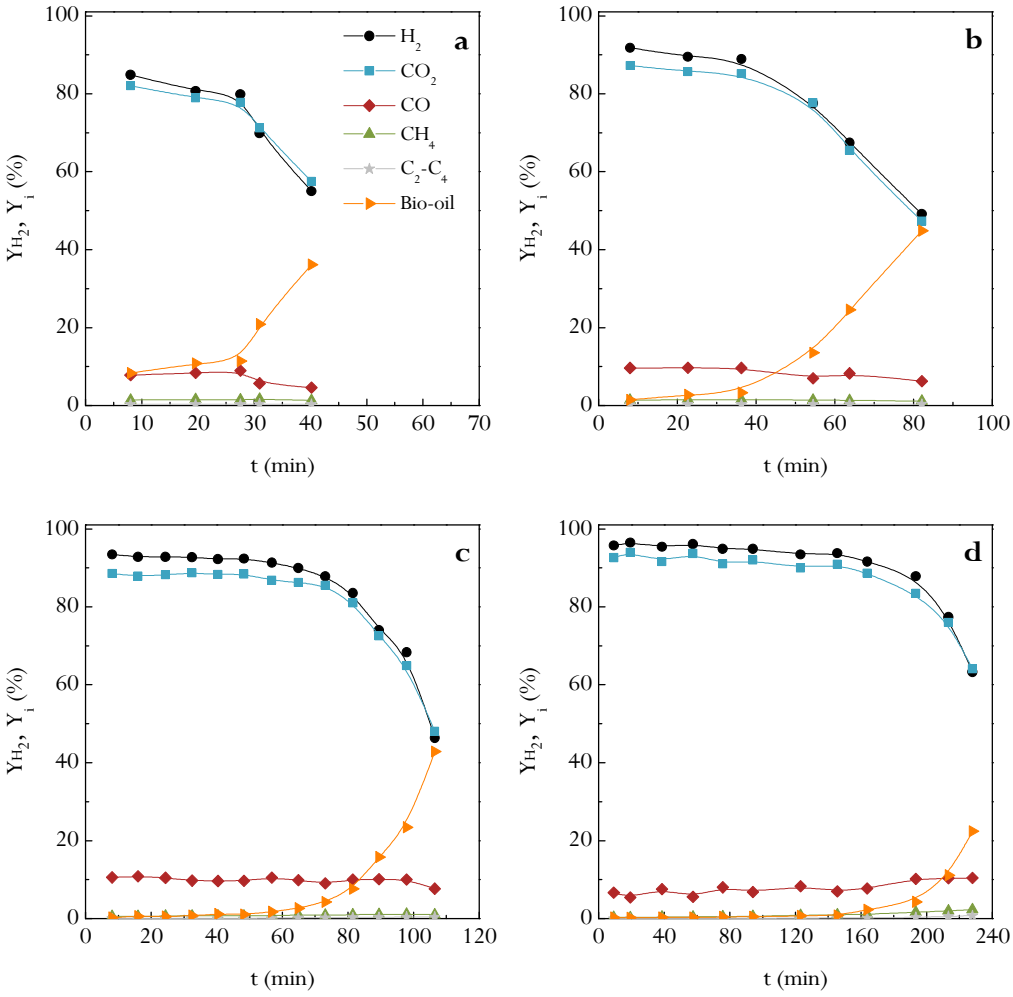

Figure 4.5. Effect of reforming space time on the evolution of product yields with time on stream with 10 (a), 15 (b), 20 (c) and 30 g_{cat} min $g_{volatiles}^{-1}$ (d). Reforming conditions: 600 °C; S/B ratio, 4.

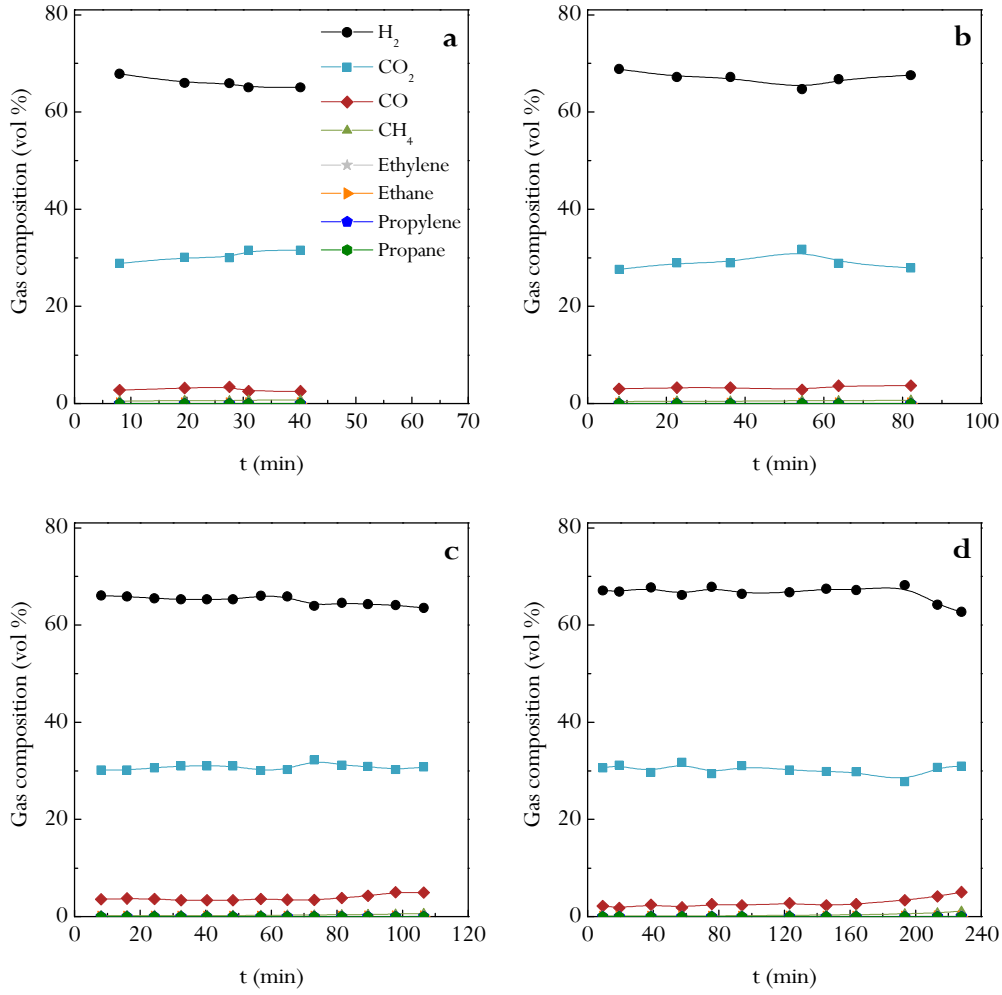

Figure 4.6. Effect of reforming space time on the evolution of gaseous product concentrations with time on stream with 10 (a), 15 (b), 20 (c) and 30 g_{cat} min $g_{volatiles}^{-1}$ (d). Reforming conditions: 600 °C; S/B ratio, 4.

4.1.1.3. Effect of steam/biomass ratio

The effect of S/B ratio on catalyst deactivation is shown in Figures 4.7, 4.8 and 4.9, in which the evolution of conversion, product yields and gaseous product concentrations with time on stream are plotted, respectively. The results correspond

to S/B ratios of 2, 3, 4 and 5 (S/C ratios of 3.9, 5.8, 7.7 and 9.7), at 600 °C and a space time of 20 g_{cat} min $g_{volatiles}^{-1}$.

The results in Figure 4.7 show that although conversion is almost complete at zero time on stream in the S/B ratio range studied, the deactivation is attenuated considerably at high S/B ratios, with the attenuation being significant from 2 to 4. These results are a consequence of the lower concentration of oxygenated compounds (which are coke precursors) in the reaction environment, the higher reforming rate of coke precursors and the higher gasification rate of the evolved coke. However, above an S/B ratio of 4, its influence on conversion is negligible, given that steam is in excess. It should noted that steam excess can saturate Ni active sites (Joensen and Rostrup-Nielsen, 2002).

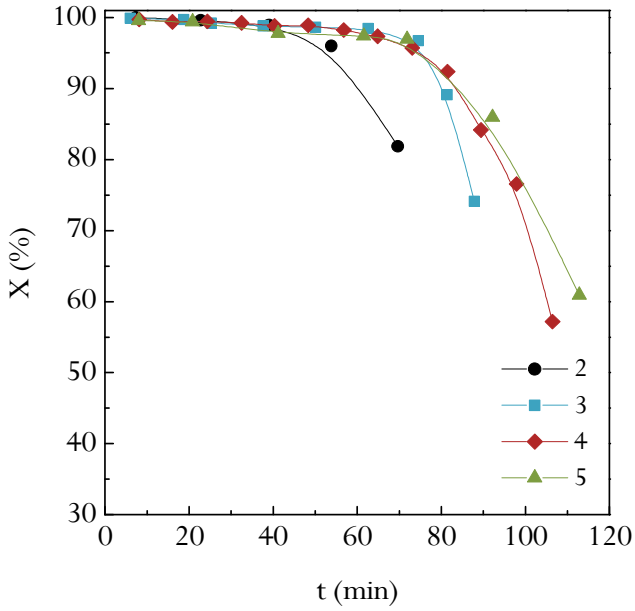

Figure 4.7. Effect of S/B ratio on the evolution of conversion with time on stream. Reforming conditions: 600 °C; space time, 20 g_{cat} min $g_{volatiles}^{-1}$.

Figure 4.8 shows the effect of S/B ratio on both the initial yields of products and catalyst deactivation. As mentioned in Section 3.3.2.3, the influence on the initial yields of products is relevant, given that higher H_2 and CO_2 yields and lower CO yield are obtained due to the enhancement of the reforming and WGS reactions.

However, the effect on deactivation is not so significant at high S/B ratios. Moreover, it should be noted that the presence of CH_4, C_2-C_4 hydrocarbons (produced by cracking reactions) and non-converted bio-oil in the reaction environment is delayed when higher S/B ratios are used. As observed, conversion and H_2 and CO_2 yields are constant for the first 70 min above an S/B ratio of 3, with the decrease being slightly less pronounced above 70 min for high S/B ratios.

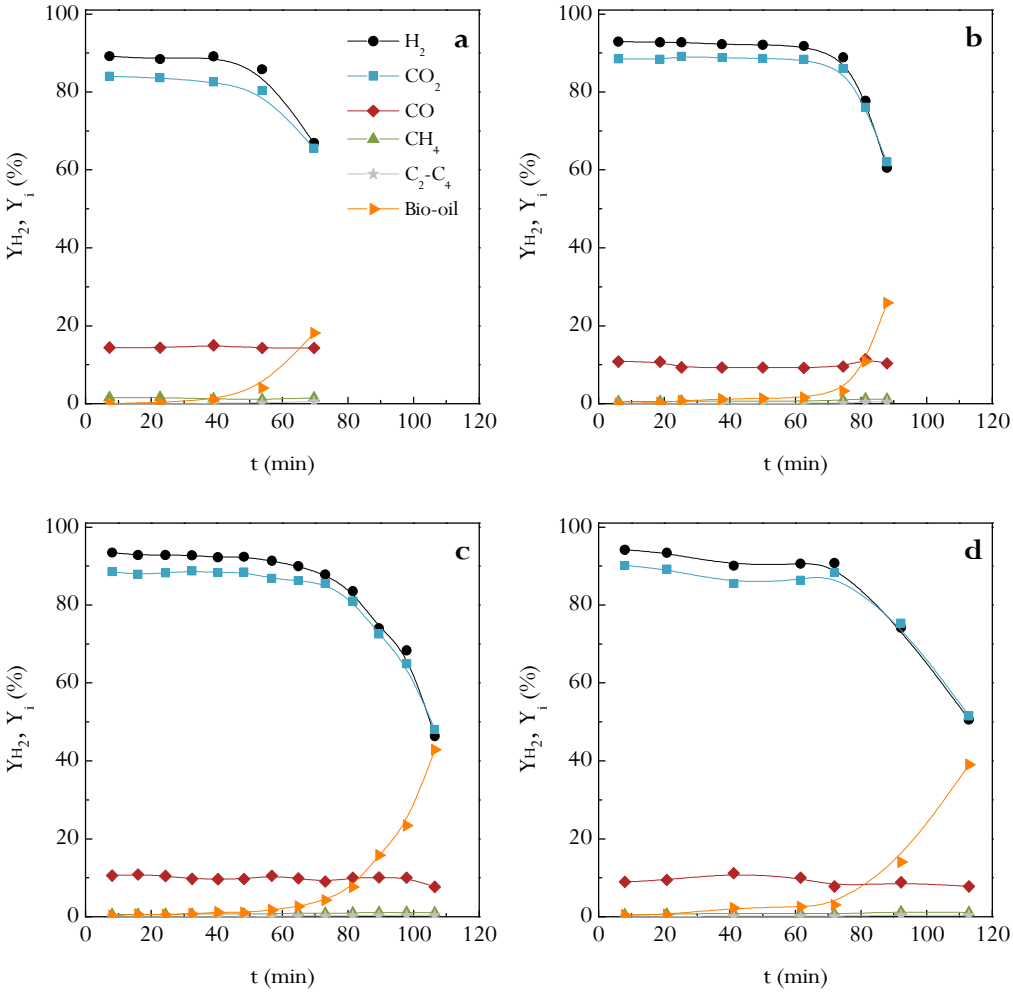

Figure 4.8. Effect of S/B ratio on the evolution of product yields with time on stream with an S/B ratio of 2 (a), 3 (b), 4 (c) and 5 (d). Reforming conditions: 600 ºC; space time, 20 g_{cat} min $g_{volatiles}^{-1}$.

The results in Figure 4.9 confirm that the deactivation does not have an impact on gaseous product concentrations, although slightly lower concentrations of CH_4 and C_2-C_4 hydrocarbons are achieved with high S/B ratios when catalyst deactivation is significant.

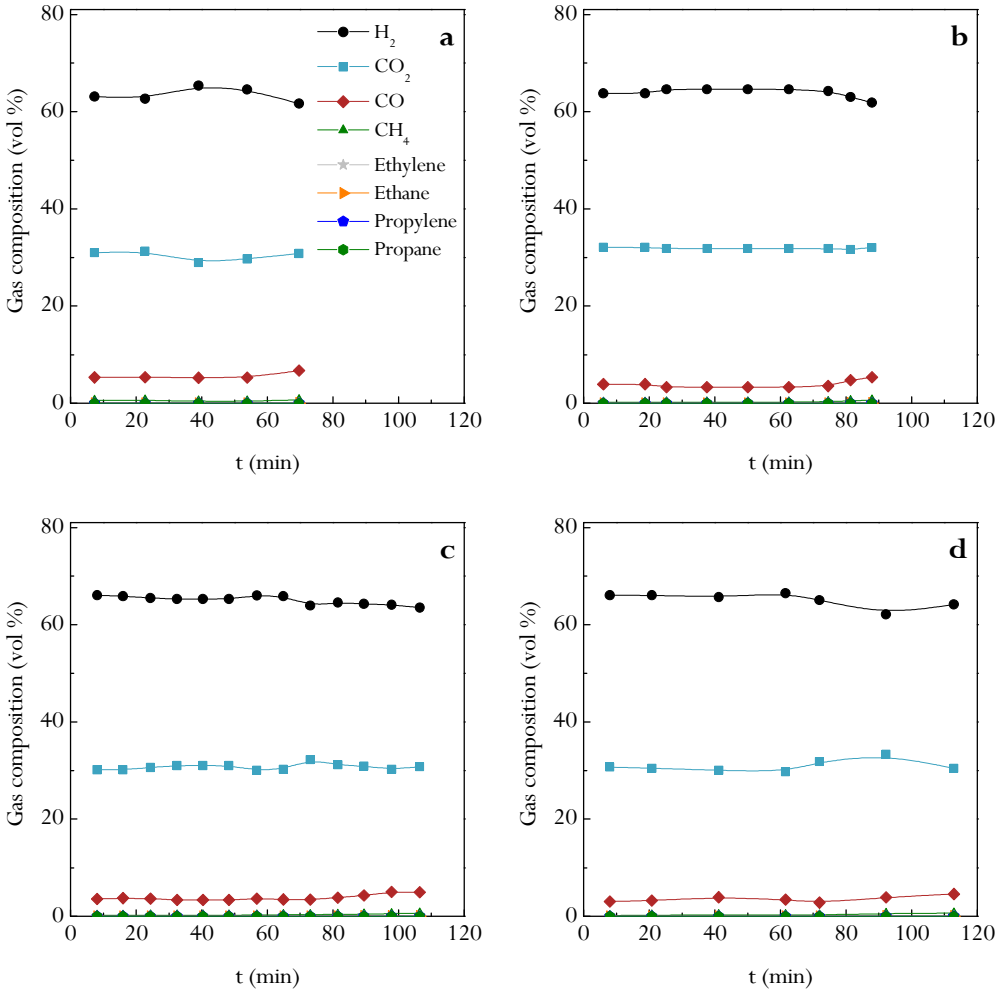

Figure 4.9. Effect of S/B ratio on the evolution of gaseous product concentrations with time on stream with an S/B ratio of 2 (a), 3 (b), 4 (c) and 5 (d). Reforming conditions: 600 °C; space time, 20 g_{cat} min $g_{volatiles}^{-1}$.

4.1.1.4. Comparison with literature results

As mentioned above, there are not many studies dealing with pyrolysis-reforming processes in which the deactivation of the catalyst and its effect on reaction indices have been investigated. Nevertheless, there is a considerable number of studies dealing with bio-oil reforming and this section describes the evolution of reaction indices compared to those obtained in the literature.

Medrano et al. (2011) obtained an initial conversion of 81 % on a Ni-Al based catalyst in the reforming of bio-oil aqueous fraction, and observed it was almost constant with time on stream. Remón et al. (2015) studied the reforming of different bio-oils and obtained full initial carbon conversion in the reforming of pine bio-oil, although it decreases to 40 % in 120 min on stream at 650 ºC, using 4 g_{cat} min $g_{organic}^{-1}$ and an S/C ratio of 7.6. The effect of temperature on conversion was also studied by Remiro et al. (2013b) in the 500-800 ºC range, with 0.22 g_{cat} h $g_{bio\text{-}oil}^{-1}$ and an S/C ratio of 12. They observed full conversion for 5 h above 700 ºC, which was attained by a thermal treatment step in which they re-polymerized lignin derived components and removed prior to the reforming step.

Concerning product yields, a similar trend to that observed in this thesis was obtained in the studies dealing with the reforming of bio-oil aqueous fraction, where a decrease in H_2 and CO_2 yields and an increase in CO and CH_4 yields were reported (Czernik et al., 2007; Medrano et al., 2011; Remiro et al., 2013b; Valle et al., 2013; Remón et al., 2015). Yan et al. (2010a) reported higher catalyst deactivation over Ni/CeO_2-ZrO_2, obtaining a value of 32 % after the first 50 min on stream.

A similar trend to that obtained in this thesis was observed for the evolution of gaseous product concentrations by Xu et al. (2010) in a fluidized bed reactor, although the concentration was maintained constant for longer than 6 h, due to the high space time used in the experiments (150 g_{cat} min $g_{bio\text{-}oil}^{-1}$).

4.1.2. Valorisation of biomass and HDPE mixtures

This section deals with the influence of HDPE co-feeding on conversion, product yields and gaseous product concentrations with time on stream. The results correspond to the experiments described in Section 3.3.3, in which the reaction indices at zero time on stream have been studied at 700 ºC, with 16.7 g_{cat} min $g_{feeding}^{-1}$ and an S/F ratio of 4. These conditions allow obtaining high conversion of volatiles from pyrolysis and so avoid operational problems.

4.1.2.1. Conversion

Figure 4.10 shows the conversion with time on stream for different HDPE/biomass mass ratios.

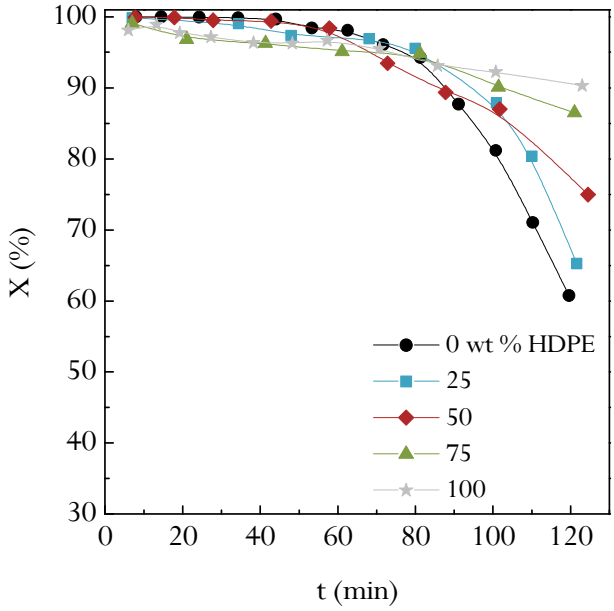

Figure 4.10. Effect of HDPE co-feeding on the evolution of conversion with time on stream. Reforming conditions: 700 °C; space time, 16.7 g_{cat} min $g_{feeding}^{-1}$; S/F ratio, 4.

As observed, the deactivation behaviour depends largely on feed composition. Thus, the conversion after 120 min continuous operation in the reforming step is around 60 % for only biomass in the feed, whereas it is higher than 90 % for only HDPE in the feed for the same time on stream. Moreover, a linear decay of catalyst activity is significant for HDPE, whereas in the case of biomass, activity is maintained for the first 60 min, with a sharp downward trend being recorded after 75 min.

The initial stable conversion period observed for only biomass in the feed is explained by the space time value exceeding the equilibrium one. The most pronounced decrease in activity observed in Figure 4.10 is obtained for only biomass in the feed, even though the effective space time for this feed is approximately 2.5 times higher than for only HDPE in the feed. These results clearly show that the oxygenated

compounds and aromatic rings (such as phenols) produced in the pyrolysis of biomass cause a much faster deactivation than the long chain hydrocarbons produced in the pyrolysis of HDPE. Likewise, Czernik et al. (2007) have reported that oxygenated compounds have a more pronounced tendency than hydrocarbons to form carbonaceous deposits on the catalyst surface, and therefore cause faster catalyst deactivation. In fact, severe reforming catalyst deactivation has been previously reported by other authors in the reforming of biomass derived oxygenates (Rioche et al., 2005; Trane et al., 2012; Lemonidou et al., 2013). The evolutions of conversion observed with time on stream for HDPE/biomass mixtures of 25/75, 50/50 and 75/25 wt % are between those corresponding to only biomass and only HDPE in the feed.

4.1.2.2. Product yields and concentrations

Figure 4.11 shows the evolution of the yields of H_2, CO_2, CO, CH_4, C_2-C_4 hydrocarbons and non-converted liquid with time on stream for different HDPE/biomass mass ratios: only biomass in the feed (a), mixtures of HDPE/biomass ratio of 25/75 (b), 50/50 (c), 75/25 wt % (d) and only HDPE in the feed (e). It should be noted that H_2 yield decreases in all cases with time on stream, although the decrease is less pronounced as HDPE/biomass mass ratio is increased, obtaining a H_2 yield of 35.0 and 64.9 % after 120 min for only biomass and only HDPE in the feed, respectively. In the same way, CO_2 follows the same tendency of H_2 yield, although CO yield does not show a clear trend. When only biomass is valorised, CO yield increases slightly with time on stream, whereas it decreases slightly when only HDPE is fed. This difference in the trend is related to the different origin of CO, given that oxygenate cracking contributes to the formation of CO in the reforming of biomass.

The decrease in activity in the reforming and WGS reactions favours the secondary cracking reactions, obtaining higher yields of CH_4 and C_2-C_4 hydrocarbons with time on stream, with the increase being more pronounced as HDPE/biomass mass ratio is increased. CH_4 yield increases from 0.2 to 3.8 % and from 0.8 to 4.6 % and C_2-C_4 hydrocarbon yield from 0.1 to 3.1 % and from 0.7 to 10.5 % in 120 min, when only biomass and only HDPE in the feed are used, respectively.

It is noteworthy that the non-converted liquid yield is lower when HDPE/biomass mass ratio is increased with time on stream, due to the lower deactivation of the catalyst when hydrocarbons are fed. Thus, 39.3 % of non-converted bio-oil is

obtained after 120 min on stream when only biomass is fed, whereas 9.7 % of non-converted waxes are obtained at the same time when there is only HDPE in the feed.

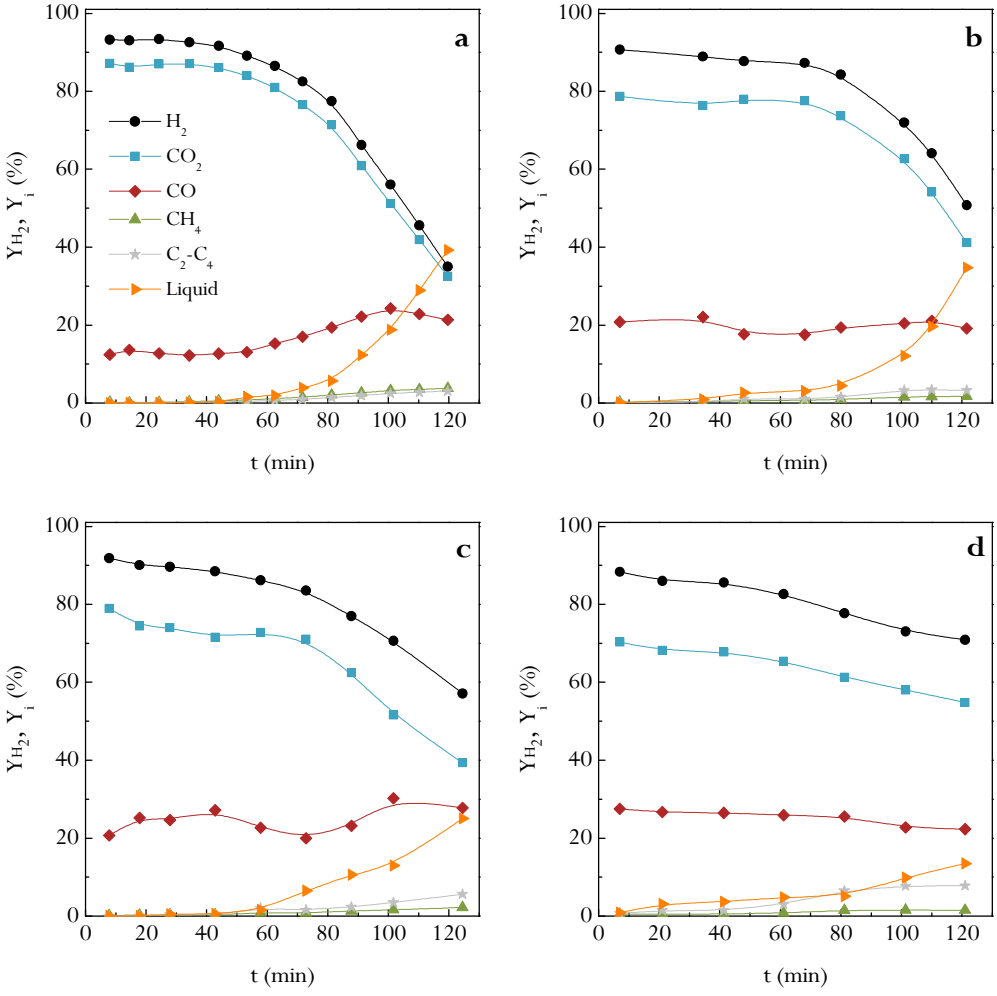

Figure 4.11. Effect of HDPE co-feeding on the evolution of product yields with time on stream with only biomass in the feed (a), HDPE/biomass mixtures of 25/75 (b), 50/50 (c), 75/25 wt % (d) and only HDPE in the feed (e). Reforming conditions: 700 °C; space time, 16.7 g_{cat} min $g_{feeding}^{-1}$; S/F ratio, 4.

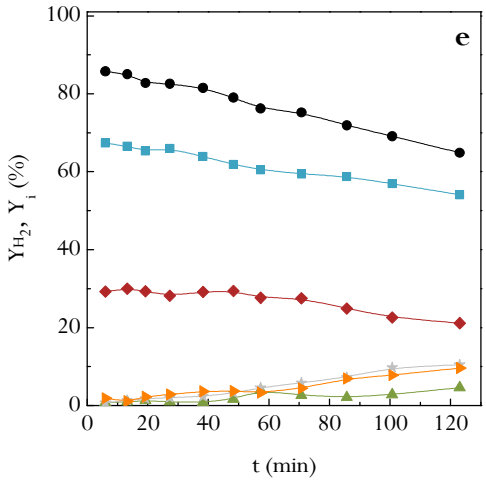

Figure 4.11. Continued.

Figure 4.12 shows the evolution of gas composition with time on stream for different feeds: only biomass (a), HDPE/biomass ratio of 25/75 (b), 50/50 (c), 75/25 wt % (d) and only HDPE (e). When there is only biomass in the feed, H_2 concentration decreases from 65.4 to 56.0 vol % in 120 min on stream, whereas it remains around 70 vol % when there is only HDPE in the feed. Moreover, when there is only biomass in the feed, CO concentration increases from 4.3 to 16.0 vol % after 120 min on stream and the opposite occurs for CO_2, i.e., it decreases from 30.2 to 24.3 vol %. This evolution of CO and CO_2 concentrations reveals a significant deactivation of the catalyst for the WGS reaction. Nevertheless, the concentrations of CO and CO_2 remain almost constant when there is only HDPE in the feed and above 75 min on stream they change slightly for the different HDPE/biomass mixtures. Therefore, when HDPE is co-fed, catalyst deactivation affecting the WGS reaction is considerably attenuated.

As noted above, the concentrations of the main gaseous products formed by secondary cracking reactions, i.e. CH_4 and C_2-C_4 hydrocarbons (mainly ethylene, ethane, propylene and propane), are initially very low for the different feeds studied, due to the catalyst activity for reforming oxygenated compounds and hydrocarbons (eqs. (3.9) and (3.14)) and for the WGS reaction (eq. (3.10)). However, when the catalyst is deactivated, CH_4 and C_2-C_4 hydrocarbon concentrations increase significantly, which is shown in detail in Figure 4.12. A similar trend (although less pronounced) is observed when 25 wt % HDPE, 50 wt % HDPE and 75 wt % HDPE are co-fed into the reactor.

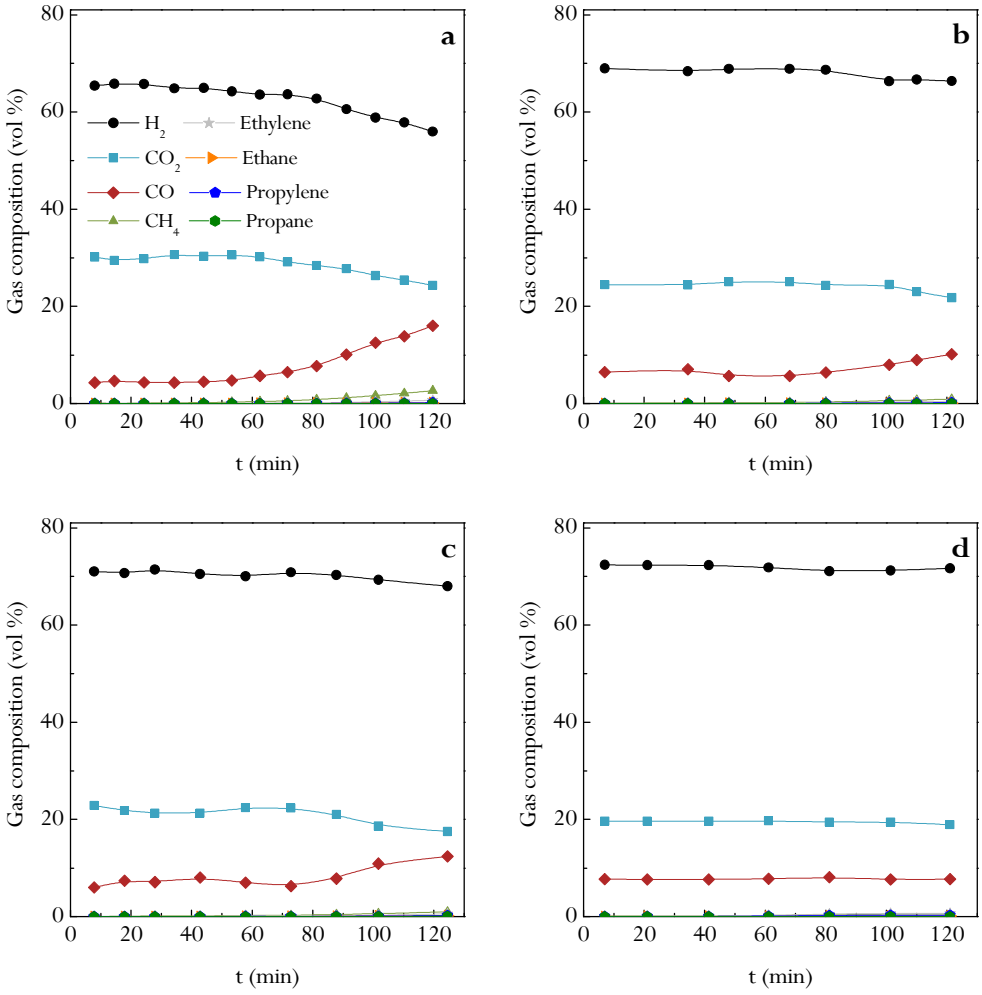

Figure 4.12. Effect of HDPE co-feeding on the evolution of gaseous product concentrations with time on stream with only biomass in the feed (a), HDPE/biomass mixtures of 25/75 (b), 50/50 (c), 75/25 wt % (d) and only HDPE in the feed (e). Reforming conditions: 700 °C; space time, 16.7 g_{cat} min $g_{feeding}^{-1}$; S/F ratio, 4.

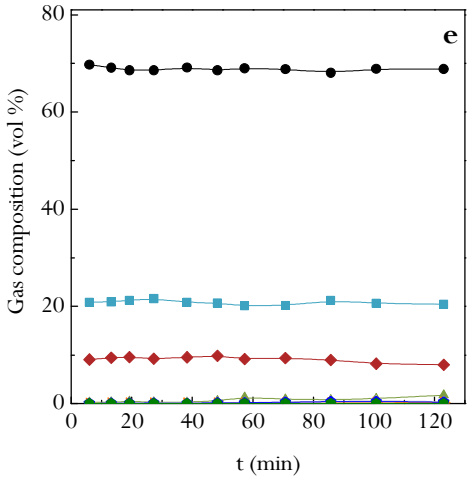

Figure 4.12. Continued.

4.2. DEACTIVATED CATALYST CHARACTERIZATION

The deactivation of the catalyst is a determining factor in the viability and operation of industrial catalytic processes. Among the different deactivation causes in the reforming reactions in which Ni is used as metallic site, the deposition of coke is the main reason of commercial catalyst deactivation, given that there are not problems related to Ni sintering (temperatures lower than 850 ºC) and S poisoning (biomass does not contain S). The deposition of coke has also been reported as the main deactivation cause in the reforming of CH_4 (Angeli et al., 2015), hydrocarbons (Wu and Williams, 2010c; Acomb et al., 2014) and oxygenated compounds, such as ethanol (Simson et al., 2011; Montero et al., 2015). The characteristics of the coke (composition/structure, morphology and reactivity) vary with the nature of the reformed compound, the type of catalyst and reaction conditions, with temperature being one of the most influential parameters. Some authors identified three types of coke in reforming processes: pyrolytic, non-filamentous and filamentous coke (Rostrup-Nielsen and Sehested, 2001). The different types of coke formed from diverse precursors have different impact on catalyst deactivation, and therefore on H_2 and other by-product yields. In this case, the study of the coke deposited on the catalyst is difficult due to the high amount of oxygenated compounds in the reaction environment, with the reactivity of these compounds being very different when they are alone or in a mixture with different organic compounds (Wu et al., 2008b; Remón et al., 2015).

The research group headed by Prof. Williams studied the Ni-based deactivated catalysts in the pyrolysis and in-line reforming of biomass in batch regime. Efika et al. (2012) verified by SEM images the presence of filamentous carbon for the NiO/Al_2O_3 catalyst, whereas the $NiO/CeO_2/Al_2O_3$ catalyst does not clearly show carbon filaments. Nahil et al. (2013) observed two different carbon oxidation peaks in the TPO experiments, obtaining one at around 450 ºC (amorphous carbon) and another one at around 550 ºC (filamentous carbon). However, when rice husk, sugar cane bagasse and wheat straw were used as feedstock, the second peak was obtained at around 650 ºC, which was assigned to graphitic carbon (Waheed and Williams, 2013). The characterization of the deactivated catalyst has also been studied in detail in bio-oil reforming processes (Davidian et al., 2007; Wu et al., 2008b; Lan et al., 2010). Yao et al. (2014) observed two different peaks corresponding to amorphous and filamentous coke in the reforming of the aqueous fraction of the bio-oil on a $Ni/\alpha\text{-}Al_2O_3$ catalyst. However, some authors reported three different peaks in the TPO curves in the deactivated $Ni\text{-}La_2O_3/\alpha\text{-}Al_2O_3$ catalyst, which are attributed to: 1)

coke deposited on Ni metal particles, whose combustion is activated by Ni particles; 2) coke deposited on Ni-La_2O_3 and/or Ni-Al_2O_3 interface, and; 3) coke deposited on the α-Al_2O_3 support, whose combustion is not catalyzed by Ni particles (Remiro et al., 2013b; Valle et al., 2013).

Concerning plastic valorisation, Wu and Williams (2010c) verified by TEM images the presence of two different types of coke deposited on Ni catalyst in the production of H_2 by pyrolysis-reforming of polypropylene (PP), which correspond to amorphous and filamentous coke, with the second one having common characteristics to carbon nanotubes and graphene, according to its graphitization degree (Helveg et al., 2011). Given that carbon nanotubes have a great potential in mechanical, thermal and electronic applications, Acomb et al. (2014) studied the simultaneous production of carbon nanotubes and H_2 in the pyrolysis-reforming of PP, improving the economics of the process.

Thus, the properties of the catalyst, reaction temperature, composition of the reaction environment (feedstock) and steam concentration are the most important factors for the production of H_2 and avoidable coke formation. Moreover, the deactivation depends to a greater extent on the morphology or location of the coke than on the total amount of coke deposited on the catalyst surface. The overall deactivation rate is a consequence of its formation rate and gasification rate, which are conditioned by temperature (Bartholomew, 2001). Particularly, high steam concentration in the reaction environment helps gasifying the amorphous coke deposited on the catalyst (main cause of active site blockage), and therefore attenuating deactivation (Remiro et al., 2013b).

This section deals with the characterization of the catalyst deactivated in the pyrolysis-reforming of biomass and biomass and HDPE mixtures. On the one hand, the effect operating variables (temperature, space time and S/B ratio) have on coke deposition has been analyzed (Section 4.2.1). On the other hand, the effect of time on stream on catalyst deactivation has been studied, analyzing the deterioration of catalyst properties (Section 4.2.2.1), the evolution of the coke (Section 4.2.2.2) and its formation mechanism (Section 4.2.2.3) for the pyrolysis-reforming of biomass. Finally, the coke deposited on the catalyst has been analyzed for biomass/HDPE mixtures valorisation (Section 4.2.3).

4.2.1. Effect of operating variables on coke deposition

In order to relate catalyst deactivation and the evolution with time on stream of the reaction indices, the coke deposited at different temperatures, space times and S/B ratios has been analyzed by temperature programmed oxidation (TPO) technique.

TPO is an effective method to determine the content of coke deposited on the catalyst and distinguish the types of coke burnt at different temperatures due to its structure (H/C ratio), position in the porous structure and relationship with the active sites. It also provides information about the location of these coke fractions (Bauer and Karge, 2006). Thus, external and internal coke can be distinguished in acid catalysts, with the external being the one burnt at lower temperatures (Valle et al., 2012; Epelde et al., 2014a). Regarding metallic or bifunctional catalysts, the coke deposited on metallic sites is burnt at lower temperatures because it is catalyzed by the metallic sites (Ereña et al., 2008; Gayubo et al., 2014; Vicente et al., 2014a,b).

It should be pointed out that time on stream differs from reaction to reaction, given that they were stopped once the catalyst was partially deactivated. Thus, the coke content in each reaction has been given by mass of biomass fed into the process.

4.2.1.1. Temperature

Figure 4.13 displays the TPO profiles of the deactivated catalyst at different reforming temperatures. Two different types of coke can be distinguished: 1) amorphous coke, which is burnt at low temperatures (< 450 ºC), activated by the Ni metal sites (encapsulating coke), and; 2) a condensed coke, which is burnt at higher temperatures, given that it corresponds to higher graphitization grade cokes. As shown in Figure 4.13, an increase in the reforming temperature involves the displacement of the maximum position of the peaks of the different types of coke towards higher combustion temperatures. In the case of the amorphous coke, a pronounced displacement is observed for the reforming temperature between 550 and 600 ºC, with the maximum of the peak being placed at around 380 and 425 ºC, respectively. In the case of the condensed coke, the effect of reforming temperature on peak position is more significant, whose maximum is placed around 550, 560, 610 and 620 ºC for the reforming temperatures of 550, 600, 650 and 700 ºC, respectively. This displacement can be explained by the evolution of the coke to more condensed structures when reforming temperature is increased (Vicente et al.,

2014c), making more difficult its combustion due to the lower hydrogenated nature of the coke and its location in the catalyst particle farther from Ni sites.

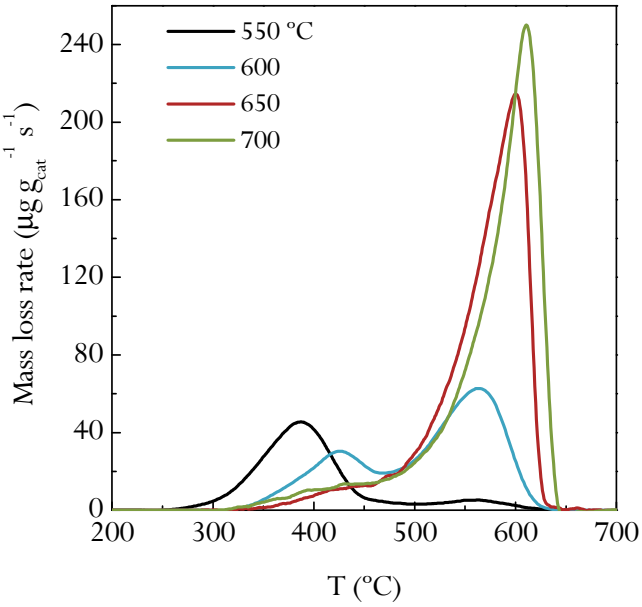

Figure 4.13. Effect of reforming temperature on the TPO profiles of the deactivated catalyst. Reforming conditions: 550-700 °C; space time, 20 g_{cat} min $g_{volatiles}^{-1}$; S/B ratio, 4.

Table 4.1 shows the coke content of the catalyst at different temperatures. It can be observed that the coke deposited at 550 °C per mass of biomass fed is higher than the obtained at 600 °C. Nevertheless, when temperature is increased in the 600-700 °C range, the coke content increases from 1.25 to 2.37 mg_{coke} g_{cat}^{-1} $g_{biomass}^{-1}$.

Comparing the results with the evolution of conversion with time on stream in Figure 4.1 (Section 4.1.1.1), it should be taken into account that catalyst deactivation is not directly related to coke content, but the nature and location influences its deactivation, which in turn it is related to the composition of the reaction medium. Thus, the proportion of amorphous and condensed coke changes at different reforming temperatures. Amorphous coke content is higher as reforming temperature is decreased, obtaining a maximum content of this type of coke at 550 °C. By relating the results with the composition in the reaction medium, it can be established that amorphous coke precursors are presumably the oxygenated

compounds contained in the bio-oil, given that their conversion is lower at low reforming temperatures, that is, when the concentration of bio-oil in the reaction medium is higher. In fact, the phenolic compounds derived from lignin pyrolysis tend to re-polymerize, but this is more difficult as temperature is increased due to their reforming.

On the contrary, the coke burnt at higher temperatures is minimum at 550 ºC, which increases when reforming temperature is increased, achieving its maximum content at 700 ºC. The higher content of this type of coke at high reforming temperatures can be related to the higher capacity of the catalyst for reforming and attenuation of WGS reaction. The higher concentration of CO at high temperatures favours the formation of structured coke by Boudouard reaction. In addition, the decomposition of CH_4 at high temperatures may contribute to the formation of this coke (Bartholomew, 2001). Nevertheless, the duration of each reaction is different, and therefore the amorphous coke can be evolved into a more condensed coke with time on stream (Vicente et al., 2014c). Consequently, the different duration of the reactions partially hinders the effect of temperature on coke content, given that for example at 550 ºC the duration of the reaction is short and, and therefore the coke does not evolve towards more condensed structures.

Table 4.1. Coke content of the catalyst deactivated at different temperatures.

T (ºC)	C_C, wt %	time on stream (min)	Biomass feed (g)	C_C, $mg_{coke}\ g_{cat}^{-1}\ g_{biomass}^{-1}$
550	5.5	20	15	3.67
600	9.9	106	80	1.25
650	19.2	111	83	2.31
700	21.3	120	90	2.37

Concerning the effect of each type of coke on catalyst activity, it should be pointed out that a similar conversion has been obtained at 600, 650 and 700 ºC when the catalyst was deactivated (Figure 4.1). Consequently, both amorphous coke and condensed coke could probably have an impact on catalyst deactivation. Although the deactivating effect of amorphous coke on Ni catalysts is well known (Wu et al., 2008a; Lan et al., 2010; Yao et al., 2014; Barbarias et al., 2016b), the condensed coke predictably also deactivates the catalyst, given that the content of amorphous coke at 700 ºC is lower than at 600 ºC and the conversion obtained when the catalyst is deactivated is similar, although the duration of the reaction is slightly higher (15

min more than at 600 ºC). Moreover, the high temperature needed for its combustion (620 ºC for a reforming temperature of 700 ºC) reveals the highly graphitic nature of the coke, which can also encapsulate Ni particles (as in the case of amorphous coke), and consequently decrease its activity (Vicente et al., 2014c).

Furthermore, the composition of biomass pyrolysis compounds (with high content of phenols and water) is not suitable for the production of nano-structured materials, and therefore the production of filamentous coke is not so clearly observed, as it has a more disorganized structure than in the valorisation of other oxygenated compounds, such as ethanol (Sánchez-Sánchez et al., 2007; Zhang et al., 2009c; Vicente et al., 2014a) or in the valorisation of hydrocarbons (Wu and Williams, 2010c; Blanco et al., 2014; Barbarias et al., 2016a).

4.2.1.2. Space time

Prior to analyzing the coke deposition on the catalyst, the effect of space time in the 10-30 g_{cat} min $g_{volatiles}^{-1}$ range has been studied by varying the amount of catalyst from 6.3 to 18.8 g, with the biomass feed rate being kept at 0.75 g min^{-1}, as mentioned in Section 2.3. As aforementioned, the fact of using different catalyst masses and times on stream in each experiment has to be considered when comparing the results.

Figure 4.14 displays the TPO results obtained in the experiments carried out using different space times and Table 4.2 the coke contents of the deactivated catalyst. The coke contents per mass of biomass in the feed decreases from 1.83 to 0.29 mg_{coke} g_{cat}^{-1} $g_{biomass}^{-1}$ when space time is increased in the 10-30 g_{cat} min $g_{volatiles}^{-1}$ range because a higher amount of catalyst enhances reforming and WGS reactions.

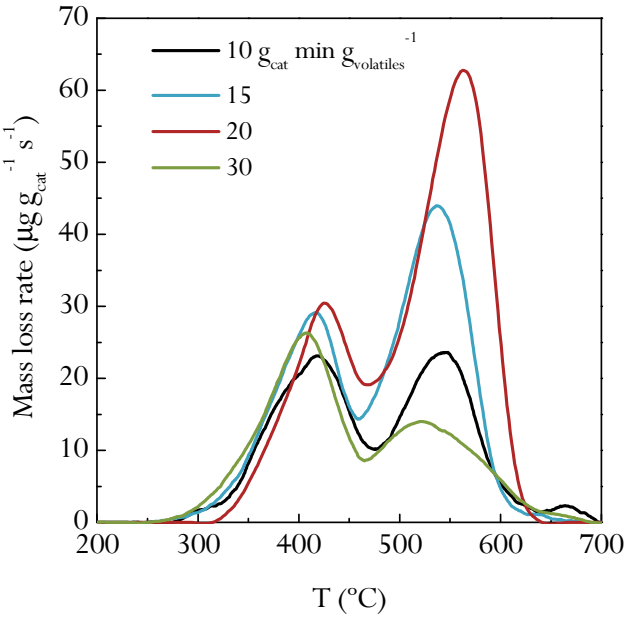

Figure 4.14. Effect of space time on TPO profiles of the deactivated catalyst. Reforming conditions: 600 ºC; space time, 10-30 g_{cat} min $g_{volatiles}^{-1}$; S/B ratio, 4.

Table 4.2. Coke contents of the deactivated catalyst at different space times.

Space time (g_{cat} min $g_{volatiles}^{-1}$)	C_C, wt %	time on stream (min)	Biomass feed (g)	C_C, mg_{coke} g_{cat}^{-1} $g_{biomass}^{-1}$
10	5.5	40	30	1.83
15	7.8	82	62	1.27
20	9.9	106	80	1.25
30	5.0	228	171	0.29

As space time is increased, the peak of amorphous coke (at low temperatures) appears approximately at the same temperature, but considering the higher amount of catalyst used and the higher duration of the reaction at higher space times, the total amount of amorphous coke increases (Figure 4.14). This result can be explained by the thermal origin of this coke, which is produced by re-polymerization of phenolic compounds of the bio-oil deposited on the catalyst surface (Remiro et al., 2013a,b),

and it thus increases with space time due to the higher contact time between these compounds and the catalyst. Moreover, a displacement of the condensed coke peaks can be observed when space time is increased due to the higher duration of the reactions, and therefore a higher evolution of the coke to a more condensed structure. Nevertheless, the content of condensed coke decreases when a space time of 30 g_{cat} min $g_{volatiles}^{-1}$ is used due to the lower concentration of coke precursors (CO, CH_4 and C_2-C_4 hydrocarbons) in the reaction medium, which is a consequence of an excess of catalyst used in this experiment. This result is interesting from an industrial point of view, given that under these conditions coke deposition on the catalyst is considerably reduced.

4.2.1.3. Steam/biomass ratio

As in the case of space time, when interpreting the results, it should be taken into account that the catalyst mass used in the experiment has been varied in the 10-25 g range, at the same time as biomass feeding rate has also been changed in the 0.6-1.5 g min^{-1} range, in order to maintain the same space time in all the experiments (20 g_{cat} min $g_{volatiles}^{-1}$) and modify as little as possible the fluid dynamic conditions of the reactors.

Figure 4.15 displays the TPO profiles obtained at different S/B ratios and Table 4.3 shows the effect S/B ratio has on coke content. Thus, coke content decreases from 1.38 to 0.69 mg_{coke} g_{cat}^{-1} $g_{biomass}^{-1}$ when S/B ratio is increased from 2 to 5, given that the higher amount of steam in the reaction medium leads to a lower concentration of coke precursors by the enhancement of reforming and WGS reactions. In addition, coke gasification is also favoured at high S/B ratios (Garcia et al., 2000; Wang et al., 2007; Fu et al., 2014).

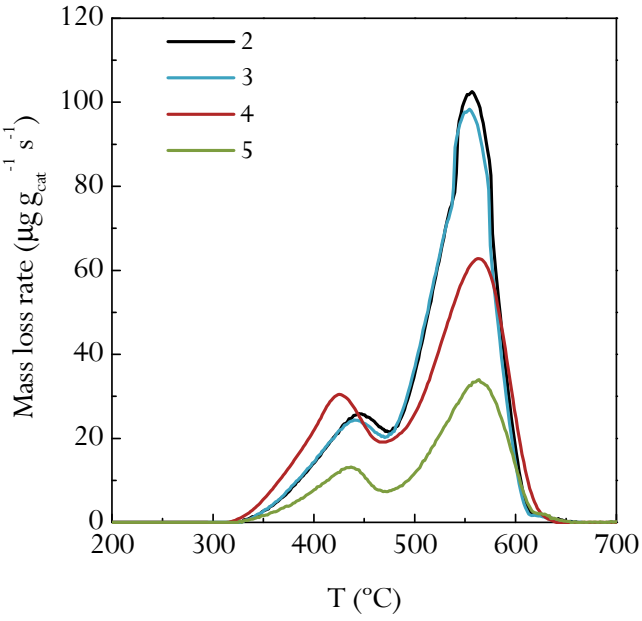

Figure 4.15. Effect of S/B ratio on the TPO profiles of the deactivated catalyst. Reforming conditions: 600 ºC; space time, 20 g_{cat} min $g_{volatiles}^{-1}$; S/B ratio, 2-5.

Table 4.3. Coke contents of the deactivated catalyst at different S/B ratios.

S/B ratio	C_C, wt %	time on stream (min)	Biomass feed (g)	C_C, $mg_{coke}\ g_{cat}^{-1}\ g_{biomass}^{-1}$
2	14.5	70	105	1.38
3	11.3	82	82	1.38
4	9.9	106	80	1.25
5	4.7	113	68	0.69

Furthermore, although it seems in Figure 4.15 that amorphous coke increases for an S/B ratio of 4, the effect is hindered by the different catalyst masses used in the experiments. Consequently, considering that fact, both the amorphous coke and the condensed one decrease in the whole S/B ratio studied.

4.2.2. Effect of time on stream on catalyst deactivation

4.2.2.1. Deterioration of catalyst properties

Physical properties

The deterioration with time on stream of the physical properties of the catalyst has been studied by N_2 adsorption-desorption, using the methodology and the equipment described in Section 2.4.2.1. The study has been carried out for the valorisation of biomass, using conditions in which the deactivation is relatively severe and assessing the effect of incipient deposition of coke and the evolution of deposition with time on stream. The conditions used are as follows: 600 ºC; space time, 20 g_{cat} min $g_{volatiles}^{-1}$; S/B ratio, 4. The sampling has been performed by removing a small amount of catalyst at different times on stream. It can be pointed out that the use of the fluidized bed and a uniform activity of the catalyst guarantee representative sampling.

Figure 4.16 shows the N_2 adsorption-desorption isotherms for the fresh and deactivated catalysts at different times on stream. Moreover, Table 4.4 shows the values of specific surface, pore volume and average pore size, which have been determined from the results in Figure 4.16. The isotherm of the fresh catalyst exhibits a characteristic hysteresis of H3 isotherms and at pressures higher than 0.4 shows the hysteresis cycle typical of mesoporous materials (the average pore size is 122 Å), with the adsorption of N_2 being higher at pressures close to unity. The values of specific surface BET and pore volume are relatively low.

These results indicate that coke deposition partially blocks the porous structure of the catalyst, reducing the specific surface by half in 50 min on stream, whereas the average pore size increases considerably because blockage by coke largely affects the smaller pores. Nevertheless, above 50 min, both specific surface and pore volume increase with time on stream, due to the higher amount of coke formed in the catalyst and the contribution of coke properties to these results.

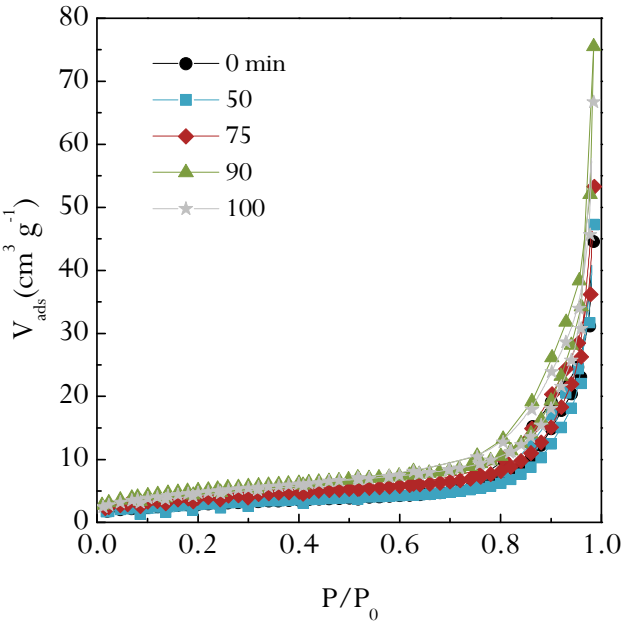

Figure 4.16. N_2 adsorption-desorption isotherms of the catalyst at different time on stream. Operating conditions: 600 °C; space time, 20 g_{cat} min $g_{volatiles}^{-1}$; S/B ratio, 4.

Table 4.4. Evolution of physical properties of the catalyst with time on stream. Operating conditions: 600 °C; space time, 20 g_{cat} min $g_{volatiles}^{-1}$; S/B ratio, 4.

Time, min	S_{BET}, m^2 g^{-1}	V_{pore}, cm^3 g^{-1}	d_{pore}, Å
0	19.00	0.040	122
50	10.20	0.072	292
75	13.84	0.081	257
90	17.95	0.114	285
100	17.05	0.101	243

Metallic properties

Table 4.5 shows the evolution of Ni crystallite size with time on stream. These values have been calculated applying the equation of Debye-Scherred (eq. (2.2)) to the diffraction bands $2\theta = 52^{\circ}$ obtained from XRD difractograms, which cannot be shown due to the confidentiality agreements signed with the supplier. As observed, the crystallite size is similar above 50 min on stream, which allowed ruling out sintering as the cause of catalyst deactivation.

Table 4.5. Evolution of Ni crystallite size with time on stream. Operating conditions: 600 ºC; space time, 20 g_{cat} min $g_{volatiles}^{-1}$; S/B ratio, 4.

Time, min	Crystallite size, nm
0	25
50	35
75	36
90	38
100	38

4.2.2.2. Evolution of coke

Temperature programmed oxidation (TPO)

Figure 4.17 shows the evolution with time on stream of coke content in the catalyst, which has been calculated based on TPO profiles of coke combustion. As observed, coke content increases slowly for the first 50 min, whereas it increases exponentially to a value of around 10 wt % at 100 min, blocking the porous structure of the catalyst. At this point, the catalyst is partially deactivated, with conversion being lower than 60 % (Section 4.1.1).

In Figure 4.18, the TPO profiles of the deactivated catalyst at different times on stream have been plotted. As observed, the coke evolves with time on stream, from an amorphous coke with a notable fraction burning below 450 ºC to a more condensed coke with a fraction burning above this temperature. Above 50 min, the increase in coke content is very fast and it is a condensed coke, with the peak of combustion being at 520 ºC for 50 min on stream, which is moved to 560 ºC for 100 min on stream.

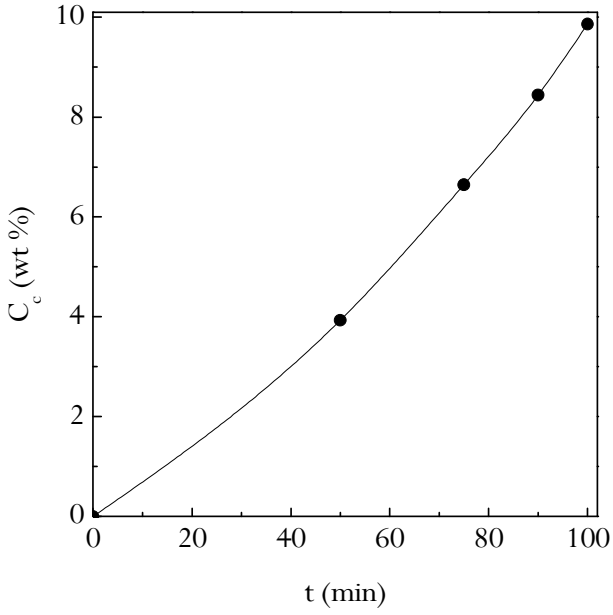

Figure 4.17. Evolution with time on stream of coke content in the catalyst. Operating conditions: 600 °C; space time, 20 g_{cat} min $g_{volatiles}^{-1}$; S/B ratio, 4.

The evolution and displacement of the TPO profiles is a consequence of the changes produced in the composition and location of the coke. The results show that the coke evolves progressively into a more condensed structure with time on stream, which is farther from Ni metallic sites, and therefore its combustion is not catalyzed. Moreover, it should be taken into account that the evolution of the coke is conditioned by its gasification, with the amorphous coke being the most affected because it is a less condensed structure (higher H/C ratio) and its gasification is catalyzed by Ni metallic sites (Remiro et al., 2013b).

Nahil et al. (2013) studied the catalyst deactivation in the pyrolysis-catalytic gasification of biomass using a bi-functional Ni-Mg-Al-CaO catalyst, obtaining two different peaks during the TPO experiments, which correspond to amorphous and filamentous coke (at 450 and 550 °C), with the filamentous being the one burnt at higher temperatures. Yao et al. (2014) studied the deactivation of different catalysts in the reforming of the aqueous fraction of the bio-oil, obtaining the oxidation of amorphous coke between 350 and 440 °C and that of the filamentous one at around 520 °C. Nevertheless, a temperature of 650 °C is needed to burn the condensed coke

produced in the rice husk, sugar cane bagasse and wheat straw pyrolysis-reforming process (Waheed and Williams, 2013). As commented above, some authors obtained three different peaks in the TPO profiles, which can be attributed to the complexity of the catalyst or high coke deposition (Remiro et al., 2013b; Valle et al., 2013; Angeli et al., 2014). Chen et al. (2016) studied a Ni/CaAlO$_x$ catalyst, obtaining two or three peaks depending on the molar ratio of Ca:Al used in the catalyst. Similar results were obtained by Medrano et al. (2011) during the catalytic steam reforming of the aqueous fraction of pyrolysis liquids after 2 h reaction with different catalysts. A Ni-Al based catalyst led to three different peaks, whereas when a modifier was introduced, only two peaks were detected. Thus, it is noteworthy that the quantity of the coke and the position of the peaks obtained in the TPO profiles depend on the feedstock, properties of the catalyst and experimental conditions used in the process.

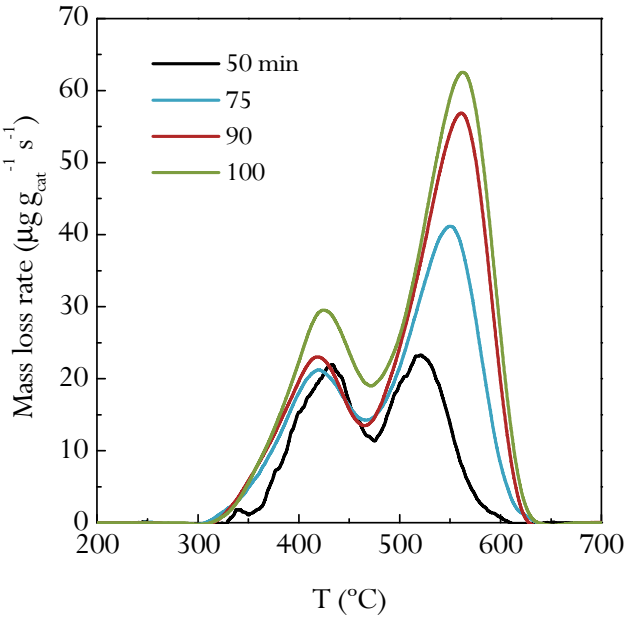

Figure 4.18. Evolution with time on stream of coke combustion in the catalyst (TPO profiles). Operating conditions: 600 ºC; space time, 20 g_{cat} min $g_{volatiles}^{-1}$; S/B ratio, 4.

Scanning electron microscopy (SEM)

Figure 4.19 shows the images of scanning electron microscopy (SEM) of the catalyst deactivated for different times on stream. These images complement the results obtained in the TPO analysis.

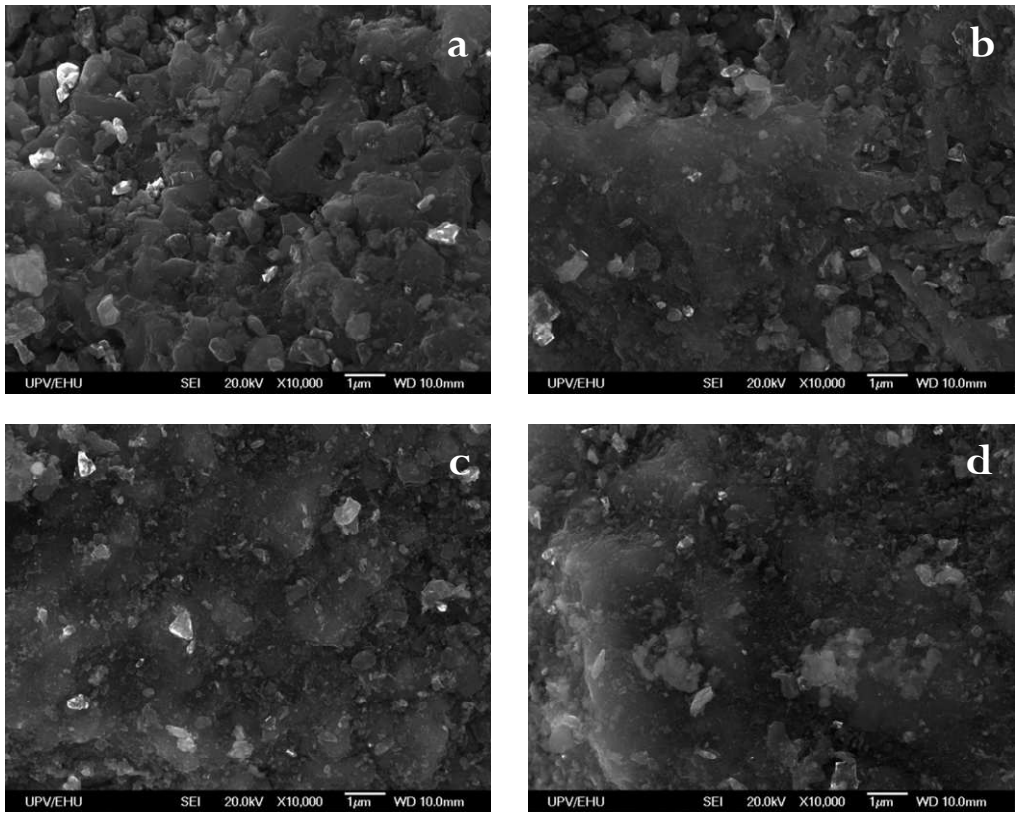

Figure 4.19. SEM images of the catalyst deactivated for different times on stream: 50 (a), 75 (b), 90 (c) and 100 min (d). Operating conditions: 600 °C; space time, 20 g_{cat} min $g_{volatiles}^{-1}$; S/B ratio, 4.

In this figure, the presence of amorphous coke is observed, which is more condensed when time on stream increases. Moreover, no filamentous coke is observed in these images. Nevertheless, the presence of filamentous carbon on NiO/Al_2O_3 catalyst was reported by Efika et al. (2012) in the pyrolysis-reforming of biomass, whereas $NiO/CeO_2/Al_2O_3$ does not lead to fibrous coke. Carbon whiskers were also observed by Medrano et al. (2011) by SEM images in the catalytic steam reforming of

bio-oil aqueous fraction on a Ni-Al catalyst modified with Ca or Mg. Yao et al. (2014) also studied different modified Ni-Al catalysts and observed that filamentous carbon was deposited on Ni-Zn-Al and Ni-Mg-Al catalysts, while the deposition of fibrous coke was moderate on Ni-Ca-Al catalyst. Lan et al. (2010) compared the reforming of bio-oil in fixed and fluidized bed reactors, with the amount of carbon nanofibres being higher when the fixed bed reactor was used.

Transmission electron microscopy (TEM)

Figure 4.20 shows the images of transmission electron microscopy (TEM) of the catalyst deactivated at 90 and 100 min on stream. The images of the catalyst for other times on stream are omitted, given that they do not provide more information. In these images, Ni^0 particles are identified as dark areas, and it is observed that all Ni^0 particles are coated with amorphous coke for 90 min (Figure 4.20a). Moreover, for 100 min on stream, a higher amount of coke is observed in the image (Figure 4.20b), which evolves to a more condensed coke.

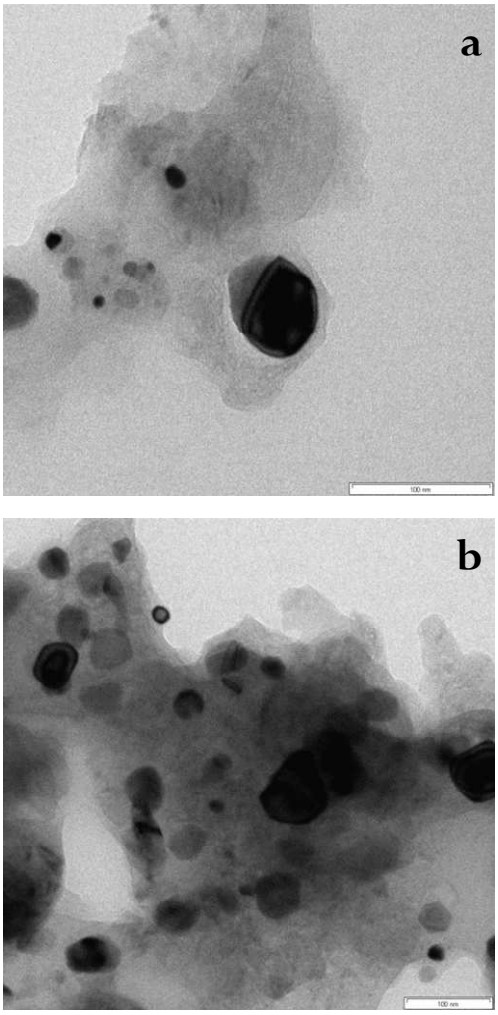

Figure 4.20. TEM images of the catalyst deactivated for different times on stream: 90 (a) and 100 min (b). Operating conditions: 600 ºC; space time, 20 g_{cat} min $g_{volatiles}^{-1}$; S/B ratio, 4.

4.2.2.3. Coke formation mechanism

Figure 4.21 shows the reaction steps involved in the reforming of biomass pyrolysis volatiles (Remiro et al., 2013b). As observed in this scheme, the oxygenated compounds derived from biomass pyrolysis are assumed to be the coke precursors. According to step 2, more coke is produced as the concentration of the oxygenated compounds in the reaction environment is higher. Therefore, the deactivation occurs

in parallel with the main reactions (reforming and WGS), which has been previously reported in the valorisation of bio-oil (Gayubo et al., 2005, 2009; Valle et al., 2012; Remiro et al., 2013b).

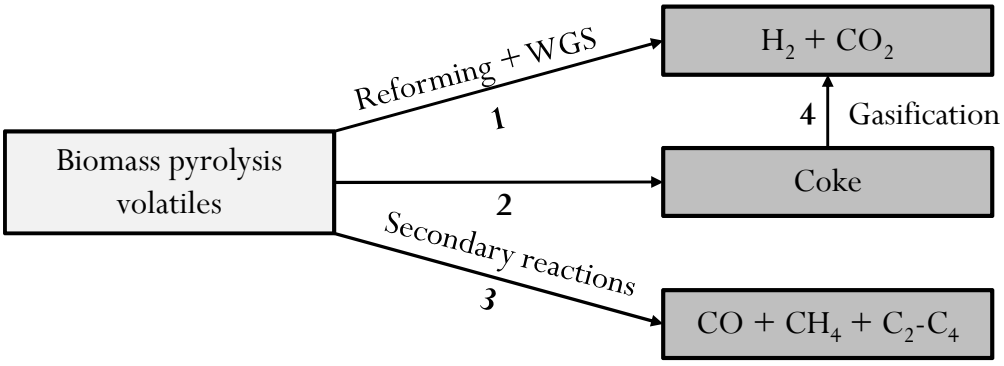

Figure 4.21. Reaction steps for the reforming of biomass pyrolysis volatiles (Remiro et al., 2013b).

Figure 4.22 shows the routes of coke formation and evolution in the catalytic steam reforming of pyrolysis volatiles from biomass, which have been previously discussed by Remiro et al. (2013b) for bio-oil reforming. As observed, the active precursor (C^*), which is adsorbed on the metal sites of the catalyst, reacts in parallel to form coke ($C^* + C^* \rightarrow$ coke) or gaseous products by gasification ($C^* + H_2O \rightarrow CO + H_2$), methanation ($C^* + 2H_2 \leftrightarrow CH_4$) and Boudouard ($C^* + CO_2 \leftrightarrow 2CO$) reactions.

The importance of these reactions together with the reforming of volatiles from biomass strongly depends on the operating conditions used for the process. When the catalyst is fresh, reforming and WGS reactions will be the main reactions, whereas secondary reactions will take place as the catalyst is being deactivated, producing CO, CH_4 and C_2-C_4 hydrocarbons as by-products, which are potential reactants for the formation of C^* precursors and coke, following the reactions shown in Figure 4.22.

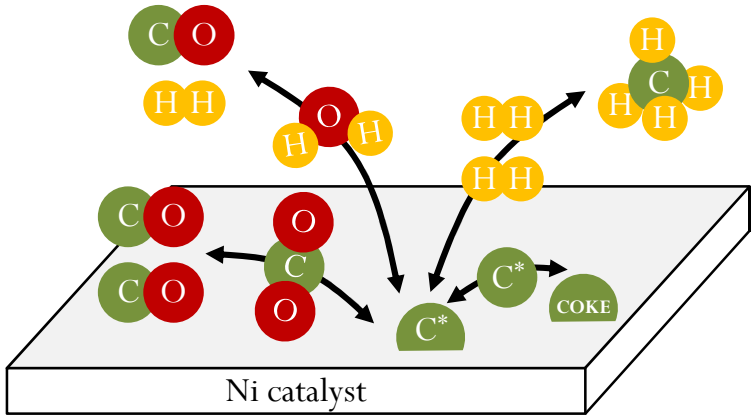

Figure 4.22. Routes for coke formation and evolution in the catalytic steam reforming of bio-oil over Ni catalysts (Remiro et al., 2013b).

In order to minimize coke formation, the catalyst composition and operating conditions play an essential role in the transformation of C^* precursor into gases, and therefore in the formation of C-O active bonds rather than C-C bonds. Furthermore, the gasification of C^* precursors is also enhanced with high steam concentration in the reaction environment. Other factors, such as Ni particle size or the incorporation of different promoters to Ni particles, can also be relevant in order to attenuate C-C bond formation and blockage of Ni particles.

4.2.3. Coke formation for biomass and HDPE valorisation

In order to explain the influence of feed composition on the evolution of conversion with time on stream, the coke has been characterized by temperature programmed oxidation (TPO) and transmission electron microscopy images (TEM). The scanning electron microscopy (SEM) images of the catalyst are omitted, given that they do not provide further information.

4.2.3.1. Temperature programmed oxidation (TPO)

Figure 4.23 displays the TPO profiles of the catalyst deactivated in the runs with three types of feeds studied: only biomass, 50/50 wt % HDPE/biomass mixture and only HDPE. In the valorisation of only biomass, a main peak at around 600 °C is observed, which corresponds to a polyaromatic and structured coke, with a small shoulder at around 425 °C related to the coke whose combustion is activated by Ni

metallic sites. This coke is related to the carbon whiskers reported by Trane-Restrup and Jensen (2015) in the steam reforming of furfural and guaiacol at 600 °C. Yao et al. (2014) also observed two different coke oxidation peaks in the steam reforming of the aqueous fraction of the bio-oil, with the deposition of filamentous coke being moderate when a Ni-Ca-Al catalyst was used. However, Montero et al. (2015) studied the steam reforming of ethanol on a Ni/La_2O_3-αAl_2O_3 catalyst and a main peak at around 500 °C with a shoulder at a lower temperature (at 430 °C) was observed, which correspond to filamentous and amorphous cokes, respectively.

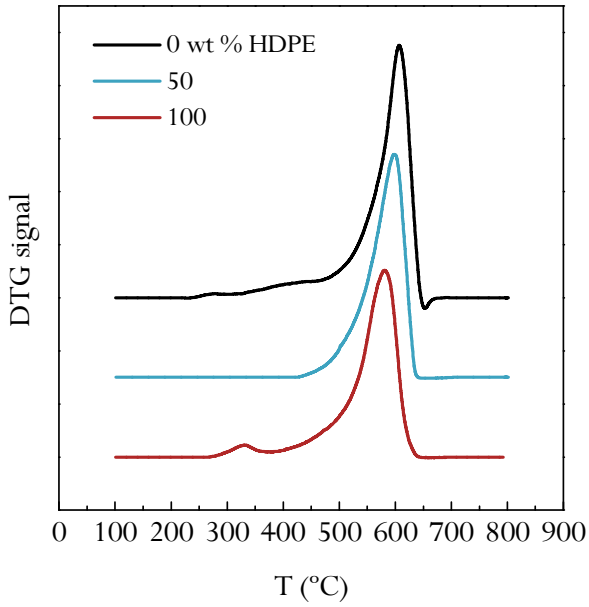

Figure 4.23. TPO profiles of the cokes deposited for only biomass, 50/50 wt % HDPE/biomass mixture and only HDPE in the feed. Operating conditions: 700 °C; space time, 16.7 g_{cat} min $g_{feeding}^{-1}$; S/F ratio, 4.

Furthermore, in the steam reforming of the pyrolysis products of only HDPE, a main peak at 580 °C with a shoulder at 450 °C were observed. The main peak corresponds to a structured and filamentous coke similar to that obtained by Wu and Williams (2010c) and Acomb et al. (2014) in the reforming of polypropylene (PP), as observed in TEM images, and will be discussed later. Nevertheless, the low porous volume of the catalyst used in this work (0.04 cm^3 g^{-1}) leads to a lower amount and less developed internal coke, and therefore its combustion is more favoured and takes place at lower temperatures. Moreover, it should pointed out that the peak of

structured coke is obtained at slightly lower temperature than in the case of biomass, with the coke being more condensed in the case of biomass valorisation, due to the different nature of the reactants and operating conditions (effective space time and S/C ratio) (Helveg et al., 2011). The peaks for the mixtures of biomass and HDPE are between those corresponding to the individual feeds.

4.2.3.2. Transmission electron microscopy (TEM)

Figure 4.24 shows TEM images of the catalyst deactivated using different feeds: only biomass (a), 25 wt % HDPE in the feed (b), 50 wt % HDPE in the feed (c), 75 wt % HDPE in the feed (d) and only HDPE (e). Differences in the structure and nature of the coke are observed, which are due to the different composition of the volatiles fed into the reforming step. The images show dark spots corresponding to Ni active sites, with the coke deposited fully covering the Ni crystals (encapsulating coke) and being mainly non-structured for only biomass in the feed (Figure 4.24a). The presence of amorphous and non-structured coke has also been observed in the catalytic steam reforming of CH_4 (Angeli et al., 2015), different hydrocarbons (Wu and Williams, 2010c; Barbarias et al., 2016b) and oxygenated compounds (Montero et al., 2015; Trane-Restrup and Jensen, 2015). The high combustion temperature observed in the TPO profile (600 ºC) is evidence that it is a very condensed coke.

However, the structure of the coke changes when HDPE is co-fed, with its nature being more filamentous as HDPE content in the feed is increased. This filamentous coke has already been observed in the reforming of polyolefin pyrolysis products (Wu and Williams, 2010c; Acomb et al., 2014). Alvarez et al. (2014a) also reported that no filamentous coke was observed when only biomass was used in the pyrolysis-reforming study of biomass and plastics mixtures. However, filamentous coke appeared when plastic/biomass ratio was increased, with the total content of coke being higher.

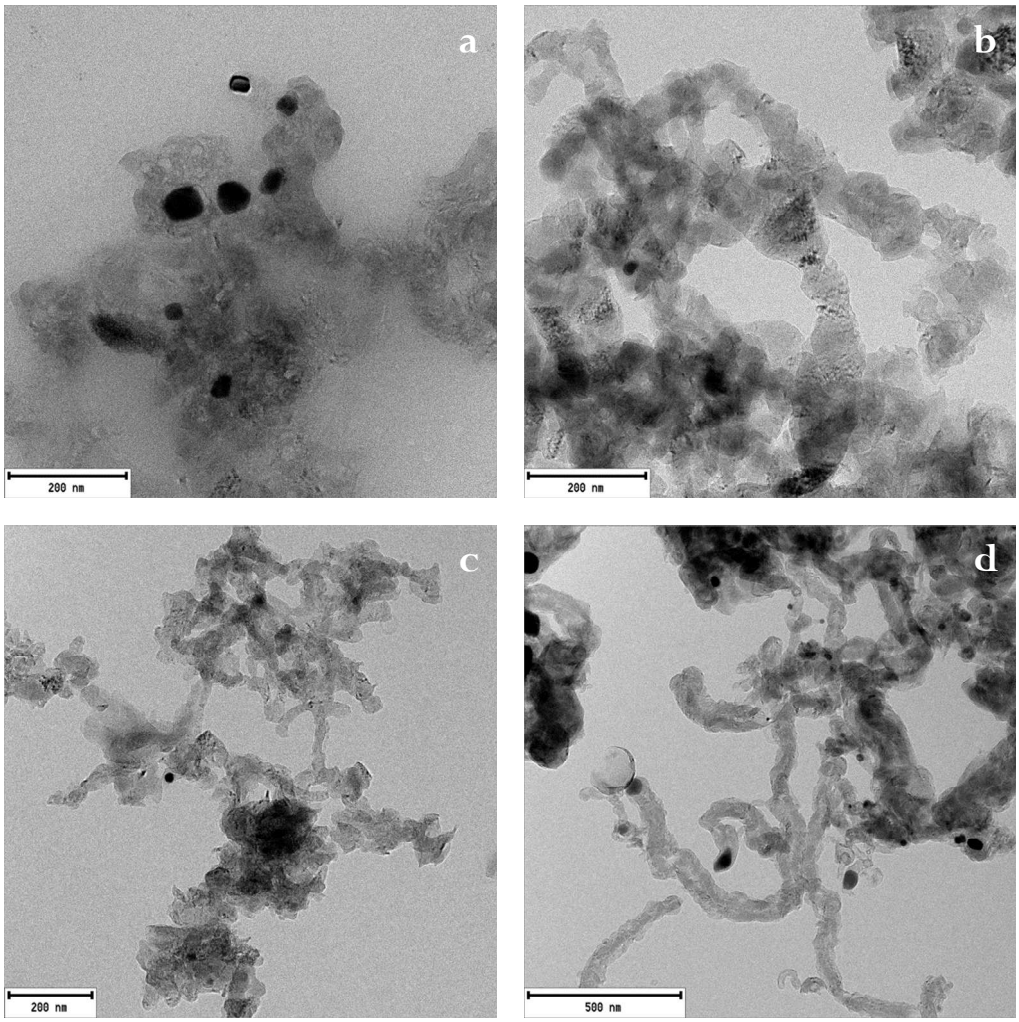

Figure 4.24. TEM images of the coke deposited on the catalyst for only biomass (a), HDPE/biomass mixtures of 25/75 (b), 50/50 (c), 75/25 wt % (d) and only HDPE in the feed (e). Operating conditions: 700 ºC; space time, 16.7 g_{cat} min $g_{feeding}^{-1}$; S/F ratio, 4.

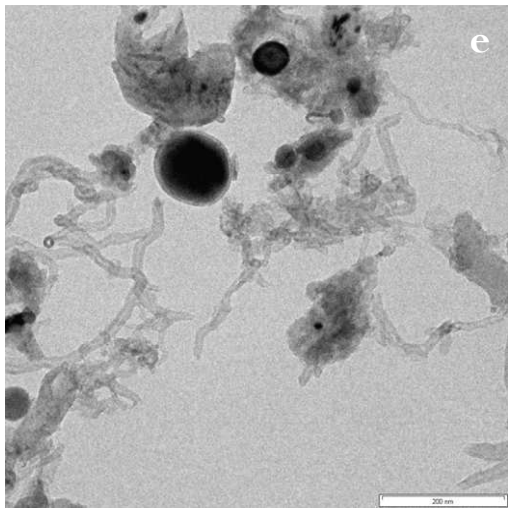

Figure 4.24. Continued.

Consequently, the faster deactivation observed for biomass and the attenuation of the deactivation when HDPE is co-fed are attributed to the different nature of the coke. The amorphous coke formed in the reforming of oxygenated compounds derived from biomass pyrolysis encapsulates Ni sites, causing a fast deactivation of the catalyst, whereas the structured and filamentous coke formed, mainly in the reforming of hydrocarbons derived from HDPE pyrolysis, does not block Ni active sites, even though its progressive deposition hinders reactant flow towards Ni particles (Latorre et al., 2011; Barbarias et al., 2016b). This interpretation of the deactivation results is consistent with the fast deactivation of the catalyst in the reforming of oxygenated compounds (DME, ethanol and bio-oil), which is attributable to the encapsulation of Ni sites by the amorphous coke formed by the condensation of intermediate oxygenates (Remiro et al., 2013a,b; Gayubo et al., 2014; Vicente et al., 2014a,c; Montero et al., 2015). Deactivation is lower in the reforming of the hydrocarbons produced in polyolefin pyrolysis, in which the coke is mainly structured (Wu and Williams, 2010c; Acomb et al., 2014).

4.3. REGENERATION OF THE CATALYST

In order to study the regeneration of the catalyst the reforming step has been carried out under the following operating conditions: 600 ºC; space time, 20 g_{cat} min $g_{volatiles}^{-1}$; S/B ratio, 4. After the reaction, the combustion of the coke has been performed in situ in the reforming reactor, with the temperature and air concentration ramp shown in Figure 4.25. Thus, first of all the regeneration has been carried out at 600 ºC for the first 90 min, increasing the concentration of air each 15 min from 10 to 100 vol %, in order to avoid a sudden increase of the temperature in the catalyst. Subsequently, the temperature has been increased from 600 to 700 ºC in 60 min and maintained at this temperature for another 60 min. The elimination of coke has been followed monitoring the concentration of CO_2 at the reactor outlet. Once the combustion of coke has been finished, the catalyst has been reduced again using the same conditions described in Section 2.3.2 (710 ºC, 10:90 vol % H_2:N_2). This process was repeated for 6 consecutive reforming/regeneration cycles.

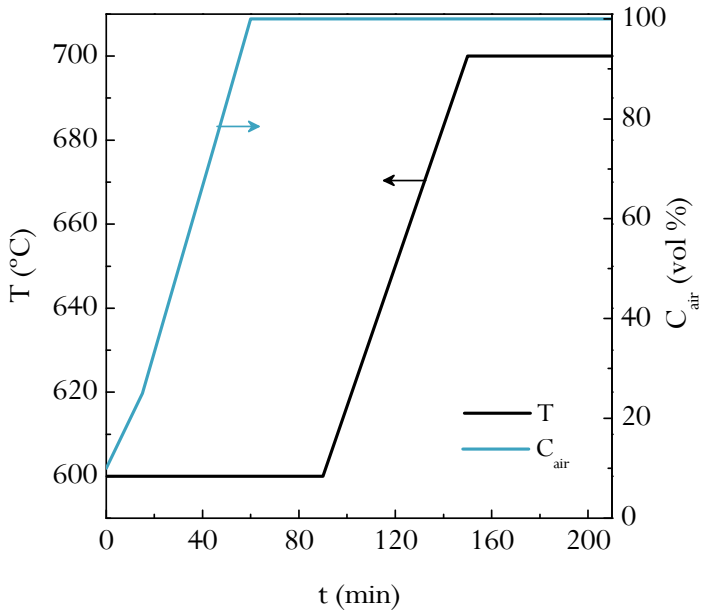

Figure 4.25. Temperature and air concentration ramp used for the regeneration of the catalyst.

4.3.1. Evolution of reaction indices with time on stream

Figure 4.26 shows the evolution of conversion with time on stream during 6 consecutive reforming/regeneration cycles. As observed, the catalyst recovers only partially its activity when is regenerated and the initial conversion decreases from the first to the fifth cycle from 99.7 to 87.6 %. Subsequent to the fifth cycle, the initial conversion is almost constant. This decrease in conversion at zero time on stream could be due to the sintering of Ni crystallites. Moreover, the evolution of conversion with time on stream follows a trend, in which the decrease is faster as the number of cycles is increased and similar subsequent to the fifth cycle. This trend is characteristic in autocatalytic deactivation mechanisms, which as in this case are accelerated by the progressively higher concentration of amorphous coke precursors (bio-oil oxygenated compounds).

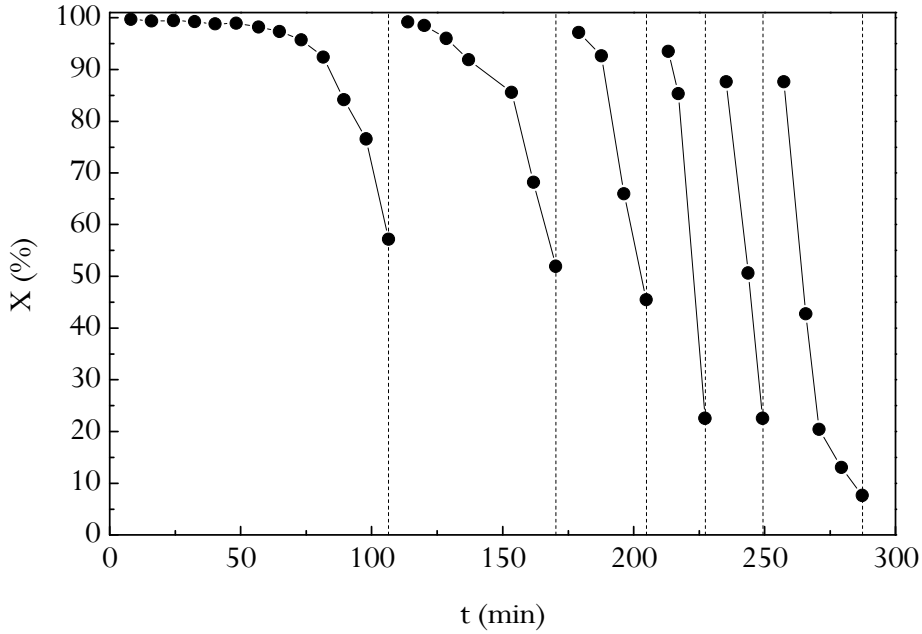

Figure 4.26. Evolution of conversion with time on stream for 6 consecutive reforming/regeneration cycles. Reforming conditions: 600 ºC; space time, 20 g_{cat} min $g_{volatiles}^{-1}$; S/B ratio, 4.

This irreversible deactivation is evident when the evolution with time on stream of the product yields is monitored (Figure 4.27). It can be pointed out that initial H_2 and CO_2 yields decrease from 93.5 to 68.0 % and from 88.6 to 67.0 %, respectively,

in the fifth cycle and it is stabilized subsequent to this cycle, with the trend being similar to that obtained for the conversion. On the contrary, the initial CO, CH_4 and C_2-C_4 hydrocarbons yields increase when the number of reforming/regeneration cycles is higher until the fifth cycle. The increase in by-product yields as catalyst sintering progresses is due to the attenuation in the rates reactions of CH_4 and C_2-C_4 hydrocarbons reforming and CO conversion by WGS reaction. In addition, the decomposition reactions of bio-oil oxygenated compounds are favoured with the lower activity of Ni sites, increasing therefore the production of these by-products.

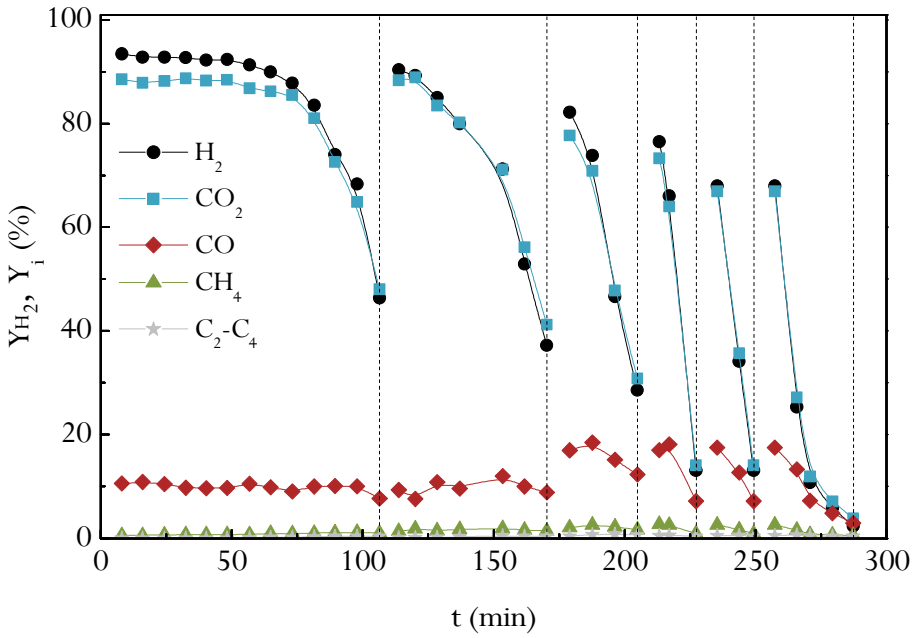

Figure 4.27. Evolution of product yields with time on stream for 6 consecutive reforming/regeneration cycles. Reforming conditions: 600 ºC; space time, 20 g_{cat} min $g_{volatiles}^{-1}$; S/B ratio, 4.

The effect of Ni sintering can also be observed in Figure 4.28, where the evolution with time on stream of gaseous product composition is plotted. The initial composition of H_2 decreases and CO increases as the number of reforming/regeneration cycles is increased, following the same trend as conversion and product yields. The lower H_2 and higher CO concentrations are explained by the lower activity of the catalyst for reforming and WGS reactions. Above the fifth cycle, the initial H_2 and CO concentrations are almost constant and the catalyst is stabilized, although its activity is maintained for less than 20 min, which is essential for a

successful scale-up of the technology. In previous studies by our research group, Montero (2015) also obtained a partial recovery of the catalyst activity in the steam reforming of ethanol on Ni/La_2O_3-αAl_2O_3 catalyst, suggesting the convenience of exploring reactivation methodologies of metallic sites in Ni catalysts.

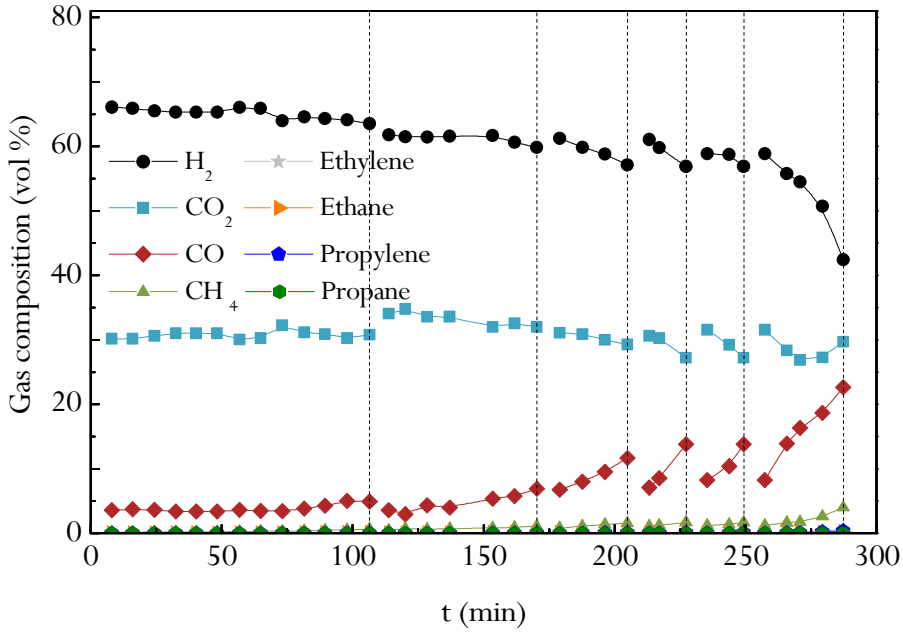

Figure 4.28. Evolution of the gaseous product composition with time on stream for 6 consecutive reforming/regeneration cycles. Reforming conditions: 600 ºC; space time, 20 g_{cat} min $g_{volatiles}^{-1}$; S/B ratio, 4.

4.3.2. Deactivated catalyst characterization

The deactivated catalyst has been analyzed by TPO in order to study the content and nature of the coke deposited on the catalyst. The TPO profiles for different reforming/regeneration cycles have been plotted in Figure 4.29. In the first cycle, two different types of coke are observed, which correspond to amorphous and condensed cokes, as mentioned in Section 4.2. It has also been pointed out that condensed coke content increases with time on stream. Thus, the high peak obtained for the condensed coke in the first cycle is mainly attributable to the high duration of the reaction (106 min), whereas in the second cycle this peak is significantly lower due to the lower duration (64 min) of the reaction. As the number of regeneration

cycles is increased, the catalyst activity decreases, and so does its capacity for reforming and WGS reactions. Between the third and sixth cycles, the duration of the reactions is short (in the 18-38 min range), and so the condensed coke is not evolved and the deposited coke is exclusively amorphous. Table 4.6 shows the coke content of deactivated catalyst for different reforming/regeneration cycles and, as observed, coke content is mainly related to the duration of each reaction.

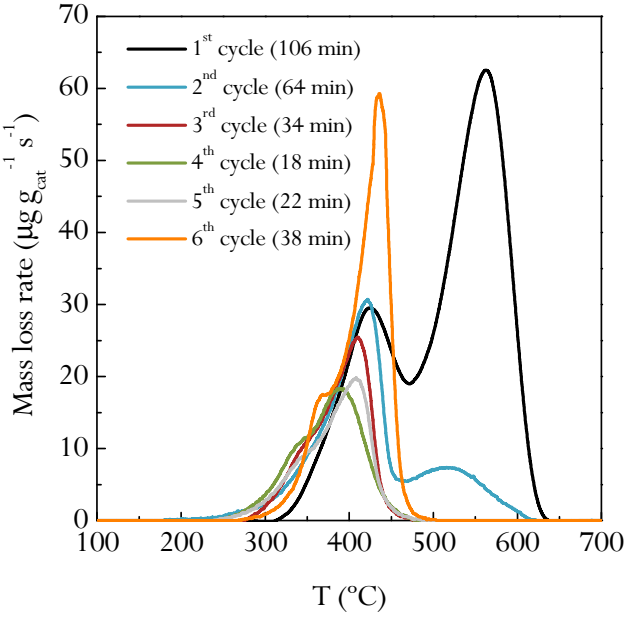

Figure 4.29. TPO profiles of deactivated catalysts for 6 consecutive reforming/regeneration cycles. Reforming conditions: 600 ºC; space time, 20 g_{cat} min $g_{volatiles}^{-1}$; S/B ratio, 4.

Table 4.6. Coke content (wt %) of the deactivated catalyst for 6 consecutive reforming/regeneration cycles. Reforming conditions: 600 ºC; space time, 20 g_{cat} min $g_{volatiles}^{-1}$; S/B ratio, 4.

Cycle	C_C, wt %
1 (106 min)	9.9
2 (64 min)	3.8
3 (34 min)	2.3
4 (18 min)	2.1
5 (22 min)	2.0
6 (38 min)	4.3

4.3.3. Regenerated catalyst characterization

The regenerated catalyst has also been characterized by X-ray diffraction (XRD) and temperature programmed reduction (TPR). Based on the results obtained in X-ray diffraction, Table 4.7 shows the Ni crystallite size obtained for different reforming/regeneration cycles, which have been calculated applying the equation of Debye-Scherrer (eq. 2.2). As observed, the size increases considerably as the number of reforming/regeneration cycles is increased, being evident the importance of Ni sintering.

Table 4.7. Evolution of Ni crystallite size for 6 consecutive reforming/ regeneration cycles. Reforming conditions: 600 ºC; space time, 20 g_{cat} min $g_{volatiles}^{-1}$; S/B ratio, 4.

Cycle	Crystallite size, nm
Fresh	25
1	40
2	48
3	50
4	55
5	55

Figure 4.30 shows the TPR profiles obtained for four different catalysts: fresh catalyst and catalysts regenerated after the first, third and fifth cycles. The fresh catalyst shows a main peak at around 550 ºC, attributed to the reduction of NiO interacting with the α-Al_2O_3 support, and another peak at 700 ºC, which corresponds to the spinel $NiAl_2O_4$. Nevertheless, once the catalyst has been deactivated and regenerated, the position of the main peak is displaced towards a lower temperature, whereas the peak corresponding to the spinel $NiAl_2O_4$ is displaced to a higher temperature. Moreover, a shoulder can be observed in the main peak subsequent to the first cycle, which is attributable to the reduction of NiO with weak interaction with the α-Al_2O_3 support.

It is evident that the reducibility of the catalyst is lower once the coke is burnt in the first cycle. Moreover, a lower temperature is required to reduce the catalyst as the number of cycles is increased. This trend can be explained by the lower dispersion of the Ni particles due to the higher Ni crystallite sizes, thus decreasing the intensity of the metal-support interaction and easing its reduction.

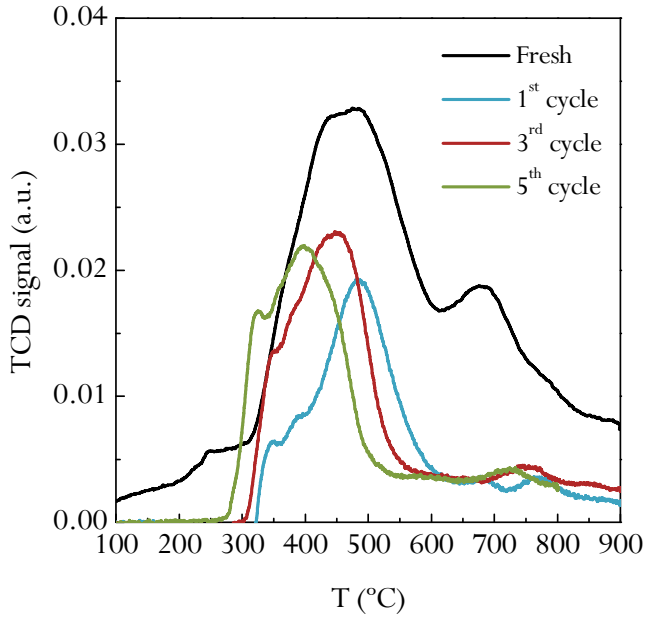

Figure 4.30. TPR profiles of deactivated catalysts for consecutive reforming/ regeneration cycles. Reforming conditions: 600 ºC; space time, 20 g_{cat} min $g_{volatiles}^{-1}$; S/B ratio, 4.

Consequently, the catalyst is irreversibly deactivated by Ni sintering, presumably during the regeneration step carried out at 700 °C, which is a fact that should be checked and, if this cause is true, less severe regeneration conditions should be chosen to preserve the metallic structure of the catalyst.

5

KINETIC MODELLING OF STEAM REFORMING IN THE PYROLYSIS-REFORMING OF BIOMASS

5. KINETIC MODELLING OF STEAM REFORMING IN THE PYROLYSIS-REFORMING OF BIOMASS

The aim of this chapter is to quantify the effect reaction conditions (temperature, space time and time on stream) have on product distribution in the catalytic steam reforming of volatiles from biomass pyrolysis. Therefore, a kinetic model is needed for the simulation and optimization of reforming conditions and for further studies of scaling up of the pyrolysis-reforming process.

The background on kinetic modelling of steam reforming of bio-oil is very limited and refers exclusively to the reforming of bio-oil model compounds, such as, ethanol, acetone, glycerol, acetol or acetic acid. Thus, steam reforming of two representative components in the aqueous fraction of bio-oil, acetone and ethanol, has been investigated by González-Gil et al. (2015), who described the process by means of five and two reactions, respectively. Wang et al. (2013b) studied the steam reforming of glycerol on a Ni-Mg-Al catalyst, and based on a kinetic model assuming only the reaction of glycerol reforming. Kinetics of acetol steam reforming, as a representative of the ketonic fraction in the bio-oil, has been satisfactorily studied by Dubey et al. (2012) in a fixed bed reactor over a wide temperature range, acetol concentration and space time, on a commercial 5 % Pt/C catalyst. First-order kinetic equations have been proposed by Román Galdámez et al. (2005) in the steam reforming of acetic acid for the formation of H_2 and CO_2 and the disappearance of CH_4 and C_2.

The kinetic model for this process has been studied in two steps:

1- A kinetic model corresponding to zero time on stream (fresh catalyst) has been established based on a compromise between simplicity and realism in the quantification of product distribution. Thus, a kinetic scheme with four reaction steps has been selected and expressions for the reaction rates of each step and the corresponding kinetic parameters have been determined (Section 5.1).

2- The kinetic model corresponding to zero time on stream has been coupled with a deactivation kinetic equation, which quantifies the decrease in catalyst activity with time on stream (Section 5.2).

5.1. KINETIC MODELLING AT ZERO TIME ON STREAM

Due to the lack of studies in the literature about kinetic modelling of the reforming of bio-oil or biomass pyrolysis volatiles, this one has been based on previous works of our research group for the kinetic modelling of the reforming of other oxygenated compounds, such as DME (Oar-Arteta, 2014) or ethanol (Montero, 2015), and for the reforming of hydrocarbons (Barbarias, 2015).

In this section, the theoretical background (Section 5.1.1) and the methodology of kinetic parameter calculation (Section 5.1.2) are described. Subsequently, a calculation program has been developed for the integration of the kinetic equations (Section 5.1.3). In Section 5.1.4, a kinetic scheme has been proposed based on the experimental results and the consideration of elementary steps in the catalytic reforming reactions. Finally, the kinetic model, the corresponding constants and the fitting to the experimental results are shown (Section 5.1.5).

The methodology for the kinetic data analysis follows the recommendations by Toch et al. (2015) for the kinetic modelling of catalytic processes. The basis are similar to those established in previous works of our research group, in which the effect of catalyst deactivation by coke deposition has been quantified (Mier et al., 2010; Epelde et al., 2014b; Pérez-Uriarte et al., 2017).

5.1.1. Reaction rate equations and mass balance

The kinetic values have been obtained in a fluidized catalytic bed reactor, in which ideal plug flow without radial concentration gradients has been assumed for the gas (Figure 5.1). Moreover, an isothermal bed has been considered, as temperature differences at radial and longitudinal positions are lower than 1 ºC. Change in molar total flow rate, F_T, has been considered along the reactor, since the reaction proceeds with an increase in the number of moles. Consequently, the mass conservation equation for each component i in a differential element of the reactor volume (in which the catalyst mass is W), is defined as follows:

$$\frac{dF_i}{dW} = \frac{d(F_T \cdot x_i)}{dW} = F_T \frac{dx_i}{dW} + x_i \frac{dF_T}{dW} = (r_i)_0 \qquad (5.1)$$

where W is the catalyst mass, x_i the molar fraction of component i on a wet basis, and $(r_i)_0$ is the formation rate of each component i in the reaction medium.

Based on eq. (5.1), the evolution of composition of each component along the reactor can be obtained:

$$\frac{dx_i}{dW} = \frac{(r_i)_0}{F_T} - \frac{x_i}{F_T}\frac{dF_T}{dW} \tag{5.2}$$

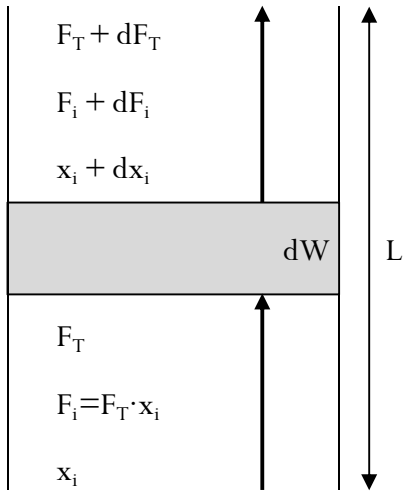

Figure 5.1. Differential element of catalyst mass in the catalytic bed.

The evolution of molar fraction with catalyst mass, and therefore with the longitudinal position in the reactor, is calculated by integrating eq. (5.2). Accordingly, the kinetic equations have been established considering the different reaction steps of the kinetic scheme in which component i is involved.

$$(r_i)_0 = \sum^{j} (\upsilon_i)_j (r_j)_0 \tag{5.3}$$

where $(\upsilon_i)_j$ is the stoichiometric coefficient of component i in the step j of the kinetic scheme, and $(r_j)_0$ the reaction rate of step j.

5.1.2. Calculation of the kinetic parameters

The calculation of the parameters for the kinetic model proposed has been carried out by non-linear multiple regression methodology, fitting the experimental results of x_i vs. W to the calculated ones by integrating eq. (5.2) and determining the best fit kinetic parameters. Computing of the models has been achieved by minimizing an error objective function (FO) defined as the weighted sum of squares of the differences between the experimental and calculated values of molar fractions:

$$FO = \sum_{i=1}^{n_c} w_i \phi_i = \sum_{i=1}^{n_c} w_i \sum_{j=1}^{p} (x_{i,j}^{*} - x_{i,j})^2 \qquad (5.4)$$

where w_i is the weight factor for each component i in the kinetic scheme, ϕ_i is the sum of squares of the residuals for each component i, $x_{i,j}^{*}$ is the molar fraction (on a wet basis) of component i at the experimental condition j, $x_{i,j}$ is the corresponding predicted value, n_c is the number of components in the kinetic scheme and p is the total number of experimental conditions.

In eq. (5.4), the weight factors are calculated as:

$$w_i = \frac{1}{\sum_{j=1}^{p} x_i} \qquad (5.5)$$

The application of eq. (5.5) gives similar results to those obtained by calculating the weight factors from the variances of the experimental result distributions.

In addition, regression coefficients (R^2) have been calculated based on the SST (*Total Sum of Squares*) and the SSE (*Sum of Squares of the Error*), which is calculated as:

$$SSE = \sum_{i=1}^{n_c} \sum_{j=1}^{p} (x_{i,j}^{*} - x_{i,j})^2 \qquad (5.6)$$

The parameters of best fit are the kinetic constants for each step j, which are expressed as functions of Arrhenius equation. To reduce the correlation between frequency factor and activation energy, the reparameterized Arrhenius equation has

been used by expressing the kinetic constant of each step (k_j) as a function of its corresponding value (k_j^*) at a reference temperature (T^*). Therefore, the parameters subjected to optimization in the kinetic model have been the kinetic constants at the reference temperature (650 ºC) and the corresponding activation energies:

$$k_j = k_j^* \exp\left[-\frac{E_j}{R}\left(\frac{1}{T}-\frac{1}{T^*}\right)\right] \quad (5.7)$$

5.1.3. Calculation program

For the integration of the kinetic equations and application of non-linear multiple regression, a calculation program has been developed in MATLAB, whose flow diagram is shown in Figure 5.2.

The main program (called "main.m") is used as an interface of input and output data and results and this program calls to non-linear regression subroutines in order to integrate the conservation equations. The input data required and the methodology are as follows:

1) An Excel file containing the kinetic values at all the experimental conditions: temperature and catalyst mass values, and molar fractions of the components of the kinetic scheme on a wet basis (x_i).

2) Identification of the kinetic model to be fitted (formulation of the differential equation set to be integrated).

3) Initial guess values for the kinetic parameters to be optimized.

The objective function to be minimized (using MATLAB *fminsearch* function) is related to the error between the experimental data and the data predicted by the proposed kinetic model, and is obtained from a series of functions that compute the error by integrating the differential equations of the model using the MATLAB *ode15s* function. Finally, model simulations are plotted and results are displayed in an Excel file.

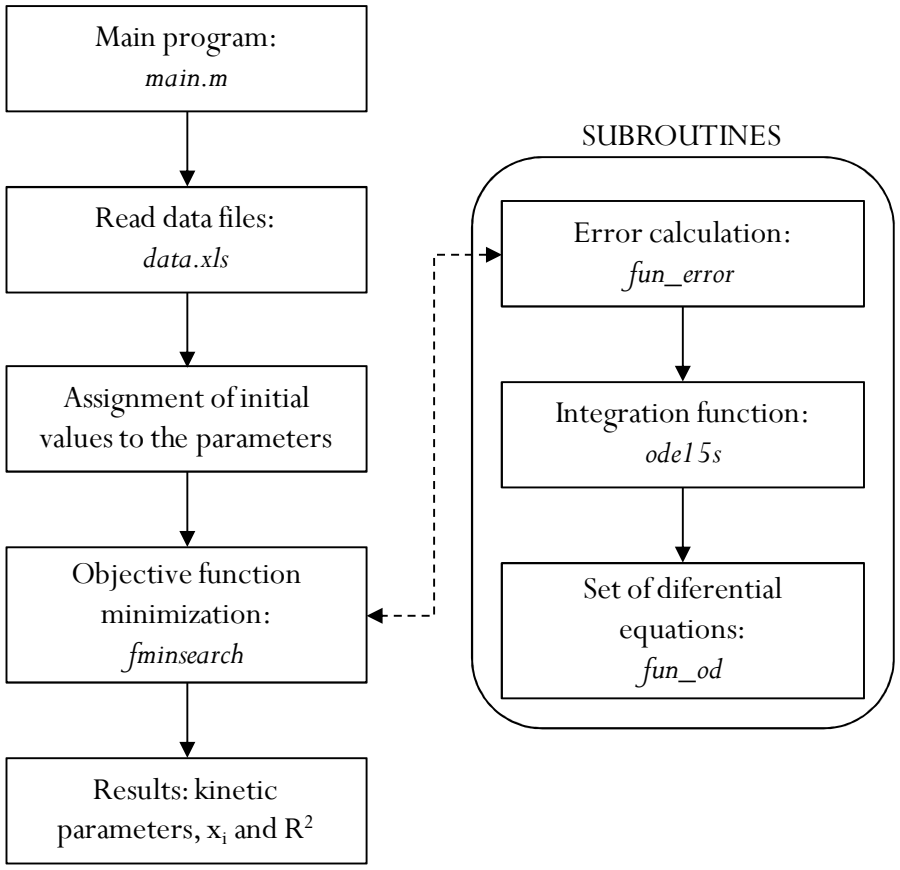

Figure 5.2. Flow diagram for the calculation of the kinetic parameters at zero time on stream.

5.1.4. Experimental results and reaction scheme

In order to establish the kinetic scheme, the product distribution at zero space time has been considered by taking into account the thermal cracking reactions. This cracking has been studied by carrying out experiments without catalyst and using a sand bed. The significance of the cracking reactions has been determined at the temperatures at which the reforming step has been performed, with the presence of CH_4, C_2-C_4 hydrocarbon fraction and oxygenated compounds, which occurs according to the following reaction:

$$C_nH_mO_k \rightarrow C_xH_yO_z + C_aH_b + CH_4 + CO + CO_2 + C \qquad (5.8)$$

The kinetic results for the modelling have been obtained by pyrolysis-reforming of biomass experiments at three different temperatures (600, 650 and 700 °C) and five values of space time for each temperature (2.5, 5, 10, 15 and 20 g_{cat} min $g_{volatiles}^{-1}$). A steam/biomass ratio (S/B) of 4 has been used in all the experiments, given that almost the maximum H_2 yield is reached at these conditions, as shown in Section 3.3.2.3.

The operating conditions of the pyrolysis step have been the same used in previous sections, which have been detailed for the biomass in Section 2.3.1. The results of the kinetic modelling have been the molar fractions of H_2, CO_2, CO, H_2O, CH_4, C_2-C_4 hydrocarbons and non-reacted oxygenated compounds ($C_nH_mO_k$). These values have been obtained by extrapolation at zero time on stream of the evolution of molar fractions with time on stream. Moreover, the results obtained in the catalytic cracking experiments without catalyst (with sand) have been used at zero space time.

Figure 5.3 shows the effect of catalyst mass on the molar fraction of each component at different temperatures. When temperature and space time are increased, reforming and WGS reactions are enhanced and therefore, H_2 and CO_2 molar fractions increase.

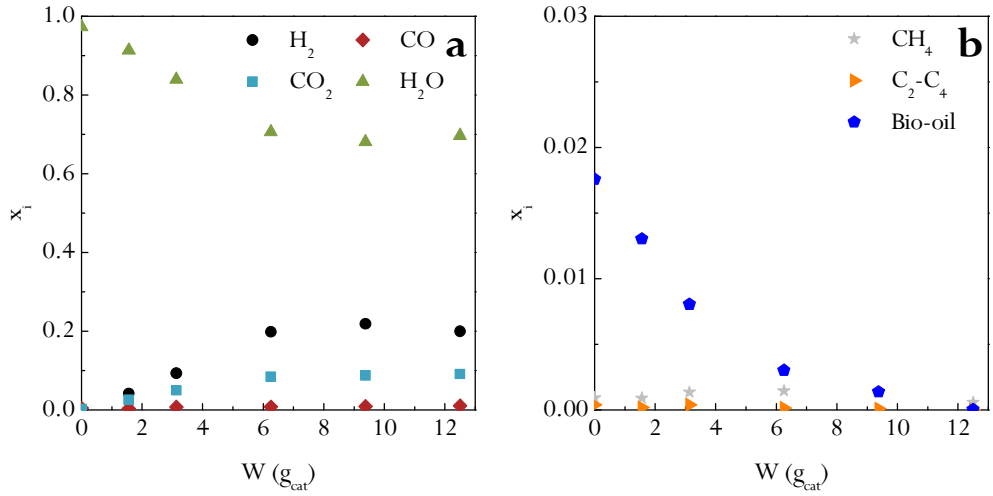

Figure 5.3. Effect of catalyst mass on product molar fractions at different reforming temperatures, 600 °C (a, b), 650 °C (c, d) and 700 °C (e, f).

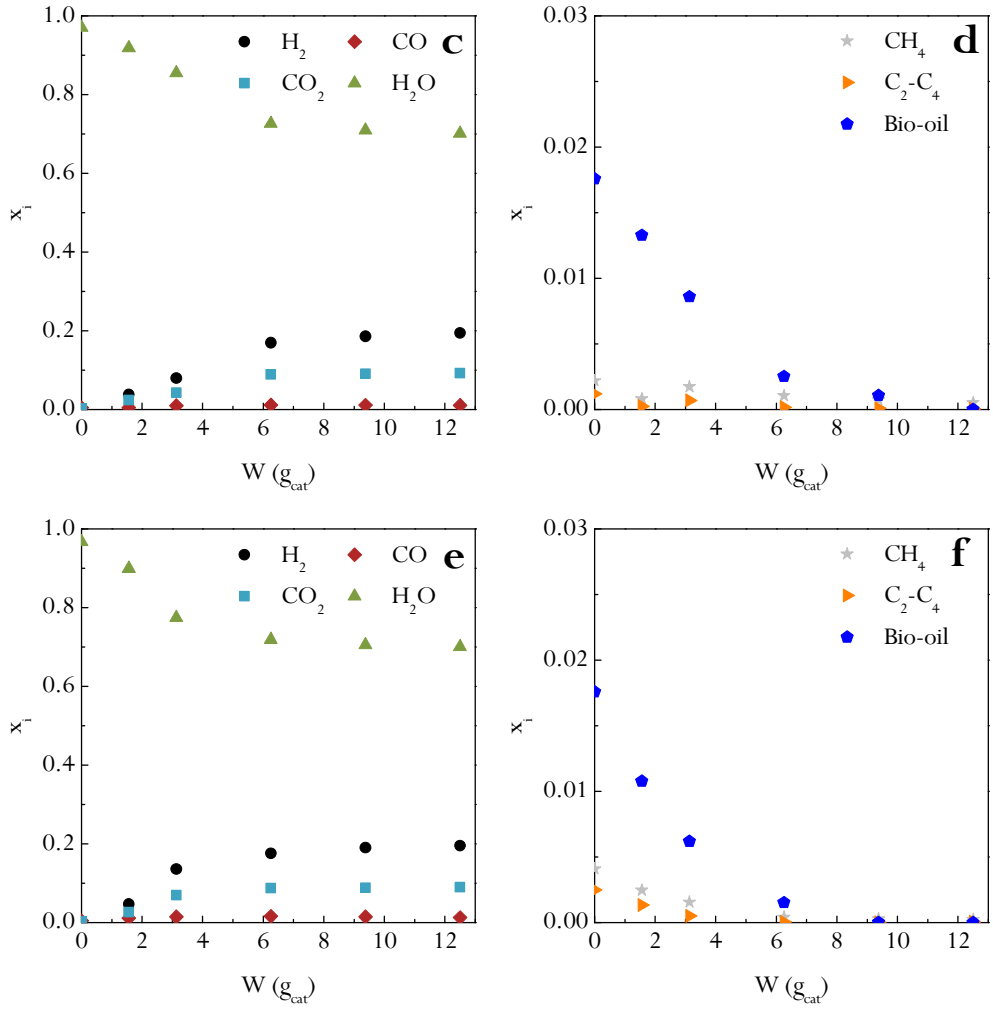

Figure 5.3. Continued.

The results at zero space time evidence the low CH_4 yield and the insignificant coke amount deposited on the sand bed in the temperature range studied.

Figure 5.3a (reforming temperature 600 °C) shows that H_2 concentration increases when the catalyst mass is increased, obtaining a maximum value with 9.4 g of catalyst (15 g_{cat} min $g_{volatiles}^{-1}$) due to the reforming reactions of the compounds in the feed (eqs. (5.9), (5.11) and (5.12)). The full reforming of oxygenated compounds is achieved with a space time of 20 g_{cat} min $g_{volatiles}^{-1}$.

At 650 ºC (Figure 5.3c,d), the reaction rate is similar for the reforming reaction, and the highest H_2 and CO_2 concentrations are achieved with a catalyst mass of 12.5 g (20 g_{cat} min $g_{volatiles}^{-1}$), when all oxygenated compounds are reformed.

Finally, at 700 ºC (Figure 3e, f), the reforming reaction rate is higher, given that the concentration of oxygenated compounds decreases rapidly and H_2 concentration increases. In this case, almost full conversion is obtained with a catalyst mass of 9.4 g (15 g_{cat} min $g_{volatiles}^{-1}$). This space time is lower than that corresponding to the same situation in the 600-650 ºC range.

Accordingly, considering the trends observed in Figure 5.3, the following kinetic scheme has been proposed for the reforming step (Figure 5.4):

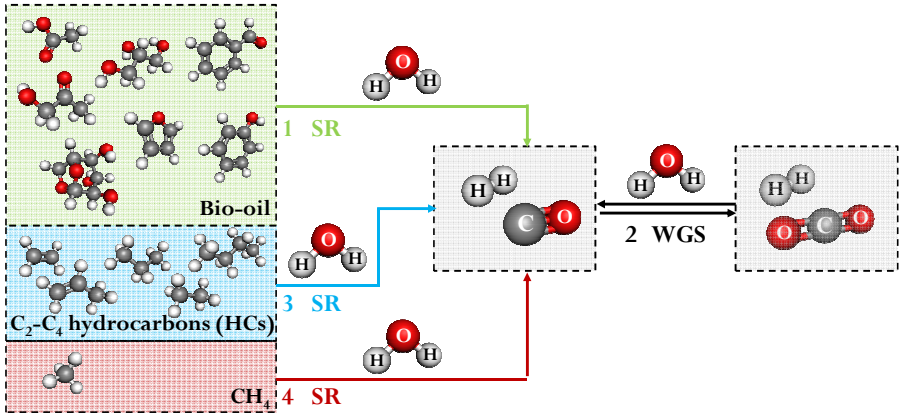

Figure 5.4. Kinetic scheme proposed for the reforming of biomass pyrolysis volatiles.

The reactions of the kinetic scheme proposed in Figure 5.4 are as follows:

1. Reforming of oxygenated compounds ($C_nH_mO_k$):

$$C_nH_mO_k + (n-k)H_2O \rightarrow \left(n + \frac{m}{2} - k\right)H_2 + nCO \qquad (5.9)$$

2. *Water Gas Shift* reaction (WGS):

$$CO + H_2O \leftrightarrow H_2 + CO_2 \qquad (5.10)$$

3. Reforming of C_2-C_4 hydrocarbon fraction:

$$C_nH_m + nH_2O \rightarrow nCO + \left(n + \frac{m}{2}\right)H_2 \quad (5.11)$$

4. Reforming of CH_4:

$$CH_4 + H_2O \rightarrow 3H_2 + CO \quad (5.12)$$

5.1.5. Proposed kinetic model

Table 5.1 shows the proposed kinetic model, in which a first order reaction for each reactant has been considered in the individual reactions of the kinetic scheme (Figure 5.4).

Table 5.1. Description of the kinetic model at zero time on stream.

Step	Kinetic equations	
1	$(r_1)_0 = k_1 \cdot x_{CnHmOk} \cdot x_{H2O}$	(5.13)
2	$(r_2)_0 = k_{WGS} \cdot (x_{CO} \cdot x_{H2O} - x_{H2} \cdot x_{CO2} / K_{WGS})$	(5.14)
3	$(r_3)_0 = k_3 \cdot x_{C2\text{-}C4} \cdot x_{H2O}$	(5.15)
4	$(r_4)_0 = k_4 \cdot x_{CH4} \cdot x_{H2O}$	(5.16)

The equilibrium constant of the WGS reaction (K_{WGS}) has been calculated with the following expression:

$$K = \exp\left[a + b\frac{1}{T} + c\log(T) + dT + eT^2 + f\frac{1}{T^2}\right] \quad (5.17)$$

where parameters (a-f) have been calculated based on thermodynamic principles, using the methodology described by Smith (2007). These values are set out in Table 5.2.

Table 5.2. Parameters of the equilibrium constant of the WGS reaction.

	a	b	c	d	e	f
K_{WGS}	$-1.8\ 10^{1}$	$5.8\ 10^{3}$	$1.8\ 10^{0}$	$-2.7\ 10^{-4}$	$0\ 10^{0}$	$-5.8\ 10^{4}$

Table 5.3 shows the kinetic parameters (kinetic constants at the reference temperature and the corresponding activation energies) for the equations in Table 5.1. These values have been calculated by the methodology described in Section 5.1.2.

Table 5.3. Kinetic parameters for the model proposed.

Parameter	
k_1^0, mol g_{cat}^{-1} min^{-1}	$5.5\ 10^{-2}$
k_{WGS}^0, mol g_{cat}^{-1} min^{-1}	$4.4\ 10^{-1}$
k_3^0, mol g_{cat}^{-1} min^{-1}	$3.0\ 10^{-2}$
k_4^0, mol g_{cat}^{-1} min^{-1}	$5.2\ 10^{-2}$
E_1^0, kJ mol^{-1}	14.5
E_{WGS}^0, kJ mol^{-1}	30.0
E_3^0, kJ mol^{-1}	33.7
E_4^0, kJ mol^{-1}	20.7
R^2	0.997

It should be noted that the activation energy for the reforming of bio-oil oxygenated compounds is low, 14.5 kJ mol^{-1}, whereas those corresponding to the reforming of CH_4 and C_2-C_4 hydrocarbons and WGS reaction are more sensitive to temperature in the 600-700 °C range.

Figure 5.5 shows the quality of the fit for the proposed kinetic model by comparing the evolution of the experimental results of product molar fractions with catalyst mass (dots) and those calculated using the model (lines). The fitting is adequate and the proposed model predicts reasonably well the effect temperature and catalyst mass (or space time) have on product distribution at zero time on stream.

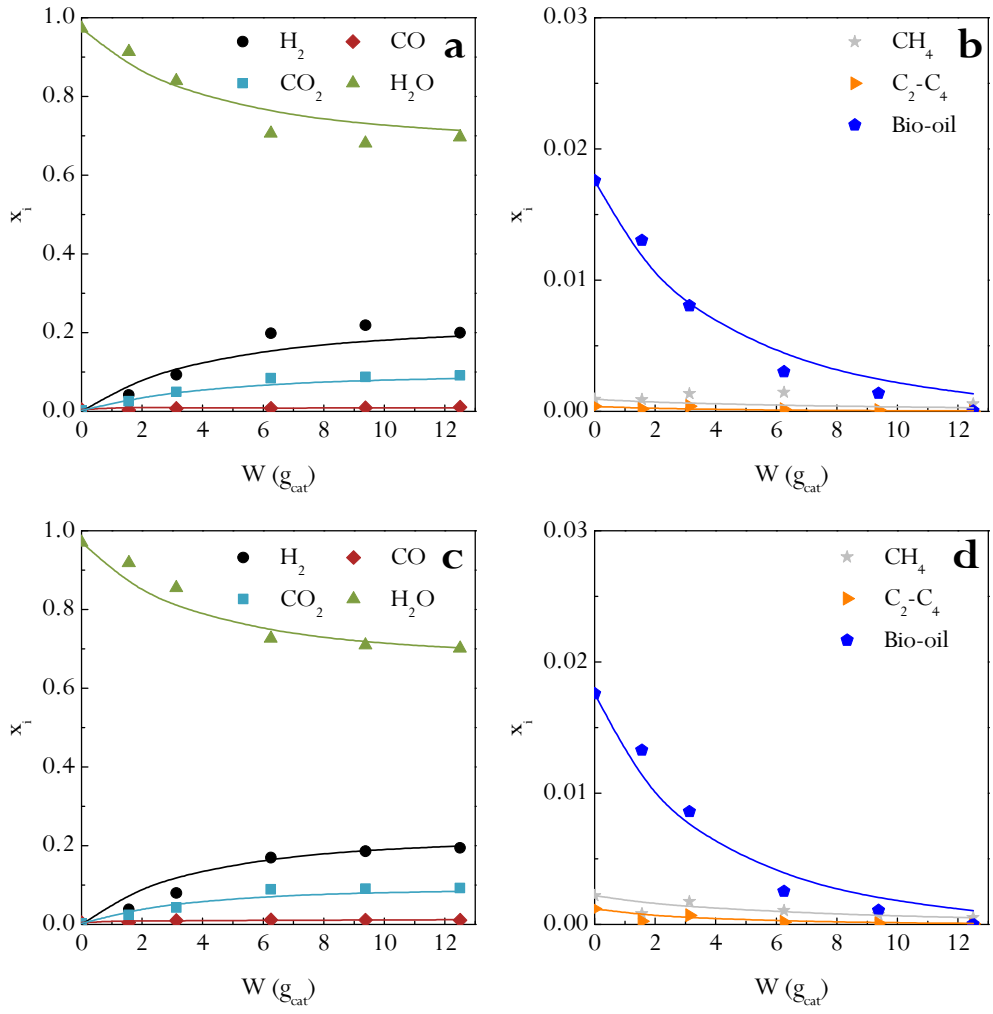

Figure 5.5. Comparison of the experimental results of evolution of product molar fractions with catalyst mass (dots) with those predicted using the model (lines) at 600 °C (a, b), 650 °C (c, d) and 700 °C (e, f).

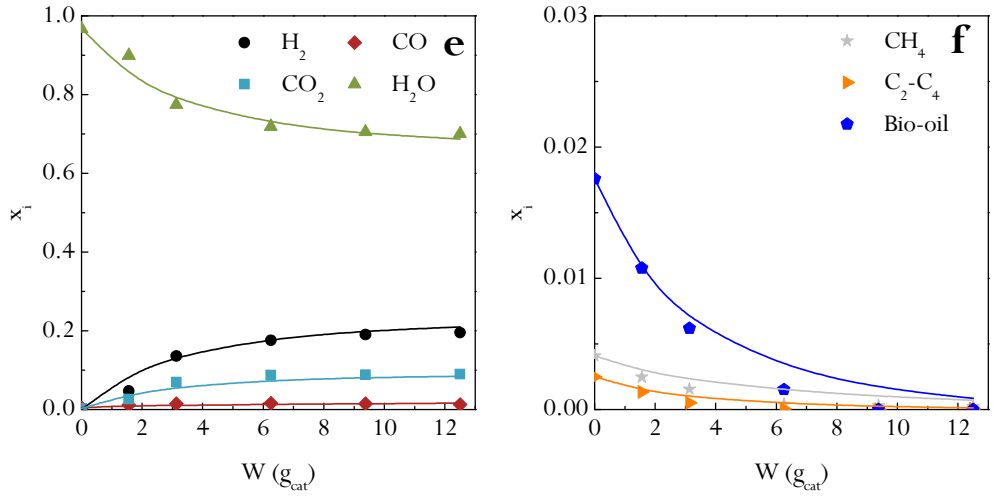

Figure 5.5. Continued.

5.2. KINETIC MODELLING OF THE DEACTIVATION

As shown in Section 4.1, the product yields change with time on stream due to catalyst deactivation. Given that deactivation is fast, a kinetic model that quantifies its effect is required for establishing an operation strategy, such as reaction/regeneration cycles or catalyst circulation in the fluidized bed reactor. Based on the coke study in Section 4.2 and the relationship between its deposition and reaction medium composition, the oxygenates in the bio oil are presumably the main coke precursors, which is an essential premise for establishing a deactivation kinetic equation.

5.2.1. Methodology

5.2.1.1. Consideration of deactivation in the kinetic equations

A non-selective deactivation model has been considered, and therefore the same activity parameter has been used for the different steps of the kinetic scheme (reforming of oxygenated compounds, C_2-C_4 and CH_4, and WGS reaction, Figure 5.4). Activity has been defined as the ratio between the reaction rate at time t and the reaction rate at zero time on stream for each component i:

$$a = \frac{r_i}{(r_i)_0} \tag{5.18}$$

Consequently, the reaction rate of component i at time t has been calculated from the reaction rate at zero time on stream, $(r_j)_0$, eqs. (5.13)-(5.16). The general expression for the kinetic equations is as follows:

$$r_i = \sum^{j} (\upsilon_i)_j (r_j)_0 a \tag{5.19}$$

5.2.1.2. Calculation of the kinetic parameters

A similar methodology as that for zero time on stream has been used to calculate the kinetic parameters. The fitting has been carried out by multiple non-linear regression of the experimental molar fractions with time on stream, solving the mass conservation equation for each component i (eq. (5.1)) together with the deactivation kinetic equation. The optimization in the fitting has been carried out by minimizing an error objective function (FO), eq. (5.4), defined in Section 5.1.2.

Given that the experimental values have been obtained in a fluidized bed reactor, there is no longitudinal profile of activity along the reactor, but activity is uniform at each time in the catalytic bed. Therefore, perfect mix is assumed for the solid and plug flow for the gas.

Similarly as in the kinetic modelling at zero time, the kinetic constants have been reparameterized. Furthermore, the kinetic parameters calculated previously at zero time on stream have been used in the fitting (Table 5.3). Therefore, the kinetic constant of deactivation at the reference temperature (650 ºC) and the corresponding activation energy have been optimized.

5.2.2. Experimental results

The experimental values used for the fitting have been obtained at 600, 650 and 700 ºC, with a catalyst mass of 12.5 g and reaction times of 105, 110 and 120 min, respectively.

The evolution of the experimental molar fractions of products with time on stream at each temperature is shown in Figure 5.6 (dots). Due to the deactivation of the catalyst, the molar fractions of H_2 and CO_2 decrease with time on stream, while that of CO increases. Moreover, those corresponding to H_2O and the non-reacted oxygenated compound fraction also increase with time on stream due to the decrease in catalyst activity. Furthermore, secondary reactions, such as cracking reactions, are enhanced, which leads to higher molar fractions of CH_4 and C_2-C_4 hydrocarbons.

5.2.3. Proposed kinetic model

The kinetic equation for the deactivation considers a catalyst deactivation rate proportional to the concentration of oxygenated compounds:

$$-\frac{da}{dt} = k_d x_{CnHmOk} a \tag{5.20}$$

where x_{CnHmOk} is the molar fraction of oxygenated compounds, k_d is the kinetic constant of deactivation and a the activity defined as the ratio between the reaction rates at t time and zero time on stream (eq. (5.18)).

Table 5.4 shows the reaction rates of the proposed kinetic scheme considering catalyst deactivation. The equilibrium constant of the WGS reaction has been calculated using eq. (5.17) with the parameters shown in Table 5.2.

Table 5.4. Description of the kinetic scheme considering deactivation.

Step	Kinetic equations	
1	$r_1 = k_1 \cdot x_{CnHmOk} \cdot x_{H2O} \cdot a$	(5.21)
2	$r_2 = k_{WGS} \cdot (x_{CO} \cdot x_{H2O} - x_{H2} \cdot x_{CO2} / K_{WGS}) \cdot a$	(5.22)
3	$r_3 = k_3 \cdot x_{C2\text{-}C4} \cdot x_{H2O} \cdot a$	(5.23)
4	$r_4 = k_4 \cdot x_{CH4} \cdot x_{H2O} \cdot a$	(5.24)

The values calculated for the deactivation rate constant at the reference temperature (650 ºC) and the corresponding activation energy have been 1.6 10^0 min^{-1} and 18.6 kJ mol^{-1}, respectively, with R^2 being 0.997. This low value of activation energy is evidence of a little effect of temperature in the 600-700 ºC range.

The adequate fit of the kinetic model is shown in Figure 5.6, in which the experimental data (dots) are compared with those predicted by the model (lines) for three temperatures, 600 ºC (a, b), 650 ºC (c, d) and 700 ºC (e, f). As observed the model satisfactorily predicts the evolution of product molar fractions with time on stream. Therefore, the consideration of oxygenated compounds as coke precursor is a solid premise.

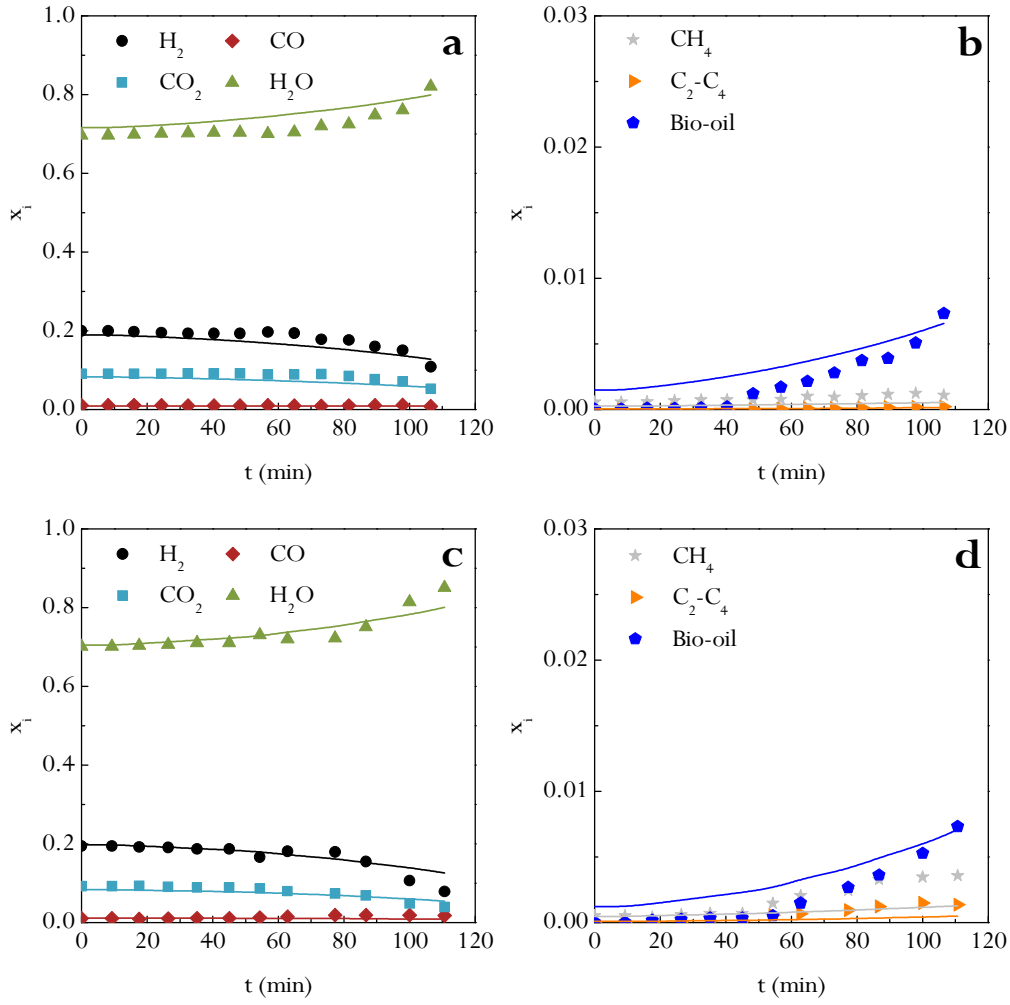

Figure 5.6. Comparison of the experimental results for the evolution of product molar fractions with time on stream (dots) with those predicted by the model (lines) at 600 ºC (a, b), 650 ºC (c, d) and 700 ºC (e, f).

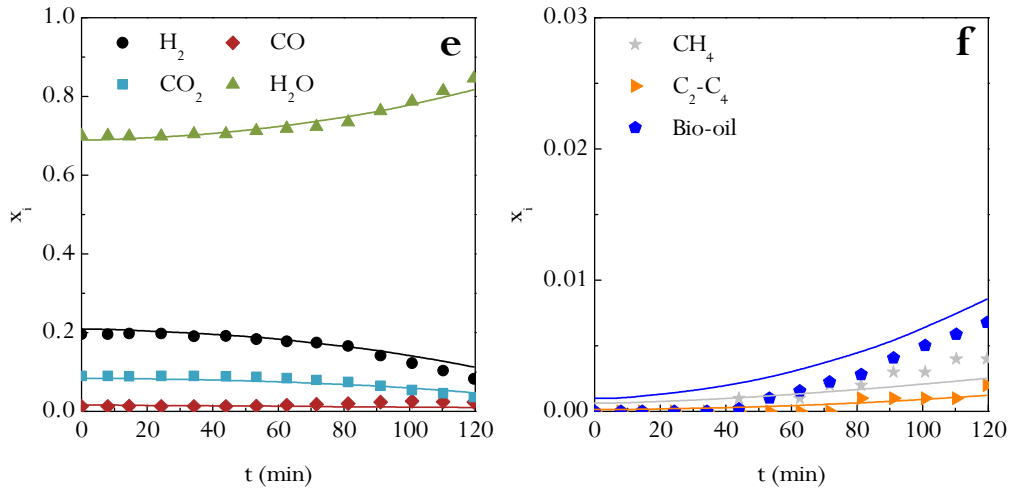

Figure 5.6. Continued.

However, a remarkable deviation is observed for the molar fractions of oxygenated compounds because, on the one hand, scale is larger (these molar fractions are smaller than those for the reforming products) and, on the other, the formation of these byproducts is affected by the cracking of oxygenated compounds leading to CH_4 and C_2-C_4, which not considered in the kinetic model due to the difficulty involved.

In any case, these gaps correspond to the prediction of secondary products (which will be improved in later works) and the proposed model adequately quantifies the distribution of the main products in the reforming reaction with time on stream (H_2, CO_2, CO and H_2O) over a wide range of operating conditions.

6

SUMMARY

6. SUMMARY

H_2 production from biomass and biomass/plastic mixtures has been studied in a two-step continuous process, with the first step being the pyrolysis of the feed and the second one the catalytic steam reforming of volatiles from the previous pyrolysis step. The process has been carried out using a laboratory-scale plant provided with a conical spouted bed reactor, which is suitable for the pyrolysis of both biomass and plastics, and a fluidized bed reactor for the in-line reforming step. The selection of these reactors is based on our research group's prior experience and each reactor's suitability and capability for performing the corresponding reactions.

Biomass and high density polyethylene (HDPE) are the materials used as feed in the process. Furthermore, the biomass used in this study is pine wood, which has been ground and sieved to a particle size in the 1-2 mm range. The HDPE has been provided in the form of chippings with a particle diameter of around 4 mm.

The reforming step has involved a Ni based catalyst, which is commercialised by *Süd Chemie* for CH_4 reforming (G90 LDP or ReforMax® 330). The catalyst has been ground and sieved to a particle size in the 0.4-0.8 mm range. The physical properties of the fresh catalyst have been measured by N_2 adsorption-desorption in a *Micromeritics ASAP 2010* apparatus. Moreover, the reducibility and nature of the metallic species have been determined by temperature programmed reduction (TPR) in a *Micromeritics AutoChem 2920*.

The volatile stream leaving the reforming reactor has been analyzed in-line by means of a GC *Agilent 6890,* and the non-condensable gases by a microGC *Varian 4900*. The results obtained from these analyses have been used to calculate the reaction indices: conversion, products yields (H_2, CO_2, CO, CH_4, C_2-C_4 hydrocarbons and non-reacted bio-oil), gaseous product concentrations (H_2, CO_2, CO, CH_4 and C_2-C_4 hydrocarbons), specific gas yield and production, H_2 production, and reacted steam.

The operating conditions in the first step (fast pyrolysis in a conical spouted bed reactor) are as follows: 500 ºC, solid feeding rate, 0.6-1.5 g min^{-1}, sand bed (0.3-0.355 mm), 50 g, and; water flow rate, 3 mL min^{-1}, which corresponds to a steam flow rate of 3.73 NL min^{-1}. The pyrolysis step by feeding steam has been studied to compare the product yields with those previously obtained by our research group when feeding N_2 as fluidizing agent. The low temperature and short residence time of the volatiles in the reactor and the good features of the conical spouted bed reactor

make it possible to obtain a stream composed mainly of oxygenates (from biomass), and waxes (C_{21+}) and gasoil (C_{12}-C_{20}) (from HDPE), which is reformed without operational problems.

The parametric study of the catalytic steam reforming of biomass pyrolysis volatiles has been carried out using the following operating variables: temperature, 550-700 °C, space time, 2.5-30 g_{cat} min $g_{volatiles}^{-1}$, and; steam/biomass ratio, 2-5.

A minimum temperature of 600 °C and a space time of 20 g_{cat} min $g_{volatiles}^{-1}$ are required to attain full conversion with an S/B ratio of 4. Under these conditions, a H_2 yield and production of 93.5 % and 11.0 wt %, respectively are attained, with these values being higher than those obtained by most of the studies in the literature dealing with the pyrolysis-reforming of biomass and steam reforming of bio-oil. The highest H_2 yield and production of 95.8 % and 11.7 wt %, respectively, have been obtained at the highest space time studied (30 g_{cat} min $g_{volatiles}^{-1}$). Moreover, an increase in the S/B ratio shifts the reforming and WGS reactions, leading to an increase in H_2 yield.

Furthermore, in order to study the effect of different feeds on the pyrolysis-reforming process, only biomass in the feed, only HDPE in the feed and different biomass/plastic mixtures (25/75 wt %, 50/50 wt % and 75/25 wt %) have been used and their effect on product yields has been analyzed, using a temperature of 700 °C, with a space time of 16.7 g_{cat} min $g_{feeding}^{-1}$ and a steam/feeding ratio of 4.

The different composition of the volatiles produced in the pyrolysis step of biomass and HDPE leads to different results in the reforming step. Thus, co-feeding plastics enhances H_2 production, which increases from 10.9 wt % with only biomass in the feed to 37.3 wt % with only HDPE in the feed, with this difference being directly related to the C and H content of the feedstocks. The linear increase in H_2 production shows there is no significant synergetic effect when co-feeding HDPE into the pyrolysis reactor.

The viability of the reforming step, and therefore of the proposed pyrolysis-reforming strategy, is conditioned by catalyst deactivation by coke deposition. Thus, especial attention has been paid to catalyst's deactivation study. Furthermore, the nature and content of the coke have been determined by several techniques (TPO, SEM and TEM), identifying two different types of coke: amorphous and more structured. Moreover, the effect feeding (biomass, HDPE and different mixtures) has on catalyst deactivation has been studied. Biomass processing causes a much faster

deactivation than HDPE processing, which is explained by the different nature of the coke deposited on the catalyst, with the amorphous coke being the main deactivating one, which is the main type of coke in biomass valorisation. The origin of this coke is related to the adsorption on metallic sites of oxygenated compounds in the reaction medium and their degradation towards amorphous and encapsulating aromatic structures. However, the co-feeding of HDPE leads to the formation of a structured and filamentous coke, whose presence has a lower impact on catalyst activity.

An original kinetic model has been proposed for the reforming of volatiles derived from biomass pyrolysis. The kinetic scheme takes into account the individual steps of steam reforming of pyrolysis products (oxygenated compounds, CH_4 and C_2-C_4 hydrocarbons), and the WGS reaction. The presence of CO and CO_2 has also been considered in the feed into the reforming step, given that these are by-products derived from oxygenate cracking. In this reforming kinetic model, the reaction rate of each individual step has been formulated as elemental regarding each reactant.

The kinetic parameters (kinetic constants at the reference temperature and the corresponding activation energies) of the different reaction steps have been determined by using non-linear multiple regression to fit the experimental results of concentrations at the reactor outlet (molar fraction of H_2, CO_2, CO, H_2O, CH_4, C_2-C_4 hydrocarbons and non-reacted oxygenates) to those calculated by integrating the kinetic equation for the formation of each component at zero time on stream.

The kinetic model at zero time on stream has been coupled with a deactivation kinetic equation, which has been formulated by fitting the experimental results of each component's evolution of concentrations in the reaction medium with time on stream to the model. The deactivation kinetic equation has an expression dependent on non-reacted oxygenate concentration (main products in biomass pyrolysis).

The full kinetic model proposed suitably predicts the experimental results obtained in the reforming of volatiles from biomass pyrolysis, in a wide range of operating conditions (600-700 ºC, space time, 0-20 g_{cat} min $g_{volatiles}^{-1}$, and time on stream up to 2 h). It is therefore a suitable tool for further simulation, optimization, and scaling up studies.

7

CONCLUSIONS

7. CONCLUSIONS

This thesis has led to the following conclusions of interest for future research, knowledge transfer, and the industrial implementation of biomass valorisation for H_2 production.

Proposed two-step system

The pyrolysis of biomass and biomass/HDPE mixtures in a conical spouted bed reactor and the in-line reforming of pyrolysis volatiles in a fluidized bed reactor have proven to be a viable strategy for the production of H_2. The development of this original continuous two-step process has several practical advantages, both from an operational point of view and for the performance of catalytic reforming, due to the separation of the pyrolysis and reforming steps. Moreover, the two reactors connected in series operate in continuous regime with separate control. Thus, high H_2 yield and production have been obtained without operational problems, except those related to catalyst deactivation, which can be solved by regenerating the catalyst and operating with catalyst circulation in the fluidized bed reactor. In addition, this direct strategy is an attractive and novel alternative to the indirect bio-oil reforming process, in which the operational problems associated with bio-oil handling are avoided.

Biomass and HDPE pyrolysis step

The conical spouted bed reactor is suitable for the continuous pyrolysis of biomass and biomass/HDPE mixtures. On the one hand, the conical spouted bed reactor allows handling solids of irregular texture, as is the case of biomass particles, and on the other, the vigorous cyclic movement of the biomass and sand particles coated with melted plastic minimises segregation problems and avoids bed defluidization when biomass/HDPE mixtures are valorised. These conditions, together with high mass and heat transfer rates between phases, allow operating at relatively low pyrolysis temperatures (500 °C), minimising the energy required in the process.

Furthermore, the low residence time of the volatiles in the conical spouted bed reactor limits secondary reactions, favouring the selective production of primary pyrolysis products. Thus, the pyrolysis conditions used maximise bio-oil production,

with its yield being 75.3 wt %. Moreover, the gas and char yields are 7.3 wt % and 17.3 wt %, respectively. Regarding plastic valorisation, the fast pyrolysis of HDPE in a conical spouted bed reactor does not produce any solid fraction. The main products are the long-chain hydrocarbons making up the diesel fraction (C_{12}-C_{20}) and waxes (C_{21+}), with a total yield of up to 90 wt %. The yields of gases and gasoline range hydrocarbons are low, 1.5 and 5.6 wt %, respectively. Thus, the product stream made up of volatiles may be treated in the reforming step, given that it is a suitable and constant stream due to the continuous operation system.

Steam atmosphere in the pyrolysis step has a limited effect on product distribution at 500 ºC, with the results being similar to those previously obtained using N_2 as fluidizing agent. This inert nature of steam is of major interest for process viability, given that the costs of the gases are reduced, and the problem related to their separation prior to the catalytic reforming step is avoided.

Catalytic reforming step of biomass pyrolysis volatiles

The Ni commercial catalyst (G90LDP) is highly active for the reforming of the volatiles produced by biomass pyrolysis (bio-oil oxygenated compounds, CH_4 and C_2-C_4 hydrocarbons).

Temperature, space time and S/B ratio have a major influence on product distribution. Thus, a minimum temperature of 600 ºC and a space time of 20 g_{cat} min $g_{volatiles}^{-1}$ are required for full conversion with an S/B ratio of 4. Once this temperature has been reached, a further increase to 700 ºC had a limited effect on product yield and composition, with H_2 yield and production in this temperature range being around 93.5 % and 11.0 wt %, respectively.

An increase in space time enhances both the reforming and the WGS reaction, leading to an increase in the yields of H_2 and CO_2. Thus, at the highest space time studied, a H_2 yield was obtained of 95.8 % of the maximum allowable by stoichiometry. Similarly, the main effect of increasing the S/B ratio is the shifting of the reforming and WGS reactions, thereby improving H_2 yield. However, an increase in this ratio involves higher process heating requirements.

Catalytic reforming step of the volatiles from the pyrolysis of biomass/HDPE mixtures

The joint valorisation of both feedstocks is an interesting strategy because it increases process flexibility and improves process yields. Thus, conversion above 98 % is achieved in all the runs performed with several HDPE/biomass mixtures, due to the relatively high space time used (16.7 g_{cat} min $g_{feeding}^{-1}$). In the valorisation of HDPE, a minimum temperature of 700 ºC has been used for attaining complete conversion, instead of the 600 ºC required for only biomass, thereby enhancing the reforming reactions and providing higher H_2 yields with lower catalyst deactivation.

In fact, a higher HDPE content in the feed enhances the production of both gaseous stream and H_2, i.e., H_2 production increases linearly with HDPE content in the feed, from 10.9 wt % for only biomass to 37.3 wt % for only HDPE. This increase in H_2 production is explained by the biomass feedstock's low H and high O contents, which are a drawback for high H_2 production.

Comparing this strategy to the gasification process, it may be concluded that the pyrolysis-reforming process leads to a H_2-rich gaseous product, obtaining a maximum concentration of around 70 vol % when only HDPE is valorised, whereas synthesis gas is the main product (maximum H_2 concentration of 58 vol % when only HDPE is valorised) in the gasification. Consequently, the higher yield and production of H_2 achieved with this two-step pyrolysis-reforming strategy, its capability to jointly valorise biomass and plastic mixtures, and the lower temperatures required compared to gasification, make this a promising process for producing H_2 from renewable raw materials and wastes.

Effect of operating conditions on deactivation

An increase in temperature in the 550-600 ºC range increases initial conversion and, in turn, attenuates the decrease in conversion and H_2 yield with time on stream. However, the effect temperature has on conversion and H_2 yield in the 600-700 ºC is slight, and a similar evolution of these reaction indices with time on stream is obtained.

The role of space time on catalyst deactivation is important for identifying the compounds that may be coke precursors in the reaction medium. The fast catalyst deactivation for low space time values allows identifying the oxygenated compounds of the bio-oil as the main coke precursors, whose concentration is higher under these

conditions. Consequently, a higher H_2 yield is obtained at high space time values, with the decrease being from 84.9 to 55.0 % in 40 min with 10 g_{cat} min $g_{volatiles}^{-1}$ and from 95.8 to 63.3 % in 230 min with 30 g_{cat} min $g_{volatiles}^{-1}$.

An increase in S/B ratio to a value of 4 effectively attenuates catalyst deactivation by favouring the gasification/reforming of the coke precursors, whose presence in the reaction medium decreases. However, an increase in the ratio above this value does not have a noticeable effect.

Furthermore, it has been proven that the composition of the feed significantly affects catalyst deactivation in the reforming step. Biomass processing leads to much faster deactivation, with this result being especially remarkable when the effective space time (by mass unit of C reformed) is approximately 2.5 times that of only HDPE in the feed. Thus, after 120 min continuous operation, conversion dropped from 100 % to approximately 90 % and 60 %, respectively, for only HDPE and only biomass in the feed. Consequently, the co-feeding of HDPE with biomass is a suitable strategy for attenuating catalyst deactivation.

Origin of catalyst deactivation

The fluidized bed reactor for the reforming step allows operating for long periods of time without operating problems due to coke deposition, thereby improving the fixed bed reactor's performance. However, coke deposition on the catalyst surface decreases H_2 and CO_2 yields and increases CO, CH_4, C_2-C_4 hydrocarbons and non-converted bio-oil yields with time on stream. Nevertheless, the catalyst's loss of activity is not only related to the amount of coke deposited on the catalyst, but also to the effect coke nature has on catalyst activity.

In addition, the catalyst's physical properties are affected by coke deposition with time on stream, decreasing the specific surface area and pore volume (meso and micropores), whereas pore diameter increases considerably, given that blocking by coke affects the smaller pores to a greater extent. Regarding the catalyst's metallic properties, Ni crystallite size is similar above 50 min time on stream, and therefore sintering at 600 ºC can be discarded as the main cause of deactivation.

The TPO, SEM and TEM analyses of the deactivated catalysts at different times on stream reveal two different types of coke: 1) amorphous coke, which encapsulates the Ni active sites and whose combustion is catalyzed at low temperatures, and 2) condensed coke, which is burnt at higher temperatures and has a more structured

nature. The coke evolves with time on stream from amorphous to more condensed structures.

Reforming temperature has a considerable effect on the amount and nature of the coke in the 550-700 ºC range. Thus, a lower content of amorphous coke is obtained at high temperatures for two different reasons: 1) the concentration of bio-oil oxygenated compounds in the reaction medium is lower, and 2) coke gasification is favoured. However, high temperatures lead to higher yields of secondary products (CO, CH_4 and C_2-C_4 hydrocarbons) in the reaction medium, which favour the formation of condensed coke. Furthermore, an increase in space time and S/B ratio considerably reduces the amount of coke deposited on the catalyst, as reforming and WGS reactions are enhanced under these conditions.

Regarding the coke deposited in the valorisation of biomass and HDPE mixtures, it may be concluded that the effect of reaction medium composition on coke nature is important. The co-feeding of HDPE leads to the formation of structured and filamentous coke, whose presence has a lower impact on catalyst activity. Catalyst deactivation by coke is therefore attenuated when HDPE is co-fed, due to the lower content of oxygenated compounds in the reaction medium.

Catalyst regeneration

The catalyst used in the reforming of biomass pyrolysis volatiles has been partially regenerated by coke combustion. Initial conversion and H_2 yield decrease from the first to the fifth cycle, from 99.7 to 87.6 % and from 93.5 to 68.0 %, respectively. However, beyond the fifth cycle, the catalyst follows a similar trend for conversion and H_2 yield with time on stream, as the catalyst has stabilized by this point.

The characterization of regenerated catalysts shows that sintering is probably the cause of irreversible catalyst deactivation. Ni crystallite size increases as reforming/regeneration cycles are increased, thereby decreasing dispersion and its activity for reforming and WGS reactions. The increase in Ni crystallite size leads to the formation of exclusively amorphous coke.

Consequently, the results obtained by six consecutive reforming/regeneration cycles reveal the catalyst's loss of activity, presumably in the regeneration step (performed at 700 ºC). Nevertheless, a stable evolution of conversion and product yields with time on stream has been achieved beyond the fifth cycle, which is significant from an industrial point of view.

Kinetic modelling of steam reforming in the pyrolysis-reforming of biomass

The validity of the kinetic model for quantifying the distribution of products (H_2, CO_2, CO, H_2O, CH_4, C_2-C_4 hydrocarbons and non-converted bio-oil) has been verified. This model has been established considering a scheme with four different reactions: reforming of bio-oil oxygenated compounds, C_2-C_4 hydrocarbons and CH_4, and the WGS reaction. The model suitably fits the experimental results of molar fraction for the compounds at the reactor outlet, in the 600-700 °C and 0-20 g_{cat} min $g_{volatiles}^{-1}$ ranges.

Likewise, a deactivation kinetic equation dependant on the concentration of bio-oil oxygenated compounds has been proposed because these are probably the main coke precursors. The consideration of the deactivation kinetic equation together with the kinetic modelling at zero time on stream enables a reasonably accurate prediction to be made of the effect operating conditions (temperature in the 600-700 °C range and space time between 0 and 20 g_{cat} min $g_{volatiles}^{-1}$) have on the evolution with time on stream of the concentration of the main compounds in the reaction medium.

The kinetic model is useful for simulating the pyrolysis-reforming process, in which the second step is carried out in a fluidized bed with catalyst circulation, with the regeneration step being carried out in another interconnected fluidized bed.

8

NOMENCLATURE

8. NOMENCLATURE

a	Catalyst activity
A_{ox}, A_{HC}	Chromatographic areas of oxygenated compounds and hydrocarbons
C_{air}	Air concentration, vol %
C_C	Coke content, wt %
d_{MO}	Average crystallite size, L
d_{pore}	Pore diameter, L
E_j	Activation energy of the step j, $L^2\ T^{-2}$
F_{H2}, F_{H2}^o	Molar flow rate of H_2 and the maximum allowable by stoichiometry, mol T^{-1}
F_i, F_T	Molar flow rate of product i and total molar flow rate, mol T^{-1}
$F_{volatiles}$	Molar flow rate of pyrolysis volatiles, mol T^{-1}
f_{ox}, f_{HC}	Response factor of oxygenates and hydrocarbons
GHSV, G_{C1}HSV	Gas hourly space velocity and gas hourly space velocity in equivalent CH_4 units, T^{-1}
HHV, LHV	High and low heating value, $L^2\ T^{-2}$
H_T, H_C, D_C, D_i, D_0	Design parameters of the spouted bed reactor: total height, height of the conical section, diameter of the conical section, diameter of the bed bottom and diameter of the gas inlet, respectively, L
k	Scherrer constant
k_d	Kinetic constant of deactivation, T^{-1}

k_j, k_j^*	Kinetic constant of the step j at T temperature and at reference temperature (650 ºC), mol M^{-1} T^{-1}
K_{WGS}	Equilibrium constant of the WGS reaction
L	Length, L
LHSV	Liquid hourly space velocity, T^{-1}
L_r, D_r	Design parameters of the fluidized bed reactor: height and internal diameter, respectively, L
m_0, m_{gas}, m_{H2}	Mass flow rate of the feed, of the gas produced and of the H_2 produced, M T^{-1}
m_{CO2}	Mass of CO_2 generated in the combustion, M
m_{ox}, m_{HC}	Mass of oxygenates and hydrocarbons, M
M_W	Molecular weight, M mol^{-1}
n_c	Number of components in the kinetic scheme
p	Total number of experimental conditions
P	Pressure, M L^{-1} T^{-2}
P_0	Adsorbate vapour pressure, M L^{-1} T^{-2}
P_{gas}, P_{H2}	Gas and H_2 production, wt %
Q_{gas}	Volumetric flow rate of the gas produced, L^3 T^{-1}
R	Gas constant, L^2 T^{-2} K^{-1}
R^2	Regression coefficient
R_{steam}	Reacted steam, wt %
$(r_i)_0$, r_i	Formation rate of the component i at zero time on stream and at t time, mol M^{-1} T^{-1}

$(r_j)_0$, r_j	Reaction rate of the step j at zero time on stream and at t time, mol M^{-1} T^{-1}
S/B, S/C, S/F	Steam/biomass ratio, steam/C ratio and steam/feed ratio
S_{BET}	BET specific surface, L^2 M^{-1}
t	Time, T
T, T^*	Temperature and reference temperature, K
T_P, T_G, T_R	Pyrolysis, gasification and reforming temperature, K
u	Gas velocity in the conical spouted bed reactor, L T^{-1}
V_{ads}	Volume of the N_2 adsorbed, L^3 M^{-1}
V_{pore}	Pore volume, L^3 M^{-1}
W	Catalyst mass, M
WHSV, W_BHSV	Weight hourly space velocity and bio-oil weight hourly space velocity, T^{-1}
w_i	Weight factor for the component i
X	Conversion, %
x_i	Molar fraction of component i in the reaction medium
$x_{i,j}$, $x_{i,j}^*$	Predicted and experimental molar fractions of component i at experimental condition j
Y_{gas}	Specific gas yield, L^3 M^{-1}
Y_{H2}	H_2 yield, %
Y_i	Yield of C containing compound i, %

Symbols

ΔH	Enthalpy, $L^2\ T^{-2}$
ΔP	Pressure drop in the conical spouted bed reactor, $M\ L^{-1}\ T^{-2}$
β	Width of the average width of the diffraction peak of the sample
γ	Angle of the conical section
θ	Position of the diffraction peak corresponding to the metal
λ	Lenght of the radiation wave
ρ	Density, $M\ L^{-3}$
τ	Space time, $M\ T\ M^{-1}$
$(\upsilon_i)_j$	Stoichiometric coefficient of component i in the step j of the kinetic scheme
ϕ_i	Sum of squares of the residuals for the component i

Abbreviations

BCC	Brown coal char
BTX	Benzene, toluene, xylene
CFB	Circulating fluidized bed
CSBR	Conical spouted bed reactor
DFB	Dual fluidized bed
DME	Dimethyl ether

DTG	Derivative thermogravimetric
EDX	Energy-dispersive X-ray spectroscopy
ER	Equivalent ratio
FCC	Fluid catalytic cracking
FID	Flame ionization detector
FO	Error objective function
GC	Gas chromatograph
HC	Hydrocarbon
HDO	Hydrodeoxygenation
HDPE, LDPE	High density polyethylene, low density polyethylene
ICP-AES	Inductively coupled plasma atomic emission spectroscopy
MFC	Mass flow controller
MS	Mass spectrometer
PET, PP, PS	Polyethylene terephtalate, polypropylene, polystyrene
RHC	Rice husk char
SEM, TEM	Scanning electron microscopy, transmission electron microscopy
SR	Steam reforming
SSE	Sum of squares of the error
SST	Total sum of squares
TCD	Thermal conductivity detector

TG	Thermogravimetric
TPO, TPR	Temperature programmed oxidation, temperature programmed reduction
WGS	Water Gas Shift
XRD	X-ray diffraction

9

BIBLIOGRAPHY

9. BIBLIOGRAPHY

Abdoulmoumine, N., Adhikari, S., Kulkarni, A., Chattanathan, S., A review on biomass gasification syngas cleanup. *Appl. Energy,* **155**, 294-307 (2015).

Acomb, J.C., Wu, C., Williams, P.T., Control of steam input to the pyrolysis-gasification of waste plastics for improved production of hydrogen or carbon nanotubes. *Appl. Catal.,B,* **147**, 571-584 (2014).

Aguado, R., *Combustión y Pirólisis de Residuos de Madera en Spouted Bed Cónico,* PhD Thesis, University of the Basque Country, Bilbao, 1999.

Aguado, R., Olazar, M., San José, M.J., Aguirre, G., Bilbao, J., Pyrolysis of sawdust in a conical spouted bed reactor. Yields and product composition. *Ind. Eng. Chem. Res.,* **39**, 1925-1933 (2000).

Ahmad, A.A., Zawawi, N.A., Kasim, F.H., Inayat, A., Khasri, A., Assessing the gasification performance of biomass: A review on biomass gasification process conditions, optimization and economic evaluation. *Renewable Sustainable Energy Rev.,* **53**, 1333-1347 (2016).

Ahmed, I.I., Gupta, A.K., Kinetics of woodchips char gasification with steam and carbon dioxide. *Appl. Energy,* **88**, 1613-1619 (2011).

Ahmed, I.I., Nipattummakul, N., Gupta, A.K., Characteristics of syngas from co-gasification of polyethylene and woodchips. *Appl. Energy,* **88**, 165-174 (2011).

Alauddin, Z.A.B.Z., Lahijani, P., Mohammadi, M., Mohamed, A.R., Gasification of lignocellulosic biomass in fluidized beds for renewable energy development: A review. *Renewable Sustainable Energy Rev.,* **14**, 2852-2862 (2010).

Alberton, A.L., Souza, M.M.V.M., Schmal, M., Carbon formation and its influence on ethanol steam reforming over Ni/Al_2O_3 catalysts. *Catal. Today,* **123**, 257-264 (2007).

Altzibar, H., Lopez, G., Olazar, M., Bilbao, J., Effect of temperature on fine particle drying in a draft-tube conical spouted bed. *Chem. Eng. Technol.,* **34**, 1130-1135 (2011).

Altzibar, H., Lopez, G., Bilbao, J., Olazar, M., Minimum spouting velocity of conical spouted beds equipped with draft tubes of different configuration. *Ind. Eng. Chem. Res.,* **52**, 2995-3006 (2013).

Alvarez, J., Kumagai, S., Wu, C., Yoshioka, T., Bilbao, J., Olazar, M., Williams, P.T., Hydrogen production from biomass and plastic mixtures by pyrolysis-gasification. *Int. J. Hydrogen Energy,* **39**, 10883-10891 (2014a).

Alvarez, J., Lopez, G., Amutio, M., Bilbao, J., Olazar, M., Bio-oil production from rice husk fast pyrolysis in a conical spouted bed reactor. *Fuel,* **128**, 162-169 (2014b).

Alvarez, J., Lopez, G., Amutio, M., Bilbao, J., Olazar, M., Upgrading the rice husk char obtained by flash pyrolysis for the production of amorphous silica and high quality activated carbon. *Bioresour. Technol.,* **170**, 132-137 (2014c).

Alvarez, J., Amutio, M., Lopez, G., Barbarias, I., Bilbao, J., Olazar, M., Sewage sludge valorization by flash pyrolysis in a conical spouted bed reactor. *Chem. Eng. J.,* **273**, 173-183 (2015).

Amutio, M., *Estrategias para la Pirólisis Rápida de Biomasa en Reactor Spouted Bed Cónico,* PhD Thesis, University of the Basque Country, Bilbao, 2011.

Amutio, M., Lopez, G., Aguado, R., Artetxe, M., Bilbao, J., Olazar, M., Effect of vacuum on lignocellulosic biomass flash pyrolysis in a conical spouted bed reactor. *Energy Fuels,* **25**, 3950-3960 (2011).

Amutio, M., Lopez, G., Artetxe, M., Elordi, G., Olazar, M., Bilbao, J., Influence of temperature on biomass pyrolysis in a conical spouted bed reactor. *Resour. Conserv. Recycl.,* **59**, 23-31 (2012a).

Amutio, M., Lopez, G., Aguado, R., Bilbao, J., Olazar, M., Biomass oxidative flash pyrolysis: Autothermal operation, yields and product properties. *Energy Fuels,* **26**, 1353-1362 (2012b).

Amutio, M., Lopez, G., Alvarez, J., Moreira, R., Duarte, G., Nunes, J., Olazar, M., Bilbao, J., Flash pyrolysis of forestry residues from the Portuguese Central Inland Region within the framework of the BioREFINA-Ter project. *Bioresour. Technol.,* **129**, 512-518 (2013).

Amutio, M., Lopez, G., Alvarez, J., Olazar, M., Bilbao, J., Fast pyrolysis of eucalyptus waste in a conical spouted bed reactor. *Bioresour. Technol.,* **194**, 225-232 (2015).

Anex, R.P., Aden, A., Kazi, F.K., Fortman, J., Swanson, R.M., Wright, M.M., Satrio, J.A., Brown, R.C., Daugaard, D.E., Platon, A., Kothandaraman, G., Hsu, D.D., Dutta, A., Techno-economic comparison of biomass-to-transportation fuels via pyrolysis, gasification, and biochemical pathways. *Fuel,* **89**, S29-S35 (2010).

Angeli, S.D., Pilitsis, F.G., Lemonidou, A.A., Methane steam reforming at low temperature: Effect of light alkanes' presence on coke formation. *Catal. Today,* **242**, 119-128 (2015).

Anis, S., Zainal, Z.A., Tar reduction in biomass producer gas via mechanical, catalytic and thermal methods: A review. *Renewable Sustainable Energy Rev.,* **15**, 2355-2377 (2011).

Antal Jr., M.J., Allen, S.G., Schulman, D., Xu, X., Divilio, R.J., Biomass gasification in supercritical water. *Ind. Eng. Chem. Res.,* **39**, 4040-4053 (2000).

Anuar Sharuddin, S.D., Abnisa, F., Wan Daud, W.M.A., Aroua, M.K., A review on pyrolysis of plastic wastes. *Energy Convers. Manage.,* **115**, 308-326 (2016).

Arabiourrutia, M., *Productos y Cinética de la Pirólisis Térmica y Catalítica de Neumáticos en Spouted Bed Cónico,* PhD Thesis, University of the Basque Country, Bilbao, 2007.

Arauzo, J., Radlein, D., Piskorz, J., Scott, D.S., A new catalyst for the catalytic gasification of biomass. *Energy Fuels,* **8**, 1192-1196 (1994).

Arauzo, J., Radlein, D., Piskorz, J., Scott, D.S., Catalytic Pyrogasification of Biomass. Evaluation of Modified Nickel Catalysts. *Ind. Eng. Chem. Res.,* **36**, 67-75 (1997).

Artetxe, M., *Producción de Olefinas a partir de Polietileno por Pirólisis y Craqueo en línea,* PhD Thesis, University of the Basque Country, Bilbao, 2012.

Artetxe, M., Lopez, G., Amutio, M., Elordi, G., Bilbao, J., Olazar, M., Light olefins from HDPE cracking in a two-step thermal and catalytic process. *Chem. Eng. J.,* **207-208**, 27-34 (2012a).

Artetxe, M., Lopez, G., Elordi, G., Amutio, M., Bilbao, J., Olazar, M., Production of light olefins from polyethylene in a two-step process: Pyrolysis in a conical spouted bed and downstream high-temperature thermal cracking. *Ind. Eng. Chem. Res.,* **51**, 13915-13923 (2012b).

Artetxe, M., Nahil, M.A., Olazar, M., Williams, P.T., Steam reforming of phenol as biomass tar model compound over Ni/Al_2O_3 catalyst. *Fuel,* **184**, 629-636 (2016).

Artetxe, M., Alvarez, J., Nahil, M.A., Olazar, M., Williams, P.T., Steam reforming of different biomass tar model compounds over Ni/Al_2O_3 catalysts. *Energy Convers. Manage.,* **136**, 119-126 (2017).

Asadullah, M., Biomass gasification gas cleaning for downstream applications: A comparative critical review. *Renewable Sustainable Energy Rev.,* **40**, 118-132 (2014).

Assaf, P.G.M., Nogueira, F.G.E., Assaf, E.M., Ni and Co catalysts supported on alumina applied to steam reforming of acetic acid: Representative compound for the aqueous phase of bio-oil derived from biomass. *Catal. Today,* **213**, 2-8 (2013).

Atutxa, A., Aguado, R., Gayubo, A.G., Olazar, M., Bilbao, J., Kinetic description of the catalytic pyrolysis of biomass in a conical spouted bed reactor. *Energy Fuels,* **19**, 765-774 (2005).

Azadi, P., Farnood, R., Review of heterogeneous catalysts for sub- and supercritical water gasification of biomass and wastes. *Int. J. Hydrogen Energy,* **36**, 9529-9541 (2011).

Aznar, M.P., Caballero, M.A., Sancho, J.A., Francés, E., Plastic waste elimination by co-gasification with coal and biomass in fluidized bed with air in pilot plant. *Fuel Process. Technol.,* **87**, 409-420 (2006).

Bae, Y.J., Ryu, C., Jeon, J., Park, J., Suh, D.J., Suh, Y., Chang, D., Park, Y., The characteristics of bio-oil produced from the pyrolysis of three marine macroalgae. *Bioresour. Technol.,* **102**, 3512-3520 (2011).

Balat, M., Balat, M., Kirtay, E., Balat, H., Main routes for the thermo-conversion of biomass into fuels and chemicals. Part 1: Pyrolysis systems. *Energy Convers. Manage.,* **50**, 3147-3157 (2009).

Balat, H., Kirtay, E., Hydrogen from biomass - Present scenario and future prospects. *Int. J. Hydrogen Energy,* **35**, 7416-7426 (2010).

Baliban, R.C., Elia, J.A., Floudas, C.A., Biomass to liquid transportation fuels (BTL) systems: Process synthesis and global optimization framework. *Energy Environ. Sci.,* **6**, 267-287 (2013).

Barbarias, I., *Proceso de Pirólisis y Reformado en Línea para la Producción de H_2 a partir de Residuos Plásticos,* PhD Thesis, University of the Basque Country, Bilbao, 2015.

Barbarias, I., Lopez, G., Alvarez, J., Artetxe, M., Arregi, A., Bilbao, J., Olazar, M., A sequential process for hydrogen production based on continuous HDPE fast pyrolysis and in-line steam reforming. *Chem. Eng. J.,* **296**, 191-198 (2016a).

Barbarias, I., Lopez, G., Amutio, M., Artetxe, M., Alvarez, J., Arregi, A., Bilbao, J., Olazar, M., Steam reforming of plastic pyrolysis model hydrocarbons and catalyst deactivation. *Appl. Catal., A,* **527**, 152-160 (2016b).

Barbarias, I., Lopez, G., Artetxe, M., Arregi, A., Santamaria, L., Bilbao, J., Olazar, M., Pyrolysis and in-line catalytic steam reforming of polystyrene through a two-step reaction system. *J. Anal. Appl. Pyrolysis,* **122**, 502-510 (2016c).

Bartholomew, C.H., Mechanisms of catalyst deactivation. *Appl. Catal., A,* **212**, 17-60 (2001).

Basagiannis, A.C., Verykios, X.E., Reforming reactions of acetic acid on nickel catalysts over a wide temperature range. *Appl. Catal., A,* **308**, 182-193 (2006).

Basagiannis, A.C., Verykios, X.E., Steam reforming of the aqueous fraction of bio-oil over structured $Ru/MgO/Al_2O_3$ catalysts. *Catal. Today,* **127**, 256-264 (2007a).

Basagiannis, A.C., Verykios, X.E., Catalytic steam reforming of acetic acid for hydrogen production. *Int. J. Hydrogen Energy,* **32**, 3343-3355 (2007b).

Bauer, F., Karge, H.G., Characterization of coke on zeolites. *Mol. Sieves,* **5** ,249-364 (2006).

Ben, H., Ragauskas, A.J., Pyrolysis of kraft lignin with additives. *Energy Fuels,* **25**, 4662-4668 (2011).

Bennett, N.M., Helle, S.S., Duff, S.J.B., Extraction and hydrolysis of levoglucosan from pyrolysis oil. *Bioresour. Technol.,* **100**, 6059-6063 (2009).

Berdugo Vilches, T., Marinkovic, J., Seemann, M., Thunman, H., Comparing Active Bed Materials in a Dual Fluidized Bed Biomass Gasifier: Olivine, Bauxite, Quartz-Sand, and Ilmenite. *Energy Fuels,* **30**, 4848-4857 (2016).

Berruti, F., Briens, C., Converting agricultural wastes into valuable green fuels and green chemicals. *Pyne Newsletter,* **23**, 3-4 (2007).

Bertero, M., De La Puente, G., Sedran, U., Fuels from bio-oils: Bio-oil production from different residual sources, characterization and thermal conditioning. *Fuel,* **95**, 263-271 (2012).

Bertero, M., Sedran, U., Conversion of pine sawdust bio-oil (raw and thermally processed) over equilibrium FCC catalysts. *Bioresour. Technol.,* **135**, 644-651 (2013).

Bhattacharya, P., Steele, P.H., Hassan, E.B.M., Mitchell, B., Ingram, L., Pittman Jr., C.U., Wood/plastic copyrolysis in an auger reactor: Chemical and physical analysis of the products. *Fuel,* **88**, 1251-1260 (2009).

Bilbao, J., Olazar, M., Romero, A., Arandes, J.M., Design and operation of a jet spouted bed reactor with continuous catalyst feed in the benzyl alcohol polymerization. *Ind. Eng. Chem. Res.,* **26**, 1297-1304 (1987).

Bimbela, F., Oliva, M., Ruiz, J., García, L., Arauzo, J., Hydrogen production by catalytic steam reforming of acetic acid, a model compound of biomass pyrolysis liquids. *J. Anal. Appl. Pyrolysis,* **79**, 112-120 (2007).

Bimbela, F., Chen, D., Ruiz, J., García, L., Arauzo, J., Ni/Al coprecipitated catalysts modified with magnesium and copper for the catalytic steam reforming of model compounds from biomass pyrolysis liquids. *Appl. Catal., B,* **119-120**, 1-12 (2012).

Bimbela, F., Oliva, M., Ruiz, J., García, L., Arauzo, J., Hydrogen production via catalytic steam reforming of the aqueous fraction of bio-oil using nickel-based coprecipitated catalysts. *Int. J. Hydrogen Energy,* **38**, 14476-14487 (2013).

Blanco, P.H., Wu, C., Williams, P.T., Influence of Ni/SiO_2 catalyst preparation methods on hydrogen production from the pyrolysis/reforming of refuse derived fuel. *Int. J. Hydrogen Energy,* **39**, 5723-5732 (2014).

Boateng, A.A., Daugaard, D.E., Goldberg, N.M., Hicks, K.B., Bench-scale fluidized-bed pyrolysis of switchgrass for bio-oil production. *Ind. Eng. Chem. Res.,* **46**, 1891-1897 (2007).

Boucher, M.E., Chaala, A., Pakdel, H., Roy, C., Bio-oils obtained by vacuum pyrolysis of softwood bark as a liquid fuel for gas turbines. Part II: Stability and ageing of bio-oil and its blends with methanol and a pyrolytic aqueous phase. *Biomass Bioenergy,* **19**, 351-361 (2000).

Brachi, P., Chirone, R., Miccio, F., Miccio, M., Picarelli, A., Ruoppolo, G., Fluidized bed co-gasification of biomass and polymeric wastes for a flexible end-use of the syngas: Focus on bio-methanol. *Fuel,* **128**, 88-98 (2014).

Braimakis, K., Atsonios, K., Panopoulos, K.D., Karellas, S., Kakaras, E., Economic evaluation of decentralized pyrolysis for the production of bio-oil as an energy carrier for improved logistics towards a large centralized gasification plant. *Renewable Sustainable Energy Rev.,* **35**, 57-72 (2014).

Bridgwater, A.V., Meier, D., Radlein, D., An overview of fast pyrolysis of biomass. *Org. Geochem.,* **30**, 1479-1493 (1999).

Bridgwater, A.V., Peacocke, G.V.C., Fast pyrolysis processes for biomass. *Renewable Sustainable Energy Rev.,* **4**, 1-73 (2000).

Bridgwater, A.V., Fast pyrolysis reactors worldwide. *Pyne Newsletter,* **27**, 18-20 (2010).

Bridgwater, A.V., Review of fast pyrolysis of biomass and product upgrading. *Biomass Bioenergy,* **38**, 68-94 (2012).

Bulushev, D.A., Ross, J.R.H., Catalysis for conversion of biomass to fuels via pyrolysis and gasification: A review. *Catal. Today,* **171**, 1-13 (2011).

Butler, E., Devlin, G., Meier, D., McDonnell, K., A review of recent laboratory research and commercial developments in fast pyrolysis and upgrading. *Renewable Sustainable Energy Rev.,* **15**, 4171-4186 (2011).

Cai, J., Liu, R., Research on water evaporation in the process of biomass pyrolysis. *Energy Fuels,* **21**, 3695-3697 (2007).

Calzavara, Y., Joussot-Dubien, C., Boissonnet, G., Sarrade, S., Evaluation of biomass gasification in supercritical water process for hydrogen production. *Energy Convers. Manage.,* **46**, 615-631 (2005).

Cao, J., Shi, P., Zhao, X., Wei, X., Takarada, T., Catalytic reforming of volatiles and nitrogen compounds from sewage sludge pyrolysis to clean hydrogen and synthetic gas over a nickel catalyst. *Fuel Process. Technol.,* **123**, 34-40 (2014).

Carlson, T.R., Tompsett, G.A., Conner, W.C., Huber, G.W., Aromatic production from catalytic fast pyrolysis of biomass-derived feedstocks. *Top. Catal.,* **52**, 241-252 (2009).

Carpenter, D.L., Bain, R.L., Davis, R.E., Dutta, A., Feik, C.J., Gaston, K.R., Jablonski, W., Phillips, S.D., Nimlos, M.R., Pilot-scale gasification of corn stover, switchgrass, wheat straw, and wood: 1. Parametric study and comparison with literature. *Ind. Eng. Chem. Res.,* **49**, 1859-1871 (2010).

Chan, F.L., Tanksale, A., Review of recent developments in Ni-based catalysts for biomass gasification. *Renewable Sustainable Energy Rev.,* **38**, 428-438 (2014).

Chen, D., Zhou, J., Zhang, Q., Zhu, X., Evaluation methods and research progresses in bio-oil storage stability. *Renewable Sustainable Energy Rev.,* **40**, 69-79 (2014).

Chen, F., Wu, C., Dong, L., Jin, F., Williams, P.T., Huang, J., Catalytic steam reforming of volatiles released via pyrolysis of wood sawdust for hydrogen-rich gas production on Fe-Zn/Al_2O_3 nanocatalysts. *Fuel,* **158**, 999-1005 (2015).

Chen, F., Wu, C., Dong, L., Vassallo, A., Williams, P.T., Huang, J., Characteristics and catalytic properties of Ni/$CaAlO_x$ catalyst for hydrogen-enriched syngas production from pyrolysis-steam reforming of biomass sawdust. *Appl. Catal., B,* **183**, 168-175 (2016).

Chhiti, Y., Salvador, S., Commandré, J., Broust, F., Couhert, C., Wood bio-oil noncatalytic gasification: Influence of temperature, dilution by an alcohol and ash content. *Energy Fuels,* **25**, 345-351 (2011).

Chiaramonti, D., Bonini, M., Fratini, E., Tondi, G., Gartner, K., Bridgwater, A.V., Grimm, H.P., Soldaini, I., Webster, A., Baglioni, P., Development of emulsions from biomass pyrolysis liquid and diesel and their use in engines - Part 1: Emulsion production. *Biomass Bioenergy,* **25**, 85-99 (2003).

Chum, H., Diebold, J., Scahill, J., Johnson, D., Black, S., Schroeder, H., Kreibich, R.E., Biomass pyrolysis oil feedstocks for phenolic adhesives. *ACS Symp. Ser.,* **385**, 135-151 (1989).

Corella, J., Toledo, J.M., Molina, G., A review on dual fluidized-bed biomass gasifiers. *Ind. Eng. Chem. Res.,* **46**, 6831-6839 (2007).

Cui, H., Grace, J.R., Spouting of biomass particles: A review. *Bioresour. Technol.,* **99**, 4008-4020 (2008).

Czernik, S., French, R., Feik, C., Chornet, E., Hydrogen by catalytic steam reforming of liquid byproducts from biomass thermoconversion processes. *Ind. Eng. Chem. Res.,* **41**, 4209-4215 (2002).

Czernik, S., French, R.J., Production of hydrogen from plastics by pyrolysis and catalytic steam reform. *Energy Fuels,* **20**, 754-758 (2006).

Czernik, S., Evans, R., French, R., Hydrogen from biomass-production by steam reforming of biomass pyrolysis oil. *Catal. Today,* **129**, 265-268 (2007).

Czernik, S., French, R., Distributed production of hydrogen by auto-thermal reforming of fast pyrolysis bio-oil. *Int. J. Hydrogen Energy,* **39**, 744-750 (2014).

Dai, X., Wu, C., Li, H., Chen, Y., The fast pyrolysis of biomass in CFB reactor. *Energy Fuels,* **14**, 552-557 (2000).

Davidian, T., Guilhaume, N., Iojoiu, E., Provendier, H., Mirodatos, C., Hydrogen production from crude pyrolysis oil by a sequential catalytic process. *Appl. Catal., B,* **73**, 116-127 (2007).

De Lasa, H., Salaices, E., Mazumder, J., Lucky, R., Catalytic steam gasification of biomass: Catalysts, thermodynamics and kinetics. *Chem. Rev.,* **111**, 5404-5433 (2011).

de Miguel Mercader, F., Groeneveld, M.J., Kersten, S.R.A., Venderbosch, R.H., Hogendoorn, J.A., Pyrolysis oil upgrading by high pressure thermal treatment. *Fuel,* **89**, 2829-2837 (2010).

del Remedio Hernández, M., García, A.N., Marcilla, A., Catalytic flash pyrolysis of HDPE in a fluidized bed reactor for recovery of fuel-like hydrocarbons. *J. Anal. Appl. Pyrolysis,* **78**, 272-281 (2007).

Demirbas, A., Competitive liquid biofuels from biomass. *Appl. Energy,* **88**, 17-28 (2011).

DeSisto, W.J., Hill, N., Beis, S.H., Mukkamala, S., Joseph, J., Baker, C., Ong, T., Stemmler, E.A., Wheeler, M.C., Frederick, B.G., Van Heiningen, A., Fast pyrolysis of pine sawdust in a fluidized-bed reactor. *Energy Fuels,* **24**, 2642-2651 (2010).

Devi, L., Ptasinski, K.J., Janssen, F.J.J.G., A review of the primary measures for tar elimination in biomass gasification processes. *Biomass Bioenergy,* **24**, 125-140 (2002).

Devi, L., Ptasinski, K.J., Janssen, F.J.J.G., Van Paasen, S.V.B., Bergman, P.C.A., Kiel, J.H.A., Catalytic decomposition of biomass tars: Use of dolomite and untreated olivine. *Renewable Energy,* **30**, 565-587 (2005).

Di Blasi, C., Modeling chemical and physical processes of wood and biomass pyrolysis. *Prog. Energy Combust. Sci.,* **34**, 47-90 (2008).

Di Blasi, C., Combustion and gasification rates of lignocellulosic chars. *Prog. Energy Combust. Sci.,* **35**, 121-140 (2009).

Di Carlo, A., Borello, D., Sisinni, M., Savuto, E., Venturini, P., Bocci, E., Kuramoto, K., Reforming of tar contained in a raw fuel gas from biomass gasification using nickel-mayenite catalyst. *Int. J. Hydrogen Energy,* **40**, 9088-9095 (2015).

Ding, N., Azargohar, R., Dalai, A.K., Kozinski, J.A., Catalytic gasification of cellulose and pinewood to H_2 in supercritical water. *Fuel,* **118**, 416-425 (2014).

Domine, M.E., Van Veen, A.C., Schuurman, Y., Mirodatos, C., Coprocessing of oxygenated biomass compounds and hydrocarbons for the production of sustainable fuel. *ChemSusChem,* **1**, 179-181 (2008).

Domínguez, C.M., Ocón, P., Quintanilla, A., Casas, J.A., Rodriguez, J.J., Highly efficient application of activated carbon as catalyst for wet peroxide oxidation. *Appl. Catal., B,* **140-141**, 663-670 (2013).

Donatelli, A., Iovane, P., Molino, A., High energy syngas production by waste tyres steam gasification in a rotary kiln pilot plant. Experimental and numerical investigations. *Fuel,* **89**, 2721-2728 (2010).

Dubey, V.R., Vaidya, P.D., Kinetics of steam reforming of acetol over a Pt/C catalyst. *Chem. Eng. J.,* **180**, 263-269 (2012).

Effendi, A., Gerhauser, H., Bridgwater, A.V., Production of renewable phenolic resins by thermochemical conversion of biomass: A review. *Renewable Sustainable Energy Rev.,* **12**, 2092-2116 (2008).

Efika, C.E., Wu, C., Williams, P.T., Syngas production from pyrolysis-catalytic steam reforming of waste biomass in a continuous screw kiln reactor. *J. Anal. Appl. Pyrolysis,* **95**, 87-94 (2012).

Elif, D., Nezihe, A., Hydrogen production by supercritical water gasification of fruit pulp in the presence of Ru/C. *Int. J. Hydrogen Energy,* **41**, 8073-8083 (2016).

Elliott, D.C., Hart, T.R., Neuenschwander, G.G., Rotness, L.J., Olarte, M.V., Zacher, A.H., Solantausta, Y., Catalytic hydroprocessing of fast pyrolysis bio-oil from pine sawdust. *Energy Fuels,* **26**, 3891-3896 (2012).

Elordi, G., *Pirólisis Térmica y Catalítica de Poliolefinas en un Reactor de Spouted Bed Cónico,* PhD Thesis, University of the Basque Country, Bilbao, 2010.

Elordi, G., Olazar, M., Lopez, G., Artetxe, M., Bilbao, J., Product yields and compositions in the continuous pyrolysis of high-density polyethylene in a conical spouted bed reactor. *Ind. Eng. Chem. Res.,* **50**, 6650-6659 (2011a).

Elordi, G., Olazar, M., Lopez, G., Artetxe, M., Bilbao, J., Continuous polyolefin cracking on an HZSM-5 zeolite catalyst in a conical spouted bed reactor. *Ind. Eng. Chem. Res.,* **50**, 6061-6070 (2011b).

Elordi, G., Olazar, M., Lopez, G., Castaño, P., Bilbao, J., Role of pore structure in the deactivation of zeolites (HZSM-5, Hß and HY) by coke in the pyrolysis of polyethylene in a conical spouted bed reactor. *Appl. Catal., B,* **102**, 224-231 (2011c).

Elordi, G., Olazar, M., Castaño, P., Artetxe, M., Bilbao, J., Polyethylene cracking on a spent FCC catalyst in a conical spouted bed. *Ind. Eng. Chem. Res.,* **51**, 14008-14017 (2012a).

Elordi, G., Olazar, M., Artetxe, M., Castaño, P., Bilbao, J., Effect of the acidity of the HZSM-5 zeolite catalyst on the cracking of high density polyethylene in a conical spouted bed reactor. *Appl. Catal., A,* **415-416**, 89-95 (2012b).

Epelde, E., Aguayo, A.T., Olazar, M., Bilbao, J., Gayubo, A.G., Modifications in the HZSM-5 zeolite for the selective transformation of ethylene into propylene. *Appl. Catal., A,* **479**, 17-25 (2014a).

Epelde, E., Aguayo, A.T., Olazar, M., Bilbao, J., Gayubo, A.G., Kinetic model for the transformation of 1-butene on a K-modified HZSM-5 catalyst. *Ind. Eng. Chem. Res.,* **53**, 10599-10607 (2014b).

Ereña, J., Sierra, I., Olazar, M., Gayubo, A.G., Aguayo, A.T., Deactivation of a CuO-ZnO-Al_2O_3/γ-Al_2O_3 catalyst in the synthesis of dimethyl ether. *Ind. Eng. Chem. Res.,* **47**, 2238-2247 (2008).

Erkiaga, A., Lopez, G., Amutio, M., Bilbao, J., Olazar, M., Steam gasification of biomass in a conical spouted bed reactor with olivine and γ-alumina as primary catalysts. *Fuel Process. Technol.,* **116**, 292-299 (2013a).

Erkiaga, A., Lopez, G., Amutio, M., Bilbao, J., Olazar, M., Syngas from steam gasification of polyethylene in a conical spouted bed reactor. *Fuel,* **109**, 461-469 (2013b).

Erkiaga, A., *Gasificación con vapor de Biomasa y Plásticos en Spouted Bed Cónico,* PhD Thesis, University of the Basque Country, Bilbao, 2014.

Erkiaga, A., Lopez, G., Amutio, M., Bilbao, J., Olazar, M., Influence of operating conditions on the steam gasification of biomass in a conical spouted bed reactor. *Chem. Eng. J.,* **237** ,259-267 (2014).

Erkiaga, A., Lopez, G., Barbarias, I., Artetxe, M., Amutio, M., Bilbao, J., Olazar, M., HDPE pyrolysis-steam reforming in a tandem spouted bed-fixed bed reactor for H_2 production. *J. Anal. Appl. Pyrolysis,* **116**, 34-41 (2015).

Faix, A., Schweinle, J., Schöll, S., Becker, G., Meier, D., (GTI-tcbiomass) life-cycle assessment of the BTO ®-process (biomass-to-oil) with combined heat and power generation. *Environ. Prog. Sustainable Energy,* **29**, 193-202 (2010).

Fermoso, J., Rubiera, F., Chen, D., Sorption enhanced catalytic steam gasification process: A direct route from lignocellulosic biomass to high purity hydrogen. *Energy Environ. Sci.,* **5**, 6358-6367 (2012).

Fernandez-Akarregi, A.R., Makibar, J., Lopez, G., Amutio, M., Olazar, M., Design and operation of a conical spouted bed reactor pilot plant (25 kg/h) for biomass fast pyrolysis. *Fuel Process. Technol.,* **112**, 48-56 (2013).

Font Palma, C., Modelling of tar formation and evolution for biomass gasification: A review. *Appl. Energy,* **111**, 129-141 (2013).

Franco, C., Pinto, F., Gulyurtlu, I., Cabrita, I., The study of reactions influencing the biomass steam gasification process. *Fuel,* **82**, 835-842 (2003).

Fratini, E., Bonini, M., Oasmaa, A., Solantausta, Y., Teixeira, J., Baglioni, P., SANS analysis of the microstructural evolution during the aging of pyrolysis oils from biomass. *Langmuir,* **22**, 306-312 (2006).

French, R., Czernik, S., Catalytic pyrolysis of biomass for biofuels production. *Fuel Process. Technol.,* **91**, 25-32 (2010).

Fu, P., Yi, W., Li, Z., Bai, X., Zhang, A., Li, Y., Li, Z., Investigation on hydrogen production by catalytic steam reforming of maize stalk fast pyrolysis bio-oil. *Int. J. Hydrogen Energy,* **39**, 13962-13971 (2014).

Gaisan, B., *Aspectos Básicos de la Tecnología de Pirólisis de Plásticos en un Reactor de Spouted Bed Cónico,* PhD Thesis, University of the Basque Country, Bilbao, 2002.

Gao, N., Li, A., Quan, C., A novel reforming method for hydrogen production from biomass steam gasification. *Bioresour. Technol.,* **100**, 4271-4277 (2009).

García, L., Salvador, M.L., Arauzo, J., Bilbao, R., Catalytic steam gasification of pine sawdust. Effect of catalyst weight/biomass flow rate and steam/biomass ratios on gas production and composition. *Energy Fuels,* **13**, 851-859 (1999).

Garcia, L., French, R., Czernik, S., Chornet, E., Catalytic steam reforming of bio-oils for the production of hydrogen: Effects of catalyst composition. *Appl. Catal., A,* **201**, 225-239 (2000).

Garcia, L., Benedicto, A., Romeo, E., Salvador, M.L., Arauzo, J., Bilbao, R., Hydrogen production by steam gasification of biomass using Ni-Al coprecipitated catalysts promoted with magnesium. *Energy Fuels,* **16**, 1222-1230 (2002).

Garcia-Garcia, I., Acha, E., Bizkarra, K., Martinez De Ilarduya, J., Requies, J., Cambra, J.F., Hydrogen production by steam reforming of m-cresol, a bio-oil model compound, using catalysts supported on conventional and unconventional supports. *Int. J. Hydrogen Energy,* **40**, 14445-14455 (2015).

Garcia-Perez, M., Adams, T.T., Goodrum, J.W., Geller, D., Das, K.C., Production and fuel properties of pine chip bio-oil/biodiesel blends. *Energy Fuels,* **21**, 2363-2372 (2007).

Gayubo, A.G., Aguayo, A.T., Atutxa, A., Valle, B., Bilbao, J., Undesired components in the transformation of biomass pyrolysis oil into hydrocarbons on an HZSM-5 zeolite catalyst. *J. Chem. Technol. Biotechnol.,* **80**, 1244-1251 (2005).

Gayubo, A.G., Valle, B., Aguayo, A.T., Olazar, M., Bilbao, J., Attenuation of catalyst deactivation by cofeeding methanol for enhancing the valorisation of crude bio-oil. *Energy Fuels,* **23**, 4129-4136 (2009).

Gayubo, A.G., Valle, B., Aguayo, A.T., Olazar, M., Bilbao, J., Pyrolytic lignin removal for the valorization of biomass pyrolysis crude bio-oil by catalytic transformation. *J. Chem. Technol. Biotechnol.,* **85**, 132-144 (2010a).

Gayubo, A.G., Valle, B., Aguayo, A.T., Olazar, M., Bilbao, J., Olefin production by catalytic transformation of crude bio-oil in a two-step process. *Ind. Eng. Chem. Res.,* **49**, 123-131 (2010b).

Gayubo, A.G., Vicente, J., Ereña, J., Oar-Arteta, L., Azkoiti, M.J., Olazar, M., Bilbao, J., Causes of deactivation of bifunctional catalysts made up of CuO-ZnO-Al_2O_3 and desilicated HZSM-5 zeolite in DME steam reforming. *Appl. Catal., A,* **483**, 76-84 (2014).

Gil, J., Corella, J., Aznar, M.P., Caballero, M.A., Biomass gasification in atmospheric and bubbling fluidized bed: Effect of the type of gasifying agent on the product distribution. *Biomass Bioenergy,* **17**, 389-403 (1999).

Gil, M.V., Fermoso, J., Rubiera, F., Chen, D., H_2 production by sorption enhanced steam reforming of biomass-derived bio-oil in a fluidized bed reactor: An assessment of the effect of operation variables using response surface methodology. *Catal. Today,* **242**, 19-34 (2015).

Gollakota, A.R.K., Reddy, M., Subramanyam, M.D., Kishore, N., A review on the upgradation techniques of pyrolysis oil. *Renewable Sustainable Energy Rev.,* **58**, 1543-1568 (2016).

Gong, F., Yang, Z., Hong, C., Huang, W., Ning, S., Zhang, Z., Xu, Y., Li, Q., Selective conversion of bio-oil to light olefins: Controlling catalytic cracking for maximum olefins. *Bioresour. Technol.,* **102**, 9247-9254 (2011).

González-Borja, M.A., Resasco, D.E., Anisole and guaiacol hydrodeoxygenation over monolithic Pt-Sn catalysts. *Energy Fuels,* **25**, 4155-4162 (2011).

González-Gil, R., Chamorro-Burgos, I., Herrera, C., Larrubia, M.A., Laborde, M., Mariño, F., Alemany, L.J., Production of hydrogen by catalytic steam reforming of oxygenated model compounds on Ni-modified supported catalysts. Simulation and experimental study. *Int. J. Hydrogen Energy,* **40**, 11217-11227 (2015).

Göransson, K., Söderlind, U., Zhang, W., Experimental test on a novel dual fluidised bed biomass gasifier for synthetic fuel production. *Fuel,* **90**, 1340-1349 (2011a).

Göransson, K., Söderlind, U., He, J., Zhang, W., Review of syngas production via biomass DFBGs. *Renewable Sustainable Energy Rev.,* **15**, 482-492 (2011b).

Goyal, H.B., Seal, D., Saxena, R.C., Bio-fuels from thermochemical conversion of renewable resources: A review. *Renewable Sustainable Energy Rev.,* **12**, 504-517 (2008).

Graça, I., Ribeiro, F.R., Cerqueira, H.S., Lam, Y.L., de Almeida, M.B.B., Catalytic cracking of mixtures of model bio-oil compounds and gasoil. *Appl. Catal., B,* **90**, 556-563 (2009).

Guan, G., Kaewpanha, M., Hao, X., Abudula, A., Catalytic steam reforming of biomass tar: Prospects and challenges. *Renewable Sustainable Energy Rev.,* **58**, 450-461 (2016).

Güngören Madenoglu, T., Boukis, N., Saglam, M., Yüksel, M., Supercritical water gasification of real biomass feedstocks in continuous flow system. *Int. J. Hydrogen Energy,* **36**, 14408-14415 (2011).

Guo, X., Wang, S., Guo, Z., Liu, Q., Luo, Z., Cen, K., Pyrolysis characteristics of bio-oil fractions separated by molecular distillation. *Appl. Energy,* **87**, 2892-2898 (2010b).

Guo, Y., Wang, S.Z., Xu, D.H., Gong, Y.M., Ma, H.H., Tang, X.Y., Review of catalytic supercritical water gasification for hydrogen production from biomass. *Renewable Sustainable Energy Rev.,* **14**, 334-343 (2010a).

Harmanos, H. L. *Detectors and Data Handling in Modern Practice of Gas Chromatography,* John Wiley & Sons, Inc., New York, 1997.

He, M., Xiao, B., Hu, Z., Liu, S., Guo, X., Luo, S., Syngas production from catalytic gasification of waste polyethylene: Influence of temperature on gas yield and composition. *Int. J. Hydrogen Energy,* **34**, 1342-1348 (2009).

Heidenreich, S., Foscolo, P.U., New concepts in biomass gasification. *Prog. Energy Combust. Sci.,* **46**, 72-95 (2015).

Helveg, S., Sehested, J., Rostrup-Nielsen, J.R., Whisker carbon in perspective. *Catal. Today,* **178**, 42-46 (2011).

Hernández, J.J., Aranda, G., Barba, J., Mendoza, J.M., Effect of steam content in the air-steam flow on biomass entrained flow gasification. *Fuel Process. Technol.,* **99**, 43-55 (2012).

Hew, K.L., Tamidi, A.M., Yusup, S., Lee, K.T., Ahmad, M.M., Catalytic cracking of bio-oil to organic liquid product (OLP). *Bioresour. Technol.,* **101**, 8855-8858 (2010).

Hilten, R.N., Bibens, B.P., Kastner, J.R., Das, K.C., In-line esterification of pyrolysis vapor with ethanol improves Bio-oil quality. *Energy Fuels,* **24**, 673-682 (2010).

Hilten, R.N., Das, K.C., Comparison of three accelerated aging procedures to assess bio-oil stability. *Fuel,* **89**, 2741-2749 (2010).

Hilten, R.N., Das, K., Kastner, J.R.,Bibens, B.P., Production of higher quality bio-oil by in line esterification of pyrolysis vapors. *US Patent US8900416 B2* (2014).

Himmelblau, D.A., Method and apparatus for producing water-soluble resin and resin product made by that method. *US Patent 5034498* (1991).

Hong, C., Gong, F., Fan, M., Zhai, Q., Huang, W., Wang, T., Li, Q., Selective production of green light olefins by catalytic conversion of bio-oil with Mg/HZSM-5 catalyst. *J. Chem. Technol. Biotechnol.,* **88**, 109-118 (2013).

Hou, T., Yuan, L., Ye, T., Gong, L., Tu, J., Yamamoto, M., Torimoto, Y., Li, Q., Hydrogen production by low-temperature reforming of organic compounds in bio-oil over a CNT-promoting Ni catalyst. *Int. J. Hydrogen Energy,* **34**, 9095-9107 (2009).

Hu, X., Lu, G., Investigation of the steam reforming of a series of model compounds derived from bio-oil for hydrogen production. *Appl. Catal., B,* **88**, 376-385 (2009).

Hu, X., Lu, G., Comparative study of alumina-supported transition metal catalysts for hydrogen generation by steam reforming of acetic acid. *Appl. Catal., B,* **99**, 289-297 (2010).

Huber, G.W., Iborra, S., Corma, A., Synthesis of transportation fuels from biomass: Chemistry, catalysts, and engineering. *Chem. Rev.,* **106**, 4044-4098 (2006).

Ikura, M., Stanciulescu, M., Hogan, E., Emulsification of pyrolysis derived bio-oil in diesel fuel. *Biomass Bioenergy,* **24**, 221-232 (2003).

Ingram, L., Mohan, D., Bricka, M., Steele, P., Strobel, D., Crocker, D., Mitchell, B., Mohammad, J., Cantrell, K., Pittman Jr., C.U., Pyrolysis of wood and bark in an auger reactor: Physical properties and chemical analysis of the produced bio-oils. *Energy Fuels,* **22**, 614-625 (2008).

Iovane, P., Donatelli, A., Molino, A., Influence of feeding ratio on steam gasification ofpalm shells in a rotary kiln pilot plant. Experimental and numerical investigations. *Biomass Bioenergy,* **56**, 423-431 (2013).

Jiang, X., Ellis, N., Upgrading bio-oil through emulsification with biodiesel: Thermal stability. *Energy Fuels,* **24**, 2699-2706 (2010).

Jin, H., Lu, Y., Guo, L., Zhang, X., Pei, A., Hydrogen production by supercritical water gasification of biomass with homogeneous and heterogeneous catalyst. *Adv. Condens. Matter Phys.,* **2014** (2014).

Joensen, F., Rostrup-Nielsen, J.R., Conversion of hydrocarbons and alcohols for fuel cells. *J. Power Sources,* **105**, 195-201 (2002).

Kan, T., Xiong, J., Li, X., Ye, T., Yuan, L., Torimoto, Y., Yamamoto, M., Li, Q., High efficient production of hydrogen from crude bio-oil via an integrative process between gasification and current-enhanced catalytic steam reforming. *Int. J. Hydrogen Energy,* **35**, 518-532 (2010).

Kan, T., Strezov, V., Evans, T.J., Lignocellulosic biomass pyrolysis: A review of product properties and effects of pyrolysis parameters. *Renewable Sustainable Energy Rev.,* **57**, 126-1140 (2016).

Kantarelis, E., Yang, W., Blasiak, W., Production of liquid feedstock from biomass via steam pyrolysis in a fluidized bed reactor. *Energy Fuels,* **27**, 4748-4759 (2013).

Karmakar, M.K., Datta, A.B., Generation of hydrogen rich gas through fluidized bed gasification of biomass. *Bioresour. Technol.,* **102**, 1907-1913 (2011).

Kaushal, P., Tyagi, R., Steam assisted biomass gasification-an overview. *Can. J. Chem. Eng.,* **90**, 1043-1058 (2012).

Kechagiopoulos, P.N., Voutetakis, S.S., Lemonidou, A.A., Vasalos, I.A., Sustainable hydrogen production via reforming of ethylene glycol using a novel spouted bed reactor. *Catal. Today,* **127**, 246-255 (2007).

Kechagiopoulos, P.N., Voutetakis, S.S., Lemonidou, A.A., Vasalos, I.A., Hydrogen production via reforming of the aqueous phase of bio-oil over Ni/olivine catalysts in a spouted bed reactor. *Ind. Eng. Chem. Res.,* **48**, 1400-1408 (2009).

Kim, Y., Parker, W., A technical and economic evaluation of the pyrolysis of sewage sludge for the production of bio-oil. *Bioresour. Technol.,* **99**, 1409-1416 (2008).

Kirtay, E., Recent advances in production of hydrogen from biomass. *Energy Convers. Manage.,* **52**, 1778-1789 (2011).

Koike, M., Ishikawa, C., Li, D., Wang, L., Nakagawa, Y., Tomishige, K., Catalytic performance of manganese-promoted nickel catalysts for the steam reforming of tar from biomass pyrolysis to synthesis gas. *Fuel,* **103**, 122-129 (2013).

Koppatz, S., Pfeifer, C., Hofbauer, H., Comparison of the performance behaviour of silica sand and olivine in a dual fluidised bed reactor system for steam gasification of biomass at pilot plant scale. *Chem. Eng. J.,* **175**, 468-483 (2011).

Kothari, R., Buddhi, D., Sawhney, R.L., Comparison of environmental and economic aspects of various hydrogen production methods. *Renewable Sustainable Energy Rev.,* **12**, 553-563 (2008).

Kruse, A., Supercritical water gasification. *Biofuels, Bioprod. Biorefin.,* **2**, 415-437 (2008).

Kumagai, S., Alvarez, J., Blanco, P.H., Wu, C., Yoshioka, T., Olazar, M., Williams, P.T., Novel Ni-Mg-Al-Ca catalyst for enhanced hydrogen production for the pyrolysis-gasification of a biomass/plastic mixture. *J. Anal. Appl. Pyrolysis,* **113**, 15-21 (2015).

Kunwar, B., Cheng, H.N., Chandrashekaran, S.R., Sharma, B.K., Plastics to fuel: a review. *Renewable Sustainable Energy Rev.,* **54**, 421-428 (2016).

Lan, P., Xu, Q., Zhou, M., Lan, L., Zhang, S., Yan, Y., Catalytic steam reforming of fast pyrolysis bio-oil in fixed bed and fluidized bed reactors. *Chem. Eng. Technol.,* **33**, 2021-2028 (2010).

Lan, P., Xu, Q., Lan, L., Ren, Z., Zhang, S., Yan, Y., A model for carbon deposition during hydrogen production by the steam reforming of bio-oil. *Energy Sources Part A,* **36**, 250-258 (2014a).

Lan, P., Lan, L.H., Xie, T., Liao, A.P., The preparation of syngas by the reforming of bio-oil in a fluidized-bed reactor. *Energy Sources Part A,* **36**, 242-249 (2014b).

Latifi, M., Berruti, F., Briens, C., Thermal and catalytic gasification of bio-oils in the Jiggle Bed Reactor for syngas production. *Int. J. Hydrogen Energy,* **40**, 5856-5868 (2015).

Latorre, N., Cazaña, F., Martínez-Hansen, V., Royo, C., Romeo, E., Monzón, A., Ni-Co-Mg-Al catalysts for hydrogen and carbonaceous nanomaterials production by CCVD of methane. *Catal. Today,* **172**, 143-151 (2011).

Laurent, E., Delmon, B., Study of the hydrodeoxygenation of carbonyl, carboxylic and guaiacyl groups over sulfided CoMo/γ-Al_2O_3 and NiMo/γ-Al_2O_3 catalysts. I. Catalytic reaction schemes. *Appl. Catal., A,* **109**, 77-96 (1994).

Lédé, J., Broust, F., Ndiaye, F., Ferrer, M., Properties of bio-oils produced by biomass fast pyrolysis in a cyclone reactor. *Fuel,* **86**, 1800-1810 (2007).

Lemonidou, A.A., Kechagiopoulos, P., Heracleous, E.,Voutetakis, S. Steam Reforming of Bio-oils to Hydrogen*, The Role of Catal. for the Sustain. Prod. of Bio-Fuels and Bio-Chem.*, 467-493 (2013).

Levin, D.B., Chahine, R., Challenges for renewable hydrogen production from biomass. *Int. J. Hydrogen Energy,* **35**, 4962-4969 (2010).

Li, D., Ishikawa, C., Koike, M., Wang, L., Nakagawa, Y., Tomishige, K., Production of renewable hydrogen by steam reforming of tar from biomass pyrolysis over supported Co catalysts. *Int. J. Hydrogen Energy,* **38**, 3572-3581 (2013).

Li, D., Koike, M., Chen, J., Nakagawa, Y., Tomishige, K., Preparation of Ni-Cu/Mg/Al catalysts from hydrotalcite-like compounds for hydrogen production by steam reforming of biomass tar. *Int. J. Hydrogen Energy,* **39**, 10959-10970 (2014).

Li, H., Xu, Q., Xue, H., Yan, Y., Catalytic reforming of the aqueous phase derived from fast-pyrolysis of biomass. *Renewable Energy,* **34**, 2872-2877 (2009b).

Li, J., Xiao, B., Yan, R., Xu, X., Development of a supported tri-metallic catalyst and evaluation of the catalytic activity in biomass steam gasification. *Bioresour. Technol.,* **100**, 5295-5300 (2009a).

Li, Q., Hu, G., Supply chain design under uncertainty for advanced biofuel production based on bio-oil gasification. *Energy,* **74**, 576-584 (2014).

Li, Q., Zhang, Y., Hu, G., Techno-economic analysis of advanced biofuel production based on bio-oil gasification. *Bioresour. Technol.,* **191**, 88-96 (2015).

Liu, S., Chen, M., Chu, L., Yang, Z., Zhu, C., Wang, J., Chen, M., Catalytic steam reforming of bio-oil aqueous fraction for hydrogen production over Ni-Mo supported on modified sepiolite catalysts. *Int. J. Hydrogen Energy,* **38**, 3948-3955 (2013).

Lopez, G., *Pirólisis Atmosférica y a Vacío de Neumáticos con Alimentación Continua en un Reactor Spouted Bed Cónico,* PhD Thesis, University of the Basque Country, Bilbao, 2008.

Lopez, G., Olazar, M., Amutio, M., Aguado, R., Bilbao, J., Influence of tire formulation on the products of continuous pyrolysis in a conical spouted bed reactor. *Energy Fuels,* **23**, 5423-5431 (2009).

Lopez, G., Olazar, M., Aguado, R., Elordi, G., Amutio, M., Artetxe, M., Bilbao, J., Vacuum pyrolysis of waste tires by continuously feeding into a conical spouted bed reactor. *Ind. Eng. Chem. Res.,* **49**, 8990-8997 (2010).

Lopez, G., Erkiaga, A., Artetxe, M., Amutio, M., Bilbao, J., Olazar, M., Hydrogen Production by High Density Polyethylene Steam Gasification and In-Line Volatile Reforming. *Ind. Eng. Chem. Res.,* **54**, 9536-9544 (2015a).

Lopez, G., Erkiaga, A., Amutio, M., Bilbao, J., Olazar, M., Effect of polyethylene co-feeding in the steam gasification of biomass in a conical spouted bed reactor. *Fuel,* **153**, 393-401 (2015b).

Lopez, G., Alvarez, J., Amutio, M., Arregi, A., Bilbao, J., Olazar, M., Assessment of steam gasification kinetics of the char from lignocellulosic biomass in a conical spouted bed reactor. *Energy,* **107**, 493-501 (2016).

Lu, Q., Li, W., Zhu, X., Overview of fuel properties of biomass fast pyrolysis oils. *Energy Convers. Manage.,* **50**, 1376-1383 (2009).

Lu, Y.J., Guo, L.J., Ji, C.M., Zhang, X.M., Hao, X.H., Yan, Q.H., Hydrogen production by biomass gasification in supercritical water: A parametric study. *Int. J. Hydrogen Energy,* **31**, 822-831 (2006).

Lu, Y.J., Jin, H., Guo, L.J., Zhang, X.M., Cao, C.Q., Guo, X., Hydrogen production by biomass gasification in supercritical water with a fluidized bed reactor. *Int. J. Hydrogen Energy,* **33**, 6066-6075 (2008).

Lu, Y.J., Guo, L., Zhang, X., Ji, C., Hydrogen production by supercritical water gasification of biomass: Explore the way to maximum hydrogen yield and high carbon gasification efficiency. *Int. J. Hydrogen Energy,* **37**, 3177-3185 (2012).

Luo, S., Xiao, B., Hu, Z., Liu, S., Guo, X., He, M., Hydrogen-rich gas from catalytic steam gasification of biomass in a fixed bed reactor: Influence of temperature and steam on gasification performance. *Int. J. Hydrogen Energy,* **34**, 2191-2194 (2009).

Luo, S., Zhou, Y., Yi, C., Syngas production by catalytic steam gasification of municipal solid waste in fixed-bed reactor. *Energy,* **44**, 391-395 (2012).

Ma, Z., Zhang, S., Xie, D., Yan, Y., A novel integrated process for hydrogen production from biomass. *Int. J. Hydrogen Energy,* **39**, 1274-1279 (2014).

Mahinpey, N., Gomez, A., Review of gasification fundamentals and new findings: Reactors, feedstock, and kinetic studies. *Chem. Eng. Sci.,* **148**, 14-31 (2016).

Makibar, J., Fernandez-Akarregi, A.R., Alava, I., Cueva, F., Lopez, G., Olazar, M., Investigations on heat transfer and hydrodynamics under pyrolysis conditions of a pilot-plant draft tube conical spouted bed reactor. *Chem. Eng. Process. Process Intensif.,* **50**, 790-798 (2011).

Makibar, J., Fernandez-Akarregi, A.R., Amutio, M., Lopez, G., Olazar, M., Performance of a conical spouted bed pilot plant for bio-oil production by poplar flash pyrolysis. *Fuel Process. Technol.,* **137**, 283-289 (2015).

Marquevich, M., Czernik, S., Chornet, E., Montané, D., Hydrogen from biomass: Steam reforming of model compounds of fast-pyrolysis oil. *Energy Fuels,* **13**, 1160-1166 (1999).

Matsumura, Y., Minowa, T., Potic, B., Kersten, S.R.A., Prins, W., Van Swaaij, W.P.M., Van De Beld, B., Elliott, D.C., Neuenschwander, G.G., Kruse, A., Antal Jr., M.J., Biomass gasification in near- and super-critical water: Status and prospects. *Biomass Bioenergy,* **29**, 269-292 (2005).

Medrano, J.A., Oliva, M., Ruiz, J., García, L., Arauzo, J., Catalytic steam reforming of model compounds of biomass pyrolysis liquids in fluidized bed reactor with modified Ni/Al catalysts. *J. Anal. Appl. Pyrolysis,* **85**, 214-225 (2009).

Medrano, J.A., Oliva, M., Ruiz, J., García, L., Arauzo, J., Hydrogen from aqueous fraction of biomass pyrolysis liquids by catalytic steam reforming in fluidized bed. *Energy,* **36**, 2215-2224 (2011).

Mei, Y., Wu, C., Liu, R., Hydrogen production from steam reforming of bio-oil model compound and byproducts elimination. *Int. J. Hydrogen Energy,* **41**, 9145-9152 (2016).

Meier, D., Faix, O., State of the art of applied fast pyrolysis of lignocellulosic materials - A review. *Bioresour. Technol.,* **68**, 71-77 (1999).

Melero, J.A., Iglesias, J., Garcia, A., Biomass as renewable feedstock in standard refinery units. Feasibility, opportunities and challenges. *Energy Environ. Sci.,* **5**, 7393-7420 (2012).

Mellin, P., Kantarelis, E., Zhou, C., Yang, W., Simulation of bed dynamics and primary products from fast pyrolysis of biomass: Steam compared to nitrogen as a fluidizing agent. *Ind. Eng. Chem. Res.,* **53**, 12129-12142 (2014).

Miao, Z., Shastri, Y., Grift, T.E., Hansen, A.C., Ting, K.C., Lignocellulosic biomass feedstock transportation alternatives, logistics, equipment configurations, and modeling. *Biofuels, Bioprod. Biorefin.,* **6**, 351-362 (2012).

Miccio, F., Piriou, B., Ruoppolo, G., Chirone, R., Biomass gasification in a catalytic fluidized reactor with beds of different materials. *Chem. Eng. J.,* **154**, 369-374 (2009).

Michel, R., Rapagnà, S., Burg, P., Mazziotti di Celso, G., Courson, C., Zimny, T., Gruber, R., Steam gasification of Miscanthus X Giganteus with olivine as catalyst production of syngas and analysis of tars (IR, NMR and GC/MS). *Biomass Bioenergy,* **35**, 2650-2658 (2011a).

Michel, R., Rapagnà, S., Di Marcello, M., Burg, P., Matt, M., Courson, C., Gruber, R., Catalytic steam gasification of Miscanthus X giganteus in fluidised bed reactor on olivine based catalysts. *Fuel Process. Technol.,* **92**, 1169-1177 (2011b).

Mier, D., Aguayo, A.T., Gamero, M., Gayubo, A.G., Bilbao, J., Kinetic modeling of n-butane cracking on HZSM-5 zeolite catalyst. *Ind. Eng. Chem. Res.,* **49**, 8415-8423 (2010).

Milne, T.A., Brennan, A.H.,Glenn, B.H., Sourcebook of methods of analysis for biomass and biomass conversion processes. *Elsevier ISBN: 1851665277* (1989).

Moens, L., Black, S.K., Myers, M.D., Czernik, S., Study of the neutralization and stabilization of a mixed hardwooc bio-oil. *Energy Fuels,* **23**, 2695-2699 (2009).

Mohan, D., Pittman Jr., C.U., Steele, P.H., Pyrolysis of wood/biomass for bio-oil: A critical review. *Energy Fuels,* **20**, 848-889 (2006).

Molino, A., Chianese, S., Musmarra, D., Biomass gasification technology: The state of the art overview. *J. Energy Chem.,* **25**, 10-25 (2016).

Montero, C., Valle, B., Bilbao, J., Gayubo, A.G., Analysis of Ni/La_2O_3-αAl_2O_3 catalyst deactivation by coke deposition in the ethanol steam reforming. *Chem. Eng. Trans.,* **37**, 481-486 (2014).

Montero, C., *Condiciones de Proceso y Modelado Cinético del Reformado con Vapor de Etanol sobre Catalizador* Ni/La_2O_3-Al_2O_3, PhD Thesis, University of the Basque Country, Bilbao, 2015.

Montero, C., Ochoa, A., Castaño, P., Bilbao, J., Gayubo, A.G., Monitoring Ni^0 and coke evolution during the deactivation of a Ni/La_2O_3-αAl_2O_3 catalyst in ethanol steam reforming in a fluidized bed. *J. Catal.,* **331**, 181-192 (2015).

Mortensen, P.M., Grunwaldt, J., Jensen, P.A., Knudsen, K.G., Jensen, A.D., A review of catalytic upgrading of bio-oil to engine fuels. *Appl. Catal., A,* **407**, 1-19 (2011).

Mullen, C.A., Boateng, A.A., Mihalcik, D.J., Goldberg, N.M., Catalytic fast pyrolysis of white oak wood in a bubbling fluidized bed. *Energy Fuels,* **25**, 5444-5451 (2011).

Müller, S., Ensyn Technologies. *Pyne Newsletter,* **27**, 11-12 (2010).

Nahil, M.A., Wang, X., Wu, C., Yang, H., Chen, H., Williams, P.T., Novel bi-functional Ni-Mg-Al-CaO catalyst for catalytic gasification of biomass for hydrogen production with in situ CO_2 adsorption. *RSC Adv.,* **3**, 5583-5590 (2013).

Namioka, T., Saito, A., Inoue, Y., Park, Y., Min, T., Roh, S., Yoshikawa, K., Hydrogen-rich gas production from waste plastics by pyrolysis and low-temperature steam reforming over a ruthenium catalyst. *Appl. Energy,* **88**, 2019-2026 (2011).

Narobe, M., Golob, J., Klinar, D., Francetic, V., Likozar, B., Co-gasification of biomass and plastics: Pyrolysis kinetics studies, experiments on 100kW dual fluidized bed pilot plant and development of thermodynamic equilibrium model and balances. *Bioresour. Technol.,* **162**, 21-29 (2014).

Narváez, I., Orío, A., Aznar, M.P., Corella, J., Biomass gasification with air in an atmospheric bubbling fluidized bed. Effect of six operational variables on the quality of the produced raw gas. *Ind. Eng. Chem. Res.,* **35**, 2110-2120 (1996).

Navarro, R.M., Guil-Lopez, R., Gonzalez-Carballo, J.M., Cubero, A., Ismail, A.A., Al-Sayari, S.A., Fierro, J.L.G., Bimetallic MNi/Al_2O_3-La catalysts (M = Pt, Cu) for acetone steam reforming: Role of M on catalyst structure and activity. *Appl. Catal., A,* **474**, 168-177 (2014).

Navarro, R.M., Guil-Lopez, R., Ismail, A.A., Al-Sayari, S.A., Fierro, J.L.G., Ni- and PtNi-catalysts supported on Al_2O_3 for acetone steam reforming: Effect of the modification of support with Ce, La and Mg. *Catal. Today,* **242**, 60-70 (2015).

Nigam, P.S., Singh, A., Production of liquid biofuels from renewable resources. *Prog. Energy Combust. Sci.,* **37**, 52-68 (2011).

Oar-Arteta, L., *Desarrollo del Catalizador y Modelado Cinético del Reformado con Vapor de Dimetil Éter,* PhD Thesis, University of the Basque Country, Bilbao, 2014.

Oasmaa, A., Leppämäki, E., Koponen, P., Levander, J., Tapola, E., Physical characterisation of biomass-based pyrolysis liquids application of standard fuel oil analyses. *VTT Publications,* **306**, ISBN 951-38-5051-X (1997).

Ogi, T., Nakanishi, M., Fukuda, Y., Matsumoto, K., Gasification of oil palm residues (empty fruit bunch) in an entrained-flow gasifier. *Fuel,* **104**, 28-35 (2013).

Olaleye, A.K., Adedayo, K.J., Wu, C., Nahil, M.A., Wang, M., Williams, P.T., Experimental study, dynamic modelling, validation and analysis of hydrogen production from biomass pyrolysis/gasification of biomass in a two-stage fixed bed reaction system. *Fuel,* **137**, 364-374 (2014).

Olazar, M., San Jose, M.J., Aguayo, A.T., Arandes, J.M., Bilbao, J., Stable operation conditions for gas-solid contact regimes in conical spouted beds. *Ind. Eng. Chem. Res.,* **31**, 1784-1792 (1992).

Olazar, M., San José, M.J., Aguayo, A.T., Arandes, J.M., Bilbao, J., Design factors of conical spouted beds and jet spouted beds. *Ind. Eng. Chem. Res.,* **32**, 1245-1250 (1993a).

Olazar, M., San Jose, M.J., Penas, F.J., Aguayo, A.T., Arandes, J.M., Bilbao, J., A model for gas flow in jet spouted beds. *Can. J. Chem. Eng.,* **71**, 189-194 (1993b).

Olazar, M., San Jose, M.J., Penas, F.J., Aguayo, A.T., Bilbao, J., Stability and hydrodynamics of conical spouted beds with binary mixtures. *Ind. Eng. Chem. Res.,* **32**, 2826-2834 (1993c).

Olazar, M., San José, M.J., Aguayo, A.T., Arandes, J.M., Bilbao, J., Pressure drop in conical spouted beds. *Chem. Eng. J.,* **51**, 53-60 (1993d).

Olazar, M., San José, M.J., Zabala, G., Bilbao, J., New reactor in jet spouted bed regime for catalytic polymerizations. *Chem. Eng. Sci.,* **49**, 4579-4588 (1994a).

Olazar, M., San Jose, M.J., Penas, F.J., Arandes, J.M., Bilbao, J., Gas flow dispersion in jet-spouted beds. Effect of geometric factors and operating conditions. *Ind. Eng. Chem. Res.,* **33**, 3267-3273 (1994b).

Olazar, M., San José, M.J., Llamosas, R., Bilbao, J., Hydrodynamics of sawdust and mixtures of wood residues in conical spouted beds. *Ind. Eng. Chem. Res.,* **33**, 993-1000 (1994c).

Olazar, M., San José, M.J., Llamosas, R., Alvarez, S., Bilbao, J., Study of local properties in conical spouted beds using an optical fiber probe. *Ind. Eng. Chem. Res.,* **34**, 4033-4039 (1995a).

Olazar, M., San José, M.J., Peñas, F.J., Aguayo, A.T., Arandes, J.M., Bilbao, J., A simplified model for gas flow in conical spouted beds. *Chem. Eng. J.,* **56**, 19-25 (1995b).

Olazar, M., San José, M.J., Aguado, R., Bilbao, J., Solid flow in jet spouted beds. *Ind. Eng. Chem. Res.,* **35**, 2716-2724 (1996).

Olazar, M., Arandes, J.M., Zabala, G., Aguayo, A.T., Bilbao, J., Design and Operation of a Catalytic Polymerization Reactor in a Dilute Spouted Bed Regime. *Ind. Eng. Chem. Res.,* **36**, 1637-1643 (1997).

Olazar, M., San José, M.J., Aguado, R., Gaisán, B., Bilbao, J., Bed voidage in conical sawdust beds in the transition regime between spouting and jet spouting. *Ind. Eng. Chem. Res.,* **38**, 4120-4122 (1999).

Olazar, M., Aguado, R., San José, M.J., Bilbao, J., Kinetic study of fast pyrolysis of sawdust in a conical spouted bed reactor in the range 400-500 °C. *J. Chem. Technol. Biotechnol.,* **76**, 469-476 (2001).

Olazar, M., San José, M.J., Alvarez, S., Morales, A., Bilbao, J., Design of Conical Spouted Beds for the Handling of Low-Density Solids. *Ind. Eng. Chem. Res.,* **43**, 655-661 (2004).

Olazar, M., Aguado, R., San José, M.J., Alvarez, S., Bilbao, J., Minimum spouting velocity for the pyrolysis of scrap tyres with sand in conical spouted beds. *Powder Technol.,* **165**, 128-132 (2006).

Ollero, P., Serrera, A., Arjona, R., Alcantarilla, S., The CO_2 gasification kinetics of olive residue. *Biomass Bioenergy,* **24**, 151-161 (2002).

Orío, A., Corella, J., Narváez, I., Performance of Different Dolomites on Hot Raw Gas Cleaning from Biomass Gasification with Air. *Ind. Eng. Chem. Res.,* **36**, 3800-3808 (1997).

Ortiz-Toral, P.J., Satrio, J., Brown, R.C., Shanks, B.H., Steam reforming of bio-oil fractions: Effect of composition and stability. *Energy Fuels,* **25**, 3289-3297 (2011).

Osada, M., Yamaguchi, A., Hiyoshi, N., Sato, O., Shirai, M., Gasification of sugarcane bagasse over supported ruthenium catalysts in supercritical water. *Energy Fuels,* **26**, 3179-3186 (2012).

Panigrahi, S., Dalai, A.K., Chaudhari, S.T., Bakhshi, N.N., Synthesis gas production from steam gasification of biomass-derived oil. *Energy Fuels,* **17**, 637-642 (2003).

Pant, K.K., Mohanty, P., Agarwal, S., Dalai, A.K., Steam reforming of acetic acid for hydrogen production over bifunctional Ni-Co catalysts. *Catal. Today,* **207**, 36-43 (2013).

Papadikis, K., Gu, S., Bridgwater, A.V., Computational modelling of the impact of particle size to the heat transfer coefficient between biomass particles and a fluidised bed. *Fuel Process. Technol.,* **91**, 68-79 (2010).

Parajuli, R., Dalgaard, T., Jørgensen, U., Adamsen, A.P.S., Knudsen, M.T., Birkved, M., Gylling, M., Schjørring, J.K., Biorefining in the prevailing energy and materials crisis: A review of sustainable pathways for biorefinery value chains and sustainability assessment methodologies. *Renewable Sustainable Energy Rev.,* **43**, 244-263 (2015).

Park, H.J., Park, Y., Kim, J.S., Influence of reaction conditions and the char separation system on the production of bio-oil from radiata pine sawdust by fast pyrolysis. *Fuel Process. Technol.,* **89**, 797-802 (2008).

Park, H.J., Park, K., Jeon, J., Kim, J., Ryoo, R., Jeong, K., Park, S.H., Park, Y., Production of phenolics and aromatics by pyrolysis of miscanthus. *Fuel,* **97**, 379-384 (2012).

Park, Y., Namioka, T., Sakamoto, S., Min, T., Roh, S., Yoshikawa, K., Optimum operating conditions for a two-stage gasification process fueled by polypropylene by means of continuous reactor over ruthenium catalyst. *Fuel Process. Technol.,* **91**, 951-957 (2010).

Parthasarathy, P., Narayanan, K.S., Hydrogen production from steam gasification of biomass: Influence of process parameters on hydrogen yield - A review. *Renewable Energy,* **66**, 570-579 (2014).

Peacocke, G.V.C., Madrali, E.S., Li, C., Güell, A.J., Wu, F., Kandiyoti, R., Bridgwater, A.V., Effect of reactor configuration on the yields and structures of pine-wood derived pyrolysis liquids: A comparison between ablative and wire-mesh pyrolysis. *Biomass Bioenergy,* **7**, 155-167 (1994).

Peacocke, G.V.C., Bridgwater, A.V., Production of liquids in high yields by ablative fast pyrolysis. *Biomass for Energy, Environment, Agriculture and Industry,* **1-3**, 1749-1756 (1995).

Pereira, E.G., Da Silva, J.N., De Oliveira, J.L., MacHado, C.S., Sustainable energy: A review of gasification technologies. *Renewable Sustainable Energy Rev.,* **16**, 4753-4762 (2012).

Pérez-Uriarte, P., Ateka, A., Gayubo, A.G., Cordero-Lanzac, T., Aguayo, A.T., Bilbao, J., Deactivation kinetics for the conversion of dimethyl ether to olefins over a HZSM-5 zeolite catalyst. *Chem. Eng. J.,* **311**, 367-377 (2017).

Pfeifer, C., Hofbauer, H., Development of catalytic tar decomposition downstream from a dual fluidized bed biomass steam gasifier. *Powder Technol.,* **180**, 9-16 (2008).

Pinto, F., Franco, C., André, R.N., Miranda, M., Gulyurtlu, I., Cabrita, I., Co-gasification study of biomass mixed with plastic wastes. *Fuel,* **81**, 291-297 (2002).

Popp, J., Lakner, Z., Harangi-Rákos, M., Fári, M., The effect of bioenergy expansion: Food, energy, and environment. *Renewable Sustainable Energy Rev.,* **32**, 559-578 (2014).

Predel, M., Kaminsky, W., Pyrolysis of mixed polyolefins in a fluidized-bed reactor and on a pyro-GC/MS to yield aliphatic waxes. *Polym. Degrad. Stab.,* **70**, 373-385 (2000).

Preto, F., Overview of pyrolysis experience in Canada, *IEA Task 34 Meeting,* Espoo, Finlandia (2010).

Pütün, A.E., Biomass to bio-oil via fast pyrolysis of cotton straw and stalk. *Energy Sources,* **24**, 275-285 (2002).

Quitete, C.P.B., Tavares, R.P.A., Bittencourt, R.C.P., Souza, M.M.V.M., Coking Study of Nickel Catalysts Using Model Compounds. *Catal. Lett.,* **146**, 1435-1444 (2016).

Radlein, D., Piskorz, J.,Majerski, P., Method of upgrading biomass pyrolysis liquids for use as fuels and as a source of chemicals by reaction with alcohols. *European Patent EP 0718392 A1* (1996).

Ramos, M.C., Navascués, A.I., García, L., Bilbao, R., Hydrogen production by catalytic steam reforming of acetol, a model compound of bio-oil. *Ind. Eng. Chem. Res.,* **46**, 2399-2406 (2007).

Rapagnà, S., Jand, N., Foscolo, P.U., Catalytic gasification of biomass to produce hydrogen rich gas. *Int. J. Hydrogen Energy,* **23**, 551-557 (1998).

Rapagnà, S., Jand, N., Kiennemann, A., Foscolo, P.U., Steam-gasification of biomass in a fluidised-bed of olivine particles. *Biomass Bioenergy,* **19**, 187-197 (2000).

Rapagnà, S., Virginie, M., Gallucci, K., Courson, C., Di Marcello, M., Kiennemann, A., Foscolo, P.U., Fe/olivine catalyst for biomass steam gasification: Preparation, characterization and testing at real process conditions. *Catal. Today,* **176**, 163-168 (2011).

Rapagnà, S., Gallucci, K., Di Marcello, M., Foscolo, P.U., Nacken, M., Heidenreich, S., Matt, M., First Al_2O_3 based catalytic filter candles operating in the fluidized bed gasifier freeboard. *Fuel,* **97**, 718-724 (2012).

Remiro, A., Valle, B., Aguayo, A.T., Bilbao, J., Gayubo, A.G., Steam reforming of raw bio-oil in a fluidized bed reactor with prior separation of pyrolytic lignin. *Energy Fuels,* **27**, 7549-7559 (2013a).

Remiro, A., Valle, B., Aguayo, A.T., Bilbao, J., Gayubo, A.G., Operating conditions for attenuating Ni/La_2O_3-αAl_2O_3 catalyst deactivation in the steam reforming of bio-oil aqueous fraction. *Fuel Process. Technol.,* **115**, 222-232 (2013b).

Remiro, A., Valle, B., Aramburu, B., Aguayo, A.T., Bilbao, J., Gayubo, A.G., Steam reforming of the bio-oil aqueous fraction in a fluidized bed reactor with in situ CO_2 capture. *Ind. Eng. Chem. Res.,* **52**, 17087-17098 (2013c).

Remiro, A., Valle, B., Oar-Arteta, L., Aguayo, A.T., Bilbao, J., Gayubo, A.G., Hydrogen production by steam reforming of bio-oil/bio-ethanol mixtures in a continuous thermal-catalytic process. *Int. J. Hydrogen Energy,* **39**, 6889-6898 (2014).

Remón, J., Medrano, J.A., Bimbela, F., García, L., Arauzo, J., Ni/Al-Mg-O solids modified with Co or Cu for the catalytic steam reforming of bio-oil. *Appl. Catal., B,* **132-133**, 433-444 (2013).

Remón, J., Broust, F., Valette, J., Chhiti, Y., Alava, I., Fernandez-Akarregi, A.R., Arauzo, J., Garcia, L., Production of a hydrogen-rich gas from fast pyrolysis bio-oils: Comparison between homogeneous and catalytic steam reforming routes. *Int. J. Hydrogen Energy,* **39**, 171-182 (2014).

Remón, J., Broust, F., Volle, G., García, L., Arauzo, J., Hydrogen production from pine and poplar bio-oils by catalytic steam reforming. Influence of the bio-oil composition on the process. *Int. J. Hydrogen Energy,* **40**, 5593-5608 (2015).

Ren, S., Lei, H., Wang, L., Bu, Q., Chen, S., Wu, J., Hydrocarbon and hydrogen-rich syngas production by biomass catalytic pyrolysis and bio-oil upgrading over biochar catalysts. *RSC Adv.,* **4**, 10731-10737 (2014).

Rennard, D., French, R., Czernik, S., Josephson, T., Schmidt, L., Production of synthesis gas by partial oxidation and steam reforming of biomass pyrolysis oils. *Int. J. Hydrogen Energy,* **35**, 4048-4059 (2010).

Rezaei, P.S., Shafaghat, H., Daud, W.M.A.W., Production of green aromatics and olefins by catalytic cracking of oxygenate compounds derived from biomass pyrolysis: A review. *Appl. Catal., A,* **469**, 490-511 (2014).

Rioche, C., Kulkarni, S., Meunier, F.C., Breen, J.P., Burch, R., Steam reforming of model compounds and fast pyrolysis bio-oil on supported noble metal catalysts. *Appl. Catal., B,* **61**, 130-139 (2005).

Román Galdámez, J., García, L., Bilbao, R., Hydrogen production by steam reforming of bio-oil using coprecipitated Ni-Al catalysts. Acetic acid as a model compound. *Energy Fuels,* **19**, 1133-1142 (2005).

Rostrup-Nielsen, J.R., Sehested, J., Whisker carbon revisited. *Stud. Surf. Sci. Catal.,* **139**, 1-12 (2001).

Ruoppolo, G., Ammendola, P., Chirone, R., Miccio, F., H_2-rich syngas production by fluidized bed gasification of biomass and plastic fuel. *Waste Manage.,* **32**, 724-732 (2012).

Saad, J.M., Nahil, M.A., Williams, P.T., Influence of process conditions on syngas production from the thermal processing of waste high density polyethylene. *J. Anal. Appl. Pyrolysis,* **113**, 35-40 (2015).

Safari, F., Salimi, M., Tavasoli, A., Ataei, A., Non-catalytic conversion of wheat straw, walnut shell and almond shell into hydrogen rich gas in supercritical water media. *Chin. J. Chem. Eng.,* **24**, 1097-1103 (2016).

Salehi, E., Azad, F.S., Harding, T., Abedi, J., Production of hydrogen by steam reforming of bio-oil over Ni/Al_2O_3 catalysts: Effect of addition of promoter and preparation procedure. *Fuel Process. Technol.,* **92**, 2203-2210 (2011).

San José, M.J., Olazar, M., Aguayo, A.T., Arandes, J.M., Bilbao, J., Expansion of spouted beds in conical contactors. *Chem. Eng. J.,* **51**, 45-52 (1993).

San José, M.J., Olazar, M., Peñas, F.J., Bilbao, J., Segregation in conical spouted beds with binary and ternary mixtures of equidensity spherical particles. *Ind. Eng. Chem. Res.,* **33**, 1838-1844 (1994).

San José, M.J., Olazar, M., Peñas, F.J., Arandes, J.M., Bilbao, J., Correlation for calculation of the gas dispersion coefficient in conical spouted beds. *Chem. Eng. Sci.,* **50**, 2161-2172 (1995).

San José, M.J., Olazar, M., Alvarez, S., Bilbao, J., Local bed voidage in conical spouted beds. *Ind. Eng. Chem. Res.,* **37**, 2553-2558 (1998a).

San José, M.J., Olazar, M., Alvarez, S., Izquierdo, M.A., Bilbao, J., Solid cross-flow into the spout and particle trajectories in conical spouted beds. *Chem. Eng. Sci.,* **53**, 3561-3570 (1998b).

San José, M.J., Olazar, M., Alvarez, S., Morales, A., Bilbao, J., Local porosity in conical spouted beds consisting of solids of varying density. *Chem. Eng. Sci.,* **60**, 2017-2025 (2005a).

San José, M.J., Alvarez, S., de Salazar, A.O., Olazar, M., Bilbao, J., Influence of the particle diameter and density in the gas velocity in jet spouted beds. *Chem. Eng. Process. Process Intensif.,* **44**, 153-157 (2005b).

San José, M.J., Alvarez, S., Morales, A., Olazar, M., Bilbao, J., Solid cross-flow into the spout and particle trajectories in conical spouted beds consisting of solids of different density and shape. *Chem. Eng. Res. Des.,* **84**, 487-494 (2006).

San José, M.J., Alvarez, S., De Salazar, A.O., Olazar, M., Bilbao, J., Operating conditions of conical spouted beds with a draft tube. Effect of the diameter of the draft Tube and of the height of entrainment zone. *Ind. Eng. Chem. Res.,* **46**, 2877-2884 (2007).

Sánchez-Sánchez, M.C., Navarro, R.M., Fierro, J.L.G., Ethanol steam reforming over Ni/La-Al_2O_3 catalysts: Influence of lanthanum loading. *Catal. Today,* **129**, 336-345 (2007).

Sanna, A., Advanced Biofuels from Thermochemical Processing of Sustainable Biomass in Europe. *Bioenergy Res.,* **7**, 36-47 (2014).

Scott, D.S., Piskorz, J., Radlein, D., Liquid products from the continuous flash pyrolysis of biomass. *Ind. Eng. Chem. Process Des. Dev.,* **24**, 581-588 (1985).

Serrano-Ruiz, J.C., Dumesic, J.A., Catalytic routes for the conversion of biomass into liquid hydrocarbon transportation fuels. *Energy Environ. Sci.,* **4**, 83-99 (2011).

Seyedeyn-Azad, F., Salehi, E., Abedi, J., Harding, T., Biomass to hydrogen via catalytic steam reforming of bio-oil over Ni-supported alumina catalysts. *Fuel Process. Technol.,* **92**, 563-569 (2011).

Seyedeyn Azad, F., Abedi, J., Salehi, E., Harding, T., Production of hydrogen via steam reforming of bio-oil over Ni-based catalysts: Effect of support. *Chem. Eng. J.,* **180**, 145-150 (2012).

Seyedeyn-Azad, F., Abedi, J., Sampouri, S., Catalytic steam reforming of aqueous phase of bio-oil over Ni-based alumina-supported catalysts. *Ind. Eng. Chem. Res.,* **53**, 17937-17944 (2014).

Shen, Y., Yoshikawa, K., Recent progresses in catalytic tar elimination during biomass gasification or pyrolysis - A review. *Renewable Sustainable Energy Rev.,* **21**, 371-392 (2013).

Shen, Y., Zhao, P., Shao, Q., Ma, D., Takahashi, F., Yoshikawa, K., In-situ catalytic conversion of tar using rice husk char-supported nickel-iron catalysts for biomass pyrolysis/gasification. *Appl. Catal., B,* **152-153**, 140-151 (2014a).

Shen, Y., Areeprasert, C., Prabowo, B., Takahashi, F., Yoshikawa, K., Metal nickel nanoparticles in situ generated in rice husk char for catalytic reformation of tar and syngas from biomass pyrolytic gasification. *RSC Adv.,* **4**, 40651-40664 (2014b).

Shen, Y., Chen, M., Sun, T., Jia, J., Catalytic reforming of pyrolysis tar over metallic nickel nanoparticles embedded in pyrochar. *Fuel,* **159**, 570-579 (2015).

Shie, J., Tsou, F., Lin, K., Steam plasmatron gasification of distillers grains residue from ethanol production. *Bioresour. Technol.,* **101**, 5571-5577 (2010).

Sikarwar, V.S., Zhao, M., Clough, P., Yao, J., Zhong, X., Memon, M.Z., Shah, N., Anthony, E.J., Fennell, P.S., An overview of advances in biomass gasification. *Energy Environ. Sci.,* **9**, 2939-2977 (2016).

Simson, A., Farrauto, R., Castaldi, M., Steam reforming of ethanol/gasoline mixtures: Deactivation, regeneration and stable performance. *Appl. Catal., B,* **106**, 295-303 (2011).

Smith, J. M. *Introducción a la Termodinámica en Ingeniería Química,* McGraw-Hill - Interamericana de México*,* México, 2007.

Smith, C.R., Buzan, E.M., Lee, J.W., Potential impact of biochar water-extractable substances on environmental sustainability. *ACS Sustainable Chem. Eng.,* **1**, 118-126 (2013).

Somerville, C., Youngs, H., Taylor, C., Davis, S.C., Long, S.P., Feedstocks for lignocellulosic biofuels. *Science,* **329**, 790-792 (2010).

Takanabe, K., Aika, K., Seshan, K., Lefferts, L., Catalyst deactivation during steam reforming of acetic acid over Pt/ZrO_2. *Chem. Eng. J.,* **120**, 133-137 (2006a).

Takanabe, K., Aika, K., Inazu, K., Baba, T., Seshan, K., Lefferts, L., Steam reforming of acetic acid as a biomass derived oxygenate: Bifunctional pathway for hydrogen formation over Pt/ZrO_2 catalysts. *J. Catal.,* **243**, 263-269 (2006b).

Tan, Z., Xu, X., Liu, Y., Zhang, C., Zhai, Y., Liu, P., Li, Y., Zhang, R., Upgrading bio-oil model compounds phenol and furfural with in situ generated hydrogen. *Environ. Prog. Sustainable Energy,* **33**, 751-755 (2014).

Toch, K., Thybaut, J.W., Marin, G.B., A systematic methodology for kinetic modeling of chemical reactions applied to n-hexane hydroisomerization. *AIChE J.,* **61**, 880-892 (2015).

Trane, R., Dahl, S., Skjøth-Rasmussen, M.S., Jensen, A.D., Catalytic steam reforming of bio-oil. *Int. J. Hydrogen Energy,* **37**, 6447-6472 (2012).

Trane-Restrup, R., Dahl, S., Jensen, A.D., Steam reforming of ethanol: Effects of support and additives on Ni-based catalysts. *Int. J. Hydrogen Energy,* **38**, 15105-15118 (2013).

Trane-Restrup, R., Jensen, A.D., Steam reforming of cyclic model compounds of bio-oil over Ni-based catalysts: Product distribution and carbon formation. *Appl. Catal., B,* **165**, 117-127 (2015).

Trippe, F., Fröhling, M., Schultmann, F., Stahl, R., Henrich, E., Techno-economic assessment of gasification as a process step within biomass-to-liquid (BtL) fuel and chemicals production. *Fuel Process. Technol.,* **92**, 2169-2184 (2011).

Uchimiya, M., Hiradate, S., Antal, M.J., Dissolved Phosphorus Speciation of Flash Carbonization, Slow Pyrolysis, and Fast Pyrolysis Biochars. *ACS Sustainable Chem. Eng.,* **3**, 1642-1649 (2015).

Umeki, K., Yamamoto, K., Namioka, T., Yoshikawa, K., High temperature steam-only gasification of woody biomass. *Appl. Energy,* **87**, 791-798 (2010).

Uzun, B.B., Apaydin-Varol, E., Ates, F., Özbay, N., Pütün, A.E., Synthetic fuel production from tea waste: Characterisation of bio-oil and bio-char. *Fuel,* **89**, 176-184 (2010).

Valle, B., Gayubo, A.G., Aguayo, A.T., Olazar, M., Bilbao, J., Selective production of aromatics by crude bio-oil valorization with a nickel-modified HZSM-5 zeolite catalyst. *Energy Fuels,* **24**, 2060-2070 (2010).

Valle, B., Castaño, P., Olazar, M., Bilbao, J., Gayubo, A.G., Deactivating species in the transformation of crude bio-oil with methanol into hydrocarbons on a HZSM-5 catalyst. *J. Catal.,* **285**, 304-314 (2012).

Valle, B., Remiro, A., Aguayo, A.T., Bilbao, J., Gayubo, A.G., Catalysts of Ni/α-Al_2O_3 and Ni/La_2O_3-αAl_2O_3 for hydrogen production by steam reforming of bio-oil aqueous fraction with pyrolytic lignin retention. *Int. J. Hydrogen Energy,* **38**, 1307-1318 (2013).

Valle, B., Aramburu, B., Remiro, A., Bilbao, J., Gayubo, A.G., Effect of calcination/reduction conditions of Ni/La_2O_3-αAl_2O_3 catalyst on its activity and stability for hydrogen production by steam reforming of raw bio-oil/ethanol. *Appl. Catal., B,* **147**, 402-410 (2014).

Van de Velden, M., Baeyens, J., Boukis, I., Modeling CFB biomass pyrolysis reactors. *Biomass Bioenergy,* **32**, 128-139 (2008).

Van Rossum, G., Kersten, S.R.A., Van Swaaij, W.P.M., Catalytic and noncatalytic gasification of pyrolysis oil. *Ind. Eng. Chem. Res.,* **46**, 3959-3967 (2007).

Velez, D., *Aspectos Básicos de la Tecnología de Pirólisis de Neumáticos en un Reactor Spouted Bed Cónico,* PhD Thesis, University of the Basque Country, Bilbao, 2004.

Vicente, J., *Catalizadores y Condiciones de Proceso para la Producción de Hidrógeno mediante Reformado con Vapor de Dimetil Éter y de Etanol,* PhD Thesis, University of the Basque Country, Bilbao, 2012.

Vicente, J., Montero, C., Ereña, J., Azkoiti, M.J., Bilbao, J., Gayubo, A.G., Coke deactivation of Ni and Co catalysts in ethanol steam reforming at mild temperatures in a fluidized bed reactor. *Int. J. Hydrogen Energy,* **39**, 12586-12596 (2014a).

Vicente, J., Ereña, J., Oar-Arteta, L., Olazar, M., Bilbao, J., Gayubo, A.G., Effect of operating conditions on dimethyl ether steam reforming in a fluidized bed reactor with a CuO-ZnO-Al_2O_3 and desilicated ZSM-5 zeolite bifunctional catalyst. *Ind. Eng. Chem. Res.,* **53**, 3462-3471 (2014b).

Vicente, J., Ereña, J., Montero, C., Azkoiti, M.J., Bilbao, J., Gayubo, A.G., Reaction pathway for ethanol steam reforming on a Ni/SiO_2 catalyst including coke formation. *Int. J. Hydrogen Energy,* **39**, 18820-18834 (2014c).

Waheed, Q.M.K., Williams, P.T., Hydrogen production from high temperature pyrolysis/steam reforming of waste biomass: Rice husk, sugar cane bagasse, and wheat straw. *Energy Fuels,* **27**, 6695-6704 (2013).

Wang, C., Dou, B., Chen, H., Song, Y., Xu, Y., Du, X., Luo, T., Tan, C., Hydrogen production from steam reforming of glycerol by Ni-Mg-Al based catalysts in a fixed-bed reactor. *Chem. Eng. J.,* **220**, 133-142 (2013b).

Wang, D., Czernik, S., Montané, D., Mann, M., Chornet, E., Biomass to Hydrogen via Fast Pyrolysis and Catalytic Steam Reforming of the Pyrolysis Oil or Its Fractions. *Ind. Eng. Chem. Res.,* **36**, 1507-1518 (1997).

Wang, D., Czernik, S., Chornet, E., Production of hydrogen from biomass by catalytic steam reforming of fast pyrolysis oils. *Energy Fuels,* **12**, 19-24 (1998).

Wang, L., Hisada, Y., Koike, M., Li, D., Watanabe, H., Nakagawa, Y., Tomishige, K., Catalyst property of Co-Fe alloy particles in the steam reforming of biomass tar and toluene. *Appl. Catal., B,* **121-122**, 95-104 (2012).

Wang, S., Zhang, F., Cai, Q., Li, X., Zhu, L., Wang, Q., Luo, Z., Catalytic steam reforming of bio-oil model compounds for hydrogen production over coal ash supported Ni catalyst. *Int. J. Hydrogen Energy,* **39**, 2018-2025 (2014a).

Wang, S., Cai, Q., Zhang, F., Li, X., Zhang, L., Luo, Z., Hydrogen production via catalytic reforming of the bio-oil model compounds: Acetic acid, phenol and hydroxyacetone. *Int. J. Hydrogen Energy,* **39**, 18675-18687 (2014b).

Wang, S., Gao, B., Li, Y., Wan, Y., Creamer, A.E., Sorption of arsenate onto magnetic iron-manganese (Fe-Mn) biochar composites. *RSC Adv.,* **5**, 67971-67978 (2015).

Wang, Y., Hu, X., Song, Y., Min, Z., Mourant, D., Li, T., Gunawan, R., Li, C., Catalytic steam reforming of cellulose-derived compounds using a char-supported iron catalyst. *Fuel Process. Technol.,* **116**, 234-240 (2013a).

Wang, Z., Pan, Y., Dong, T., Zhu, X., Kan, T., Yuan, L., Torimoto, Y., Sadakata, M., Li, Q., Production of hydrogen from catalytic steam reforming of bio-oil using C12A7-O^--based catalysts. *Appl. Catal., A,* **320**, 24-34 (2007).

Wei, L., Xu, S., Liu, J., Lu, C., Liu, S., Liu, C., A novel process of biomass gasification for hydrogen-rich gas with solid heat carrier: Preliminary experimental results. *Energy Fuels,* **20**, 2266-2273 (2006).

Wei, L., Xu, S., Zhang, L., Liu, C., Zhu, H., Liu, S., Steam gasification of biomass for hydrogen-rich gas in a free-fall reactor. *Int. J. Hydrogen Energy,* **32**, 24-31 (2007).

Westerhof, R.J.M., Brilman, D.W.F., Van Swaaij, W.P.M., Kersten, S.R.A., Effect of temperature in fluidized bed fast pyrolysis of biomass: Oil quality assessment in test units. *Ind. Eng. Chem. Res.,* **49**, 1160-1168 (2010).

Wilk, V., Hofbauer, H., Conversion of mixed plastic wastes in a dual fluidized bed steam gasifier. *Fuel,* **107**, 787-799 (2013a).

Wilk, V., Hofbauer, H., Co-gasification of plastics and biomass in a dual fluidized-bed steam gasifier: Possible interactions of fuels. *Energy Fuels,* **27**, 3261-3273 (2013b).

Wilk, V., Schmid, J.C., Hofbauer, H., Influence of fuel feeding positions on gasification in dual fluidized bed gasifiers. *Biomass Bioenergy,* **54**, 46-58 (2013).

Williams, P.T., Williams, E.A., Fluidised bed pyrolysis of low density polyethylene to produce petrochemical feedstock. *J. Anal. Appl. Pyrolysis,* **51**, 107-126 (1999).

Wong, S.L., Ngadi, N., Abdullah, T.A.T., Inuwa, I.M., Current state and future prospects of plastic waste as source of fuel: A review. *Renewable Sustainable Energy Rev.,* **50**, 1167-1180 (2015).

Woolcock, P.J., Brown, R.C., A review of cleaning technologies for biomass-derived syngas. *Biomass Bioenergy,* **52**, 54-84 (2013).

Wright, M.M., Daugaard, D.E., Satrio, J.A., Brown, R.C., Techno-economic analysis of biomass fast pyrolysis to transportation fuels. *Fuel,* **89**, S2-S10 (2010).

Wu, C., Huang, Q., Sui, M., Yan, Y., Wang, F., Hydrogen production via catalytic steam reforming of fast pyrolysis bio-oil in a two-stage fixed bed reactor system. *Fuel Process. Technol.,* **89**, 1306-1316 (2008a).

Wu, C., Sui, M., Yan, Y., A comparison of steam reforming of two model bio-oil fractions. *Chem. Eng. Technol.,* **31**, 1748-1753 (2008b).

Wu, C., Williams, P.T., Hydrogen production by steam gasification of polypropylene with various nickel catalysts. *Appl. Catal., B,* **87**, 152-161 (2009a).

Wu, C., Williams, P.T., Hydrogen production from the pyrolysis-gasification of polypropylene: Influence of steam flow rate, carrier gas flow rate and gasification temperature. *Energy Fuels,* **23**, 5055-5061 (2009b).

Wu, C., Williams, P.T., Ni/CeO_2/ZSM-5 catalysts for the production of hydrogen from the pyrolysis-gasification of polypropylene. *Int. J. Hydrogen Energy,* **34**, 6242-6252 (2009c).

Wu, C., Williams, P.T., Investigation of Ni-Al, Ni-Mg-Al and Ni-Cu-Al catalyst for hydrogen production from pyrolysis-gasification of polypropylene. *Appl. Catal., B,* **90**, 147-156 (2009d).

Wu, C., Liu, R., Carbon deposition behavior in steam reforming of bio-oil model compound for hydrogen production. *Int. J. Hydrogen Energy,* **35**, 7386-7398 (2010).

Wu, C., Williams, P.T., Pyrolysis-gasification of plastics, mixed plastics and real-world plastic waste with and without Ni-Mg-Al catalyst. *Fuel,* **89**, 3022-3032 (2010a).

Wu, C., Williams, P.T., A novel Ni-Mg-Al-CaO catalyst with the dual functions of catalysis and CO_2 sorption for H_2 production from the pyrolysis-gasification of polypropylene. *Fuel,* **89**, 1435-1441 (2010b).

Wu, C., Williams, P.T., Investigation of coke formation on Ni-Mg-Al catalyst for hydrogen production from the catalytic steam pyrolysis-gasification of polypropylene. *Appl. Catal., B,* **96**, 198-207 (2010c).

Wu, C., Dong, L., Onwudili, J., Williams, P.T., Huang, J., Effect of Ni particle location within the mesoporous MCM-41 support for hydrogen production from the catalytic gasification of biomass. *ACS Sustainable Chem. Eng.,* **1**, 1083-1091 (2013).

Wu, C.Z., Yin, X.L., Yuan, Z.H., Zhou, Z.Q., Zhuang, X.S., The development of bioenergy technology in China. *Energy,* **35**, 4445-4450 (2010).

Xiao, X., Meng, X., Le, D.D., Takarada, T., Two-stage steam gasification of waste biomass in fluidized bed at low temperature: Parametric investigations and performance optimization. *Bioresour. Technol.,* **102**, 1975-1981 (2011).

Xiao, X., Cao, J., Meng, X., Le, D.D., Li, L., Ogawa, Y., Sato, K., Takarada, T., Synthesis gas production from catalytic gasification of waste biomass using nickel-loaded brown coal char. *Fuel,* **103**, 135-140 (2013).

Xie, H., Yu, Q., Wei, M., Duan, W., Yao, X., Qin, Q., Zuo, Z., Hydrogen production from steam reforming of simulated bio-oil over Ce-Ni/Co catalyst with in continuous CO_2 capture. *Int. J. Hydrogen Energy,* **40**, 1420-1428 (2015a).

Xie, H., Yu, Q., Yao, X., Duan, W., Zuo, Z., Qin, Q., Hydrogen production via steam reforming of bio-oil model compounds over supported nickel catalysts. *J. Energy Chem.,* **24**, 299-308 (2015b).

Xie, H., Yu, Q., Zuo, Z., Han, Z., Yao, X., Qin, Q., Hydrogen production via sorption-enhanced catalytic steam reforming of bio-oil. *Int. J. Hydrogen Energy,* **41**, 2345-2353 (2016).

Xie, Y., Xiao, J., Shen, L., Wang, J., Zhu, J., Hao, J., Effects of Ca-based catalysts on biomass gasification with steam in a circulating spout-fluid bed reactor. *Energy Fuels,* **24**, 3256-3261 (2010).

Xu, Q., Lan, P., Zhang, B., Ren, Z., Yan, Y., Hydrogen production via catalytic steam reforming of fast pyrolysis bio-oil in a fluidized-bed reactor. *Energy Fuels,* **24**, 6456-6462 (2010).

Xu, Q., Xie, D., Wang, F., Yan, Y., Mechanism of hydrogen production by the catalytic steam reforming of bio-oil. *Energy Sources Part A,* **35**, 1028-1038 (2013).

Xue, Y., Zhou, S., Brown, R.C., Kelkar, A., Bai, X., Fast pyrolysis of biomass and waste plastic in a fluidized bed reactor. *Fuel,* **156**, 40-46 (2015).

Yakaboylu, O., Harinck, J., Smit, K.G., De Jong, W., Supercritical water gasification of biomass: A literature and technology overview. *Energies,* **8**, 859-894 (2015).

Yan, C., Cheng, F., Hu, R., Hydrogen production from catalytic steam reforming of bio-oil aqueous fraction over Ni/CeO_2-ZrO_2 catalysts. *Int. J. Hydrogen Energy,* **35**, 11693-11699 (2010a).

Yan, C., Hu, E., Cai, C., Hydrogen production from bio-oil aqueous fraction with in situ carbon dioxide capture. *Int. J. Hydrogen Energy,* **35**, 2612-2616 (2010b).

Yang, J., Blanchette, D., de Aumia, B.,Roy, C. *Progress in Thermochemical Biomass Conversion,* Bridgwater, A.V. (Ed.), *Blackwell Sci. Publ.,* Oxford, UK (2001).

Yanik, J., Ebale, S., Kruse, A., Saglam, M., Yüksel, M., Biomass gasification in supercritical water: Part 1. Effect of the nature of biomass. *Fuel,* **86**, 2410-2415 (2007).

Yanik, J., Ebale, S., Kruse, A., Saglam, M., Yüksel, M., Biomass gasification in supercritical water: II. Effect of catalyst. *Int. J. Hydrogen Energy,* **33**, 4520-4526 (2008).

Yao, D., Wu, C., Yang, H., Hu, Q., Nahil, M.A., Chen, H., Williams, P.T., Hydrogen production from catalytic reforming of the aqueous fraction of pyrolysis bio-oil with modified Ni-Al catalysts. *Int. J. Hydrogen Energy,* **39**, 14642-14652 (2014).

Yoon, S.J., Choi, Y., Lee, J., Hydrogen production from biomass tar by catalytic steam reforming. *Energy Convers. Manage.,* **51**, 42-47 (2010).

Yung, M.M., Magrini-Bair, K.A., Parent, Y.O., Carpenter, D.L., Feik, C.J., Gaston, K.R., Pomeroy, M.D., Phillips, S.D., Demonstration and characterization of Ni/Mg/K/AD90 used for pilot-scale conditioning of biomass-derived syngas. *Catal. Lett.,* **134**, 242-249 (2010).

Zacher, A.H., Olarte, M.V., Santosa, D.M., Elliott, D.C., Jones, S.B., A review and perspective of recent bio-oil hydrotreating research. *Green Chem.,* **16**, 491-515 (2014).

Zhang, H., Xiao, R., Huang, H., Xiao, G., Comparison of non-catalytic and catalytic fast pyrolysis of corncob in a fluidized bed reactor. *Bioresour. Technol.,* **100**, 1428-1434 (2009b).

Zhang, L., Li, W., Liu, J., Guo, C., Wang, Y., Zhang, J., Ethanol steam reforming reactions over Al_2O_3·SiO_2-supported Ni-La catalysts. *Fuel,* **88**, 511-518 (2009c).

Zhang, W., Automotive fuels from biomass via gasification. *Fuel Process. Technol.,* **91**, 866-876 (2010).

Zhang, Y., Jin, B., Zhong, W., Experimental investigation on mixing and segregation behavior of biomass particle in fluidized bed. *Chem. Eng. Process. Process Intensif.,* **48**, 745-754 (2009a).

Zhang, Y., Li, W., Zhang, S., Xu, Q., Yan, Y., Steam reforming of bio-oil for hydrogen production: Effect of Ni-Co bimetallic catalysts. *Chem. Eng. Technol.,* **35**, 302-308 (2012).

Zhang, Y., Brown, T.R., Hu, G., Brown, R.C., Comparative techno-economic analysis of biohydrogen production via bio-oil gasification and bio-oil reforming. *Biomass Bioenergy,* **51**, 99-108 (2013).

Zou, J., Yang, H., Zeng, Z., Wu, C., Williams, P.T., Chen, H., Hydrogen production from pyrolysis catalytic reforming of cellulose in the presence of K alkali metal. *Int. J. Hydrogen Energy,* **41**, 10598-10607 (2016).

10

DISSEMINATION OF RESULTS

10. DISSEMINATION OF RESULTS

10.1. PUBLICATIONS DERIVED FROM THE THESIS

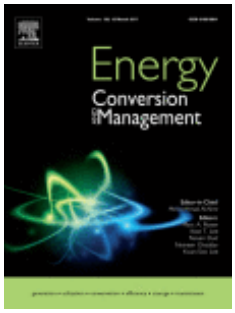

Arregi, A., Amutio, M., Lopez, G., Artetxe, M., Alvarez, J., Bilbao, J., Olazar, M.

Hydrogen-rich gas production by continuous pyrolysis and in-line catalytic reforming of pine wood waste and HDPE mixtures

Energy Convers. Manage., **136**, 192-201 (2017).

Impact factor: 4.801

Arregi, A., Lopez, G., Amutio, M., Barbarias, I., Bilbao, J., Olazar, M.

Hydrogen production from biomass by continuous fast pyrolysis and in-line steam reforming

RSC Adv., **6**, 25975-25985 (2016).

Cited by 9 publications

Impact factor: 3.289

10.2. OTHER PUBLICATIONS

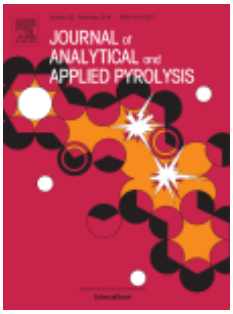

Barbarias, I., Lopez, G., Artetxe, M., Arregi, A., Santamaria, L., Bilbao, J., Olazar, M.

Pyrolysis and in-line catalytic steam reforming of polystyrene through a two-step reaction system

J. Anal. Appl. Pyrolysis, **122**, 502-510 (2016).

Cited by 1 publication

Impact factor: 3.652

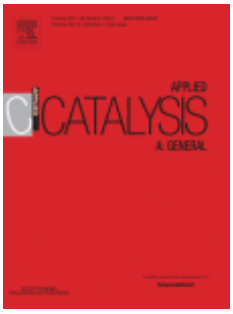

Barbarias, I., Lopez, G., Amutio, M., Artetxe, M., Alvarez, J., Arregi, A., Bilbao, J., Olazar, M.

Steam reforming of plastic pyrolysis model hydrocarbons and catalyst deactivation

Appl. Catal., A, **527**, 152-160 (2016).

Cited by 2 publications

Impact factor: 4.012

Alvarez, J., Lopez, G., Amutio, M., Artetxe, M., Barbarias, I., Arregi, A., Bilbao, J., Olazar, M.

Characterization of the bio-oil obtained by fast pyrolysis of sewage sludge in a conical spouted bed reactor

Fuel Process. Technol., **149**, 162-175 (2016).

Cited by 1 publication

Impact factor: 3.847

Barbarias, I., Lopez, G., Alvarez, J., Artetxe, M., Arregi, A., Bilbao, J., Olazar, M.

A sequential process for hydrogen production based on continuous HDPE fast pyrolysis and in-line steam reforming

Chem. Eng. J., **296**, 191-198 (2016).

Cited by 6 publications

Impact factor: 5.310

Lopez, G., Alvarez, J., Amutio, M., Arregi, A., Bilbao, J., Olazar, M.

Assessment of steam gasification kinetics of the char from lignocellulosic biomass in a conical spouted bed reactor

Energy, **107**, 493-501 (2016).

Cited by 3 publications

Impact factor: 4.292

Artetxe, M., Lopez, G., Amutio, M., Barbarias, I., Arregi, A., Aguado, R., Bilbao, J., Olazar, M.

Styrene recovery from polystyrene by flash pyrolysis in a conical spouted bed reactor

Waste Manage., **45**, 126-133 (2015).

Cited by 3 publications

Impact factor: 3.829